

The Pennsylvania State University

The Graduate School

**LIVING WITH CHANGE: AN ARCHAEOLOGICAL STUDY OF HUMAN SETTLEMENT
PATTERNS AS ENVIRONMENTAL ADAPTATIONS IN LATE HOLOCENE
MADAGASCAR**

A Dissertation in

Anthropology

by

Dylan Scott Davis

© 2022 Dylan Scott Davis

Submitted in Partial Fulfillment
of the Requirements
for the Degree of

Doctor of Philosophy

May 2022

The dissertation of Dylan Scott Davis was reviewed and approved by the following:

Kristina Douglass
Assistant Professor of Anthropology and African Studies
Joyce and Doug Sherwin Early Career Professor in the Rock Ethics Institute
Dissertation Advisor
Chair of Committee

Douglas Bird
Associate Professor of Anthropology

Rebecca Bliege-Bird
Professor of Anthropology

Guangqing Chi
Professor of Rural Sociology, Demography, and Public Health Sciences

Mary Shenk
Associate Professor Anthropology and Demography
Director of Graduate Studies, Department of Anthropology

Abstract

People on Madagascar have coped with environmental change for millennia. Present-day environmental change, however, is negatively impacting the livelihoods and sustainability of coastal communities on Madagascar. As a result of increasing climate-driven impacts on livelihoods and economic development initiatives, community settlement strategies are shifting towards increased sedentism. This dissertation investigates settlement patterns of mobile foraging populations, their drivers, and ecological effects in Late Holocene Madagascar. Specifically, I investigate environmental links to settlement patterns via remotely sensed environmental and archaeological data and radiocarbon chronology from identified archaeological deposits. While most studies of settlement distribution focus on socioecological drivers, in this project I also devote attention to the ecological legacy effects of human settlement by looking at the geochemical and spectral properties of archaeologically inhabited areas. In this way, this dissertation seeks a holistic understanding of settlement distribution in Southwest Madagascar extending from its driving forces to its long-lasting effects on ecological systems. Using a predictive modeling protocol rooted in ideal distribution models from human behavioral ecology, I use machine learning algorithms to extract culturally significant environmental variables from Sentinel-2 satellite images. These data then aid in exploring the degree to which resource distribution is correlated with settlement density, whether Allee effects account for settlement patterns, and the resulting ecological impact of foraging activity on the Malagasy landscape over thousands of years. Identified cultural deposits are visited during ground investigations to survey and excavate different areas to acquire temporal information (e.g., ^{14}C dates, ceramics, etc.). Based on this newly generated archaeological settlement record, these data are incorporated into spatial point process models (PPMs), a form of regression analysis, of archaeological settlements to investigate the relationship between environmental conditions and settlement distributions. PPMs help to reveal external ecological relationships as well as dispersive or cohesive properties between archaeological points. Finally, using an automated remote sensing procedure employing a combination of Sentinel-2 and PlanetScope imagery and random forest models, I quantify the extent of cultural niche construction resulting from foraging communities in the Velondriake Marine Protected Area in southwest Madagascar since the Late Holocene. Altogether, this dissertation demonstrates that foraging communities in Late Holocene Madagascar settled the landscape according to the principles of an ideal free distribution with Allee effects, meaning that a strong mix between environmental and social factors, including active landscape modification (or niche construction) drove settlement choice. Specifically, the presence of freshwater sources, community defense, and social cohesion were among the most significant drivers of settlement patterns, followed by marine resource access (i.e., coral reefs). Additionally, it appears that almost 20% of the Velondriake region has been anthropogenically modified, demonstrating that foraging communities leave quantifiable and long-lasting impacts on ecological systems. Over the last millennium, communities in the Velondriake region have maintained close social connections, which have shifted geographically over the last several hundred years. Settlements appear to reflect a variety of long-term and seasonal occupations that exploited a variety of marine habitats including coastal coral reefs, oceans, and mangrove forests.

Table of Contents

List of Figures.....	viii
List of Tables.....	xi
Preface.....	xii
Acknowledgements.....	xiii
Chapter 1: Introduction.....	1
The Importance of Landscape and Regional Contexts.....	3
The Velondriake Marine Protected Area and Collaborative Archaeology.....	5
A New Theoretical Approach for Settlement Archaeology.....	7
Chapter 2: A Review of Aerial and Spaceborne Remote Sensing in African Archaeology.....	13
Limitations of Recent Remote Sensing Archaeology in Africa.....	17
Trends in Remote Sensing Research in African Archaeology.....	22
Future Directions for Remote Sensing in African Archaeology.....	31
Conclusions.....	34
Chapter 3: The aerial panopticon and the ethics of archaeological remote sensing in sacred cultural spaces.....	36
Surveillance and Power: Foucauldian Dynamics.....	42
Case Study: Madagascar.....	50
<i>Local Opinions on Aerial Imagery</i>	53
Discussion.....	58
Conclusion.....	62
Chapter 4: Satellite-based remote sensing rapidly reveals extensive record of Holocene coastal settlement on Madagascar.....	64
Previous Landscape-Level Investigations on Madagascar.....	68
Methods.....	70
<i>Ideal Free Distribution Modeling</i>	70
<i>Remote sensing and predictive modeling</i>	72
<i>Processing steps of predictive modeling analysis</i>	73
Results.....	79
<i>Prediction of pre-recorded site locations</i>	80
<i>Prediction of previously unrecorded site locations</i>	82
Discussion.....	85
<i>Future Work</i>	90
Conclusions.....	91

Chapter 5: Integrating point process models, evolutionary ecology, and traditional knowledge improves landscape archaeology: A case from southwest Madagascar.....	94
Materials and Methods	102
<i>Point Process Modeling for First-Order Properties</i>	104
<i>GIS Analysis</i>	107
<i>Point Process Modeling for Second-Order Properties</i>	111
Results	112
<i>Point Process Modeling of First-Order Properties</i>	115
<i>GIS Analysis</i>	119
<i>Point Process Modeling of Second-Order Properties</i>	121
Discussion	124
Conclusions	129
Chapter 6: Remote Sensing Reveals Lasting Legacies of Land-Use by Small-Scale Communities in the southwestern Indian Ocean.....	132
Niche Construction and the Legacy of Land-Use Practices.....	137
Methods.....	141
<i>Machine Learning Algorithm</i>	142
<i>Vegetative Indices</i>	144
<i>Spatial Analysis</i>	146
Results	147
Discussion & Conclusions	151
Chapter 7: Evidence for extensive social networks as risk-mitigation strategies on Southwest Madagascar	158
<i>Sociality and resilience in the face of external pressures</i>	158
<i>Past Social Networks in SW Madagascar</i>	160
<i>Stressors and Expectations</i>	161
Materials and Methods	164
<i>Network Analysis</i>	164
<i>Assessment of sampling error on network results</i>	167
<i>Ceramic Chronologies</i>	168
<i>Paleoclimate Assessment using Bayesian Change Point Analysis (BCPA)</i>	168
Results	169
Discussion	172
<i>Early Period Network (1150-450 BP)</i>	173
<i>Middle Period Network (450-250 B.P.)</i>	174

<i>Late Period Network (250-50 B.P.)</i>	175
Conclusion.....	176
Chapter 8: Refining the settlement chronology of SW Madagascar: Results of new excavations in the Velondriake Marine Protected Area	177
Regional Background	178
Methods.....	182
Results	185
<i>Radiocarbon Chronology of Human Presence in Velondriake, Madagascar</i>	190
<i>Site Descriptions</i>	193
Chapter 9: Conclusion	219
Theoretical and Practical Contributions	219
Settlement History of the Velondriake Region of Southwest Madagascar	221
Future Research Avenues	223
<i>Understanding the relationship between climatic change and human mobility using high-resolution paleoclimate proxies</i>	224
<i>The legacy of ancient niche construction among foragers, herders, and farmers in southwest Madagascar</i>	226
Final Thoughts.....	228
Appendix A: IRB Protocols Pertaining to Geophysical Data Collection at Penn State	
230	
Appendix B: Supplemental Data for Chapter 4	234
Supplemental Code: Archaeological Distributional Analysis.....	236
Appendix C: Supplemental Information from Chapter 5	248
Appendix D: Supplemental Information from Chapter 6	269
Supplementary Figures.....	269
Supplementary Tables.....	272
Code used for Analyses.....	273
<i>R-Code</i>	273
Calculate Band Statistics for Data.....	280
<i>Javascript Code for Compiling Sentinel-2 Data</i>	292
<i>Javascript Code for Machine Learning Analysis</i>	295
Appendix E: Supplemental Information from Chapter 7	298
Calculate Raw Data Values of Network Connectivity	307
Appendix F: Supplemental Data for Chapter 8	344
Supplemental Code: Bayesian Accumulation Model for G134 (coded in R v. 4.0.2).344	

Supplemental Figures and Tables	346
References	351

List of Figures

Figure 1-1: Map of the Velondriake Marine Protected Area.	6
Figure 1-2: Approach to understanding archaeological settlement and mobility patterns used in this dissertation.	10
Figure 2-1: Map of remote sensing case studies discussed in the chapter.	17
Figure 3-1: A map of the Commune of Befandefa (which now also includes the Velondriake Marine Protected Area).	46
Figure 3-2: Examples of caves and rock shelters in Velondriake, most of which do not appear on official maps, like the one in Figure 3-1.	47
Figure 3-3: Location of study region in Southwest Madagascar.	51
Figure 3-4: MAP team member George Manahira assisting with Total Station mapping of karst topography around archaeological sites in Velondriake.	54
Figure 3-5: Community member in SW Madagascar wearing goggles and viewing live feed from drone.	56
Figure 3-6: Examples of cultural features that can easily be recorded using aerial and spaceborne imaging systems.	58
Figure 3-7: Illustration of standard versus equitable practice of remote sensing within archaeology.	59
Figure 4-1: Map of study area.	67
Figure 4-2: A 2-D scatterplot function in ENVI.	74
Figure 4-3: Processing steps of predictive modeling analysis.	78
Figure 4-4: Results of Archaeological Probability Index.	81
Figure 4-5: Density distribution of artifacts recovered from different probability locations.	82
Figure 4-6: Shows the points of some specific materials collected during survey.	85
Figure 4-7: Shows the locations of artifacts (and clusters of artifacts) recovered from grids visited throughout the study area during July and August of 2019.	86
Figure 4-8: Graphical representation of K-S empirical cumulative distribution function (ECDF) curve results reported in Table 4-8.	89
Figure 5-1: Map of study region in Southwest Madagascar.	98
Figure 5-2: Illustration of iterative modeling process.	101
Figure 5-3: Map of unweighted predictive raster with and without re-sampling.	110
Figure 5-4: First order intensity of archaeological deposits (per m ²) as a function of different environmental variables using nonparametric smoothing (rho-hat test).	113
Figure 5-5: First order intensity of archaeological deposits (per m ²) weighted by artifact counts as a function of different environmental variables using nonparametric smoothing (rho-hat test).	114
Figure 5-6: Results of testing for second-order interaction using K-, G-, and PC-functions compared to 39 simulated realizations of CSR.	115
Figure 5-7: Map of raw and kernel-smoothed Pearson residual values of PPM3, PPM4, and PPM1.	117
Figure 5-8: Results of the residual K- and G-function tests on PPM1 and best fitted models PPM3 and PPM4.	119
Figure 5-9: Residual K-function test of the best-fitting unweighted PPM with an area interaction parameter and the best-fitting weighted PPM with an area interaction parameter.	124

Figure 6-1: Illustrates the methodological workflow presented in this chapter.	134
Figure 6-2: Map of the study region.	135
Figure 6-3: Illustration of perturbation and relocation components of NCT.	140
Figure 6-4: Results of RF algorithm using a threshold of 0.7.	148
Figure 6-5: Vegetation index values for archaeological and non-archaeological locations.	149
Figure 6-6: Density of anthropogenic modifications within the study region identified by the machine learning algorithm.	151
Figure 6-7: Comparison between predictive modeling results of Davis, DiNapoli, and Douglass (2020) and this chapter.	153
Figure 7-1: Ceramic characteristics and their relative chronology.	161
Figure 7-2: Historical events and precipitation/aridity levels based on $\delta^{18}O$ data from the carbonate of a speleothem collected from Asafora Cave and from ostracods collected in laminated lake sediments at Ranobe.	162
Figure 7-3: Map of the study region, showing locations where archaeological ceramics and paleoclimate data were recovered.	163
Figure 7-4: X^2 Distance network of ceramic attributes over time.	171
Figure 8-1: Map of excavated locations reported in this chapter alongside prior excavation work in the Velondriake Marine Protected Area.	178
Figure 8-2: Illustration of chronometric hygiene procedure.	184
Figure 8-3: Radiocarbon data for all excavations in Velondriake conducted in this study except G134.	191
Figure 8-4: Bayesian age depth estimation model for G134.	192
Figure 8-5: Profile wall drawings of G123 Unit 1.	194
Figure 8-6: Profile wall drawing of G123 Unit 2.	196
Figure 8-7: Profile wall of G123 Unit 3.	199
Figure 8-8: Photo of concreted soil layer found in G123 Unit 3.	200
Figure 8-9: Profile wall drawing of G130.	203
Figure 8-10: Profile wall drawing of G58.	204
Figure 8-11: Profile wall drawing of G134.	205
Figure 8-12: Surface of Feature 1 (Left) and Feature 2 (Right) which are defined by concreted and burnt shell material.	207
Figure 8-13: Drawings of ceramic rim sherds recovered from G134.	207
Figure 8-14: Bayesian age estimation of the depth where the lithic blade was recovered from Level 8 of G134 Unit 1.	210
Figure 8-15: Shows the distribution of age estimates for a depth of 166cm based on the Bayesian age-depth estimation model reported above (Figure 8-4).	210
Figure 8-16: Profile wall drawing of G-15-20.	211
Figure 8-17: Wall profile for SAVABO Unit 1.	214
Figure 8-18: Wall profile for SAVABO Unit 2.	215
Figure 9-1: Map of corals identified for coring along the coast of Velondriake.	225
Figure 9-2: Map of the Namonte Basin in southwest Madagascar.	227
Supplemental Figure D-1: Shows results of pansharpener procedure on SWIR imagery.	269

Supplemental Figure D-2: Shows the locations of ground-verified archaeological sites (blue), non-archaeological sites (red), and randomly generated test points (black) used in the analysis.....	270
Supplemental Figure D-3: Shows violin and boxplots for annual and seasonal vegetative index values.	270
Supplemental Figure D-4: Shows the SWIR reflectance signatures for archaeological, non-archaeological, and randomly generated points within the study area.	271
Supplemental Figure D-5. Shows NDWI vegetative index values for archaeological, non-archaeological, and randomly generated points within the study area.	271
Supplemental Figure D-6. Results of Getis-Ords General G test.....	272
Supplemental Figure F-1: Bayesian age depth estimation model of G134 using only class 1 and class 2 ¹⁴ C dates.	346
Supplemental Figure F-2: Count of marine shell material recovered from G123 Unit 1.	346
Supplemental Figure F-3: Count of marine shell material recovered from G123 Unit 2.	347
Supplemental Figure F-4: Count of marine shell materials recovered from G123 Unit 3.	347
Supplemental Figure F-5: Count of marine shell material recovered from G-15-2020 by stratigraphic level.	348

List of Tables

Table 2-1: List of open-source/freely available data repositories and software platforms for remote sensing analysis.	20
Table 4-1: Quantified thresholds of probability index and their qualitative equivalent classifications.	77
Table 4-2: Confusion matrix for SVM classification.	79
Table 4-3: Producer’s and user’s accuracy for SVM classification.....	79
Table 4-4: Confusion matrix for OBIA classification.....	80
Table 4-5: User's and Producer's Accuracy for OBIA classification.	80
Table 4-6: Sum of survey results by grid probability value.....	83
Table 4-7: Descriptive statistics of probability values for specific points within survey grids where materials were recovered.	84
Table 4-8: Results of K-S tests between archaeological probability distribution and randomly generated probability distributions.....	88
Table 5-1: List of different variables incorporated in Chapter 4 and the models developed in this chapter.....	102
Table 5-2: Results of comparing the different inhomogeneous Poisson point process models using Δ AIC, Δ BIC, and their associated weights.	115
Table 5-3: Results of the chosen best fitting model (PPM3), including the parameter estimates and standard errors with a 95% confidence interval for each covariate.	118
Table 5-4: The formulas and respective covariate weights for each predictive model and the results of ground tested results in relation to each modified algorithm.	122
Table 5-5: Descriptive statistical values for raster probability values at known archaeological deposit locations (n=1030) for each created predictive model.....	123
Table 5-6: Results of comparing 6 PPMs using Δ AIC, Δ BIC, and their associated weights.....	123
Table 6-1: Accuracy assessment of random forest algorithm.	147
Table 7-1: X^2 -similarity scores and associated ceramic assemblages among select sites surveyed in 2019.	170
Table 7-2: Average Centrality Metrics for Decorative Networks.....	172
Table 8-1: Previous Radiocarbon Dates from Excavations in the Velondriake Marine Protected Area.	181
Table 8-2: Radiocarbon dates from charcoal recovered from excavation units reported in this dissertation.	186
Table 8-3: Chronometric Hygiene of charcoal samples processed via AMS.....	190
Table 8-4: G123 Unit 1 Marine Shell Material.....	195
Table 8-5: G123 Unit 2 Marine Shell Materials.....	197
Table 8-6: G123 Unit 3 Marine Shell Materials.....	201
Table 8-7: G-15-2020 marine shell materials.	213
Supplemental Table B-1: Shows list of surveyed grid locations during the summer of 2019 and materials collected from each area.	234
Supplemental Table D-1. List of PlanetScope images used for analyses.....	272
Supplemental Table F-1: Charcoal Samples and their chronometric hygiene ranks and associations.....	349

Preface

The author adopted Chapters 2-8 of this dissertation from a series of co-authored manuscripts for which Dylan S. Davis was the first author and primary contributor of all. Davis conducted all of the remote sensing, GIS, and spatial statistical analyses, in addition to archaeological surveys and data analysis resulting from surveys and excavations, including AMS preprocessing of charcoal samples. Davis was responsible for organizing excavation projects but did not personally conduct these excavations due to the COVID-19 pandemic and associated travel restrictions between the United States and Madagascar between 2020 and 2021. Davis was also responsible for writing initial drafts and revisions of all manuscripts, as well as most of the interpretations of the data produced, and creating most of the figures and tables. For Chapters 2-8 Douglass provided guidance and assisted in revisions during the peer review process and contributed to interpretations of data collected and reported on in these manuscripts. For Chapter 3, members of the Morombe Archaeological Project (MAP) team (Lahiniriko, Chrisostome, Manahira) and Olo Be Taloha Lab at Penn State (Buffa, Rasolondrainy, Creswell, Anyanwu, Ibiogba, Randolph, Ouarghidi, and Phelps) were involved in discussions of ethical issues pertaining to remote sensing and revisions to writing that culminated in the published article. For Chapter 4, members of the Morombe Archaeological Project Team conducted archaeological survey and assisted with data analysis (Andriankaja, Carnat, Chrisostome, Colombe, Fenomanana, Hubertine, Justome, Lahiniriko, Léonce, Manahira, Pierre, Roi, Soafiavy, Victorian, Voahirana). Majakahery was involved in data interpretation for Chapter 4. For Chapter 5, DiNapoli assisted in the formulation of the spatial analysis and aided in interpretation of results, writing and revising of the manuscript. For Chapter 7 Rasolondrainy and Hixon aided in data interpretation and provided relevant historical and paleoclimate datasets used in analysis. For Chapter 8, the Morombe Archaeological Project Team, led by Manahira, conducted excavations and material analysis in the field.

Acknowledgements

There are many people I wish acknowledge for their support and dedication throughout my doctoral program. First, I wish to thank the entire Morombe Archaeological Project team for their constant collaboration and assistance in conducting fieldwork in Madagascar. In particular, George “Bic” Manahira, for all of his dedication to this project and constant assistance in logistical planning and execution of fieldwork plans. This was vital for the completion of my research, especially during the COVID-19 pandemic when travel between the United States and Madagascar was impossible. I am also indebted to the local leaders and village presidents of Velondriake who granted me permission to conduct fieldwork on their lands.

I must also thank my dissertation committee members – Drs. Douglas Bird, Rebecca Bird, and Guangqing Chi – for their guidance and support. Their feedback on proposal and dissertation drafts was invaluable and helped to shape my dissertation project. I want to also acknowledge the ongoing support of my Master’s advisors, Drs. Carl Lipo and Matthew Sanger.

Next, I must extend my sincere thanks to my advisor and committee chair, Dr. Kristina Douglass, for all of her guidance and support throughout my time at Penn State. Kristina agreed to take me on as a student after the departure of my original advisor, and since that time we have developed a number of important projects and co-authored numerous manuscripts together. I am sure our academic collaborations will extend well into the future, and it is in large part because of her guidance that I am where I am today.

Finally, I want to thank my family for their constant love and support. My parents, who have supported me in all I have sought to do, including earning an undergraduate degree in anthropology, which spurred on everything I have accomplished in this dissertation. My grandparents, for always stressing the importance of education. My sister, for always trying to one-up me, therefore pushing me to do my best as well. And finally, no acknowledgement would be complete without mentioning my partner and closest confidant, Jules, who always brings optimism to every situation and encourages me at every turn.

This dissertation research is based upon work supported by the National Science Foundation (BCS-2039927), the National Geographic Society (NGS-77912R-21), the American Philosophical Society, the Explorers Club, the NASA Pennsylvania Space Grant Consortium, Sigma Xi, the Institute for Computational and Data Sciences at Penn State University, three Hill Fellowship Awards through the Department of Anthropology at Penn State, a Dickerson Family Fund Award through the African Studies Program at Penn State, the Africana Research Center at Penn State, and the Energy and Environmental Sustainability Laboratories (EESL) at Penn State. Material samples were collected and exported with authorization from the Ministry of Culture (Permit #1/21 MCC/SG/DRCC.AA) and the local community leaders in Commune de Befandefa. Any opinions, findings, and conclusions or recommendations expressed in this publication are those of the author and do not necessarily reflect the views of the aforementioned agencies.

Chapter 1: Introduction

Climate change is one of the largest threats to human security and prosperity in the modern world, with the consequences increasing in their severity as time progresses. The U.N. Intergovernmental Panel on Climate Change (IPCC) recently released an extensive report on the state of the world and its risk from climate related disasters. Among its many impacts, the climate crisis and subsequent environmental instability are resulting in a major increase of highly vulnerable populations throughout much of the world (IPCC 2022). However, the exact impact of climate and environmental instability on human mobility is a complex issue that has resulted in inconsistencies between different estimates of its actual role in human migratory strategies (Heslin et al. 2019; IPCC 2022). Archaeology can offer an important means by which to understand long-term consequences of the impact of climatic and environmental instability on human settlement and mobility (Altschul et al. 2017, 2020; Kintigh et al. 2014).

Madagascar presents one exceptional case study to address these issues, as the island has a human history of at least 2400 years and exemplifies hypervariable climatic conditions throughout this same period (Dewar and Richard 2007a; Douglass, Hixon, et al. 2019). However, large tracts of the Malagasy landscape require intensive archaeological investigation (Davis et al. 2020). Island archaeology, especially on Madagascar, has largely focused on “first contact” events and subsequent environmental change (e.g., Anderson et al. 2018; Hansford et al. 2018; Mitchell 2019; Vérin et al. 1969; exceptions include Deschamps 1959). Research on Madagascar has revealed that such studies, while important for establishing migration chronologies, do little to advance understanding about post-arrival mobility and settlement patterns (Douglass, Walz, et al. 2019; Douglass and Zinke 2015). The hyper-focus on the “first” or “earliest” inhabitants of the island have resulted in primarily “site-based” archaeological investigations that lack

regional contexts for later periods of human occupation (e.g., Dewar et al. 2013; Gommery et al. 2011; Hansford et al. 2018; Heurtebize and Vérin 1974; Vérin 1971).

While “site-based” studies have provided invaluable information pertaining to the evolution of state formation on Madagascar and chronological data over the past millennium, such work has fallen short when evaluating post-arrival mobility and settlement strategies at regional scales (Douglass and Zinke 2015). By pushing away from “site-based” archaeological research towards the evaluation of the archaeological record as a complex system with multiple scalar contexts, we will be better positioned to evaluate these phenomena and pressing questions surrounding human-environmental dynamics throughout the island’s history. Unlike site-based investigations, a landscape approach permits for exploration into the interconnections between human populations and their surroundings at multiple scales and changes in behavior over time and space (Anschuetz et al. 2001; Green and Petrie 2018).

Additional scales of analysis are particularly important for understanding human-environmental dynamics (An 2012; Davis 2020a; Elsayah et al. 2020; Lansing 2003), and are essential for capturing the wide-range of interconnected variables and scales of interaction at play between human and environmental systems. On Madagascar, where coastal communities are at increased risk from environmental change (Harris 2011; Le Manach et al. 2012), advancing understanding of how humans and environments interact is vital for conservation efforts and environmental policy development.

As such, the purpose of this dissertation is to highlight internal settlement and mobility patterns, their drivers, and long-term impacts, throughout the southwest of Madagascar via a multiproxy landscape-scale analysis. By studying archaeological settlement patterns using a variety of data (e.g., geophysical, geochemical,

archaeological, and environmental) at different scales, we can help uncover links between human mobility and environmental conditions, which in turn can contribute to mitigation planning for extreme climate events today. Environmental change is increasingly affecting modern coastal communities on Madagascar (IDMC 2020, 2021) and understanding these drivers over time can assist in developing contemporary environmental policies.

The Importance of Landscape and Regional Contexts

A crucial epistemological question among archaeologists has been the use of “sites” as analytical units (e.g., Caraher et al. 2006; Dunnell 1992; Dunnell and Dancey 1983; McCoy 2020). Opponents of the “site” concept point to its imprecision (i.e., what exactly constitutes a site?) and its disjointed connection with reality (i.e., sites do not exist, they are merely a classificatory tool). However, the “site” is a long-engrained concept and it can be difficult to look at the archaeological record through different lenses. Nonetheless, alternative archaeological frameworks have sought to diminish the utility of “sites”. Among the most noteworthy are “siteless” surveys (Dunnell and Dancey 1983)—wherein regional surveys constantly re-define units of measurement based on repeated investigation and analysis of clustering patterns; landscape archaeology—where researchers describe the archaeological record as a connected system, rather than individual “sites” (Anschuetz et al. 2001); and even viewing the archaeological record in atemporal terms (Bailey 1981, 2008)—where it is seen as a palimpsest without discrete components like “sites”.

Despite the obvious flaws with defined empiricist classes like “sites”, this concept also runs antithetical to Malagasy ontologies. Specifically, the notion of an archaeological or cultural “site” opposes the Malagasy notion of *Fomba Gasy*, or the view that people and their landscapes are dynamic, interlaced components that “root” people within a particular area (Evers and Seagle 2012). Rather than seeing specific isolated “sites” of cultural significance, it is the landscape, as a whole, that is deeply associated with traditions and

histories. As such, cultural places are not tangible objects that can always be detected and quantified as “sites” of importance. This runs counter to how most archaeological projects are organized. Thus, the adoption of a landscape or atemporal archaeology that moves past the “site” concept will not only improve archaeological research in a theoretical sense, but will also better align with Malagasy ontological systems, thereby improving archaeological interpretations on Madagascar.

Landscape analysis requires interdisciplinary integration, often combining frameworks from geography, anthropology, climatology, and demography, among others, to holistically investigate how people lived within a region over time (e.g., Anschuetz *et al.* 2001; Ingold 1993; Tilley 1994). Landscape archaeology can provide insight about human-environmental dynamics and is well suited to address archaeological questions on Madagascar centered around extinction events, migration, and anthropogenic effects on ecological systems. Globally, archaeological studies of settlement-behavior and its relationship to environmental variables are abundant (see Davis 2020), and yet Madagascar has very few such archaeological studies (exceptions include Wright 2007; Griffin 2009; Parker Pearson *et al.* 2010), especially those pertaining to its earliest human inhabitants (Battistini and Verin 1972; Davis, DiNapoli, and Douglass 2020; Douglass 2017; Douglass *et al.* 2018). This is partly because landscape approaches require geographically expansive datasets, as mentioned earlier, but also stems from the fact that large tracts of Madagascar’s landscape have seen less intense investigation than others, leaving extremely thorough data in some regions, and less so in others.

Landscape studies of ancient Malagasy populations generally focus on time periods after 1000-1100 B.P. when settlements increase in size and number (Parker Pearson *et al.* 2010). Researchers now know that humans were present on Madagascar prior to 1100 B.P., possibly extending back several thousand years (Dewar *et al.* 2013),

although this timeframe is widely debated (e.g., Anderson et al. 2018; Hansford et al. 2018, 2020; Mitchell 2019, 2020). Nonetheless, recent radiocarbon evidence suggests that the earliest recorded communities were likely migrating from areas within Madagascar (Dewar et al. 2013; Douglass, Hixon, et al. 2019; Hansford et al. 2018; Parker Pearson et al. 2010). For these earliest archaeological periods, however, landscape level analysis is lacking.

The Velondriake Marine Protected Area and Collaborative Archaeology

The southwest of Madagascar contains a rich, but highly threatened and vastly unexplored archaeological record. Some of the earliest evidence of human occupation has been found in this region (Douglass, Hixon, et al. 2019; Hansford et al. 2018), and highly variable climatic conditions have been associated with the appearance of widely diverse cultural practices among the people who live here (Douglass 2017; Radimilahy 2011; Yount et al. 2001).

This dissertation project focuses on the region containing and directly surrounding the Velondriake Marine Protected Area (VMPA). The VMPA resides in the southwest coast of Madagascar between the cities of Toliara and Morombe (Figure 1-2). It encompasses a marine and coastal region of approximately 800 km² and is home to over 10,000 people (Harris 2007). Velondriake, which translates roughly as “to live with the sea”, is home to *Vezo* people, fishing communities linked to maritime lifeways (Koechlin 1975; Langley 2006). *Vezo* actually means “to paddle”, which emphasizes their connection with marine environments (Astuti 1995). The Velondriake area is home to extensive coral reef habitats, mangrove forests, seagrass beds, and threatened terrestrial species like baobab trees and spiny forests. The formation of the VMPA was borne out of the Velondriake Association, a group of 23 different villages (initially—the number of members has since grown) with a common goal of preserving and conserving marine resources in this area

(Cripps and Harris 2009). This study centers around the village of Andavadoake, which is one of the largest member villages within the VMPA.



Figure 1-1: Map of the Velondriake Marine Protected Area, Southwest Madagascar.

The archaeology of the VMPA is a recent development, with the first comprehensive investigation of the area starting in 2011 by Douglass (2016). Douglass' work focuses on the excavation of six different areas around the modern village of

Andavadoake, where she describes several open air and rock shelter sites occupied between 3000 B.P. and the present (Douglass 2016, 2017; Douglass et al. 2019). Her work presents a more targeted analysis, however, of contexts dated between 1400 – 100 BP (Douglass et al. 2018). The region appears to have an extensive history of marine resource exploitation by human inhabitants, including resource acquisition in a range of habitats extending from coral reefs, mangroves, and intertidal zones (Davis, DiNapoli, and Douglass 2020; Douglass 2017). As this dissertation project will highlight, the settlement system in this region was shaped by environmental and sociopolitical resources and a closely connected social network of permanent and semipermanent communities (Chapter 4; Chapter 7). This dissertation also aims to acquire a better understanding of the chronology of human occupation of the VMPA using a landscape approach.

Andavadoake is the largest village within the VMPA and serves as the basecamp for the Morombe Archaeological Project (MAP), which is a collaborative community archaeology team established by Kristina Douglass in 2011 (Douglass 2016; Douglass, Morales, et al. 2019). Within this dissertation, I worked closely with the MAP team to develop research questions, plan and execute fieldwork operations, and output the results in the form of presentations, workshops, and publications. The goal of MAP is to develop a fully collaborative archaeology that seeks to include local communities at every stage of the scientific process from project formation through publication (Douglass, Morales, et al. 2019). This dissertation was made possible because of this inclusivity, and everything that follows took place in direct and consistent collaboration with local archaeologists in MAP.

A New Theoretical Approach for Settlement Archaeology

It is common within studies of archaeological settlement patterns to investigate these phenomena as they relate to environmental or ecological variables (see Kowalewski 2008). A multitude of studies framed around human behavioral ecology (HBE) modeling

have demonstrated the importance of environmental resources and ecological variables in human settlement choice (e.g., Coddington and Jones 2013; Hanna and Giovas 2019; Jazwa and Collins-Elliott 2021; Winterhalder et al. 2010). However, all too often, studies that prioritize environmental drivers can overlook social influences on behavior, which in turn can result in an incomplete understanding of demographics related both to settlement choice and the subsequent effects of these actions.

Likewise, for the purposes of modeling settlement distributions, predicting the locations of archaeological deposits, and creating systematic inventories of cultural materials, archaeologists often rely on these environmentally focused frameworks that look primarily at drivers (or “push” and “pull” factors, *sensu* Lee 1966) of settlement distribution. However, it is equally important to understand the long-term effects of settlement on a landscape, and such effects can subsequently be used to predict and prospect for archaeological materials.

In this dissertation, I put forth a multiproxy approach to settlement archaeology that seeks to investigate human settlement strategies from the perspective of feedback-loops and multiple lines of evidence (Figure 1-3). In so doing, this framework aims to balance drivers of settlement and mobility along with their resulting impacts on the involved socioecological systems. Such an approach requires multidisciplinary collaboration as it involves the use of multiple lines of evidence and methodological approaches to investigate different, but interrelated aspects of the archaeological record.

For example, within this dissertation, remote sensing can be used to record important environmental information and geophysical signatures of human activity, which in turn can directly answer questions concerning niche construction and human impact on ecological systems. When paired with spatial statistics, we can utilize remotely sensed

information to assess potential drivers of settlement and mobility, and both of these approaches can subsequently aid in archaeological survey and excavation efforts, as new cultural heritage sites can be identified. Spatial modeling also adds an ability to indirectly assess social factors that affect population distributions and can indicate patterns of social cohesion and dispersion between communities or individuals across a landscape. Archaeological evidence from excavations (e.g., ceramics, charcoal, etc.) can provide additional temporal information that then allows us to take all the aforementioned analyses to another level by tracking changes in these relationships over time. As such, the multiproxy approach presented here allows researchers to understand settlement patterns as a feedback loop between behavioral choice, subsequent (un)anticipated effects, and long-term patterns of ecological transformation. While individual studies and methods can address questions targeting specific facets of this phenomenon, they do not provide a cohesive explanation of the archaeological record.

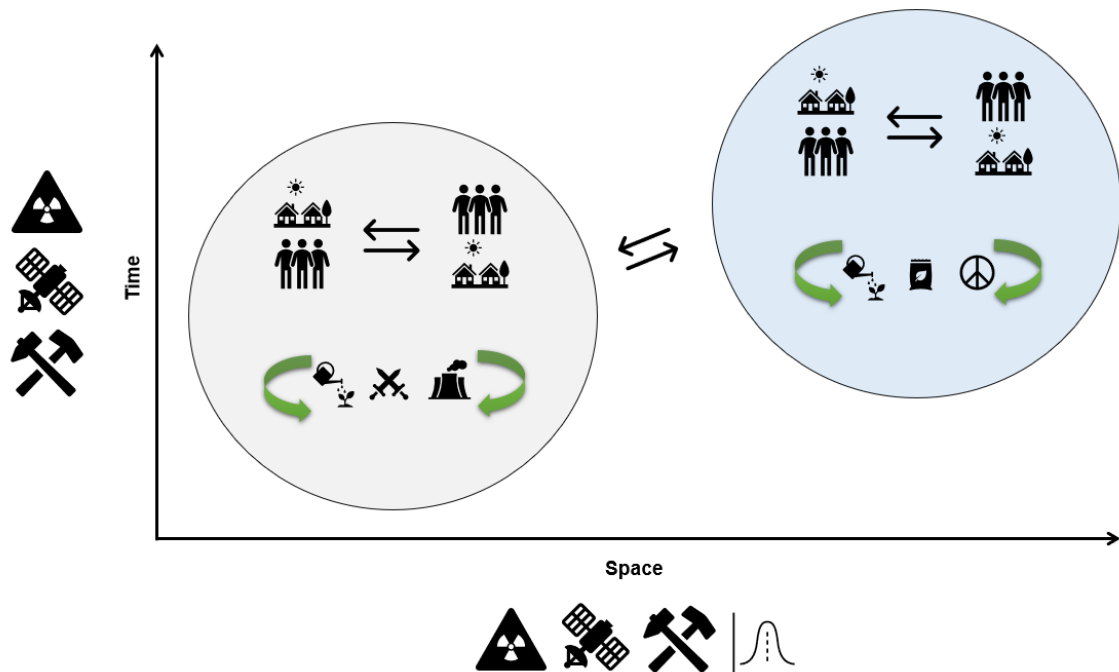


Figure 1-2: Approach to understanding archaeological settlement and mobility patterns used in this dissertation. Grey and Blue circles show two different socioeconomic systems, which each have their own set of socioeconomic feedbacks. The two systems also interact with one another as part of a larger, regional system, the spans a greater amount of geographic space. In addition, these interactions are not static, but also must be observed through a temporal lens that will subsequently change through time. Such an approach requires the integration of multiple lines of evidence provided by a myriad of approaches (indicated by symbols along x and y axis (e.g., geophysical, geochemical, archaeological, etc.).

Research Questions and Hypotheses

Using the approach outlined above, this dissertation seeks to address socioecological dynamics of settlement and mobility patterns among coastal foraging communities in the VMPA. Specifically, this study dissects the problem into four major questions: 1. To what degree was resource distribution correlated with settlement density in Late Holocene SW Madagascar? 2. What role do social ties to place and community defense play in settlement locations? 3. How do social networks shift over time with respect to climatic and sociopolitical events? And 4. Do ecological legacies of landscape modification exist in SW Madagascar and can these niche constructing activities aid in detecting ancient settlement locations and/or provide insight into the extent of anthropogenic activity across the Malagasy landscape? To address these questions, I turn to a suite of geospatial (i.e., spatial statistical modeling, remote sensing, network analysis, machine learning), archaeological (i.e., survey, excavation), and geochemical (i.e., radiocarbon isotope analysis) methods.

Summary/Conclusion

This dissertation develops a conceptual model for multiproxy geospatial landscape analysis. This framework allows for a comprehensive investigation of settlement distributions and their relationship with socioenvironmental conditions and is applied to a case study in the VMPA in southwest Madagascar over the last millennium. The

dissertation itself is comprised of an iterative research approach, and each chapter builds upon the results of the next in order to address this topic from multiple viewpoints and using different data types. Remote sensing data are central to much of this dissertation, and in Chapters 2 and 3, I discuss the latest advances in remote sensing archaeology within African archaeology, in general, and the ethical considerations that are due when using this technology, particularly in cases of culturally sensitive landscapes which are present within Southwest Madagascar. Next, in Chapter's 4 and 5, I outline the results of a set of predictive models rooted in human behavioral ecology (HBE) frameworks developed for locating archaeological deposits throughout the Velondriake study area. These models investigate settlement patterns as a function of environmental resource availability and social cohesion and serve both as prospection tools and means to explain the archaeological settlement patterns present in this area.

In Chapter 6 I present an investigation of legacy ecological effects caused by cultural niche construction in the VMPA by foraging communities over the last millennium. This entails the utilization of high-resolution satellite imagery and machine learning algorithms which enable researchers to identify archaeological deposits based on vegetation and soil properties. This chapter builds upon the prior two chapters by investigating the long-term effects of settlement on the Malagasy landscape and demonstrates the presence of an extensive niche created by mobile foraging and herding communities.

In Chapter 7 I present the results of a network analysis conducted using ceramic sherds recovered from field surveys over the past several years in the VMPA. This chapter provides additional insight into social cohesion and movement of people and ideas throughout the study region that is identified by spatial modeling in Chapter 5. In Chapter 8, I detail the results of the excavations conducted as part of this dissertation project and

discuss settlement chronologies for the VMPA, including a series of 58 new radiocarbon dates from 5 archaeological units located throughout the Velondriake region.

Finally, in Chapter 9, I summarize the most significant findings of this project and chart out the future research trajectories that will build from this dissertation. Together, this research provides a case study for how landscape archaeology focused on settlement patterns is enhanced by close community engagement and a holistic, multiproxy approach that considers settlement studies from a combination of methods that explore behavioral drivers and long-term impacts of human activities through time.

Chapter 2: A Review of Aerial and Spaceborne Remote Sensing in African Archaeology¹

Remote sensing instruments are powerful tools for producing relatively complete records of archaeological settlement patterns and human behavior at the landscape scale. Literature on aerial and spaceborne technologies (e.g., satellites, LiDAR, aerial photographs, etc.) in archaeology has demonstrated that multi- and hyper-spectral satellite sensors and aerial platforms such as LiDAR are particularly useful for tackling issues of survey coverage and site identification (Chase et al. 2012; Lasaponara and Masini 2012; Leisz 2013; Luo et al. 2019; Osicki and Sjogren 2005; Verhoeven 2017). Coupled with machine-learning algorithms, remote sensing offers an effective means to increase survey areas and the discovery of new cultural deposits (Bennett et al. 2014; Davis 2019; Davis, Lipo, et al. 2019; Trier et al. 2019). Specifically, the use of such technology allows researchers to: 1) investigate large geographic scales in a time efficient (and cost effective) manner; 2) access areas which are difficult to physically visit due to geography, lack of infrastructure, and/or political instability; and 3) achieve enhanced visibility for archaeological survey in environments with dense vegetation or otherwise challenging topography (e.g., LiDAR, SAR). The widespread use of such methods would allow Africanist archaeologists to investigate settlement distributional patterns and landscape use in multiple temporal contexts at extraordinary speeds, as case studies from other areas demonstrate (Bennett et al. 2014; Davis, Lipo, et al. 2019; Magnini and Bettineschi 2019).

¹ Davis, Dylan S., and Kristina Douglass. 2020. Aerial and Spaceborne Remote Sensing in African Archaeology: A Review of Current Research and Potential Future Avenues. *African Archaeological Review* 37(1): 9-24. DOI:10.1007/s10437-020-09373-y.

In this paper, we review landscape-scale remote sensing archaeological research conducted throughout the African continent, focusing primarily on the last two decades (Figure 2-1) and how these methods can benefit archaeological research in the face of unprecedented climatic shifts and threats to cultural heritage. Specifically, we look at approaches utilizing aerial and spaceborne remote sensing instruments and avenues of research that are yet to be fully utilized in this region. We offer several explanations for why remote sensing has been slow to break into the mainstream of Africanist archaeology. Then, we present examples from Africanist research that illustrate why these methods are essential for protecting and recording the archaeological record in the face of climate change and human impacts.

On the African continent, aerial and spaceborne remote sensing approaches have been widely applied, largely utilizing black-and-white aerial photographs to study state formation (Denbow 1979; Evers 1975; Gard and Mauny 1961; Jones 1978; Lampl 1968; Maggs 1976; Mason 1968; Mille 1970; Saumagne 1952; Seddon 1968; Wright 2007). Such studies illustrate the great potential for these approaches to expand our understanding of the archaeological record at the landscape scale and a diversity of social, economic and political processes. But again, these applications have been uneven. Studies by Jones (1978), Maggs (1976), Evers (1975), Mason (1968), and others revolutionized archaeological understanding of Iron Age settlement patterns throughout much of southern Africa. Meanwhile, on African islands, like Madagascar, aerial remote sensing has been much more limited in its archaeological applications (Fournier 1973; Mille 1970). Since the advent of commercial satellite imagery, only one study (Clark et al. 1998) has been applied in this region. Such insufficient aerial coverage of African islands have severely limited our understanding of their settlement history.

Neglecting to make use of aerial and spaceborne technologies makes it more likely that African archaeological sites and landscapes will soon be permanently lost. Climate change brings with it threats to archaeological deposits, including coastal erosion and sea-level rise (IPCC 2018; Ministère de l'Environnement, des Eaux, et des Forêts 2006; USAID 2016). Some of the sites most vulnerable to climate change contain the earliest traces of human (and early *Homo*) history (Erlandson 2012), while others represent the center of ancient global trading networks and are actively eroding (Radimilahy and Crossland 2015). Many coastal and island sites in Africa are also important for understanding past human adaptation and resilience in the face of climate and other pressures (Douglass and Cooper 2020; Thompson and Turck 2009; Turck and Thompson 2016). With today's impending climate crisis, it is imperative to learn all that we can from these sites before they are lost.

Further damage occurs from political instability and conflict (Casana and Laugier 2017; Francioni and Lenzerini 2006; Harmanşah 2015; Pollock 2016), and economic inequality (Brodie et al. 2006; Parcak et al. 2016). To address anthropological questions concerning demography, the nature of social and political organization in prehistory, and the ecological entanglements of early populations, systematic archaeological investigations are required (e.g., Stahl 2005; Verhoeven 2017). Remote sensing instruments provide the ability to survey large geographic areas much faster than traditional approaches, as has been demonstrated by many studies throughout the world (Beck et al. 2007; Bescoby 2006; Biagetti et al. 2017; Bini et al. 2018; Borie et al. 2019; Casana 2014; Cerrillo-Cuenca 2017; Davis, Lipo, et al. 2019; De Laet et al. 2007; Evans et al. 2013; Freeland et al. 2016; Guyot et al. 2018; Harrower et al. 2013; Jahjah et al. 2007; Johnson and Ouimet 2014; Klehm et al. 2019; Krasinski et al. 2016; Lasaponara et al. 2014; Lipo and Hunt 2005; Meyer et al. 2019; Schuetter et al. 2013; Thabeng et al.

2019; Zanni and Rosa 2019). This ability is vital in the face of accelerated rates of cultural heritage loss, which threatens African communities and livelihoods (Mire 2017).

Remote sensing has rapidly advanced over the past several decades, and the application of some of the more recent innovations in image processing appear underutilized within African contexts. We argue that these latest trends in remote sensing can offer a cost-effective solution for addressing the issue of systematic broadscale survey in Africa by reducing the amount of time required to investigate landscapes, thereby improving our overall understanding of landscape level phenomena throughout the region's history.

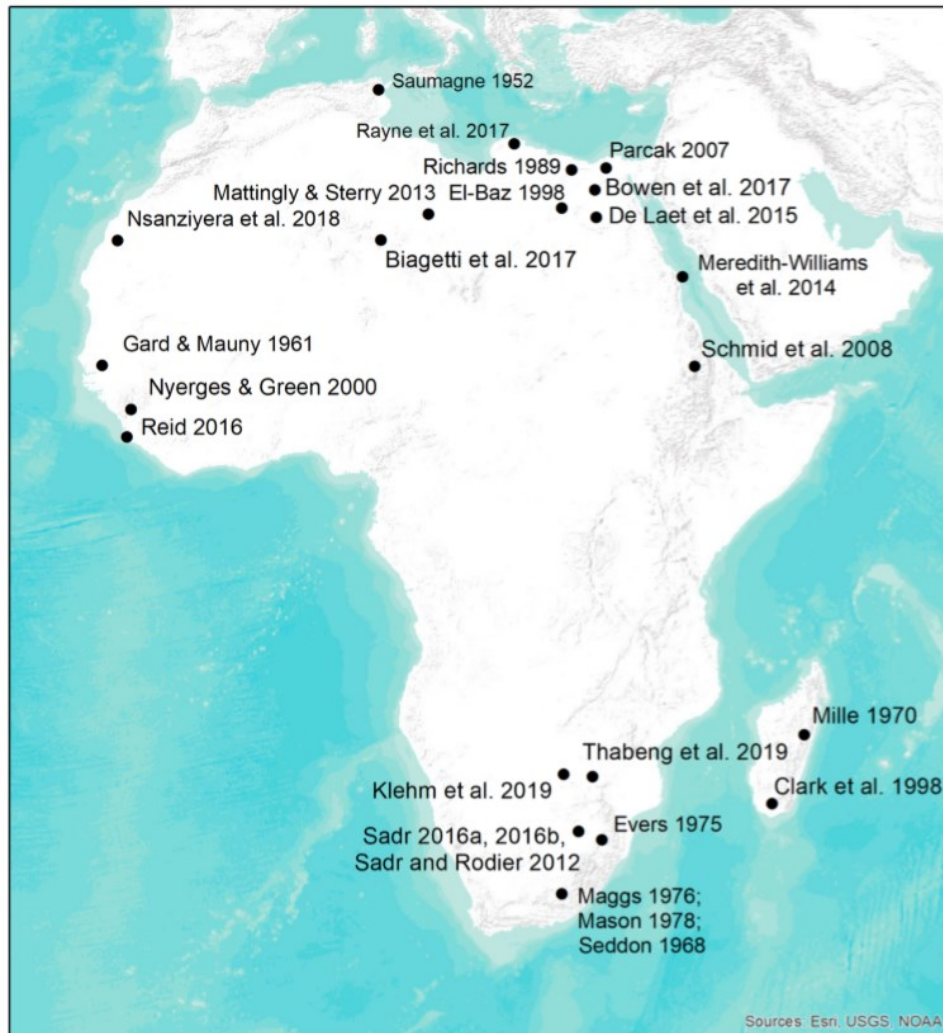


Figure 2-1: Map of remote sensing case studies discussed in the text. It provides the locations of many recent studies – and several older ones – that have demonstrated the potential of remote sensing research and the benefits of some more recent analysis techniques.

Limitations of Recent Remote Sensing Archaeology in Africa

The field of remote sensing and image analysis is constantly expanding, with an explosion of new processing techniques emerging over the past few decades. With such advances come costs, however, and oftentimes these costs prevent their utilization. For example, sensors such as LiDAR permit for the identification of topographic anomalies and have been successfully applied to archaeological prospection around the world (Cerrillo-Cuenca 2017; Davis, Lipo, et al. 2019; Evans et al. 2013; Guyot et al. 2018; Lasaponara and Masini 2013; Trier et al. 2019). However, such technologies are infrequently used for archaeology in Africa (one exception being (Sadr 2016b)) and elsewhere because the cost of LiDAR ranges from the tens-to-hundreds-of-thousands of dollars and is not affordable for most researchers. Commercial satellite imagery while less expensive (~\$20+ per km²), is still out of the financial reach of some research teams. Thus, while LiDAR and very-high-resolution satellite imagery have been used for archaeological research in other parts of the world, such applications require extensive budgets, and funding for African archaeological research is sometimes limited (Clark 1994; Robertshaw 2012). Other sensors and datasets, however, are available for free (e.g., Landsat, Sentinel-1 and 2) and provide similar capabilities.

In addition to new sensors and technologies, there have been advances in image processing methods, which have not yet been widely disseminated through the Africanist archaeology community. Specifically, the emergence of object-based image analysis (OBIA) over the past 15-20 years (Blaschke 2010) has seen major improvements in accuracy and identification capabilities for archaeological objects (see Davis 2019 for a

review; also see Magnini and Bettineschi 2019). Such techniques have been successfully applied to systematically parse through datasets for archaeological information and produce results with higher accuracy than traditional pixel-based approaches (Sevara et al. 2016). Automated methods – especially OBIA – help to save time and money on surveying (Davis, Sanger, et al. 2019), and this is particularly important in regions where sites are deteriorating due to anthropogenic and other forces.

In addition to OBIA, many advanced classification algorithms – such as random forest, support vector machine, and neural networks – are only just beginning to be utilized by Africanist archaeologists. Such approaches have produced highly accurate results in northern and southern Africa (Biagetti et al. 2017; Thabeng et al. 2019). The recent (and otherwise limited) introduction of such remote sensing techniques in Africanist archaeology may be partially explained by training opportunities for Africanist scholars as well as the abundance of research conducted by scholars outside of Africa.

Archaeological remote sensing training opportunities are offered at a myriad of African universities, museums and research institutions, with several courses offered by Nigerian, South African, and Ethiopian institutions. For example, Obafemi Awolowo University in Nigeria offers a number of training opportunities in remote sensing, and even has a Center for Remote Sensing and GIS (RECTAS). Most opportunities for remote sensing training within Africa appear to be not directly affiliated with archaeology, however. Exceptions include Addis Ababa University in Ethiopia, where the Archaeology and Heritage Management Department offers cartography courses, and the University of the Witwatersrand, which offers remote sensing courses in the Department of Geography, Archaeology, and Environmental Studies. The results of several workshops and occasional short courses in remote sensing have resulted in training manuals (Wright 2017). Additionally, the African Association of Remote Sensing of the Environment

(AARSE) holds a biannual pan-African conference at which new remote sensing methods are shared amongst a community of remote sensing experts. It would be useful for Africanist archaeology organizations to establish linkages with AARSE and encourage archaeologists to attend the AARSE conference.

While limited training within Africa cannot alone explain the dearth of archaeological remote sensing studies in the region, it is a limiting factor for Africanist scholars within Africa to utilize such methods. Because much of the funding for archaeology in Africa comes from outside the continent (Ellison et al. 1996; MacEachern 2010; Robertshaw 2012), and much of the literature pertaining to remote sensing is conducted by scholars outside of Africa, a limit in training opportunities for local archaeologists is certainly a contributing factor for the low number of recent studies when compared to other regions around the world (e.g., Europe). Robertshaw (2012: 98) also emphasizes the structural inequality in funding for African archaeology: “while the number of indigenous African archaeologists has been increasing across the continent in recent years, their access to research funds and logistical support is miniscule compared with that of their overseas colleagues” (also see Arazi 2011; MacEachern 2010).

Another possible reason for a lack of remote sensing stems from the mindset that archaeology requires the highest resolution datasets (which are usually costly to acquire). Most often, remote sensing research in archaeology is focused on directly identifying archaeological deposits in image data, and this requires high spatial resolution (~1m or less) and spectral resolution (i.e., multispectral, hyperspectral capabilities) (Beck et al. 2007). However, there is also extensive work on *indirect* identification of archaeological deposits, usually using medium-to-course resolution images (Agapiou et al. 2014; Bennett et al. 2012; Davis, Andriankaja, et al. 2020; Kirk et al. 2016). Direct investigation utilizes high resolution data in which archaeological deposits can be visualized and identified. In

contrast, indirect investigation – whereby archaeological features are not directly visible – relies on proxies to estimate the likelihood of sites being present in a given area (e.g., Kirk et al. 2016).

Where funding and resources are limited, *indirect* methods are the best option for increasing remote sensing studies in a region. Using freely available satellite imagery (e.g., Landsat, Sentinel-1, Sentinel-2), researchers can conduct analyses of vegetation patterns to identify likely cultural deposits on large (>50km²) geographic scales. Furthermore, the use of explicit theory (e.g., human behavioral ecology models [Charnov 1976; Fretwell and Lucas 1969; MacArthur and Pianka 1966]) can be used in conjunction with remote sensing to improve such predictive modeling approaches (Davis and Douglass 2020; Verhagen and Whitley 2012).

Given the abundance of freely available remote sensing datasets available with coverage for the entirety of the African continent, as well as many open-source softwares that can be used to process this imagery (see Table 2-1), it is via an *indirect* approach that remote sensing can be most easily and cost effectively integrated into archaeological research procedures in this region.

Table 2-1: List of open-source/freely available data repositories and software platforms for remote sensing analysis. While not an exhaustive list, the table provides some well-known and other less known platforms which have strong capabilities and datasets for African regions.

Resource Name	Operating Systems	Notes/Capabilities	Reference
QGIS (formerly known as Quantum GIS)	<ul style="list-style-type: none"> • Windows • MacOS • Linux 	<ul style="list-style-type: none"> • Has an extensive number of plugin software, some of which (e.g., GRASS, Orfeo) have significant remote sensing analysis capabilities, 	(QGIS Development Team 2018)

SAGA	<ul style="list-style-type: none"> • Windows • Linux • FreeBSD • MacOS 	<ul style="list-style-type: none"> • Contains many environmental modeling tools and visualization algorithms. 	(Conrad et al. 2015)
Google Earth Engine	<ul style="list-style-type: none"> • Internet based. Any operating system will run with internet connection 	<ul style="list-style-type: none"> · Repository of freely accessible image datasets · Cloud-based computer processing allows for extremely fast analysis on large datasets · Ability to conduct automated analysis algorithms 	(Gorelick et al. 2017)
R	<ul style="list-style-type: none"> • Windows • MacOS • Linux • Solaris OS 	<ul style="list-style-type: none"> • Coding platform with many remote sensing packages (e.g., raster[Hijmans 2019], RStoolbox [Lautner et al. 2019]) 	(R Core Team 2020)
Earth Explorer	<ul style="list-style-type: none"> • Internet based. Any operating system with internet can access 	<ul style="list-style-type: none"> • Remote sensing data repository for the United States Geological Service (USGS). Contains datasets ranging from satellite data to LiDAR and aerial imagery around the globe. 	https://earthexplorer.usgs.gov/
Copernicus	<ul style="list-style-type: none"> • Internet based. Any operating system with internet can access 	<ul style="list-style-type: none"> • Remote sensing data repository for the European Space Agency satellites (e.g., Sentinel 1 and 2). 	https://scihub.copernicus.eu/

While some of these open-source platforms are well known by archaeologists both within and outside of Africa (e.g., Google Earth), others are less recognized. For example, Google Earth Engine (GEE; Gorelick et al. 2017) is a free platform for educational,

research, and nonprofit groups. GEE can be used to access remote sensing imagery and analyze these data with complex image processing algorithms that otherwise require an extensive coding background or potentially costly commercial software. Researchers have demonstrated that Google Earth Engine (GEE) is adept for archaeological prospection, specifically for digitizing archaeological feature boundaries and automating feature detection (Liss et al. 2018). A recent review of GEE indicates that while its use among remote sensing specialists is on the rise, African research has not engaged with this platform in a major way (Luo et al. 2018). Considering the capabilities of GEE – both as a data repository and platform for simple-to-complex analyses – and the fact that it is free to use, there is great potential for Africanist archaeologists to integrate it into their toolkits.

Trends in Remote Sensing Research in African Archaeology

Remote sensing has a long history in archaeology (Capper 1907; Lindbergh 1929), but the applications of this technology in Africa are more recent and scarcer than in other areas. In a recent special issue of *Geosciences* published on archaeological remote sensing, Africa was only represented by two of 14 articles (Nsanziyera et al. 2018; Oduntan 2019), of which only one (Nsanziyera et al. 2018) was a case study while the other (Oduntan 2019) was a discussion of legal statutes relating to geospatial research in the region. This example is not an outlier, but represents a trend in recent remote sensing archaeology, where many of the latest developments are focused on other regions, primarily in the northern hemisphere (Davis 2019). Africa represents over 30 million km² and, while numerous studies have employed landscape level survey since the start of the 21st century, a vast amount of territory remains incompletely investigated (Figure 2-1). In Madagascar, for example, the largest African island consisting of ~500,000 km², less than 1% of the island has been systematically investigated using remote sensing techniques.

To ensure at-risk archaeological deposits are recorded in a systematic fashion, the latest advances in image processing and automated analysis methods are imperative.

Beginning in the 1950s, Africanist archaeologists have taken advantage of aerial photographs and identified thousands of archaeological sites from various time periods across the continent (e.g., Denbow 1979; Evers 1975; Jones 1978; Maggs 1976; Mason 1968; Saumagne 1952; Seddon 1968). Saumagne (1952) conducted an aerial survey of archaeological sites in Tunisia. Almost a decade later, Gard and Mauney (1961) used aerial photographs to identify monumental earthen mounds in modern-day Senegal. Following these studies, aerial vantage points were utilized by archaeologists to identify a range of different features.

Denbow (1979), for example, identified hundreds of Iron Age sites in Botswana on the basis of vegetative patterns observed in aerial photographs. Denbow's work led to a better understanding of hilltop settlement dynamics and their connection with surrounding landscapes. This landscape-level work has also allowed us to test theories about the interactions between different communities of foragers, farmers, and herders in the Bosutswe region. Recent remote sensing studies continue to build on this earlier work but have begun to pay closer attention to subtler and less well-studied components of the archaeological record (e.g., Klehm et al. 2019).

Similarly, work conducted by Maggs (1976) was foundational for Iron Age settlement studies in southern Africa (e.g., Evers 1975; Jones 1978). The information obtained from these aerial surveys allowed for the development of site typologies and the analysis of specific environmental and social contexts that affected settlement choice (Huffman 1986).

On Madagascar, Mille (1970) used aerial photographs to identify and record approximately 16,000 fortified sites in an area encompassing 47,000 km² in the central highlands (Figure 2-1). These photographs were systematically investigated to create settlement density maps which were then statistically tested to classify sites into different settlement types (Fournier 1973). Mille's (1970) study transformed archaeologists' understanding of settlement histories of the 15th-19th centuries by unveiling extensive monumental constructions throughout central Madagascar which were previously unrecorded. With this new information, Mille (1970) was able to calculate settlement densities and find connections between political transformation and settlement patterns (Fournier 1973).

While aerial photographs can provide helpful information, the interpretation of (oftentimes) black-and-white images with little-to-no spectral data is inherently limiting. Many early studies that relied on aerial photography identified the largest archaeological sites, while overlooking or under-evaluating more subtle cultural deposits (see Klehm et al. 2019:69-70 for a brief discussion). The identification of cultural deposits via aerial photographs has resulted in the identification of many large structures (e.g., Denbow 1979; Maggs 1978; Mille 1970), but very little in the way of smaller domestic structures. This stems from a combination of resolution issues, lack of multispectral bands, and the limits of human analysts in identifying certain patterns and textures in photographs. The prospection of subtle features of the archaeological record has been enhanced by advances in computer learning and improvements in sensor resolution.

Following the explosion of satellite data in the 1980s and 1990s, remote sensing applications in African archaeology began integrating multispectral sensors into analysis (e.g., Allan and Richards 1983; Clark et al. 1998; Lightfoot and Miller 1996; Richards 1989; Williams and Faure 1980). Much of this work has emerged in the last two decades using

both medium- (e.g., Sentinel 1 and 2, Landsat) and high-resolution (Worldview 2 and 3; Ikonos, etc.) sensors (Clark et al. 1998; Klehm et al. 2019; Meredith-Williams et al. 2014; Nsanziyera et al. 2018; Nyerges and Green 2000; Reid 2016; Schmid et al. 2008). The application of multispectral satellites has permitted archaeologists to use subtle differences in the electromagnetic spectrum to identify disturbed landscapes and anthropogenic activities.

For example, Clark et al. (1998) illustrate the benefits of multispectral and synthetic-aperture-radar (SAR) data - an active sensor that can detect moisture content and textural properties of ground surfaces (Chen et al. 2017) – for understanding Madagascar’s settlement history. The researchers focus on several hundred square kilometers of area (Figure 2-1) and shed light on the development of land-use throughout the region as well as insight into where the oldest archaeological contexts are located. For example, there have been many recent archaeological discoveries that place cultural contexts in association with ancient megafauna species, including elephant birds (*ratite genera Aepyornis and Mullerornis*) (Douglass 2016; Parker Pearson et al. 2010; Radimilahy 2011). In addition, Clark et al. (1998) show how archaeological deposits often produce discernable patterns that are distinct from modern day landscape boundaries. Thus, identification of temporally older cultural features can be made on the basis of their placement in the modern landscape. By so doing, remote sensing provides archaeologists with the capability of monitoring known sites as well as locating new ones.

These advances are not limited to Africanist research and have a long tradition in remote sensing archaeology around the world (Bini et al. 2018; Kirk et al. 2016; Lasaponara et al. 2014; Luo et al. 2019; Opitz and Herrmann 2018; Parcak 2009; Traviglia and Cottica 2011; Verhoeven and Sevara 2016). Multispectral sensors have also been used to develop vegetative indices that show the relative health of vegetation and can be

used as a proxy of archaeological activity (see Bennett et al. 2012; Klehm et al. 2019; Thabeng et al. 2019), and such indices have proven useful in the detection of archaeological deposits dating to different periods throughout Africa (Biagetti et al. 2017; Klehm et al. 2019; Reid 2016; Sadr 2016b; Schmid et al. 2008; Thabeng et al. 2019). Additionally, they can be used to monitor the impacts of human activities on cultural materials (Reid 2016; R  ther 2002).

Monitoring anthropogenic impacts on cultural heritage represents one major trend of remote sensing archaeology in Africa (Casana and Laugier 2017; Lasaponara and Masini 2018; Parcak 2007, 2009; Parcak et al. 2016), and is at the forefront of major projects involving the continent (e.g., EAMENA, <http://eamena.arch.ox.ac.uk/>). The Endangered Archaeology in the Middle East and North Africa (EAMENA) project (Bewley et al. 2016) has created an open-access digital database of aerial images and archaeological data with the goal of rapidly evaluating the status of cultural heritage preservation throughout the Middle East and North African region. The use of these data has resulted in numerous publications on the importance of aerial survey for cultural heritage management (e.g., Fradley and Sheldrick 2017; Hobson 2019; Rayne et al. 2017; Zerbini and Fradley 2018). Additionally, programs like UNITAR's Operational Satellite Applications Programme (UNOSAT) have resulted in thorough damage assessments to cultural heritage in Syria (UNOSAT 2014).

A second trend in Africanist archaeological remote sensing is the use of vegetative indices for the identification of archaeological materials. For example, Biagetti et al. 2017 studied early Holocene settlements in the Sahara, Schmid et al. 2008 investigated soil properties in anthropogenic environments in Ethiopia, and Reid 2016 investigated settlement patterns in Sierra Leone (Figure 2-1). In these projects, scholars calculated relative vegetation health and growth and matched these trends with areas of known

anthropogenic activity. These signatures were then used as a basis for understanding the ecological effects of human land-use (e.g., Nyerges and Green 2000) and allowed for both the indirect prospection of archaeological materials via geochemical signatures and the monitoring of cultural materials at risk of damage or destruction. Such approaches are particularly useful because they can provide important information using both high- and medium-resolution datasets (Biagetti et al. 2017). In contrast, direct detection of sites via spectral or geometric properties requires higher resolution data (see Beck et al. 2007).

A third trend in African remote sensing archaeology is the focus on mapping geomorphological properties of landscapes and their relationship to ancient settlement patterns. Such studies have successfully identified both archaeological sites and geomorphological features, such as paleolakes in the Sahara (e.g., Biagetti et al. 2017; also see El-Baz 1998) and ancient stone quarries in Egypt (De Laet et al. 2015). This approach is important, especially for studying human-environmental relationships, as it reveals interconnections between natural resources and human settlement patterns. For example, Clark et al. (1998) illustrate how specific environmental features (i.e., paleodunes) can act as markers of archaeological activity, and recent work confirms this conclusion by incorporating paleodunes among other features into a predictive model (Davis, Andriankaja, et al. 2020). Geomorphological studies in North Africa have also provided insight into where ancient rivers were located, which holds potential for identifying archaeological sites (El-Baz 1998).

Remote sensing datasets are increasingly analyzed via machine learning classification procedures, and this represents a fourth emerging trend in remote sensing archaeology in Africa, as well as globally. Semi-automated analysis techniques involve the use of statistical classifiers, machine learning algorithms, and/or specialized image processing software to aid in analyzing remote sensing datasets with greater accuracy

and speed. Such methods have been applied increasingly during the past few decades (Bennett et al. 2014; Davis 2019; Lambers 2018; Traviglia and Torsello 2017), including in Africa (Klehm et al. 2019; Reid 2016; Schmid et al. 2008; Thabeng et al. 2019). In the past year, the number of remote sensing studies utilizing automated methods in Africa has increased (e.g., Davis et al. 2020; Klehm et al. 2019; Thabeng et al. 2019), and this trend applies to global archaeology as well (Davis, Lipo, et al. 2019; Davis, Sanger, et al. 2019; Meyer et al. 2019; Trier et al. 2019; Verschoof-van der Vaart and Lambers 2019). In some instances, researchers are using automated methods solely for landscape classification, and the identification of cultural deposits remains a manual task for analysts (e.g., Biagetti et al. 2017). More recently, however, archaeological studies have utilized machine learning algorithms to directly identify archaeological materials.

Automated analysis methods have been implemented in Africa using high-resolution multispectral Worldview-2 imagery. Thabeng et al. (2019) create training data to conduct random-forest and support vector machine classifications to distinguish between anthropogenic and non-anthropogenic land-types throughout southern Africa since 900 AD. Their random forest classification uses an iterative predictive modeling approach to select ideal classes for datasets on the basis of popular consensus among the different nodes (Pal 2005). Support vector machine classification then identifies optimal separations between classes and can produce highly accurate results, even with small training data sets (Mountrakis et al. 2011). Advanced classification algorithms can thus help to automate the prospection of archaeological sites on the basis of spectral characteristics with a high rate of accuracy (>95%). There are some issues of misclassification, however, which can be resolved using object-based image analysis (OBIA) classification methods (Thabeng et al. 2019).

Another recent application of automated remote sensing is Klehm et al. (2019), who use an unsupervised classification algorithm – wherein a computer divides an image into classes without the input of a human analyst – to identify spectral signatures associated with cultural deposits in Botswana. Klehm and colleagues' (2019) draw attention to hinterland areas with less dominant archaeological features, as the focus of archaeological research in this area was historically on clusters of hilltop settlements (e.g., Denbow 1979). They identify and field test 10 new archaeological sites, of which 8 were confirmed to be Iron Age deposits (Klehm et al. 2019). Klehm et al. (2019) demonstrate the benefits of automated survey procedures, and the role that these methods can play in improving predictive modeling of archaeological site locations in areas that suffer from lack of funding and survey capabilities. As such, automated remote sensing surveys are vital for increasing our understanding of the archaeological record in areas where survey is difficult or otherwise impeded.

While (semi)automated analysis methods have advantages in terms of processing speed and identification capabilities, programming automated procedures requires training, trial and error, and time, as the processes are often quite complicated and software are not always user friendly. There are, however, many online forums and tutorials that can aid researchers in performing specific kinds of tasks (a simple search in YouTube will lead to hundreds of video tutorials using both commercial and open-source software). It should also be mentioned that there are currently no “fully-automated” archaeological remote sensing methods: every remote sensing analysis requires validation of results, usually by ground visits or other assessments of accuracy. As such, all automated procedures discussed, here and elsewhere, are truly “semi-automated” procedures.

OBIA represents a recent advancement in automated detection in archaeology (ca. mid-2000s; see (Davis 2019)). Simply, OBIA is an image-processing technique that segments an image into discrete components on the basis of one or more geometric or textural characteristics. It has been demonstrated that such methods are more accurate than traditional “pixel-based” image analysis methods (see Sevara et al. 2016) and can be used for different scales of analysis ranging from microscopic to global-scale imagery (Magnini and Bettineschi 2019). OBIA has since been followed by neural network analysis and other machine learning techniques (Verschoof-van der Vaart and Lambers 2019). Despite the improvements in the accuracy and reliability of automated detection using OBIA, archaeologists are yet to apply OBIA within African archaeology (Davis 2019a), in part due to limited training opportunities (see above) and costs often associated with such processing methods. Use of OBIA can also assist in distinguishing between anthropogenic and non-anthropogenic features (Davis, Lipo, et al. 2019; Lambers et al. 2019; Thabeng et al. 2019).

While automated methods are gaining popularity, plenty of work is still conducted using manual analysis (Mattingly and Sterry 2013; Rayne et al. 2017; Sadr 2016a, 2016b). For many researchers, manual analysis can be particularly useful, especially with open-source datasets like Google Earth. The use of manual analysis methods (including ground-testing identified results) is always a necessary component of remote sensing analysis, but complementing these with automated approaches helps to reduce biases and inconsistencies in purely manual results (Bennett et al. 2014; Davis 2019a; Verhoeven 2017; also see for example Sadr 2016b). While automated analyses introduce their own sets of assumptions and limitations, these biases are explicit and largely reproducible. Manual analysis, however, contain largely implicit biases on the part of the analyst and can introduce confounding assumptions in the analysis of remote sensing data. Part of the

slow introduction of automated methods relates to cost, as such software can be exceedingly expensive. Processing capabilities of platforms like Google Earth Engine (Gorelick et al. 2017), however, offer free access to a variety of automated image processing algorithms, as well as the ability to code specifically designed processes for those with coding backgrounds (see Table 2-1).

Future Directions for Remote Sensing in African Archaeology

Increased integration of remote sensing approaches in African archaeology will provide many avenues for future exploration and discovery. The first step is to expand remote sensing surveys into areas where such methods are largely absent and where cultural heritage is at increased risk (e.g., climate change, political instability, etc.). This large-scale effort can be accomplished through a combination of direct and indirect investigations.

Indirect investigations face challenges, however, and require innovative integrations of remote sensing methods with explicit theories and models designed to explain cultural phenomena. Such frameworks are central to disciplines such as anthropology, geography, and history. Currently, one of the fundamental limitations of most archaeological remote sensing studies is their implementation *sans* anthropological theory – with anthropological referring to frameworks mentioned previously (Thompson et al. 2011). In most remote sensing investigations, identification of patterns or objects in datasets is most commonly conducted using methods and theories exclusively from geosciences and physics.

For example, many researchers have used vegetative indices to predict the locations of cultural deposits (e.g., Biagetti et al. 2017; Kirk et al. 2016; Lasaponara and Masini 2007; Schmid et al. 2008) but most of these studies do not incorporate explicit

theoretical models – e.g., ethnography, human behavioral ecology, niche construction, etc. – when building indexes of archaeological activity. While these approaches are useful for identifying archaeological sites, they can be limiting in addressing more complex archaeological questions. For this reason, remote sensing archaeology is often published as individual case studies (Calleja et al. 2018; Davis, Sanger, et al. 2019; Lasaponara and Masini 2007; Traviglia and Cottica 2011) that demonstrate the usefulness of specific approaches but are never developed to address questions of broad anthropological significance.

Much of the recent literature employing new analytical methods for remote sensing are purely experimental, and thus are interested solely in developing methods that can be more widely applied by future work. This is inherently useful and should be encouraged. Nonetheless, some researchers have begun incorporating the results of such remote sensing analyses into broader anthropological syntheses, and this should become commonplace in future research (Borie et al. 2019; Cerrillo-Cuenca and Bueno-Ramírez 2019; Freeland et al. 2016; Inomata et al. 2018; Rutkiewicz et al. 2019).

Because of the disconnect between remote sensing applications and anthropological theory, coarser-resolution imagery is often ignored or avoided by archaeologists because they cannot directly identify deposits, save those that are extraordinarily large (such as fortifications, walls, and roadways) (Beck et al. 2007; Zanni and Rosa 2019). However, there is an abundance of freely downloadable data that is available for nearly every inch of the globe, and despite its lower resolution (~10-30m or greater), such datasets can be extremely beneficial for archaeological analyses (Agapiou et al. 2014; Borie et al. 2019; Breeze et al. 2015; Kirk et al. 2016; Zanni and Rosa 2019).

A recent study by Nsanziyera et al. (2018) makes use of anthropological variables in conjunction with geoscience frameworks and freely available remote sensing datasets to predict the locations of archaeological sites in a 1000 km² area in Morocco (Figure 2-1). By incorporating anthropological, as well as environmental variables into their model, the authors achieve ~93% accuracy, thereby demonstrating the utility of theoretically driven analyses and freely available datasets. Another recent study by Davis and colleagues (2020) developed a predictive remote sensing algorithm using freely available Sentinel-2 imagery predicated on theoretical insights from human behavioral ecology. The method successfully predicted the location of both known and previously unrecorded deposits with an accuracy of over 95%. Africanist archaeologists are well-positioned to lead the way on the integration of anthropological models and theories into applications of remote sensing, given the long tradition of theorizing population movements, the emergence of complex social, political and economic forms, regional interaction and other landscape-scale behaviors (Anquandah 1987; Ashley et al. 2016; Breunig et al. 1996; Harlan and Stemler 2011; Stahl 1985; Wynne-Jones and Fleisher 2015).

With the acquisition of remote sensing datasets at higher spatial and spectral resolutions, it is possible to directly identify archaeological deposits, rather than assign general probabilities of where these features are most likely to be located (Calleja et al. 2018; Davis, Sanger, et al. 2019; De Laet et al. 2007; Klehm et al. 2019; LaRocque et al. 2019; Lasaponara and Masini 2007; Thabeng et al. 2019; Traviglia and Torsello 2017; Trier et al. 2009). While future work should attempt to acquire and analyze high-resolution imagery (e.g., IKONOS, SPOT, Worldview, etc.), the immediate priority should be to develop robust theoretical models that can be tested using freely available imagery. This will allow the greatest number of archaeologists – regardless of financial capabilities – to begin utilizing remote sensing technologies.

In addition, future work should seek to analyze satellite imagery using a mix of automated and manual procedures. This will permit researchers to: a) eliminate observer biases that are often abundant in purely manual evaluations of remote sensing data; and b) systematically investigate entire regions in short spans of time. Automated methods, such as OBIA, can also improve our understanding of site dynamics, as these approaches can classify feature shape, size, and other morphometric properties (Davis, Sanger, et al. 2019).

Conclusions

This paper has reviewed the application of aerial and spaceborne remote sensing methods for landscape analysis in African archaeology. These techniques offer great potential to increase our knowledge of the human past and help to record and protect cultural heritage that is at risk from anthropogenic and natural forces. While Africanist archaeology has a long history of aerial surveys, the most recent advances in aerial and spaceborne technology have been slow to break into research practices in the region. With an increasingly threatened archaeological record, methods to quickly and accurately record this information are essential.

Climate-related risks are increasing rapidly (IPCC 2021) and much of the African coast is in danger of sea level rise and erosion. Equally problematic for archaeology in other regions of Africa are anthropogenic forces such as urban development and looting activity. In the case of looting, in particular, researchers have demonstrated the power of remote sensing technologies to identify cultural materials under threat (Casana and Laugier 2017; Lasaponara and Masini 2018; Lauricella et al. 2017; Parcak et al. 2016; UNOSAT 2014; Xiao et al. 2018). It is therefore necessary to increase the rate at which researchers document the archaeological record, as many African archaeological deposits are rapidly disappearing (Erlandson 2012; Parker Pearson et al. 2010).

Remote sensing can also aid in creating more robust archaeological datasets which can form the basis of large-scale landscape level studies (Davis, Sanger, et al. 2019; Freeland et al. 2016; Inomata et al. 2018; Menze and Ur 2012) and improve the speed and accuracy of mapping archaeological deposits (Hesse 2010). The speed and accuracy attainable through remote sensing survey methods are essential for future archaeological research, as datasets continue to expand.

Ultimately, the integration of remote sensing into the mainstream of Africanist archaeology is underway, and as knowledge of cost-effective datasets and processing software increases among Africanists, research using these methods should increase substantially. We emphasize many such platforms above and hope that this article assists researchers in accessing useful analytical tools. However, it is also essential that training in remote sensing techniques become a featured component of archaeology programs throughout Africa and Africanist departments more broadly. Rigorous training is especially critical for the use of techniques involving machine learning and automated analysis.

Scholars in Africa have long made important contributions to the study of landscape change, settlement histories, and spatial analysis. By incorporating remote sensing datasets into future studies, Africanist contributions will be enhanced with more complete datasets and greater geographic coverage of the diversity of Africa's human past.

Chapter 3: The aerial panopticon and the ethics of archaeological remote sensing in sacred cultural spaces²

Within archaeological remote sensing, the ethics of aerial photography are often overlooked, especially when areas of interest involve local, Indigenous, and descendant (LID) communities. While surveillance has been highlighted within the context of aerial and spaceborne remote sensing archaeology (Myers 2010), the literature on this topic is scarce. The ethical quandary surrounding surveillance parallels dilemmas of “who controls the past” (Colwell 2016), specifically in terms of who is permitted to “collect, retain, and use” large-scale datasets derived from aerial and spaceborne sensors (Cohen et al. 2020). Image data, in particular, has reinforced colonialist agendas and has had severely negative consequences in many instances for LID groups around the world (Gordon 1997; Hartmann et al. 1999; Ranger 2001). With the creation of larger remote sensing datasets with extremely fine spatio-temporal resolutions and virtually unlimited spatial coverage, issues of power and surveillance must be confronted head-on to ensure that future research is equitable and avoids repeating the many injustices of colonial era research.

A primary issue to address is the epistemological dissonance between remotely sensed and other classes of data (see Millican 2012; Thomas 1995, 2008). Knowledge produced by remote sensing instruments is often viewed as fundamentally different from other sources of archaeological and anthropological data, such as ethnohistoric information, because they are collected from the sky and are thus assumed to be disconnected from and less impactful to communities on the ground (see Hacıgüzeller

² Davis, D. S., Buffa, D., Rasolondrainy, T., Creswell, E., Anyanwu, C., Ibirogba, A., Randolph, C., Ouarghidi, A., Phelps, L. N., Lahiniriko, F., Chrisostome, Z. M., Manahira, G., & Douglass, K. (2021). The aerial panopticon and the ethics of archaeological remote sensing sacred cultural spaces. *Archaeological Prospection*, 28(3), 303–318. <https://doi.org/10.1002/ARP.1819>

2012). This creates a disconnect between local community views of space and place and the viewpoint of the aerial surveyor (Ingold 1993; Mark and Turk 2003; Rennell 2012; Thomas 1993) and serves to deny sovereignty of LID communities over the acquisition and use of remotely sensed data. The disparity in the treatment of different classes of information augments an already uneven power structure between archaeologists and LID communities. This power dynamic is critically dependent upon LID representation in scientific research, and a collaborative approach can help balance existing power structures by providing more sovereignty to LID communities.

In combination with other classes of data, remote sensing can be used to enhance archaeological and historical interpretation. For example, Wadsworth (2020) underscores how different techniques can create complementary narratives about landscapes and their history, and that researchers can combine different data sources (like remote sensing and local histories) to produce interpretations that are more meaningful for researchers and LID communities. Douglass, Walz and colleagues (2019) emphasize that such integration of multiple data sources is, in fact, necessary to minimize the risk of inaccurate or biased interpretations of how people and landscapes co-evolve. Nonetheless, remote sensing archaeology does not always take an integrative and collaborative approach. Unequal power dynamics between the observer(s) and the observed remain deeply entrenched (Eubanks 2017), and this is particularly significant when observed parties have deep histories of connection to the places that they live (i.e., LID communities).

The uses of remotely sensed imagery in archaeology have a broad range, encompassing small-scale, localized studies of specific sites and locations, broader regional surveys, and landscape-scale assessments of at-risk cultural heritage with agendas quite distinct from other academic initiatives. As such, in what follows, our

discussion is primarily targeted towards those uses of remotely sensed data that target traditional homelands of LID communities with long histories associated with the landscape under investigation, and particularly the use of high-resolution datasets where culturally-significant features can be directly identified and recorded. Nevertheless, our reflections on the ethics of remote sensing archaeology are certainly relevant to broader-scale investigations and studies using lower resolution data. Our aim is not to present a “one size fits all” solution, as different research programs will have different ethical dilemmas to face. Rather our paper seeks to spark a conversation about how archaeologists wield significant power and influence through their use of remote sensing technologies, and that this power has the potential to have real and devastating consequences on LID communities. Thus, regardless of scale or scope of the research agenda, we must confront these power dynamics to ensure that communities are not negatively impacted by our work.

Certainly, in many heritage management projects rooted in large-scale surveys, the scale of the analyses and level of detail are not always great enough to constitute a violation of privacy, *per se*. Massive archaeological undertakings of landscape mapping have advanced scholarly understandings of many regions around the world (e.g., Bewley et al. 2016; Casana 2014; Hobson 2019; Menze and Ur 2012). Nevertheless, even where such work has lower data resolutions and less direct contact with individual sites and cultural features, ethical considerations with regard to local communities remain imperative. In the context of large heritage management surveys, previous community and participatory mapping and education initiatives demonstrate some of the ways that researchers are beginning to engage local communities within landscape-scale projects (e.g., Casana 2020; Fisher et al. 2021; Parcak 2019; Yates 2018; also see community archaeology projects like The Chilterns AONB [<https://www.chilternsaonb.org/>], Whiteadder

[<https://whiteadder.aocarchaeology.com/>], among others). Additionally, these large-scale initiatives can also increase local or regional representation on project boards so that local concerns can be more consistently acknowledged and addressed.

Recently, a number of researchers have begun to address ethical issues surrounding remote sensing archaeology (e.g., Chase et al. 2020; Cohen et al. 2020; Davis and Sanger 2021; Gupta et al. 2020), but attention remains limited, particularly considering the scope of the ethical issues at stake in the use of remote sensing technologies. In addition to an ethical consideration of power imbalances resulting from aerial or spaceborne sensing, there are also legal considerations. While the proliferation of drone technology into the private and commercial sectors has been met with legal regulations on their use in some areas, laws governing aerial and spaceborne remote sensing are largely ambiguous or entirely unrelated to issues of privacy (Oduntan 2012). International aviation laws claim that nations are entitled to “complete and exclusive sovereignty” of airspace above their territorial boundaries (Haney 2015), but space law is not as concrete. Furthermore, despite the clarity of aviation laws, disputes over jurisdiction still arise. For example, Native American nations view airspace and land as part of the same continuous territory, and thus claim jurisdiction over both, while U.S. aviation regulations run counter to this sovereignty claim (Haney 2015; Reddix-Small 2014). International law, therefore, does not create a legal panacea that solves all issues of legality and ethics. There are even regions of the world where legal policies are limited, or non-existent, regarding safety and privacy of citizens in relation to aerial technologies, or how such data are used (Oduntan 2019). Since remote sensing technology has opened vast amounts of space to exploration by archaeologists, the question posed here is whether the collection and analysis of remote sensing data from locations where data collected at the ground level would otherwise be “off-limits” are ethically justifiable.

In the work presented in this thesis, my colleagues and I use satellite remote sensing to identify archaeological sites. My work on this project inspired this particular chapter and deeper probing of the ethics of remote sensing research, especially when it involves the investigation of sacred cultural spaces and communities with deep historical ties to the landscapes under study. Here, we thus primarily consider a case study from Southwest Madagascar, where diverse communities have lived for hundreds to thousands of years and where there are strict taboos (*fady or faly*) governing access to parts of the landscape, especially with regard to *vahiny*--people outside of the endogamous community (Cinner 2008). Remote sensing, however, allows outsiders to have unrestricted aerial access to these locations, and Malagasy law only requires a permit for the use of certain technologies (e.g., drones) but does not require permission from local communities for the use of remotely sensed data. Regardless of legality, we ask whether it is *ethical* for researchers to conduct geospatial analyses of the SW Malagasy landscape without the consent and collaboration of LID peoples? We suggest that the answer ultimately lies in who benefits from the sensing of these spaces and the research that comes from this action (see Cohen et al. 2020). Furthermore, we argue that the use of remotely sensed data should not adversely impact any party, especially LID communities in the region under study.

In fact, with collaborative remote sensing approaches, archaeologists have the capacity to engage with communities that have often been excluded from many past investigations because of highly mobile and transient lifeways that make the study of their connections to landscapes more difficult. Such research agendas could help empower highly vulnerable populations who have been victims of displacement and disenfranchisement. Furthermore, geospatial technologies more broadly have been leveraged in powerful ways to revision and center the histories and agency of Black,

Indigenous, and People of Color (Dunnavant 2021), as these are inscribed in land and seascapes.

We advocate approaches to the use of remote sensing technologies that engage LID communities in active collaboration and knowledge exchange. This includes discussing how remote sensing technologies work, understanding local opinions about these methods, developing research plans in consultation with LID community members and landowners prior to any aerial survey taking place, involving community members in the survey process, and maintaining transparency about the use of remotely sensed data throughout the research project. Transparency is at the heart of collaborative archaeological practice, and is central to co-producing science in a just manner (Atalay 2012; Douglass, Morales, et al. 2019; Lyons 2013; Wadsworth 2020). As Gupta et al. (2020, S47) state: “greater attention to community-driven intellectual efforts can enhance the bonds of trust between Indigenous and non-Indigenous peoples, a situation that can meaningfully address colonial practices in archaeology.”

In what follows, we outline the power imbalance that can result from aerial and spaceborne sensing in the form of a panopticon dynamic (*sensu* Foucault 1995[1975]). Next, we discuss these issues within the context of Southwest Madagascar. Our objective in the article is to critically evaluate the ways in which remote sensing archaeology can create or accentuate unequal power dynamics between local communities and researchers and their institutions. To this end, we evaluate the opinions of LID communities in Velondriake, Madagascar, about the use of remote sensing instruments (specifically drones and satellites) for documenting culturally significant places. We draw on our experiences in working with local communities in this area to challenge currently accepted assumptions about power dynamics within remote sensing archaeology. In such

a discussion, we acknowledge that some may be uncomfortable with the framing of our discussion, as we are ultimately suggesting that power must be more equitably shared between researchers and stakeholder communities--put more bluntly, we are implying that power must be ceded by researchers who have hitherto held it. At the same time, we stress that this article should not be seen as an attack on particular individuals or practices, but rather as a critical self-reflection about how to increase the equity of our research practices.

Surveillance and Power: Foucauldian Dynamics

In his book, *Discipline and Punish*, Michael Foucault (1995 [1975]) outlines the role of surveillance in the construction of a power structure between members of society. In particular, Foucault focuses on the panopticon (Bentham 1791), an architectural style employed in many European prisons wherein guards watch inmates from an elevated central tower. The guards' presence or absence in the tower is unknown to prisoners. Prisoners must, therefore, assume that guards are always present.

Much like the panopticon, remote sensing offers a "birds-eye" view of entire regions with unfettered access and visibility, and limited indication to people on the ground of when the landscape is being surveilled. Many remote sensing technologies (like aerial photography) became prominent through their military applications, including the survey of battlefields and enemy territories (Parrington 1983). RADAR technology, which has gained popularity in archaeological remote sensing (e.g., Chen et al. 2017), saw its largest development during WWII, when it was extensively used to look for enemy submarines and aircraft (Parrington, 1983). Furthermore, while satellite imagery was first proposed as a step forward for scientific research, it was an essential tool used by Russian and American agencies in the space race during the Cold War. In fact, the United States

Navy's Bureau of Aeronautics was intimately involved in the creation and launch of the first satellites (Rosenthal 1968).

The development of remote sensing techniques for military purposes may explain the lag in ethics concerns regarding these methods (Pollock 2016), as the early intent of much of this technology was espionage, which by definition does not involve consent (Gogarty and Hagger 2008). Personal property and "private" spaces are inherently revealed and all restrictions are ignored. While archaeologists may not think of their work as surveillance or espionage, the potential ramifications of using aerial or spaceborne imaging systems to photograph people's homes and property does require careful thought, especially when the bounds of an investigation involve culturally sensitive areas or communities that have historically been exploited by colonialist/imperialist agendas. Applications of remote sensing can be positive, negative, or both, but regardless these tools result in a shift of power towards the observer(s) and away from the observed. Therefore practitioners need to be conscious and intentional about how they are engaging communities in the gathering and application of remotely sensed datasets.

While the panopticon can be viewed negatively, there are also positive elements of such surveillance mechanisms. Advances in science and medicine require surveillance mechanisms to address important questions on a range of topics, and such hierarchical observation can also help to counter dominant power structures (Galič et al. 2017:23). For example, a "constitutional panopticon" flips the roles of observers and observed to oversee governmental officials and those in places of power (Brunon-Ernst 2013). Therefore, the concept of a panopticon is neutral (see Haggerty 2006), but can make positive or negative impacts depending upon how such power dynamics are exploited.

Unlimited access to remotely sensed data can therefore come at a cost: it can exert power over those living in investigated spaces (see Myers 2010). For example, local perceptions of being surveilled can induce behavioral change through fear and can limit the ability of local communities to make managerial decisions about their land and resources. Gupta et al. (2020) illustrate this issue in Canada, where legal statutes limit the authority and capacity of First Nations communities to access archaeological information compiled from "big data" sources like satellites and aerial surveys. This creates a power imbalance resembling Jeremy Bentham's (1791; also see Foucault 1995 [1975]) panopticon, wherein researchers and government employees are given total control of datasets in most instances, leaving indigenous peoples without any authority to control/manage their own cultural heritage or how this information is used. This threatens sovereignty and local rights over data access and privacy (see Myers 2010). To use these data without consulting with stakeholder communities is a breach of trust, confidentiality, and establishes an all-too-familiar power structure in which the academic elite dominates the histories and heritage of LID communities.

On Madagascar, for example, the French colonial administration undertook widespread cartographic projects in the 19th and 20th centuries which often undermined LID communities and served to solidify colonial control of land and resources (Amelot 2017). In order to protect places from surveillance, local informants sometimes deliberately left important places out of official records (Figures 3.1-3.2). With increasing availability of mapping technology (i.e., satellites, GIS, etc.), mapping these locations becomes easier, but to add such locations to new maps would be a transgression of local wishes. Not only does mapping culturally significant locations become easier, but it becomes possible without ever consulting local communities, thereby creating a top-down

power structure where the foreigner can be perceived as ever-present, always watching, and the surveilled may have little authority to object (*sensu* Foucault 1995 [1975]).

Of course, the nature of surveillance and the ethical issues that arise depend, to one degree or another, on the nature of the surveillance instrument, the region and people under watch (and their ability to object to surveillance activities), the degree of privacy that may be infringed upon by such investigations, and the plans for interpretation and use of remotely acquired data. For example, coarse-grained satellite imagery cannot detect individuals or features smaller than dozens of meters in diameter with any clarity, and thus individual privacy will likely not be in question if research only utilizes these lower-resolution datasets. In contrast, if drones are used, you can identify people, license plates, and even coins on the ground; this can certainly violate privacy. But, even in cases where individual privacy may not be infringed upon, decisions may be made based on remote sensed data that affect the autonomy and ability of communities and individuals to use and manage the landscapes they inhabit. Foucauldian power dynamics thus still operate at coarse resolutions where the degree of personal privacy infringement is low. Remote sensing archaeology should therefore strive to increase engagement with LID communities, regardless of project scope and data resolution. In what follows, we focus particularly on ethical issues as they pertain to the most significant potential breaches of local community privacy rights in the context of culturally sacred spaces. As such, while all researchers should bear in mind the arguments and problems put forth here, the degree to which our specific recommendations will be relevant will entirely depend upon the scale of the analysis taking place, the types of data employed, and the status of local communities in the region of focus.

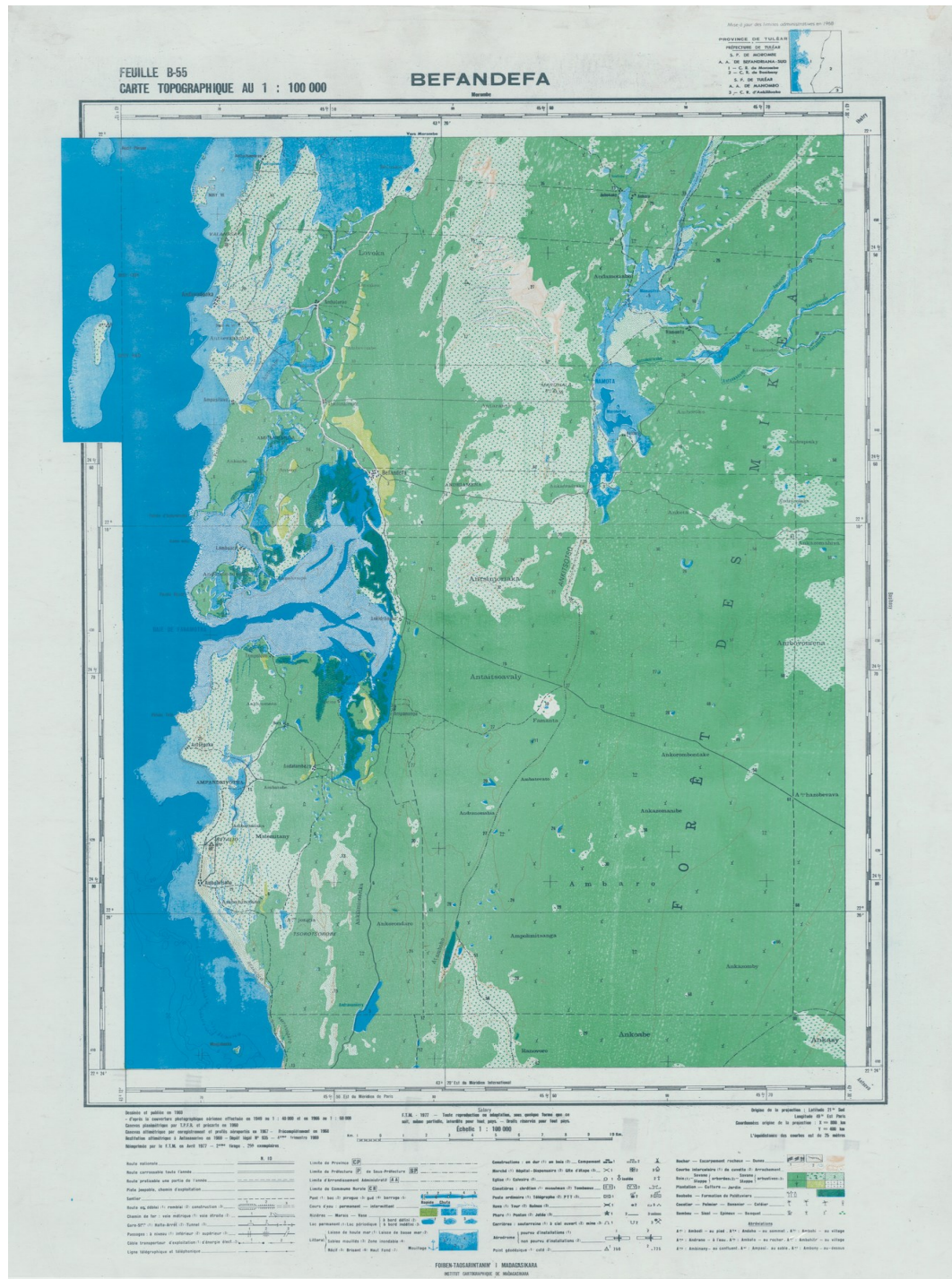


Figure 3-1: A map of the Commune of Befandefa (which now also includes the Velondriake Marine Protected Area) created by the French colonial administration. Notably, the map does not include many important landscape features like caves and rock shelters in this area. This was a conscious effort by local informants to keep these locations (many of which are sacred or places of hiding from outside interference) secret (Credit: Foiben-Taosarintanin'i Madagasikara (FTM)).



Figure 3-2: Examples of caves and rock shelters in Velondriake, most of which do not appear on official maps, like the one in Figure 3-1. Many caves and shelters are sacred to LID communities (Credit: K. Douglass).

The issues of privacy and confidentiality that arise with the use of geospatial technologies like high-resolution aerial/satellite imagery are well established by geographers. The American Association of Geographers (AAG 2009) specifically states in their code of ethics that “[d]ecisions about the collection, ownership, and analysis of geospatial data should be made with a view toward affording individuals and communities that bear the burdens of geospatial research the opportunity also to share in its benefits.” The AAG continues, stating that field-based projects should return all results and findings back to local communities and local collaborators should be included as authors on publications deriving from that research (AAG 2009).

Professional organizations in archaeology and anthropology, however, have not demonstrated a unified approach. As Dennis (2020) notes, digital archaeology (encompassing all research conducted via computer-based approaches) exists almost entirely without well-formulated ethical oversight. For example, the Society for American

Archaeology (SAA) has no specific requirements or ethics mandate for community engagement, stating that “archaeologists should reach out to, and participate in cooperative efforts” (SAA 2016, emphasis added). In contrast the American Anthropological Association (AAA) has an explicit guideline that “[a]nthropologists have an obligation to ensure that research participants have freely granted consent, and must avoid conducting research in circumstances in which consent may not be truly voluntary or informed” (AAA Ethics Forum 2012). Similarly, the Code of Ethics for the CAA (Computer Applications and Quantitative Methods in Archaeology) specifically acknowledges that their work can impact local communities and the general public. As such, the CAA “is committed to engagement and consultation with groups and individuals impacted by archaeological work carried out by CAA members, with the aim of building relationships that are respectful and mutually beneficial” (CAA International 2018). There is a growing consensus among archaeologists and anthropologists that local engagement is needed, but ethical guidelines are not uniform between regions or organizations, especially when it relates to digital research practices like remote sensing.

This inconsistency extends to the classification of human subject research (HSR) by institutional review boards (IRBs). Geographical and geospatial technologies that record or contain potentially sensitive geographic information (i.e., GPS coordinates, personal identification records, etc.) are heavily scrutinized during IRB processes (Appendix A). However, remote sensing data, which inherently contains geographic information as well as photographic documentation of cultural locations, are not always explicitly mentioned.

While the use of drones and other aerial imaging systems can monitor and record people and their activities, aerial images are only classified as HSR by the United States

Government if an investigator obtains information from a "living individual", either directly or via means that would be considered private (Resnik and Elliott 2019). For archaeological remote sensing research looking at historical, landscape-scale patterns of land-use, the absence of identifiable information about living individuals is usually interpreted as non-HSR, and therefore an IRB is not deemed necessary. As such, IRB forms (e.g., Appendix A, section 22.9) that require information about photographing or videoing "subjects" refer to people themselves, not necessarily cultural landscape features. However, landscapes are inherently cultural, and in some cases landscape features have been granted personhood status (e.g., those connected with ancestors), with all the rights that people have (e.g., Roy 2017; Warne 2019; Safi n.d.).

It is important to emphasize that landscapes are conditioned by and condition how individuals and communities use particular spaces. Therefore, they are places infused with human values which are embodied within that place (*sensu* Basso 1996; de Certeau 1984; Ingold 1993; Lepofsky et al. 2017). Landscapes and humans are inseparable. Thus, surveilling landscapes – regardless of whether individuals are present on the landscape at the time of data collection – should be thought of in critical terms that adhere to ethical standards related to cultural research. Researchers making use of aerial imagery should consider that the study of cultural landscapes and features can have the same implications as HSR, and may need to be included as such in proposals for IRB approval (see Resnik and Elliott 2019; also see AAG 2009). As mentioned earlier, some datasets simply do not have the quality to precisely locate specific cultural features, and in such instances the connection with HSR may be unnecessary; nonetheless, it is vital that remote sensing archaeologists collaborate with local communities to ensure that local perceptions of place are understood and respected.

Case Study: Madagascar

Madagascar is the fourth largest island in the world, and sits at the crossroads of the Indian Ocean, connecting the cultural spheres of the African continent and Persian Gulf to those of South and East Asia, and Indonesia (Radimilahy and Crossland 2015). The peoples of Madagascar have diverse cultural practices, beliefs and norms, which include a range of taboos (*fady* or *faly*). *Fady* are often tied to specific locations. For example, visiting certain locations can be *fady*, especially for a *vazaha* or *vahiny* (outsider) to the community (Cinner 2008; Fritz-Vietta et al. 2017; Langley 2006; Pearson and Regnier 2018). *Fady* locations are often associated with privileged or sacred knowledge, and with the rights of *razana* (ancestors; Cinner 2008). Despite strong prescriptions governing access to and use of sacred spaces, drones and satellites can scan these areas without consent from local leaders, completely disregarding and contravening the wishes of LID communities. In this sense, the Foucauldian power dynamics inherent to remote sensing make it possible to scan these areas without community consent.

Over the course of this dissertation project, remote sensing instruments were used to survey the Velondriake Marine Protected Area in southwest Madagascar (Figure 3-3). During ground surveys to test the accuracy of a predictive model of archaeological site locations derived from satellite images (Chapters 4 and 5) there were several instances in which the sampling protocol called for ground-truthing *fady* locations, such as ancestral tombs. Upon discovery of the inclusion of these sites in the survey plan, ground investigation was suspended or rerouted to avoid trespassing on restricted grounds. Because LID communities were consulted and our research team consists of local archaeologists and community members, we were cognizant of the potential for our geospatial methodology and tools to transgress local *fady* and carefully avoided trespassing on sacred spaces. Our work on this project inspired the current paper and

deeper probing of the ethics of remote sensing research. We ask whether *fady* locations should even be visible on freely available datasets (which are oftentimes produced by foreign nations or agencies).

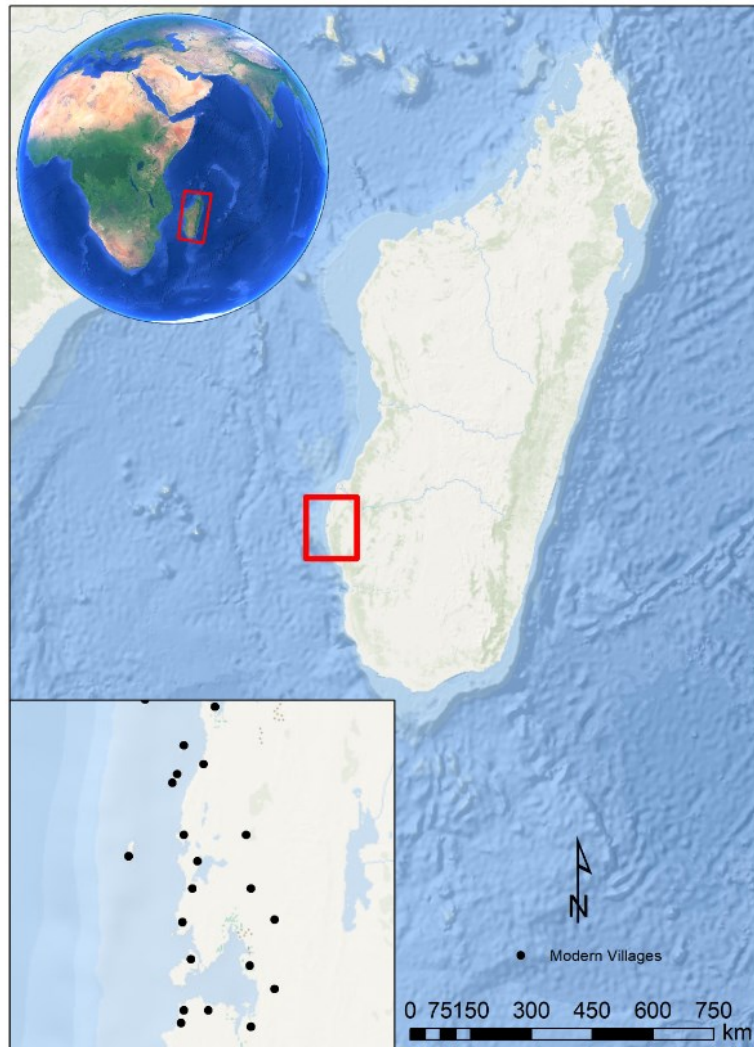


Figure 3-3: Location of study region in Southwest Madagascar. Inset map shows the Velondriake Marine Protected Area and modern day villages (black dots) located within this region. Service Layer Credits: ESRI, Garmin, GEBCO, NOAA NDGC, and other contributors. Inset map credits: Google.

On Madagascar, legal statutes regulating satellite imagery do not restrict access or require consultation with LID communities in any form. Drones, in contrast, are more heavily regulated. For example, the conditions of use for drones, detailed in the

“Instruction N°01 ACM/DRG/17 relative aux conditions d’exploitation des aéronefs télépilotés” (<http://www.acm.mg/spip.php?article35>) lays out clear and specific regulations for how and where drones can fly and record images or video.

Article 2 of this code, for example, specifies that no drone can be flown within 100m of a person unless prior consent has been given to the drone pilot from the people in question. Furthermore, the drone pilot must identify and take all necessary measures to avoid flying over property limits of the land that they are flying above, and if private land will be flown over, consultation with the landowner must be acquired. Article 3 of this code further specifies that drones are prohibited from encroaching upon prohibited areas. Anecdotally, however, we know these stipulations are often ignored by drone pilots where we work in Madagascar.

With respect to spaceborne remote sensing (i.e., satellites), Madagascar has ratified several treaties relating to space exploration and space telecommunication systems (Oduntan 2019). However, Madagascar has not signed or ratified treaties related to liability (LIAB 1972) or object registration (REG 1975; see Oduntan, 2019). Thus, in contrast to drones, the use of spaceborne data is essentially unregulated, apart from treaties deeming that data collected by such means should be shared with governments of states who are impacted. Even in these treaties, however, issues of privacy go unmentioned (e.g., The Space Treaty. 18 UST 2410, 610 UNTS 205). In fact, several UN resolutions on space activities do not require prior consent of countries targeted by satellites, which leaves many concerns regarding privacy rights of nations as well as individuals (Oduntan 2011). Therefore, remotely sensed information has the power to control without local consent and needs to be closely considered by data users (observers)

in order to avoid enforcing unequal power dynamics and/or further disempowering the observed.

Local Opinions on Aerial Imagery

The Morombe Archaeological Project (MAP), based in SW Madagascar, was established in 2011, and is grounded in collaborative and co-produced research on the co-evolution of people and landscapes. The project is guided by the fundamental principle that science is enriched and made just through collaborative and inclusive approaches (Douglass, Morales, et al. 2019). The MAP team comprises over 25 members, predominantly from the communities of Velondriake. Several MAP team members are authors on this paper. Geospatial tools and data, including drones, handheld GPS devices, total stations, and satellite imagery, are central to MAP work, particularly in reconstructing landscape-level phenomena related to human mobility and resource use (Figure 3-4).

The suite of geospatial tools used by MAP serve a variety of aims, all of which have the potential to yield sensitive information. For example, total stations produce detailed maps of individual sites, topography and landscape features. Handheld GPS units are used to record geographic coordinates of sites and artifact locations. These data are then used to make maps that include locations that are potentially sacred to the communities of Velondriake. On a larger scale, satellite imagery is used by the MAP to document settlement patterns and drivers of landscape change, while drones are used for aerial photography and videography.

Given the widespread use of geospatial technologies - especially remote sensing instruments that produce sensitive information, it is imperative to the MAP's foundation that we engage the ethics of using these tools and data. To that end, the team has

gathered information regarding local opinions about the use of drones, in particular, as drones are a newer addition to the suite of tools the project relies on. We consider this to be an important first step in establishing best practices and a collaboratively produced ethics of geospatial technologies in Malagasy archaeology.



Figure 3-4: MAP team member George Manahira assisting with Total Station mapping of karst topography around archaeological sites in Velondriake (Credit: K. Douglass).

To evaluate the opinions of LID communities in Velondriake about the use of remote sensing instruments for documenting culturally significant places we draw on our work experiences and the work done by the MAP team. Specifically, we focus on local opinions on drone imagery because of the highly visible nature of drones and their ability to record detailed photographs of culturally significant places.

We developed a series of questions to guide a critical discussion between MAP team members on the best practices for archaeologists using remote sensing technologies: 1) do team members feel that drone photography violates local customs and privacy? 2) Are people aware of what drones can see? And 3) is there interest among community members in how the technology works? Understanding local perceptions can

help to avoid unequal power dynamics by modifying remote sensing activities in accordance with local norms instead of generating discomfort or fear (and invading privacy) through detached surveillance. Thus, our critical self-reflection and discussion led to a series of clear revelations that will be central in developing a set of best practices and future efforts to generate collaborative work with geospatial technologies in Velondriake and elsewhere. Future development of best practices will involve formal interviews with LID community members beyond the MAP team and workshops to increase community familiarity with these technologies.

Based on our critical discussions, when using drones to take aerial photographs, local views on privacy appear largely dependent upon the places drones are flown. If a particular area is *fady* for people to visit or photograph in general, then drones are not an exception. As such, the photography of graves and burial sites via drone is almost never allowed, unless express permission has been granted by community leaders.

Apart from *fady* areas, there does not seem to be great concern about privacy with respect to remote sensing via drones. However, part of the reason for this likely stems from the transparent research design of MAP projects. For all projects, the MAP team meets with local community leaders to discuss the nature of all archaeological research projects. Thus, before photographs are taken or surveys are conducted, community leaders are made aware, and any concerns over any aspect of the research is addressed before work proceeds.

With respect to overall interest in drones and remote sensing technologies, we have observed that there are many community members who are curious about drones when they are used for taking photographs. Recently, the MAP incorporated a Phantom IV drone and DJI Digital FPV goggles into its project toolkit (Figure 3-5). These goggles

provide the user with a live feed of the imagery being recorded by the drone and the feeling of flying over the landscape. Team members and LID community members who attended training sessions for the use of the drone and goggles all took turns wearing the goggles and viewing this live feed. All reported a feeling of initial disorientation followed by awe at the extent of the drone's view and the clarity of the image. Older members of the community, in particular, found the technology disorienting, particularly as it allows the user to see themselves from above. The MAP team agreed that hands-on experiences with the technology afforded by the goggles significantly altered users' understanding of the power of these tools. This highlights the need to not only discuss the nature and capabilities of geospatial tools, but to create opportunities for community members to have hands-on experiences that enhance their understanding of their scope and resolution. Without an understanding of how these tools work, the collection of imagery with informed consent is difficult, if not impossible.



Figure 3-5: Community member in SW Madagascar wearing goggles and viewing live feed from drone.

In this dissertation project, the MAP team and I used satellite images to remotely identify and survey archaeological sites in Velondriake. Due to the volume of satellite imagery available, our project investigated over 1000 km² of the Velondriake area, which inevitably includes sacred spaces. According to local community members, there are approximately 54 *fady* places throughout the Velondriake area, and every village within this region has at least 3 *fady* locations. When planning each survey, team members would instantly recognize specific locations in the imagery (e.g., nearby towns, villages, and cities). Likewise, many could identify locations of prior archaeological work, or where *fady* sites were located. In multiple instances, areas detected in satellite images overlapped with *fady* areas and required changes in survey plans. In these instances, the team's collaborative discussion of the satellite data was crucial to ensuring that the research plans would avoid sacred spaces. At the same time, it highlighted an important issue with aerial and spaceborne sensors: these practically unregulated sources of data can locate sensitive cultural information that, in all other instances, would be off-limits to outsiders (Figure 3-6). This inevitably tips the scales of power towards the outside observer and away from local communities. As such, our critical reflection of this project provides important lessons for future remote sensing archaeological work, namely that collaboration with LID communities is imperative to ethical research practice.



Figure 3-6: Examples of cultural features that can easily be recorded using aerial and spaceborne imaging systems. A. Drone image of cultivation areas in the Mikea territories east of Velondriake (Credit: G. Cripps). B. PlanetView (Planet Team 2020) satellite image of cultivation areas in the Mikea territories (Credit: Imagery © Planet Inc. 2020).

Discussion

The use of remote sensing technologies has been historically dominated by institutions and scholars in the Global North, with most publications coming from Europe, Asia, and North America (Agapiou and Lysandrou 2015; Cohen et al. 2020; Davis 2020b). This places scholars and communities in other regions of the world at a disadvantage in terms of training to utilize remote sensing instruments to improve knowledge of the past, despite the fact that many datasets exist with global coverage (Davis and Douglass 2020). Furthermore, it can create an imbalance of power with respect to archaeologists and local communities in areas where knowledge of such technologies is limited (Fig. 3.7a), wherein outside researchers have the ability to record people and landscapes without local knowledge or consent (*sensu* Foucault 1995 [1975]).

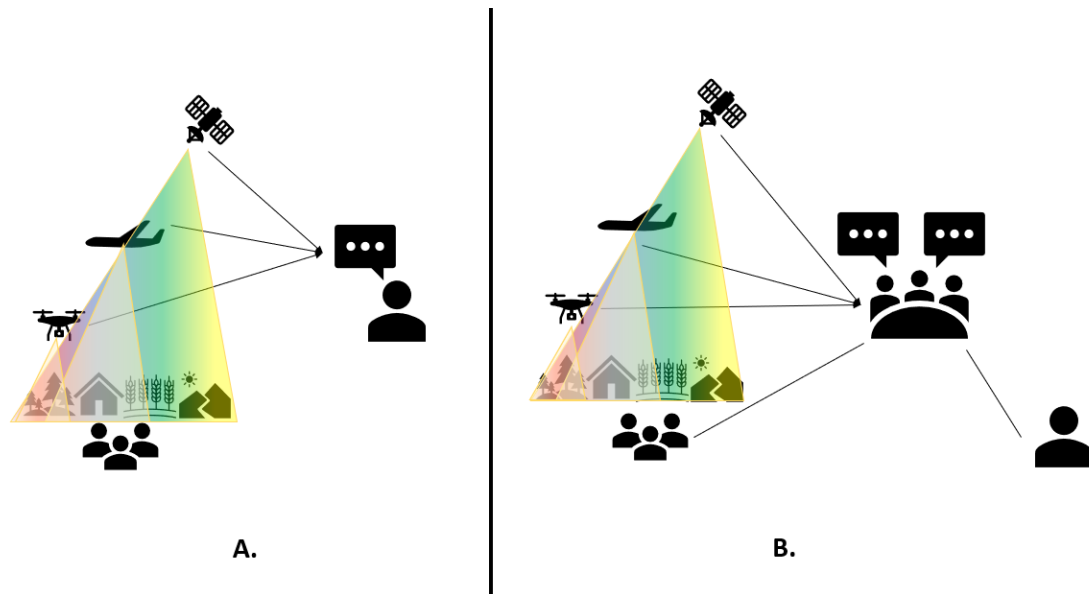


Figure 3-7: Illustration of standard versus equitable practice of remote sensing within archaeology. A. Standard means by which remote sensing archaeology is conducted. The academic acquires aerial/spaceborne datasets, develops a research agenda and analyzes that data without consent from or collaboration with LID communities. B. Proposed establishment of best practices in remote sensing archaeology centered on community collaboration and consent. The academic consults with local communities and analyzes aerial/spaceborne datasets collectively within the scope of a mutually agreed upon research agenda.

For example, within North America, Gupta et al. (2020) show how significant portions of indigenous historical and archaeological data are “owned” by the Canadian government. This leaves many First Nations communities without any control over how these data are used or disseminated. Akin to Foucault’s (1995 [1975]) notions of power, LID communities are placed at the mercy of foreign powers to monitor and protect their cultural heritage, and their sacred places are left in a perpetual state of surveillance by those who should not necessarily have access to those places, remotely or otherwise. Gupta and colleagues (2020) also state that there is growing interest among First Nations communities in this area in controlling geospatial information related to their cultural heritage. As our experience shows, local communities in Madagascar are also expressing

interest in archaeology and the geospatial technologies being used to collect this information.

The work conducted by the MAP team over the past several years has increasingly utilized drones and other remote sensing technologies in fieldwork. What is clear from field observations and discussions with LID community members in Madagascar is that photography, of any kind, requires mutual consent. While many aspects of privacy do not appear to be a major concern (i.e., photographing modern villages and houses), the scanning of sacred locales (i.e., ancestral tombs and burials, sacred caves, spaces of ritual – like the practice of *tromba* [trance] – etc.) is taboo and in violation of the wishes of LID communities. This largely coincides with the legal statutes in place within Madagascar pertaining to drone operation, where permission is needed before operating a drone within certain spaces.

Within the MAP surveys in southwest Madagascar, the level of comfort with drones is likely, in large part, due to the transparent nature of MAP practices (see Douglass, Morales, et al. 2019). Local community leaders are consulted prior to any archaeological field project and any use of drones or other methods are explicitly discussed before any work commences. By engaging with local community members before any analysis even begins, research is guided by the interests and concerns of LID communities as well as researchers (Fig. 3.7b). This helps to restructure the power dynamics involved with remote sensing technologies and avoid a panopticon-esque organization with outside researchers controlling all aspects of data collection and analysis.

This notion of mutual benefit is central to many participatory mapping approaches in geography and anthropology (Álvarez Larrain et al. 2021; Colloredo-Mansfeld et al. 2020; Dunn 2007; King 2002; Ramirez-Gomez et al. 2015). By involving local communities

in mapping projects that utilize GIS and remote sensing, research is inherently on track to adhere to many ethical standards such as providing benefits to local communities (Álvarez Larrain et al. 2021; Álvarez Larrain and McCall 2019; Ehrman-Solberg et al. 2020; Sanchez et al. 2021). For example, participatory mapping has alleviated conflicts among groups over resources (e.g., Kwaku Kyem 2004). Issues still persist in the use of participatory mapping, particularly the Eurocentric cartographic representation that is standard in GIS (see Álvarez Larrain and McCall 2019). Such views of the world do not always align with LID knowledge, and participatory projects must be careful not to force certain viewpoints onto others via Eurocentric cartographic representations of the world (Álvarez Larrain and McCall 2019; also see Dunn 2007), as this also perpetuates asymmetries of power.

As our discussions above and previous research emphasize for Madagascar (see Evers and Seagle 2012), landscapes are cultural phenomena that are inseparable from people (also see Basso 1996; de Certeau 1984; Morton 2013). As such, when using technologies to record information about landscapes, this work will inevitably have impacts on communities living in these places. While some geospatial technologies like drones can have a very invasive effect because of the high resolution of the data and the visible presence of the instrument, satellites, in contrast, are not visible to local communities but are achieving comparable image quality that can record sacred spaces at sub-meter resolution (Figure 3-6). While individuals may not be visible in such imagery, sacred places are and can be documented in great detail. The distance placed between many geospatial datasets and human subjects research have ultimately created a false dichotomy between what constitutes “human-subject” research, as some geospatial data (like GPS points) are scrutinized by IRB protocols while others (aerial and spaceborne images) are alarmingly absent (Appendix A). As such, archaeologists must be careful about what data they use

and how they share this information. Ultimately the dissemination of potentially sensitive information acquired from aerial reconnaissance should be an open dialogue with LID communities to ensure both the protection of cultural heritage and ensuring local autonomy in managing their heritage.

Conclusion

In this article, we detail how the concept of the panopticon, central in Foucaultian theories of power, apply to archaeological remote sensing. We then provide context on how we have addressed these power dynamics during fieldwork in SW Madagascar as a means of raising critical awareness about ethical issues inherent to remote sensing research. While there is ample access to global remote sensing datasets, archaeologists should be reserved in their ambitions to use these without first grappling with the ethical issues discussed here. Researchers must ask themselves is this: “Do the places I am investigating potentially contain actively sensitive or sacred sites? And if so, would I want a stranger recording places that are significant to me without my knowledge or consent?” Most likely, if the answer to the first question is “yes”, the answer to the second will not be as straightforward (or will result in “no”). Thus, there is a need to communicate with communities to ensure that consent and knowledge of research activities are established before using these powerful technologies.

While some datasets (i.e., satellite imagery) are widely (and in some cases freely) available, the use of such data with high resolutions that have the capacity to directly detect culturally important structures should be in consultation with local stakeholders (Fig. 7). In the case of newly commissioned remote sensing datasets (e.g., drone imagery, aerial remote sensing [e.g., LiDAR], etc.), conversations should take place between local communities and researchers before data collection to discuss: 1) the extent of data

collection; 2) how the data can be used; and 3) who should have access to that information.

In sum, we argue that the ethical implications of archaeological prospection efforts using remote sensing revolve most heavily around power dynamics. To alleviate such issues, a collaborative approach to archaeological remote sensing is needed to ensure that research agendas do not violate local communities' respect for privacy and traditional customs. In order to more broadly represent community concerns regarding use of these technologies, all archaeological projects using geospatial technologies should engage in a structured discussion with LID communities prior to, and throughout research projects that involves a clear set of steps: 1) create shared understanding of the scope, nature, scale, resolution of the technology or dataset in question; 2) provide hands-on experience of how different technologies operate, 3) generate a plan for the use and dissemination of these tools and data that respects LID wishes; 4) make data acquired from that tool available to LID community members. Only by making the status of external researchers and local communities equal in all elements of research can we avoid power imbalances and the ethical pitfalls that accompany such dichotomies.

Chapter 4: Satellite-based remote sensing rapidly reveals extensive record of Holocene coastal settlement on Madagascar³

The human history of Madagascar, the world's fourth largest island, is complex and involves the movement and dynamic interaction of people, plants, animals, and ideas from around the Indian Ocean (Dewar and Richard 2012; Fuller et al. 2014; Radimilahy and Crossland 2015). To-date, archaeological, genetic, and linguistic research have revealed the earliest known evidence of Madagascar's far-reaching connections; the island lies at the westernmost reach of the Austronesian expansion (Crowther et al. 2016) and multiple lines of evidence testify to the migration of Bantu peoples from the African mainland to Madagascar (Parker Pearson et al. 2010; Pierron et al. 2017). Important questions, however, regarding Madagascar's human past remain poorly resolved. The timing and nature of Madagascar's human colonization continue to generate intense debate in archaeology (Douglass, Hixon, et al. 2019), and our understanding of subsequent social, economic, political, and ecological processes is limited, both temporally and spatially (Dewar and Wright 1993; Douglass and Zinke 2015).

Research into Madagascar's early history requires new approaches to overcome existing barriers to our understanding. These include the poorly understood remains of ancient foraging and fishing communities, and the relationship between archaeological settlement patterns, environmental conditions, and climate change (e.g., Kull 2000; Parker Pearson et al. 2010; Wright 2007; Wright and Rakotoarisoa 2003). Landscape-level

³ Davis, Dylan S., Vanillah Andriankaja, Tahirisoa Lorine Carnat, Zafy Maharesy Chrisostome, Christophe Colombe, Felicia Fenomanana, Laurence Hubertine, Ricky Justome, François Lahiniriko, Harson Léonce, George Manahira, Briand Venance Pierre, Razafimagnefa Roi, Patricia Soafiavy, Faralahy Victorian, Vavisoa Voahirana, Barthélémy Manjakahery, and Kristina Douglass. 2020. Satellite-based remote sensing rapidly reveals extensive record of Holocene coastal settlement on Madagascar. *Journal of Archaeological Science*. 115:105097. DOI:10.1016/j.jas.2020.105097.

approaches are critically needed to address these research lacunae. To date, landscape-level approaches are mostly absent from archaeological studies on Madagascar (for exceptions see Dewar and Wright 1993; Mille 1970; Vérin 1986; Wright 2007; Parker Pearson et al. 2010). This is partly because ground-based landscape investigations require large investments of time and resources in the field to generate sufficient information; funding, logistics and a small number of active field archaeologists have proven to be barriers to extensive areal coverage. Innovative approaches are critically needed to expand archaeological survey coverage and document cultural heritage, particularly considering that Madagascar is experiencing increasing impacts from climate change. Climate-driven threats on the island extend to both its people and their histories (IDMC 2020; Lemahieu et al. 2018; USAID 2016).

Here we present the first satellite-based remote sensing archaeological survey of the Velondriake Marine Protected Area of southwest coastal Madagascar. Using freely available satellite imagery, image processing algorithms, predictive modeling derived from human behavioral ecology (HBE) theory and ground-truthing survey, our approach successfully identifies cultural deposits throughout a ~1400 km² area. The Velondriake (Figure 4-1) case study demonstrates how the development of a predictive model to analyze satellite imagery can rapidly expand the known record of archaeological settlements on Madagascar, filling both temporal and spatial gaps at the landscape level. Systematically documenting ephemeral components of the archaeological record at the landscape scale is essential for answering longstanding questions in archaeology surrounding human-environment interactions, social complexity, resilience, and mobility (e.g., Kintigh et al. 2014). On Madagascar, specifically, little attention has been paid to internal migration within the island, but rather focused on arrival events and migration between Madagascar and surrounding regions (Allibert 2008; Anderson et al. 2018;

Beaujard 2011; Dewar and Richard 2012; Douglass, Walz, et al. 2019; Hansford et al. 2018; Mitchell 2019; Vérin et al. 1969). By conducting landscape scale surveys of the island, we will be able to address how communities moved throughout the landscape, and how such mobility was related to environmental, political, and social developments.

Our case study also highlights the importance of integrating theoretical models with remote sensing methods in African archaeology more broadly (Davis and Douglass 2020). Drawing on lessons from research conducted using HBE and related theoretical models from other regions (e.g., Baja California (Coddington and Jones 2013), the Channel Islands (Winterhalder et al. 2010), Australia (O'Connell and Allen 2012), Polynesia (DiNapoli and Morrison 2017)), we demonstrate that it is possible to use satellite-based remote sensing to test the nature of past human-environment interaction and drivers of settlement mobility. We further demonstrate that the integration of theoretical models and satellite-based remote sensing methods holds great potential for rapidly locating previously unrecorded archaeological deposits at vast geographical scales, even when these deposits are ephemeral in nature.

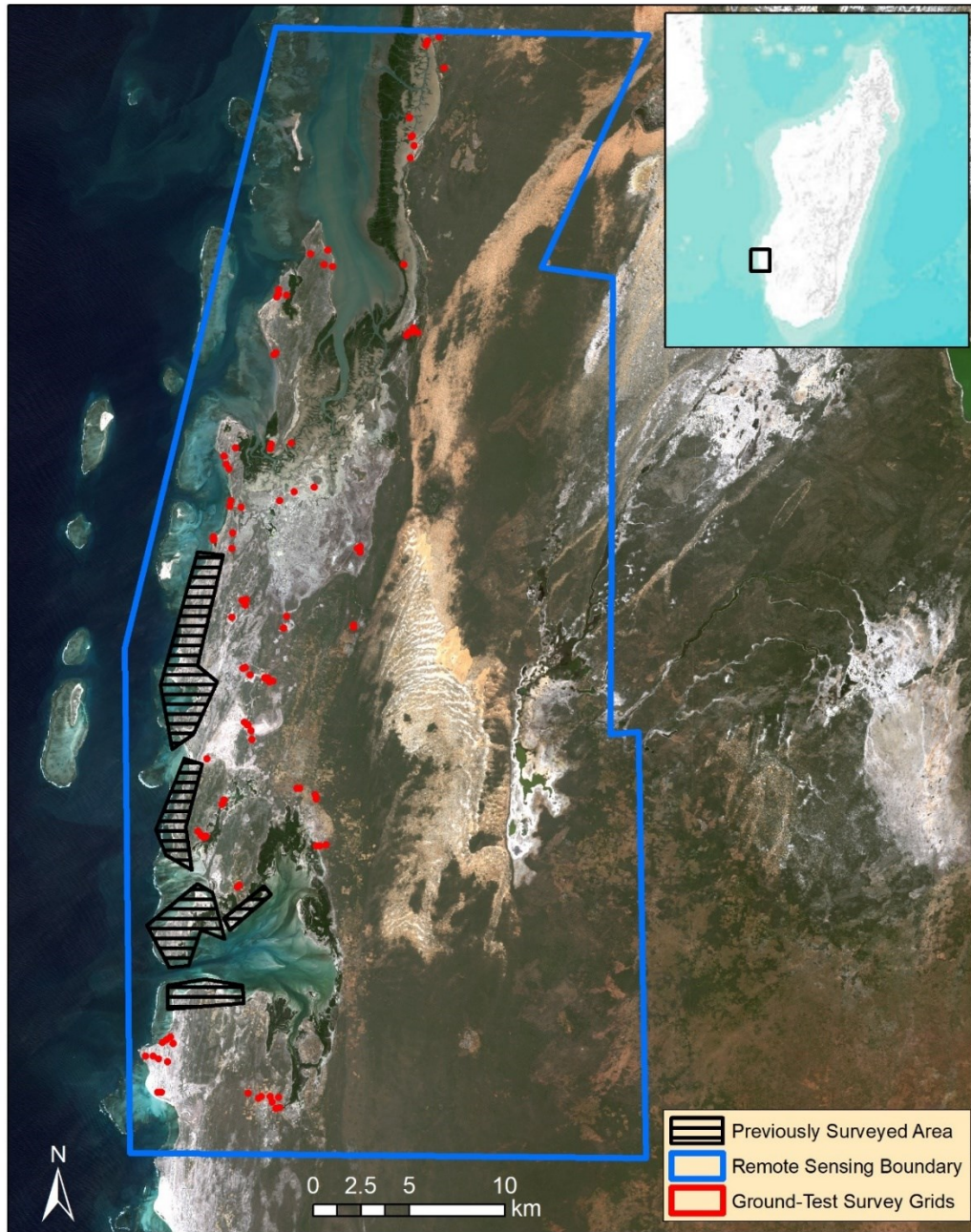


Figure 4-1: Map of study area. Inset map shows location of study area on Madagascar. Full coverage pedestrian transect survey of a portion of the research area by the Morombe Archaeological Project (MAP, 2011-2017) generated preliminary data used to build a theoretically-driven remote sensing procedure. Previously unexplored areas were then surveyed using our remote sensing imagery and the results of our predictive model of site location were then assessed using ground-truthing survey (Satellite image: Sentinel 2; Inset map source credits: Esri, GEBCO, NOAA, National Geographic, Garmin, HERE, Geonames.org).

Previous Landscape-Level Investigations on Madagascar

Most landscape-level archaeological investigations on Madagascar focus on periods from 900 B.P. to the present and highlight important demographic and political processes, including the overall increase in size and number of settlements and the rise of centers of political power (Parker Pearson et al. 2010; Wright 2007). Although the reliability of chronometric determinations for early periods has been questioned (e.g., Anderson et al. 2018; Mitchell 2019), evidence of far earlier occupations exists on Madagascar, extending the island's human record as far back as ~10,000 B.P. during the Early Holocene (Hansford et al. 2018). Recent systematic assessment of Madagascar's radiocarbon chronology supports the possibility of an Early Holocene human presence on Madagascar, despite a lack of contextual information on the nature of such an early presence (Douglass, Hixon, et al. 2019). Given the evidence for Early Holocene human activity on Madagascar and the taphonomic and sampling challenges inherent in studying Madagascar's ephemeral early forager sites (Douglass and Zinke 2015), new approaches are urgently needed to record and assess over 90% of the span of time for which human presence has been recorded on the island. Landscape-level approaches, in particular, will be critical to understanding the evolution of settlement patterns and human-environment dynamics during early periods of human occupation. A diversity of landscape-level approaches has proven useful for understanding the interplay between human behaviors and environmental contexts in other parts of the world (e.g., Coddington and Jones 2013; DiNapoli and Morrison 2017; Jazwa et al. 2017; Winterhalder et al. 2010).

Despite the critical temporal gaps in landscape-level archaeological investigations to-date, understandings of landscapes from the 10th century onwards (Crossland 2001; Pearson 1992; Sussman et al. 1994; Tucker 2004; Wallace et al. 2016) have illuminated connections between humans and their environmental surroundings. Theory from human

behavioral ecology (HBE) and historical ecology have been integrated in ethnographic work (e.g., Tucker 2004; Tucker et al. 2010), but such approaches are still scarce in archaeological contexts (e.g., Douglass, Walz, et al. 2019). For example, Tucker (2004) demonstrates how Mikea foragers' food-sharing practices are dictated by economic factors, reciprocity, kin selection, and tolerated theft. In another study by Tucker et al. (2010), HBE is used to understand risk mitigation via the practice of mixed subsistence strategies.

Recent advances in remote sensing methods and datasets (e.g., Davis et al. 2019; LaRocque et al. 2019; Thabeng et al. 2019) offer important opportunities for applications of remote sensing approaches that promise to advance and expand our understanding of the island's archaeological record, particularly with regard to early and ephemeral sites. On Madagascar, previous studies using aerial imagery successfully revealed the locations of tens-of-thousands of fortification sites dating as far back as ~600 B.P. (Mille 1970). Most recently, Clark et al. (1998) illustrated the potential of multispectral and radar instruments for recording landscape patterns that could reveal the locations of archaeological deposits. Since Clark et al.'s study, spatial and spectral resolutions in satellite imagery have increased, permitting for greater details to be captured by sensors. In turn, researchers' ability to identify subtle landscape deposits (like archaeological sites) have improved, as higher resolutions are often needed to detect such features (see Beck et al. 2007). Furthermore, advances in image processing techniques have led to a revolution in remote sensing analysis (Davis 2019; Lambers et al. 2019; Verschoof-van der Vaart and Lambers 2019). Our study demonstrates the potential for remote sensing to clarify diachronic landscape changes and their human dimensions on Madagascar, as has been achieved in other world regions (e.g., Carleton and Collard 2019; Davis 2019b; Stephens et al. 2019).

Methods

Here, we outline a preliminary study that combines HBE modeling with remote sensing survey to predict the distribution of archaeological sites on southwest Malagasy landscapes. In this discussion, “site” refers to any area containing two or more artifacts during ground surveys. Sites thus encompass artifact clusters, settlements, and any other cultural materials present in an area. The approach is based on ideal free distribution (IFD) models (see Fretwell and Lucas 1969). These models assume that individuals settle areas with the best overall suitability (with regards to available resources) and that, as population density and resource consumption increase, settlements shift to areas with lower resource suitability. Because the current study lacks absolute temporal control, the assumption is made that the earliest sites will be located in “high” suitability areas. Confirmation of this hypothesis requires further testing. Here we focus on the density and variability of cultural materials present in different suitability locations. Furthermore, we assess whether ethnographically and historically important resources (e.g. coral reefs, vegetatively productive land, distance to the coast, etc.) are good predictive variables for locating archaeological sites in southwest coastal Madagascar.

Ideal Free Distribution Modeling

Within HBE, there are a series of different optimality models (optimal foraging theory, OFT) which try to predict decision making of individuals based on costs and benefits of different actions (e.g., Blurton Jones 1986; Charnov 1976; Fretwell and Lucas 1969; MacArthur and Pianka 1966; O’Connell and Hawkes 1981). Such modeling approaches have proven useful in exploring the rationale behind observed phenomena in anthropology, including archaeological evidence of behavior and choice (e.g., Bird et al. 2016; Coddington and Bird 2015; Jazwa et al. 2017; Robinson et al. 2019; Tucker et al. 2010). Despite criticisms of OFT (see Zeder 2012), the explicit framework offered by such

approaches provides a heuristic device for exploring factors that may influence settlement choice in human populations (e.g., Stiner and Kuhn 2016).

IFD models, a type of OFT model developed by Fretwell and Lucas (1969), have been applied in various settings around the world for identifying temporal and ecological trends in population settlement distribution (see Winterhalder et al. 2010; Codding and Jones 2013; Yaworsky and Codding 2018; Hanna and Giovas 2019). IFD stems from the work of Fretwell and Lucas (1969) and operates on the principle of negative density dependence (Winterhalder et al. 2010; Yaworsky and Codding 2018). As population pressures increase, the overall resource quality of that area will degrade, thereby lowering the suitability of that habitat and its likelihood of being settled.

The IFD model, however, is simplistic, and there are biological principles that often violate its assumptions. For example, the Allee effect accounts for temporary improvements in habitat suitability caused by immigrating populations, community aggregation, and habitat modification (Fretwell and Lucas, 1969:19). One example of Allee-effect IFD comes from Neolithic farmers who modified their landscapes to increase agricultural production by clearing forestland (McClure et al. 2009). IFD-Allee models predict that individuals settling lower ranking habitats attract others to follow, thereby abandoning higher suitability areas (Winterhalder et al. 2010:473). As such, the highest suitability areas will have a slightly lower population than medium suitability locations.

There is also a variant of IFD for when access is restricted, and people establish certain controls over resources – ideal despotic distribution (IDD). IDD accounts for differences in competitive ability and resource control (Jazwa et al. 2017). In an IDD model, the opposite pattern of population distribution is expected from IFD, wherein the highest density of individuals will inhabit lower suitability habitats.

Since we currently have limited information about the resource management and land-use practices of these communities or changes in their demography at a fine resolution, we cannot definitively assess whether land-use practices led to degradation of environments as the IDD model posits. IFD models, therefore, are used as a theoretically-framed starting point, rather than IDD, so that we may begin to address this information in a theoretically sufficient manner (*sensu* Lewontin 1974).

Remote sensing and predictive modeling

For this study we use freely downloadable satellite imagery from the European Space Agency Sentinel-2 satellite (<https://scihub.copernicus.eu/dhus/#/home>). This satellite has proven useful for a wide range of disciplines, including archaeology (Agapiou et al. 2014), but its medium-to-low resolution (10m visual and near infrared (NIR), 20m NIR and short-wave infrared (SWIR)) constrains its applicability, including for the documentation and preservation of cultural heritage. Because archaeological deposits on Madagascar's southern coasts are often subtle artifact scatters, Sentinel-2 data do not have the spatial resolution necessary to directly identify these features. However, its resolution is conducive to developing a predictive model of site locations using the theoretical assumptions of IFD. While similar predictive measures have been used by other scholars (e.g., Agapiou et al. 2014; Bennett et al. 2012; Kirk et al. 2016; Lasaponara and Masini 2007), most rely on interpreting vegetative indices for soil and vegetative anomalies, and do not always utilize explicit theoretical models from anthropology.

If our method is successful – and the data conform to an IFD – we expect: 1) that high value areas will contain the greatest proportion, density, and variety of artifacts; 2) these amounts will decrease steadily in Medium, Low, and Null probability areas; and 3) that the settlements located in high probability areas will be older than those in other

locations. The third hypothesis is beyond the scope of the current paper and will be the focus of future research once sufficient temporal data become available.

Processing steps of predictive modeling analysis

1. Based on a review of available archaeological and ethnographic data, we developed a list of important resources and landscape features for communities of the southwest coast (i.e., Douglass 2016; Douglass et al. 2018; Gommery et al. 2011; Pearson 1992, 1997; Tucker 2004; Tucker et al. 2010). These data include locations of coastal archaeological sites identified by surface survey and excavation (Douglass 2016; MAP 2011-2017). Important variables that influence human settlement include: distance from the sea shore; distance from offshore coral reefs; distance from paleodunes; and the vegetative productivity of specific locations.

2. Training samples were created using the 2-D scatterplot function in ENVI to develop a total of 6 landscape classes (Figure 4-2): water, coral, bare soil, shrubs, paleodunes, and dense vegetation (i.e., mangrove forests). This method was used for training sample collection to ensure a minimal amount of spectral overlap between each land class. An initial assessment of the spectral properties of the study area led to the decision to use the NIR, Red, and Green bands (RGB 843) in order to capture the most information pertaining to vegetative health and moisture properties for landscape classification.

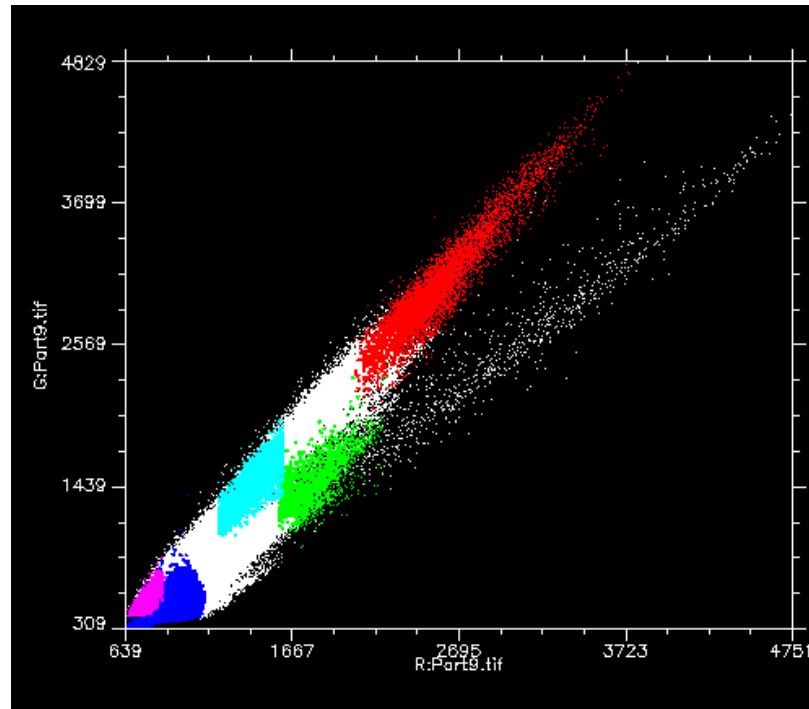


Figure 4-2: A 2-D scatterplot function in ENVI (Exelis Visual Information Solutions 2009). Each land-class can be identified by spectral values and overlaps can be minimized. Red: paleodunes; Green: coral; Cyan: shrubs; Blue: water; Magenta: dense vegetation. All white space is unclassified spectral values within the satellite image.

3. Sentinel-2 images were classified using a support vector machine (SVM) classifier in ENVI 4.7 (Exelis Visual Information Solutions 2009). SVM is a non-parametric classification technique that has gained popularity due to its ability to produce highly accurate classifications using limited training datasets (Mountrakis et al. 2011). The method works by identifying optimal separations between classes and can handle multiple classes simultaneously (Pal and Mather 2005).

4. Coral reefs in some instances were not reliably classified using pixel-based methods (i.e., SVM). We therefore used an object-based image analysis (OBIA) approach with threshold classification (see Davis 2019a; Sevara et al. 2016). Unlike pixel-based methods, object-based methods take shape, texture, and morphology into account to classify image components (Blaschke 2010; Davis 2019; Hay and Castilla 2008). This

same procedure was used to classify the locations of offshore islands, which serve to extend fishing grounds and offer safe-havens for coastal fishers during periods of political instability (Cripps 2009; Douglass 2016:72). OBIA was used to generate shapefiles of offshore island and coral locations using eCognition 9.0.1 (Trimble 2014). Multiresolution segmentation was conducted using a scale parameter of 60, shape parameter of 0.7, and compactness factor of 0.6. These parameters were chosen following trial-and-error, wherein the chosen parameters resulted in the greatest accuracy. Following this step, pixel brightness thresholds were used to extract all image objects located in areas covered by or immediately adjacent to water (as identified by SVM) that matched threshold values for coral or offshore island features. Corals within this region contained brightness values between 600 and 1150 and offshore islands contained values of 1200 or greater. The OBIA results were then assessed manually to eliminate the few errors present throughout the study region.

5. Data generated from the SVM and OBIA classifications were imported into ArcGIS 10.6.1 (ESRI 2020) and underwent several processing steps (Figure 4-3). The water and paleodune classes were extracted into their own raster layers in ArcMap and subjected to Euclidean distance tests. Euclidean distance produces a raster of distance measurements between the input (i.e., water and paleodunes) and the surrounding pixels in an image. Euclidian distance is appropriate, as opposed to a cost-distance analysis, because of the gradual landscape elevation changes in this region. While hills and other topographic features are present, there are no extreme elevation changes within the study region.

6. The final variable incorporated is vegetative productivity. To measure vegetative productivity a SAVI (soil adjusted vegetative index) was used, which takes into consideration soil properties, including moisture content (Huete 1988). Given the extreme

variance in soil reflectance characteristics on Madagascar (see Clark et al. 1998), SAVI was chosen as the most appropriate index, as opposed to NDVI (Normalized Difference Vegetation Index) and others (e.g., simple ratio, leaf area index, etc.; see Jensen 2007:384–385) that decrease in accuracy over large geographic areas with high vegetative diversity (Jensen 2007). SAVI is calculated using the formula:

$$SAVI = \frac{NIR-red}{NIR+red+L} \times (1 + L)$$

where the NIR and red bands are used, and L represents the soil adjustment factor. The best soil adjustment has been demonstrated around L = 0.5 (Huete 1988; also see Jensen 2007) and was chosen for this study. Once calculated, SAVI indices that contained values associated with the presence of shrubs and other vegetation were extracted and we conducted another Euclidean distance function to produce a distance raster of vegetative areas.

7. With all these variables together, we used the following formula to calculate overall probability of early forager settlements in ArcGIS using the raster calculator:

$$P_{Arc} = \left(\frac{1}{d_w} + \frac{1}{d_c} + \frac{1}{d_p} + \frac{1}{d_v} + \frac{1}{d_i} \right) \times 100$$

Where P_{Arc} is the probability of archaeological deposits, d_w is distance from water, d_c is the distance from coral beds, d_s is the distance from paleodunes, d_v is the distance from land with SAVI index values of .35 or better (this value represents the minimum value for shrubland), and d_i represents the distance to offshore islands. Each distance raster was inverted to produce the highest values for the lowest distance from each resource type. Once the index was calculated, we used inverse-distance weighting (IDW) interpolation to fill in gaps in the probability raster up to 100 m using the elevation void fill function in ArcMap 10.6.1 (ESRI 2018).

8. Following the development of our predictive model, we assessed the model's ability to detect *prerecorded* archaeological sites (MAP 2011-2017) and established a sampling strategy for field tests to assess the model's ability to predict the location of *previously unrecorded* cultural deposits. To accomplish this, we first compared the locations of prerecorded sites to the probability values generated by the algorithm. Then, to assess the algorithm's ability to detect previously unrecorded materials, we created a grid of 50m x 50m squares throughout the entire study area (~1400 km²). Each grid was assigned a unique identification number by ArcMap. In Excel, we randomly selected 600 ID numbers using the "randbetween" function. These 600 areas were then checked to ensure they were accessible on foot. Ultimately, a total of 145 areas were selected on the basis of proximity to other points, accessibility, and feasibility of visitation during the 2019 field season. Among the randomly selected grids, 73 contained "high" probability zones, 31 contained "medium probability", and 27 had "low" probability. Surveyors did not have any prior knowledge of the probability of locating sites to ensure an unbiased recording of materials. Table 4-1 shows the quantitative breakdown of these qualitative categories. The remaining 14 areas had null probability values and were chosen to assess false negative results.

Table 4-1: Quantified thresholds of probability index and their qualitative equivalent classifications. Class thresholds were calculated using a Natural Breaks (Jenks 1967) method.

Quantitative Values	Qualitative Ranking Equivalent
Null/Blank	Null
0-5.5	Low
5.5-11.4	Medium
>=11.5	High

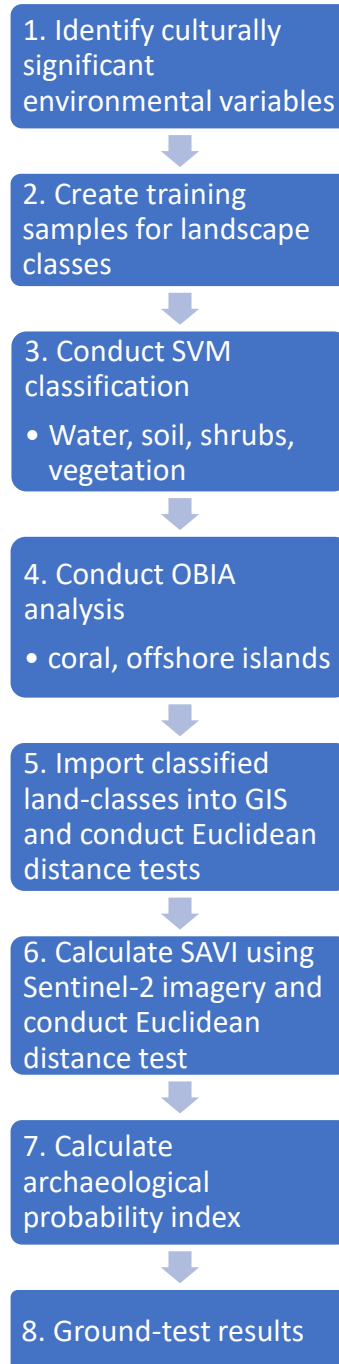


Figure 4-3: Processing steps of predictive modeling analysis.

Together, these methods produced information needed to calculate overall habitat suitability, and by extension, probability of settlement for coastal communities. Based upon the expectations of IFD, the highest suitability (and hence probability) locations will hold

the greatest number of archaeological deposits, with lower suitability areas containing fewer archaeological assemblages.

Results

SVM resulted in 93.6% accuracy (KIA = 0.931) (see Tables 4-2 and 4-3) and OBIA attained an overall accuracy of 97.7% (KIA = 0.914) for the classification of the chosen environmental land-types (Tables 4-4 and 4-5).

Table 4-2: Confusion matrix for SVM classification. Numbers are total ground-testing points.

Class	Mangroves	Dunes	Coral	Water	Forest	Shrubs	Sand/ Bare Ground	Total (# of points)
Mangroves	98876	0	0	0	2297	0	0	101173
Dunes	0	45570	0	0	0	0	343	45913
Coral	0	0	20478	0	0	0	0	20478
Water	0	0	0	126383	0	11	0	126394
Forest	2614	0	0	0	173492	0	138	176244
Shrubs	1	0	0	0	6051	31274	117	37443
Sand/Bare Ground	0	0	0	0	3	839	18103	18945
Total	101491	45570	20478	126383	181843	32124	18701	526590

Table 4-3: Producer's and user's accuracy for SVM classification

Class	Producer Accuracy (%)	User Accuracy (%)
Mangroves	97.42%	97.73%
Dunes	100.00%	99.23%
Coral	100.00%	99.96%

Water	99.99%	100.00%
Forest	95.41%	98.43%
Shrubs	97.32%	83.52%
Sand/Bare Ground	96.80%	95.56%

Table 4-4: Confusion matrix for OBIA classification. Numbers reflect amount of training objects.

Class	Islands	Coral	Total #
Islands	795	8	803
Coral	14	141	155
Total (%)	809	149	958

Table 4-5: User's and Producer's Accuracy for OBIA classification.

Class	Producer's Accuracy (%)	User's Accuracy (%)
Islands	98.3	99.0
Coral	94.6	91.0

Prediction of pre-recorded site locations

Within the entire dataset of prerecorded archaeological deposits (n = 756), we find that only five previously surveyed deposits do not fall within areas identified by the algorithm (Figure 4-4). All of these deposits are located on paleodune features, however, suggesting a strong relationship between this environmental context and human settlement. The model thus reliably predicts the location of *pre-recorded* deposits.

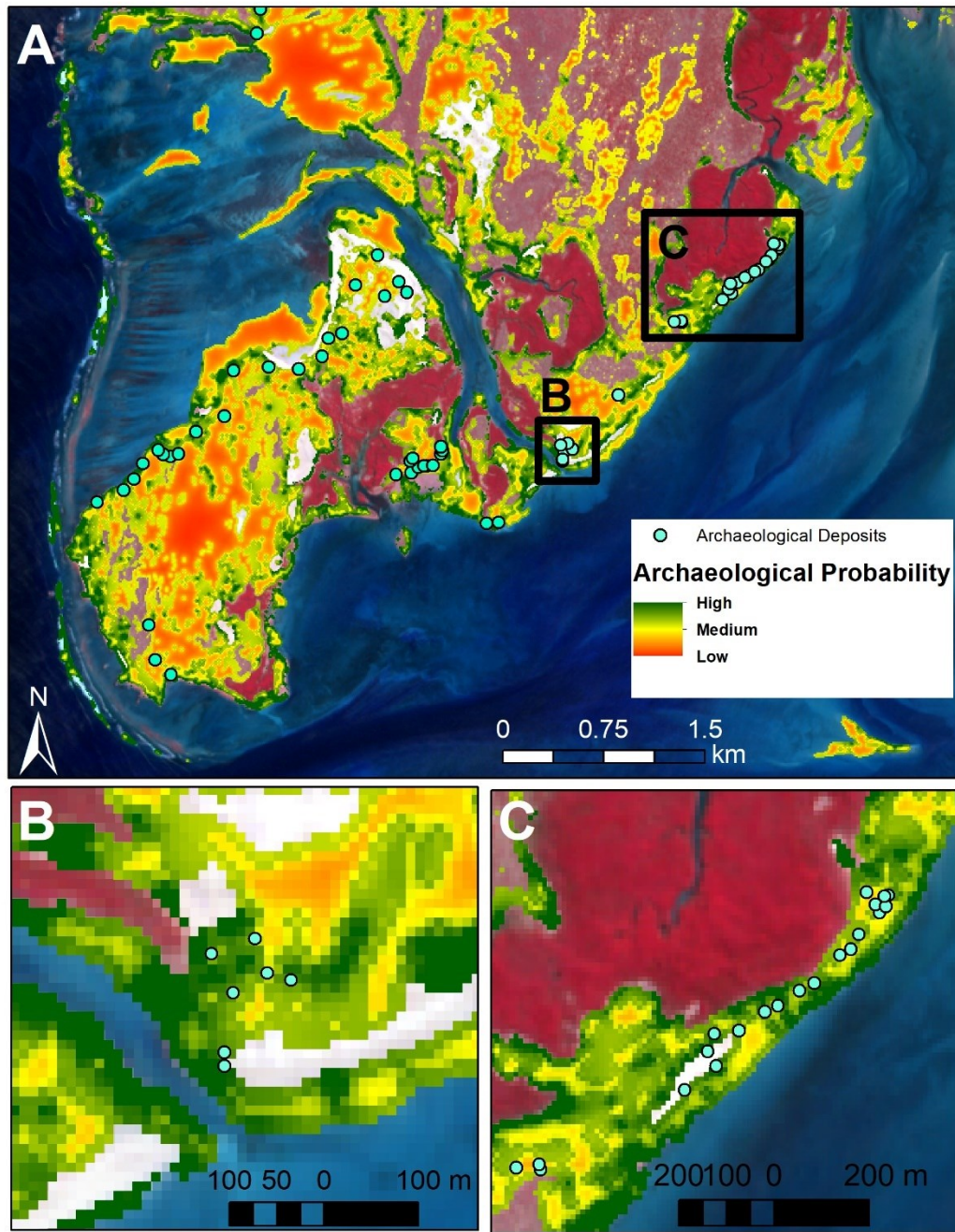


Figure 4-4: Results of Archaeological Probability Index and select pre-recorded sites. A. Sites represent those recorded by recent survey work between 2017 and 2018 and earlier surveys recorded by the MAP between 2011-2018 (see Douglass 2016). B. Shows closeup of a cluster of sites found in map A. C. Shows another cluster of sites in map A. Both clusters (B and C) fall primarily on high and medium values.

Prediction of previously unrecorded site locations

To assess the ability of the model to locate *previously unrecorded* cultural materials, ground surveys were carried out on 71 of the 145 selected sites during the summer of 2019 (Appendix B Supplemental Table B-1). A variety of different materials were recovered during surveys, ranging from ceramics and beads to elephant bird eggshell and marine shells (Table 4-6). When assessing these artifacts, we distinguished between “definitive” and “possible” human presence, with “definitive” referring to materials that were clearly made or altered by people (e.g., ceramics, modified shell, etc.) and “possible” referring to materials that are in direct association with other cultural artifacts or contexts, such as burning activity. The results largely fit the hypothesis that high suitability areas will contain the greatest proportion, density, and variety of artifacts and that these amounts will decrease steadily in Medium, Low, and Null probability areas. However, there is a slight increase in the density of artifacts within medium probability zones, suggesting a possible fit with an IFD with Allee effect model (see Fretwell and Lucas 1969; Figure 4-5).

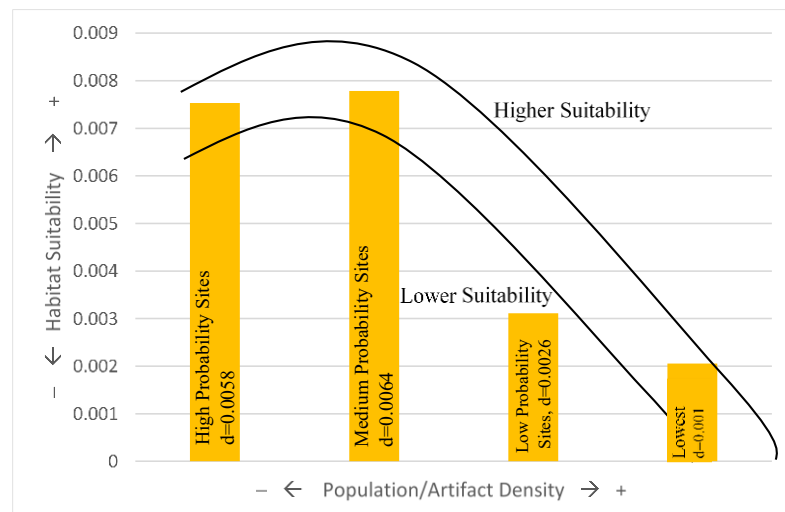


Figure 4-5: Density distribution of artifacts recovered from different probability locations. Black lines represent the IFD-Allee curves, with the top line representing population thresholds for the best habitats, and the second line showing thresholds for less suitable habitats. Temporal data is still needed to confirm conformity to an ideal distribution.

Table 4-6: Sum of survey results by grid probability value. Note, the amount of material increases between each level, with the greatest increase for high probability locations. Lower probability areas still produce artifacts, which is expected, but at lower densities and amounts, as predicted by an ideal free distribution model. The variety of artifacts also decreases with probability.

Grid Probability	Types of artifacts	Charcoal	Eggshell	Marine Shell	Faunal	Ceramics	Beads	Lithics	Botanicals	Glass	Metal	Burnt Stones	Coral	Total Materials Collected
High	9	6	186	204	35	193	26	0	0	0	1	7	1	659
Medium	8	1	88	102	6	129	3	0	0	1	0	1	0	331
Low	5	1	54	41	5	39	0	0	0	0	0	0	0	140
Null	3	0	22	13	1	0	0	0	0	0	0	0	0	36

Grid probability values are an average of raster pixel data. As such, even “high” probability grids may contain values that are lower in likelihood. Therefore, we investigated the precise locations where materials are present to see if individual materials are also accurately predicted by the model. When examining the locations of individual artifacts, we once again find a strong clustering in high probability areas (Table 4-7; Figure 4-6).

Table 4-7: Descriptive statistics of probability values for specific points within survey grids where materials were recovered. The average and most frequently occurring values are high probability, thus coinciding with the grid-level data. Note, these calculations ignore null values.

Statistic	Quantitative Value	Qualitative Value
Minimum	1.69	Low
Maximum	22.96	High
Mode	16.33	High
Mean	12.71	High

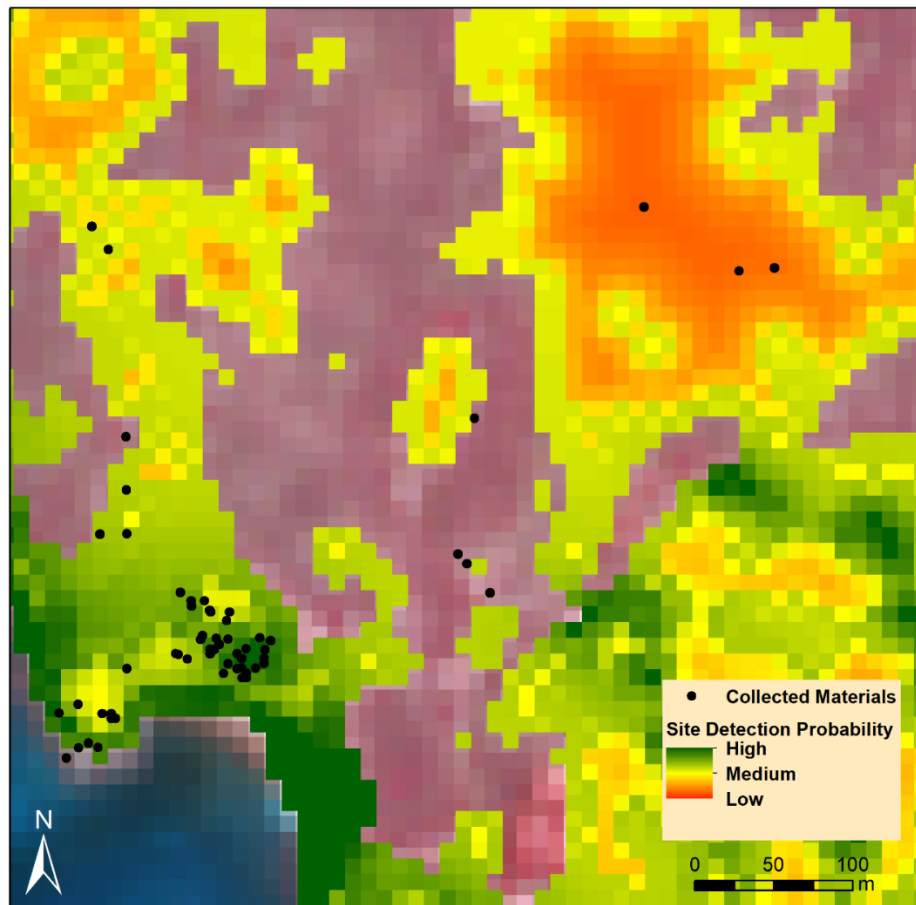


Figure 4-6: Shows the points of some specific materials collected during survey. Note how the greatest clustering takes place on the highest values, and as values decrease the number of materials follows suit.

Discussion

The distribution of materials recovered during pedestrian survey suggests that the immediate coastline is the most densely inhabited area of the study region (Figure 4-1), with material culture abundance (i.e., ceramics, beads, modified shells, etc.) steadily decreasing as one moves inland (Figure 4-7). As indicated in Table 4-6, the diversity of artifacts also decreases in lower suitability areas, suggesting possible limitations for resource acquisition. For example, in high suitability areas, metal and coral artifacts, in addition to beads and other artifact types, are present. However, in medium, low, and null

suitability areas metal and coral were not recovered, and the amount of beads and other artifacts decreases drastically. This raises the possibility that resource access may have been controlled, as the variety of materials is not even across the study region.



Figure 4-7: Shows the locations of artifacts (and clusters of artifacts) recovered from grids visited throughout the study area during July and August of 2019. Definitive human presence is signified by beads, ceramics, and burnt/worked marine shells. Possible

human presence is signified by the presence of shells and faunal remains that are burned, but not worked or modified, and an absence of ceramics or beads.

This preliminary landscape analysis illuminates several possibilities to understand settlement patterns. Archaeological deposits identified here all fall within the expectations of optimal foraging and IFD modeling frameworks. Populations settling the coast of southwest Madagascar appear to have prioritized shoreline ecosystems with ready access to resources that are still valued today. Cultural deposits found further inland are often within flood-zones during the wet season. This pattern coupled with the dearth of cultural materials exceeding 5 km from the modern coastline suggest that settlements are greatly influenced by marine resources.

Furthermore, Allee's principle (Allee and Bowen 1932) argues that community formation can produce increased fitness for a population's survival. Social ties can act as Allee effects because they can foster cooperation between individuals, thereby allowing for resource acquisition to be shared and limiting the burden on smaller groups or individuals. An Allee effect distribution would suggest that coastal foraging populations: a) actively changed and improved the suitability of the areas they inhabited (which has been documented elsewhere: see Freeman and Baggio 2017; McClure et al. 2009; Quintus and Cochrane 2018; Quiros et al. 2017); and/or b) that social networks were strong unifying factors that led to significant population movements as environmental resources shifted.

Additional support for an idealized distribution comes from Kolmogorov-Smirnov (K-S) distribution tests which reveal distinct differences between the archaeological data and other continuous distribution functions (Table 4-8; Figure 4-8; Appendix B Supplemental Code). The data are not normally distributed, nor do they conform to Gamma or Poisson patterns. Gamma distributions are often used to evaluate skewed datasets with positive values (Hogg et al. 2005) and Poisson distributions measure

spacing between randomly occurring events (Haight 1967). The results indicate that archaeological distributions are statistically different from these patterns but are closest to a uniform dispersal.

If comparing a uniform dispersal to an IFD, we can expect that in high suitability areas IFD will have greater densities than uniform distributions, but moderate distributions should be about equal (i.e., densities are distributed rather evenly across moderate suitability spaces). When looking at the comparison between the archaeological and simulated uniform distribution data, the archaeological data mostly matches this expectation. The conformity of the archaeological data to an IFD remains a hypothesis, however, as temporal information is needed. Nonetheless, the results of the K-S tests provide evidence that justifies further research into this question.

Table 4-8: Results of K-S tests between archaeological probability distribution and randomly generated probability distributions. All tests run in R (R Core Team 2020) using the stats package (see Appendix B Supplemental Code).

Compared Distribution	D-value	P-value
Normal	0.83673	< 0.00001
Gamma	0.80823	< 0.00001
Poisson	0.81229	< 0.00001
Uniform	0.13469	0.02438

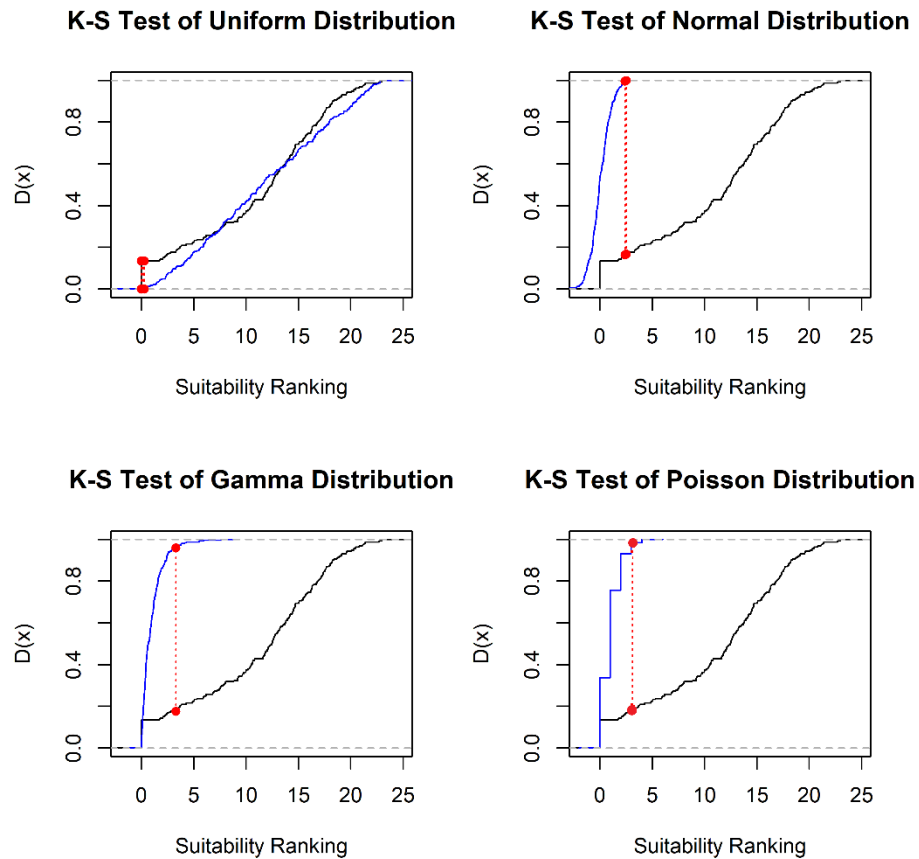


Figure 4-8: Graphical representation of K-S empirical cumulative distribution function (ECDF) curve results reported in Table 4-8. Archaeological data is represented by the black line. Simulated distribution is represented by the blue line. The red dotted line shows the maximum difference between the observed and simulated distributions.

Consistent with findings by Douglass (2016), this study also suggests a relationship in the Velondriake area between possible elephant bird (*Aepyornithidae*) nesting grounds and human settlement locations. Elsewhere on Madagascar associations between cultural contexts and elephant bird eggshell have also been noted (e.g., Parker Pearson et al. 2010; Radimilahy 2011; Battistini and Verin 1972). *Aepyornis* eggshell remains are often located in ancient paleodunes which are present along the coasts of southern Madagascar and are easily visible from medium-to-course resolution

satellite imagery (Clark et al. 1998). The identification and survey of paleodune features is likely to yield exciting new information regarding the interaction between humans and these large avifauna, and the investigation of paleodunes should be prioritized to better understand the processes that contributed to the birds' decline.

Future Work

While the results are highly positive, there is room to improve the predictive power of the algorithm developed here. Future work will look to improve the method by incorporating additional ethnographic and environmental variables that were potentially overlooked, such as groundwater levels. Looking at the results, the greatest density clusters of materials seem to occur in areas closest to offshore islands and on coastlines that contain coves sheltered by rocky coastal barriers. Conducting spatial-statistical tests can reveal the most significant variables for predicting archaeological material and will be the focus of future work.

Furthermore, the results of the surveys carried out under the direction of this remote sensing model will be used to address larger questions concerning human-environmental interaction through time. In particular, future work will integrate settlement pattern data with high resolution paleoecological and paleoclimate records, to enable modeling of human response to climate and environmental change. This will enable researchers to understand settlement and migratory patterns and their connection to environmental conditions. As fieldwork continues, temporal data will become available for many of these newly identified deposits (see Chapter 8). To date, we know that several previously excavated sites dating to ~2500 B.P. (see Douglass 2016) were re-identified as “high” likelihood by our algorithm. This suggests that other contemporaneous – and possibly earlier sites – will emerge as our ground surveys continue.

Based on preliminary analysis of ceramic decorative attributes (see Douglass 2016) recovered during ground surveys, many of the sites identified using this predictive model date to periods between 200-1000 B.P. High probability sites had the greatest range in ceramic styles, signifying longer occupational durations, while low probability sites had fewer ceramics and less variation. There were also many sites with undecorated ceramics, and an absence of ceramics, which tend to signify earlier occupations than those with decorated ceramics (Douglass 2016). Furthermore, these surveys contain only surface deposits, meaning that these dates likely represent the latest materials on sites that were occupied during earlier periods. Seeing as present sea levels were similar to those 3000 – 6000 B.P., with a 2-3m rise between 1000 and 3000 B.P. (Virah-Sawmy et al. 2009), identified sites that are near the modern coastline and lack ceramics may yield information about earlier periods of human settlement that span hundreds-to-thousands of years. Radiocarbon dates from follow-up excavations (reported in Chapter 8) confirm the presence of dense human occupation over the last 300 years and evidence of earlier human activity spanning 800-1200 years, including the presence of lithic traditions that predate ceramics in this region.

Conclusions

The method developed here is already revealing important information pertaining to settlement patterns in Southwest Madagascar. We now have evidence that coastal foragers in the past placed importance on similar environmental resources as contemporary communities. We also have additional evidence of human-megafauna interactions, which will prove useful for understanding extinction patterns and the role of terrestrial resources in coastal community lifeways. Furthermore, we have a systematic dataset that can be used to test hypotheses regarding internal mobility and migration.

Our case study illustrates the utility of HBE theory for framing predictive remote sensing analysis. The protocol described here evaluated the probability of cultural activity at an average rate of ~50 km² per hour of processing time.⁴ With greater processing power, this rate can be increased further, saving time, money, and resources by targeting high probability areas for ground survey. Additionally, all the analyses conducted here use freely available satellite imagery and can be analyzed using open-source software, including QGIS (QGIS Development Team 2018) and R (R Core Team 2020). With greater access to geo-spatial and statistical training, this work can be greatly expanded by other researchers, particularly in regions that are understudied in archaeology.

The acquisition of remote sensing datasets at higher spatial and spectral resolutions will allow researchers to directly identify archaeological deposits on Madagascar, rather than assign general probabilities for where these features are located (e.g., Calleja et al. 2018; Davis et al. 2019; De Laet et al. 2007; Guyot et al. 2018; Lasaponara and Masini 2007; LaRocque et al. 2019; Traviglia and Cottica 2011; Trier et al. 2009; Thabeng et al. 2019). Because remote sensing surveys can often only identify locations of the largest-scale features – and thereby bias our understanding towards specific activities, the use of theoretical models can help to direct ground survey efforts in conjunction with remote sensing data to reduce some of these biases by identifying a greater variety of cultural activities. The method developed here makes it possible to

⁴ This ratio was calculated on the basis of the average time allocation for each section of the study area. The region was divided into 3 parts totaling ~1400 km², with each section requiring approximately 6-8 hours of computer processing time for the SVM classification and another 2 hours of manual processing time to create the final probability map. Total, this procedure can be achieved with high levels of time- and cost-efficiency which can be cut down even further depending upon computing power and processing speeds. Computer used for analysis had an Intel® Core™ i7-4790 CPU @ 3.60 GHz Processor with 32.0 GB of RAM.

identify early deposits on Madagascar which are currently at risk of disappearing due to erosion and sea-level change. We must act quickly to uncover the fragile remains of the earliest settlers of Madagascar, as these components represent an actively disappearing cultural landscape. Threats to cultural heritage from environmental factors such as erosion and sea level rise, are exacerbated by urban development and other anthropogenic factors (Douglass 2016; Parker Pearson et al. 2010; Wright and Rakotoarisoa 2003; Wright 2007).

Uncovering and preserving these data requires an expansion of remote sensing surveys – via satellites, drones, and other instruments – to rapidly and systematically survey vast geographic space. There have been calls in recent years to expand systematic survey of Madagascar’s landscape (Douglass and Zinke 2015; Parker Pearson et al. 2010), including the often-neglected areas inland from the immediate coastline (Douglass et al. 2018). While our study looks at coastal areas in the Southwest, the method can easily be expanded to inland regions of Madagascar.

Note: Supplemental files for this chapter are available in Appendix B and from the Penn State ScholarSphere repository at: <https://doi.org/10.26207/1a47-pw11>.

Chapter 5: Integrating point process models, evolutionary ecology, and traditional knowledge improves landscape archaeology: A case from southwest Madagascar⁵

Predictive modeling has been a staple of landscape-scale archaeological investigations for decades (Bettinger 1980; Custer et al. 1986; Jochim 1976; Judge and Sebastian 1988; Plog and Hill 1971; Verhagen and Whitley 2012). These models are critical not only for the identification of archaeological features but also for better understanding the processes underlying their distributional patterns. The methods employed for the development of predictive models in archaeology are varied and often integrate expert knowledge, geographic information systems (GIS), remote sensing analysis (Custer et al. 1986; Kirk et al. 2016; Klehm et al. 2019), linear regression (Alexakis et al. 2011; van Leusen et al. 2005; Parker 1985; Warren 1990) and other approaches (see refs. (Howey et al. 2016; Verhagen and Whitley 2012)). Other spatial statistical methods can also be used for developing such models, but, to-date, have been underutilized in archaeology. Predictive modeling in archaeology is also often limited by the lack of explicit theoretical frameworks to interpret patterns in the archaeological record (Davis and Douglass 2020; Verhagen and Whitley 2012). As we demonstrate below, the integration of theory from human behavioral ecology (HBE) into predictive models allows us to test hypotheses about processes driving human settlement on a landscape and improve our interpretations of settlement patterns.

⁵ Davis, D. S., DiNapoli, R. J., & Douglass, K. (2020). Integrating point process models, evolutionary ecology, and traditional knowledge improves landscape archaeology: A case from Southwest Madagascar. *Geosciences*. 10(8), 267 <https://www.mdpi.com/2076-3263/10/8/287>.

One example of an underutilized statistical method is point process modeling. Point processes are the mechanisms that produce a point pattern (i.e., spatial distribution of points). Point process models (PPMs) represent a large class of spatially-explicit models that are used to evaluate the underlying processes responsible for different properties of spatial patterns (see (Baddeley et al. 2015)). A core strength of point process modeling is the ability to characterize and distinguish between the effects of the first- and second-order properties of a point process.

A fundamental principle of point pattern analysis is the distinction between the first- and second-order properties of spatial point processes (for a detailed discussion see ref (O'Sullivan and Perry 2013:41–43)). The first-order property is the *intensity* of the underlying process and refers to variability in the density of points across a study region. The intensity includes both the average number of points per unit area and the degree to which density varies with location, which can be spatially variable (i.e., an inhomogeneous process) or constant within a given region (i.e., homogenous process) (Baddeley et al. 2015). On a landscape, the first-order intensity of a point pattern often results from a relationship between the density of a class of points and external variables. For example, freshwater (external variable) may influence the distribution of archaeological materials (class of points) on a landscape, such as increased settlement density near freshwater sources, or the density of trees (class of points) may be influenced by changes in altitude (external variable).

The second-order property is the *interaction* or dependence between points in a point pattern, which results from a process whereby points influence the locations of other points. This second-order property is typically characterized by different degrees of clustering or dispersion. In human settlements, for example, second-order properties can consist of processes related to population interaction (e.g., social or kinship networks, conflict, territoriality, etc.) that might result in different degrees of settlement nucleation or

spacing. As first- and second-order properties are distinct and result from different kinds of processes, distinguishing between these two properties is a major focus of point pattern analysis that is critical for accurately modeling and explaining spatial processes (Baddeley et al. 2015; Bevan, Crema, et al. 2013; DiNapoli et al. 2019; O'Sullivan and Perry 2013).

For instance, it is possible that a first-order trend may be mistaken for second-order interaction simply because points have spatially varying density. In human settlements, for example, we might confuse a first-order trend, such as higher density near water sources, for second-order settlement clustering, when in fact the pattern may be sufficiently accounted for by the first-order effect. It is also possible for a model to under account for settlement clustering or dispersion by not including a second-order interaction component. Thus, attempting to account for the effects of both first- and second-order interaction should be a primary concern in settlement pattern analyses (Carrero-Pazos et al. 2019; Davis, DiNapoli, Sanger, et al. 2020; DiNapoli et al. 2019). PPMs offer a range of statistical tools to better investigate the relative importance of different factors responsible for spatial patterns in the archaeological record, including second-order properties. Thus, PPMs can allow archaeologists to distinguish between first- and second-order effects in settlement patterns even when data on social interaction remain unknown or poorly understood. This is critical particularly in areas where archaeological investigation is still nascent. While the use of PPMs in archaeology as explanatory tools has increased in recent years (Bevan, Jobbová, et al. 2013; Bevan and Conolly 2011; Bevan and Lake 2016; Bevan and Wilson 2013; Brandolini and Carrer 2020; Carrero-Pazos 2019; Carrero-Pazos et al. 2019, 2020; DiNapoli et al. 2019; Eve and Crema 2014; Knitter and Nakoinz 2018; Spencer and Bevan 2018; Vernon et al. 2020a), they are still relatively underutilized, and few studies have explicitly used them for predictive modeling of site distributions (Hamer et al. 2019).

In what follows, we employ and assess the efficacy of PPMs for iteratively refining predictive models for archaeological survey, using southwest Madagascar as a case study. Madagascar is the fourth largest island on Earth and contains a vast archaeological record, but areal coverage through survey or excavation remains limited in many parts of the island. The region is also important for understanding human history, as it sits at the crossroads of a number of major migration routes and trade networks in the Indian Ocean (Beaujard 2007, 2011; Boivin et al. 2013; Radimilahy and Crossland 2015). Despite decades of research, however, there is still significant debate about the timing and nature of the island's initial settlement by people and the subsequent expansion of settlements across the island (Anderson et al. 2018; Douglass, Hixon, et al. 2019; Hansford et al. 2018; Mitchell 2019).

In the southwest of Madagascar, communities traditionally practice a mixed economy consisting of foraging, fishing, herding and farming (Astuti 1995; Iida 2005; Koechlin 1975; Tucker et al. 2010; Yount et al. 2001). Cultural identity in the region is tied to ancestral clan affiliation as well as dominant subsistence practices (Yount et al. 2001). The coastal region is occupied by Vezo (who are primarily fishers), Masikoro (who are primarily agropastoralists), and Mikea (who primarily occupy and forage in the forests further inland) (Koechlin 1975; Yount et al. 2001). While there is evidence that foraging populations were extant on Madagascar for thousands of years (Dewar et al. 2013; Douglass, Hixon, et al. 2019; Hansford et al. 2018), the exact timing of human arrival in the southwest and elsewhere on the island is still subject to intense debate among archaeologists (Anderson et al. 2018; Mitchell 2019). Based upon limited evidence, it is likely that these early human populations were small foraging communities that occupied areas around river valleys (Parker Pearson et al. 2010) and karst landscapes along the island's coasts (Dewar et al. 2013; Douglass 2016). To better understand settlement patterns on the southwest coast, Davis and colleagues (Davis, Andriankaja, et al. 2020)

developed an HBE-based remote sensing/GIS predictive model for locating Late Holocene archaeological deposits in coastal southwestern Madagascar and interpreting their distribution (Figure 5-1).

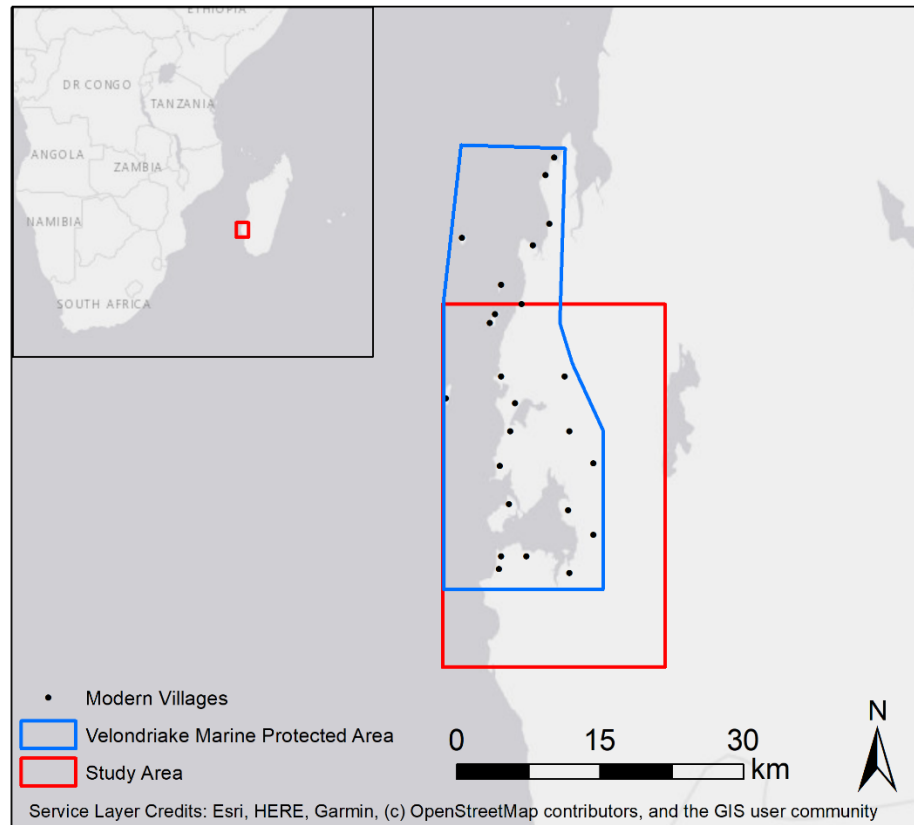


Figure 5-1: Map of study region in Southwest Madagascar. The region contains the Velondriake Marine Protected Area and has been increasingly documented by archaeologists over the past several years.

The model developed by in the previous chapter (Davis, Andriankaja, et al. 2020) is rooted in the ideal-free distribution (IFD) model (Fretwell and Lucas 1969; Weitzel and Coddling 2020). Using the theoretical predictions of an IFD (i.e., communities will first choose to settle the most suitable habitats, identified on the basis of resource availability, followed by lower suitability regions) the team compiled a list of important ecological variables, which were recorded in ethnohistoric records (Douglass et al. In Preparation).

The invaluable insight provided by such traditional ecological knowledge (TEK) has been well established (Cooper and Sheets 2012; Huntington et al. 2004; Lane 2015). In particular, TEK has increased archaeology's ability to inform the present by tracing feedback loops between human behavior and environmental change (Cooper and Duncan 2019; Lefale 2010). They then digitized these features using satellite imagery and automated image analysis procedures and developed a predictive model rooted in the assumption that the closer a point on the landscape is to these resources, the higher the likelihood of people settling these locations (Davis, Andriankaja, et al. 2020). During ground testing of the algorithm (reported in Chapter 4), more than 1000 individual artifacts were recovered from 74 locations throughout the study area in Southwest Madagascar, with most of these materials coming from locations ranked as having a "high probability" of containing archaeological deposits.

Nonetheless, in 20% of instances, the predictive model ranked an area as "high probability" where no archaeological materials were recorded during pedestrian survey. The occurrence of false positives leaves room for improvement in the development of the model and also challenges the starting theoretical assumptions of IFD that framed the model. One overlooked factor is that these false positives may result from the omission of important variables in the construction of the model. Another possibility is that certain resources are more important to populations in this area than others, meaning that a uniformly weighted model may not fit as well as a model where some variables are more highly ranked. Site preservation in this region is quite poor, and so false positives could also be related to the disappearance of archaeological sites or visibility issues due to dense vegetation (especially in regions further inland).

It is also possible that second-order properties (e.g., settlement nucleation or spacing) are leading to greater densities of archaeological material in some areas of high

probability, but not in others, which suggests that first-order trends do not fully account for spatial patterns on this landscape. This would support the possibility raised earlier (Davis, Andriankaja, et al. 2020) of an Allee-effect, or positive density dependence (a second-order property), on the distribution of sites, whereby areas with mid-level suitability will attract greater population densities because of habitat modifications and community aggregation (Bliege Bird et al. 2020; Fretwell and Lucas 1969:19; Winterhalder et al. 2010). Such community aggregation in lower-suitability environments can also be caused by territoriality, as predicted by the ideal despotic distribution (IDD) model (another model centered on second-order properties) (Bell and Winterhalder 2014; Fretwell and Lucas 1969; Jazwa et al. 2017; Summers 2005). Allee-effects and IDD's will result in second-order properties (i.e. clustering) not accounted for by a first-order trend and can be characterized with PPMs.

By iteratively developing and evaluating different models, we can improve their accuracy and be better positioned to explain emerging patterns in the archaeological record (Figure 5-2). In this article, we demonstrate how archaeologists can test the importance of different factors in a model for accurately predicting the location of archaeological deposits. This process allows us to improve the predictive model discussed in the previous chapter (Davis, Andriankaja, et al. 2020) to increase the number of true positive detections while limiting false positives when directing field surveys.

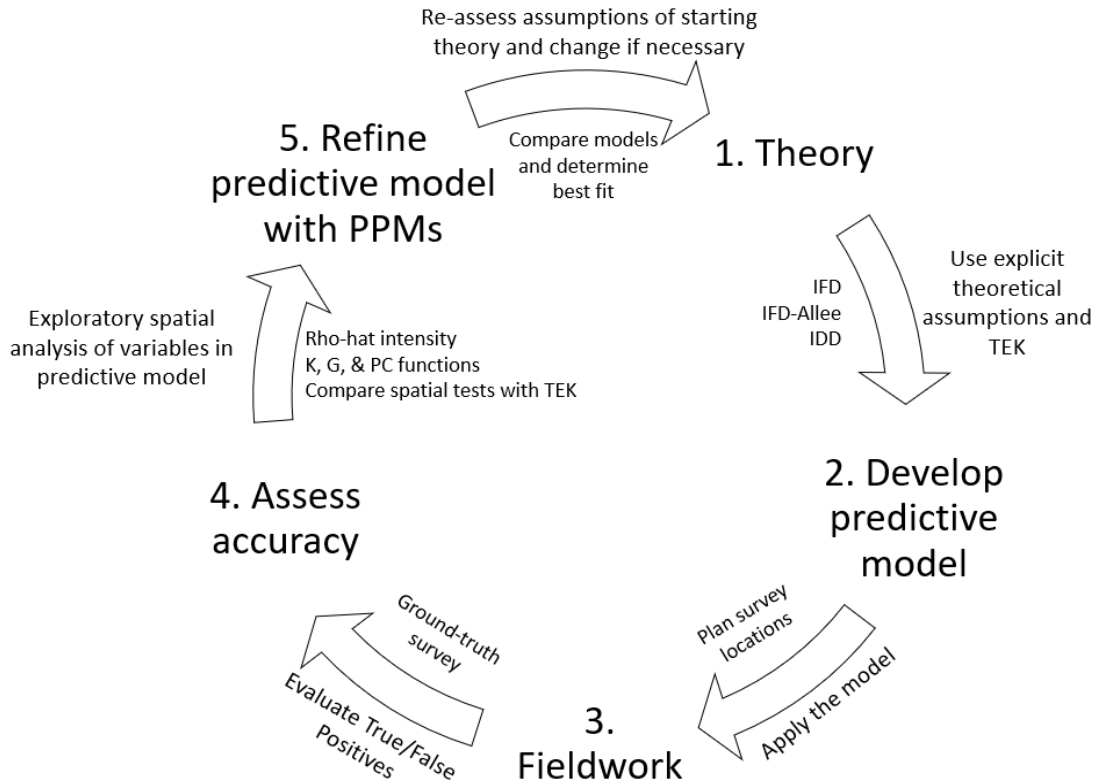


Figure 5-2: Illustration of iterative modeling process. This method permits for simultaneous and constant re-evaluation of the current predictive model and interpretation of the archaeological record.

Building on this previous work by incorporating PPMs allows us to refine the current predictive algorithm for Madagascar and improve its utility for future archaeological investigations. In particular, we demonstrate how PPMs can be used to characterize different environmental variables that predict the first-order intensity of archaeological deposits and also to what degree second-order clustering or dispersion properties improve predictive accuracy. This approach thus aids in understanding the relative importance of different variables and processes responsible for spatial patterns in the archaeological record.

Materials and Methods

To re-evaluate the previous (Davis, Andriankaja, et al. 2020) predictive model, we take the previous set of variables incorporated into this model as well as some new variables that were previously excluded (Table 5-1). The environmental variables used by previously (Davis, Andriankaja, et al. 2020) were generated via automated remote sensing analysis and vegetative index calculations. The same data are used here and are freely available from the Davis et al. (Davis, Andriankaja, et al. 2020) publication's supplemental documents (see Appendix C or <https://doi.org/10.26207/1a47-pw11>).

Table 5-1: List of different variables incorporated in Chapter 4 (Davis, Andriankaja, et al. 2020) and the models developed in this chapter.

Variable	Davis, Andriankaja, et al. (2020)	This Study
Vegetative Productivity	Yes	Yes
Coral Reefs	Yes	Yes
Offshore Islands	Yes	Yes
Distance to the Ocean	Yes	Yes
Paleodunes	Yes	Yes
Rocky outcrops	No	Yes
Depth to bedrock	No	Yes

The algorithm in Chapter 4 (Davis, Andriankaja, et al. 2020) considered the distance from any given point on the landscape to vegetatively productive regions (quantified via soil adjusted vegetation index (SAVI) values (Huete 1988)), paleodune features (where many recorded archaeological sites in this area are located), offshore islands (which were important refuges from warfare and banditry, as well as important fishing grounds), and coral reefs. In addition to these variables, field observations indicate that rocky outcrops along much of the coastline appear associated with the presence of archaeological deposits. This is potentially related to freshwater access (Tucker 2020) as well as defense and survival strategies. Oral histories from coastal dwelling Vezo

communities in the Southwest of Madagascar indicate that limestone outcrops often provide good locations for hiding from marauders (Langley 2006). Ethnographic and archaeological sources also suggest that freshwater availability is particularly important when selecting village locations (Beaujard 2011; Douglass, Walz, et al. 2019; Iida 2005; Langley 2006; Tucker et al. 2010). The outcrops act as rainwater reservoirs and are still used by communities in the region today for gathering freshwater.

Because freshwater source data is not available for the study region, we also use depth to bedrock as a proxy (Fishman et al. 2011; Gabrielli et al. 2012). The shallower the bedrock depth, the closer to the surface, and more accessible, groundwater reservoirs are expected to be. Depth to bedrock and soil data used for our analysis (Hengl et al. 2015) are freely available from the International Soil Reference and Information Centre (ISRIC) Data Hub (<https://data.isric.org/geonetwork/srv/eng/catalog.search#/home>). While groundwater hydrology is far more complicated than a metric of depth to bedrock (Appels et al. 2015; Gabrielli et al. 2012; Hopp and McDonnell 2009), shallow bedrock has been the source of water exploitation for populations in other parts of the world (Brosnan et al. 2018; Fishman et al. 2011). The geology of southwest Madagascar is largely sedimentary, with geologically recent deposits comprised of limestone, sand, and other alluvial soils (Brenan 1972; Douglass 2017).

In order to evaluate the overall importance of first and second-order properties (e.g., Allee effect clustering on the archaeological record, as suggested by (Davis, Andriankaja, et al. 2020)), we use exploratory point pattern analyses and then build a series of PPMs. Archaeological survey data collected over the past several years by the Morombe Archaeological Project (MAP) (Douglass, Morales, et al. 2019) are used as the basis of knowledge about the archaeological record. Archaeological points were recorded as artifact clusters (comprised of a mix of materials including ceramic sherds, marine shell

tools, faunal remains, and charcoal) during survey of the model reported in Chapter 4 (Davis, Andriankaja, et al. 2020), and thus each point can represent multiple artifacts at a given location. If some data points represent a single artifact while others represent multiple artifacts, density calculations and the overall intensity of the point pattern can be affected. To ensure that spatial tests are not being skewed due to this fact, we ran all spatial tests twice, once by incorporating the total number of materials as a spatial weight, and once without weighting, to see if artifact counts had any spatial effects on the point pattern. Survey locations were chosen using a stratified random strategy and surveyors were not given information about the model's predictions of site locations, in order to avoid survey bias.

Point Process Modeling for First-Order Properties

First, we explore first-order trends between the intensity of archaeological deposits in our study area and different covariates (i.e., environmental variables) using nonparametric smoothing (rho-hat function in the *spatstat* package) (Baddeley et al. 2015). The rho-hat function plots the intensity of a point pattern as a function of a given covariate (Baddeley et al. 2015). In other words, the rho-hat function quantifies the degree to which the density of archaeological deposits is related to a specific variable (e.g., how archaeological deposits are accounted for by vegetation).

Next, we investigate whether the settlement pattern in our study area exhibits significant degrees of clustering or dispersion (i.e., second-order interactions) by performing K-, G-, and pair correlation (PC) function tests on the archaeological point pattern. Each of these summary functions assesses the degree of clustering or dispersion in a point pattern but are somewhat distinct. The K-function (Ripley 1977) calculates the average number of points within a specified radius and is standardized by the intensity of those points (i.e., the number of points is divided by the total area encompassed by point

locations). The G-function calculates nearest neighbor distance distribution values for each data point (Baddeley et al. 2015). The PC function assesses whether a point-pattern is significantly more clustered or dispersed than expected for a random pattern, but is not cumulative like the other functions (Baddeley et al. 2015; Stoyan and Stoyan 1994).

The significance of potential clustering or dispersion is assessed by comparing the empirical archaeological patterns to simulated realizations of a random null model. We assess the significance of second-order interaction in these functions using simulation envelopes of a null model of complete spatial randomness (CSR) with 39 Monte Carlo iterations (equivalent to $p = 0.05$). Significant clustering is inferred when the empirical function (i.e., the archaeological point pattern) is above the simulation envelope. Likewise, significant dispersion between points is inferred when the empirical function is below the simulation envelope. Areas of the empirical function within the envelope are consistent with CSR (i.e., not significantly different from a random pattern).

Following these exploratory analyses of first- and second-order properties we develop a series of PPMs, following similar recent applications (Davis, DiNapoli, Sanger, et al. 2020; DiNapoli et al. 2019; Eve and Crema 2014). Our initial PPMs focus on modeling first-order trends and consist of: a homogenous Poisson model (which models the archaeological point pattern as a random process [i.e., CSR]), and two inhomogeneous Poisson models (which model the point pattern as a function of environmental covariates): the Chapter 4 (Davis, Andriankaja, et al. 2020) model and a new model combining all of the assessed environmental variables (see Table 5-1). We identify the best fitting model for the settlement pattern using multi-model selection tools, specifically the Akaike Information Criterion (AIC) and Bayesian Information Criterion (BIC) (Akaike 1974; Burnham and Anderson 2002; Schwarz 1978) and a stepwise selection procedure. These model selection tools evaluate how well a statistical model fits

a dataset given a tradeoff between model fit and overall complexity of the data (Burnham and Anderson 2002). The lower the difference in information criteria score (e.g., ΔAIC and ΔBIC) and the higher the weight (W_i), the better the model. Stepwise selection determines the best fitting model by evaluating how each covariate affects the fit of the overall model and dropping covariates if they result in a higher AIC or BIC score (Venables and Ripley 2002).

We assess the fit between the best-fitting models and the empirical data in multiple ways. We first evaluate the fit by calculating the raw and kernel-smoothed residual values of our best fitting model and the original model (Davis, Andriankaja, et al. 2020) to quantify any deviations between the first-order trend of the fitted model and the empirical data. In other words, the residuals illustrate the goodness-of-fit between the actual locations of archaeological deposits and the locations predicted by the PPM. Raw residuals estimate the bias within a model and kernel-smoothed residuals use a geographically weighted average of the residuals to account for spatial variance in the raw residual values (Baddeley et al. 2005).

We then evaluate the second-order component of the best-fitting models using residual-K and G-functions. These functions assess the fit between the second-order component PPM and the empirical point pattern (i.e., archaeological material distributions) by comparing their K- and G-function estimates with a “compensator”, which is an estimate of the mean value of the K- or G-function (Baddeley et al. 2011). In simpler terms, residual K- and G-functions assess the goodness-of-fit between the predictions of a PPM and the archaeological data in terms of their interpoint relationships (i.e., clustering or dispersion between archaeological points). If the PPM is a good fit to the data, the residual-K and G-functions should lie within the simulation envelope. If the empirical function lies above or below the simulation envelope, this suggests that the empirical pattern is more clustered

or dispersed than is accounted for in the model, respectively. In such cases of poor second-order fit, we can improve the models by explicitly including a second-order interaction clustering or dispersion parameter.

GIS Analysis

Next, using the model selection results of the best-fitting inhomogeneous model, we generate rasterized probability maps (i.e., a series of pixel values situated in geographic space that contain probability values) of places where archaeological sites are expected in ArcGIS 10.7 (ESRI 2020). Using raster maps, we evaluate the probability scores of different regions within the study area directly with locations of identified archaeological deposits. These maps, in turn, can be used to direct further ground surveys in Madagascar. We create different probability maps by assigning differential weights to each covariate in order of their relative importance. We determine differential weighted values for each covariate based on the rho-hat intensity functions and coefficient estimates from the best-fitting PPM. The greater the intensity measurement and the stronger the coefficient estimates, the greater that covariate's effect on the archaeological point distribution. By evaluating the difference in intensity and coefficient estimates associated with each covariate we can establish orders of magnitude by which each covariate influences the resulting archaeological point pattern. These values can then be translated into associated rankings (or weights) for each variable.

For example, in this study we are concerned with the relationship of covariates that explain intensities of archaeological deposits at different distances. As such, if we look at three different variables (A, B, and C) we can examine: 1) whether all three variables are negatively or positively correlated with archaeological points (i.e., as distance from each variable increases, does the number of archaeological materials decrease or increase, respectively) based on coefficient estimates; and 2) the intensity values of the

archaeological points that each variable accounts for based on the rho-hat function and fitted values of the model coefficients. For example, if variable A has a negative relationship with the archaeological point pattern that is three times as strong as variable B, and B is twice as negatively related with C, we can use this information as a guide to which variables are most important. Following evaluation of the fitted coefficients, if variable A accounts for 3-times the intensity of a point pattern at small-distances than B, and B accounts for 2-times the intensity of C, we can weight (or rank) variable A at three times that of B and B at twice that of C.

We create different weighted rasters using the raster calculator tool in ArcGIS. Following the creation of these probability rasters, we assess each model by comparing surveyed locations from 2019 (which were used to test the model in Chapter 4 (Davis, Andriankaja, et al. 2020) with the probability values assigned by the model. If archaeological deposits are recorded in areas that were not predicted (or had low probability values) this indicates a poor fit for that predictive model. In contrast, if deposits are recorded in areas with high probability values, this indicates a better-fitting predictive model. The GIS analysis can be performed in open source platforms as well (e.g., QGIS (QGIS Development Team 2018)), and necessary code used for raster calculations is provided in a Supplemental R-markdown document (Appendix C; <https://www.mdpi.com/2076-3263/10/8/287>).

Ethnographic data are also incorporated into weighting decisions when explicit information pertaining to the importance of resources is available. For example, ethnohistoric records indicate that coastal Vezo communities in southwest Madagascar place great importance on freshwater availability, access to coral reefs and fisheries, and that rock outcrops have served as a defensive strategy for hiding from foreign invaders (Douglass et al. In Preparation; Iida 2005; Koechlin 1975; Langley 2006). Marine and

freshwater resource availability and defensability of the area are a common rationale for settling an area, and the lack of freshwater or defensability are most frequently referenced for why people move (Douglass et al. In Preparation). As such, results from the prior intensity metrics and coefficient estimates are compared with these ethnographic data, and where discrepancies arise (e.g., statistical tests suggest that marine resources are not strongly influencing archaeological points, but ethnohistoric records indicate a strong connection), favor is given to the ethnohistoric data.

Before creating the new probability models in ArcGIS 10.7 (ESRI 2020), the depth to bedrock data is resampled using nearest neighbor interpolation from its original 250m resolution to a resolution of 10m to match the other datasets derived from Sentinel-2 satellite imagery. We resample the dataset iteratively in ArcGIS 10.7 (ESRI 2020) using the resample tool to achieve the best results, from 250m to 10m.⁶ When not resampled, the inclusion of this data into raster calculations makes resulting datasets too coarse to direct meaningful ground investigations (Figure 5-3).

⁶ Resampling was conducted four times, first from 250m to 150m, second from 150m to 75m, third from 75m to 35m, and fourth from 35m to 10m.

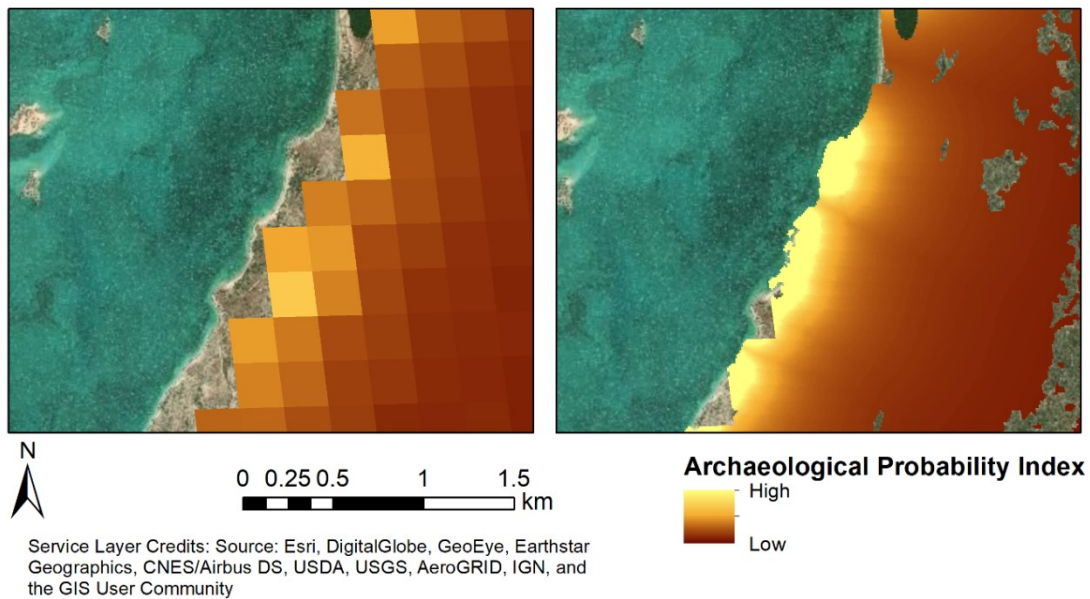


Figure 5-3: Map of unweighted predictive raster with and without re-sampling. Left: shows the unweighted predictive raster without resampling depth to bedrock data from 150m to 10m. Right: shows the results of the unweighted predictive raster after resampling depth to bedrock data from 150m to 10m. Resampling makes the results more easily interpretable, and by extension, usable for archaeological survey.

For all models, we take the inverse of the distances from all variables from any given point within the study area (except for bedrock, which is the depth not the distance). This follows the previous chapter’s (Davis, Andriankaja, et al. 2020) assumption (and the theoretical assumption of IFD) that the closer a point is to these variables the higher the likelihood of human occupation.

Finally, the probability maps are evaluated against each other and the original model in Chapter 4 (Davis, Andriankaja, et al. 2020) to determine the most accurate predictive model for archaeological prospection. Accuracy is calculated based on the same 2019 surveys used to ground-truth the original model (see Davis, Andriankaja, et al. 2020). In all surveyed regions we calculate the probability value assigned by each raster.

Because each raster provides only the probability of archaeological materials, and not a definitive “yes” or “no” to the presence of cultural deposits, we used a natural breaks method (Jenks 1967) to define “true” or “false” negatives and positives based on the threshold between “high”, “medium”, and “low” probability locations. “True positives” are considered as all surveyed locations identified as having “high” likelihood of containing archaeological deposits that did indeed contain artifacts while “false positives” are all surveyed areas identified as “high” likelihood of containing archaeological materials that did not contain any artifacts. Medium and low likelihood areas are not included in these assessments because the algorithm expects that you might find material, but you might not, thus it cannot be counted as a “true” positive or negative. All spatial analyses are conducted in R (R Core Team 2020) using the *spatstat* package (Baddeley et al. 2015) and the code is freely available (see Supplemental File). We also use *MuMIn* (Barton 2019), *maptools* (Bivand and Lewin-Koh 2019), *raster* (Hijmans 2019), *rgdal* (Bivand et al. 2019), *rgeos* (Bivand and Rundel 2019), *sp* (Bivand et al. 2013; Pebesma and Bivand 2005), and *MASS* (Venables and Ripley 2002) packages.

Point Process Modeling for Second-Order Properties

The best-performing weighted raster and the unweighted raster are imported into R and used to create two PPMs with these rasters as the sole covariates. The unweighted raster created in ArcGIS (representing the best-fitting model PPM3) is compared against the weighted model, rather than direct comparison with PPM3 to prevent issues in model selection resulting from differences in the number of covariates. A model with six covariates is inherently more complex than a model with one covariate, which can result in higher AIC/BIC scores for the more complex model.

To assess whether the weighted model is a better fit to the data, we compare it with the unweighted PPM using the same multi-model selection approach detailed above

(Akaike 1974; Burnham and Anderson 2002; Schwarz 1978). We then assess second-order interactions by building new models that include an Area Interaction process, which accounts for clustering or dispersion at multiple scales (Baddeley and van Lieshout 1995). For these area interaction models, the value of the irregular parameter r is selected by minimizing AIC. We construct three PPMs that add this second-order parameter to the original Davis et al. (Davis, Andriankaja, et al. 2020) model, the best-fitting unweighted model, and the best-fitting weighted model. Each of these new PPMs is compared to the other models without second-order properties using multi-model selection. If second-order processes are influencing the archaeological distributional pattern (as predicted by an Allee effect or IDD model), then we expect that the best fitting model will consist of both first-order properties (i.e., environmental variables) and second-order interactions (e.g., clustering).

Results

We first present the rho-hat intensity functions, which measure the first-order intensity of archaeological deposits in relation to specific environmental covariates. We examine these patterns using both weighted and unweighted datasets. Figures 5.4 and 5.5 show that certain covariates have a greater effect on the intensity of the archaeological point pattern. Specifically, bedrock and rocky outcrops have the strongest negative relationship with the intensity of archaeological points (meaning that intensities are highest at lower distances), while the distance to the ocean, dunes, and vegetation values have a weaker negative intensity relationship with archaeological points. These relationships fluctuate, however, as marine resources seem to cycle between increased and decreased intensity over a distance of 250 m. When accounting for the number of artifacts present in each area using a spatial weight, both unweighted (Figure 5-4) and weighted (Figure 5-5)

results present very similar patterns. This suggests that the effects of different covariates are not strongly influenced by artifact count.

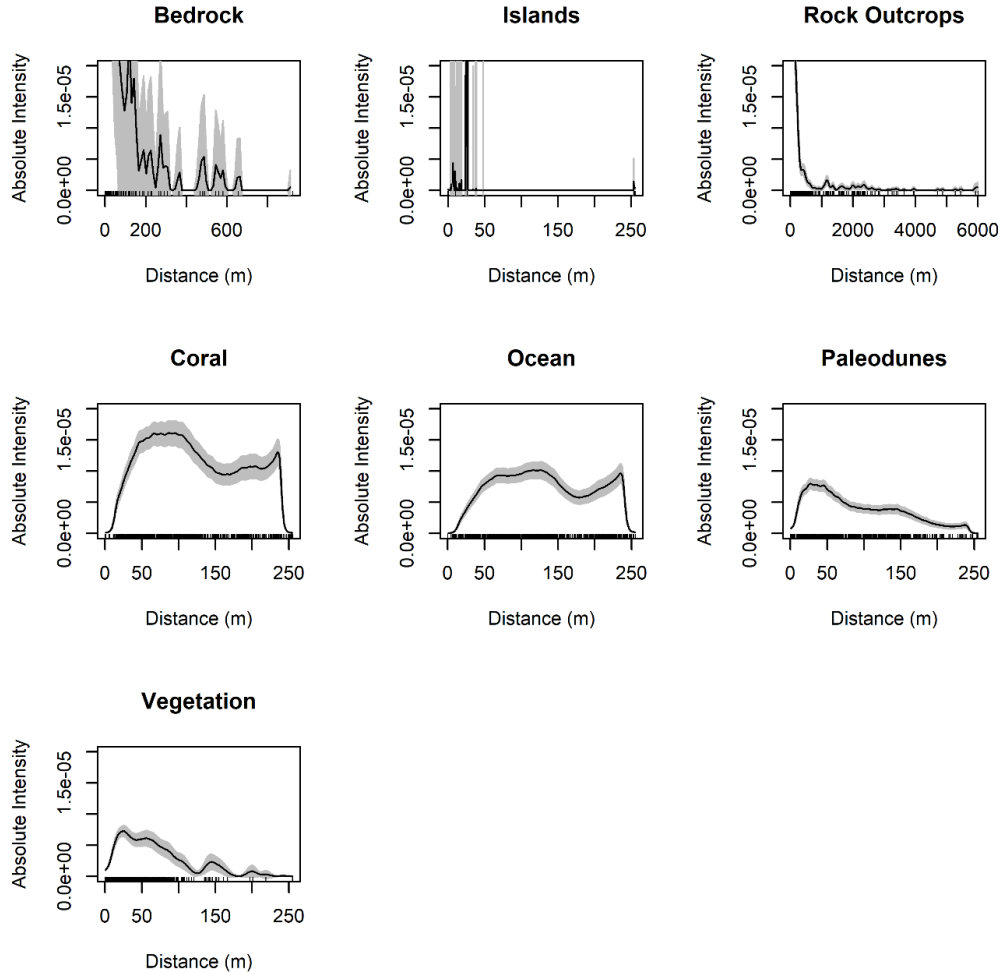


Figure 5-4: First order intensity of archaeological deposits (per m²) as a function of different environmental variables using nonparametric smoothing (rho-hat test). Euclidian distance measurements were used for distance (m) calculations.

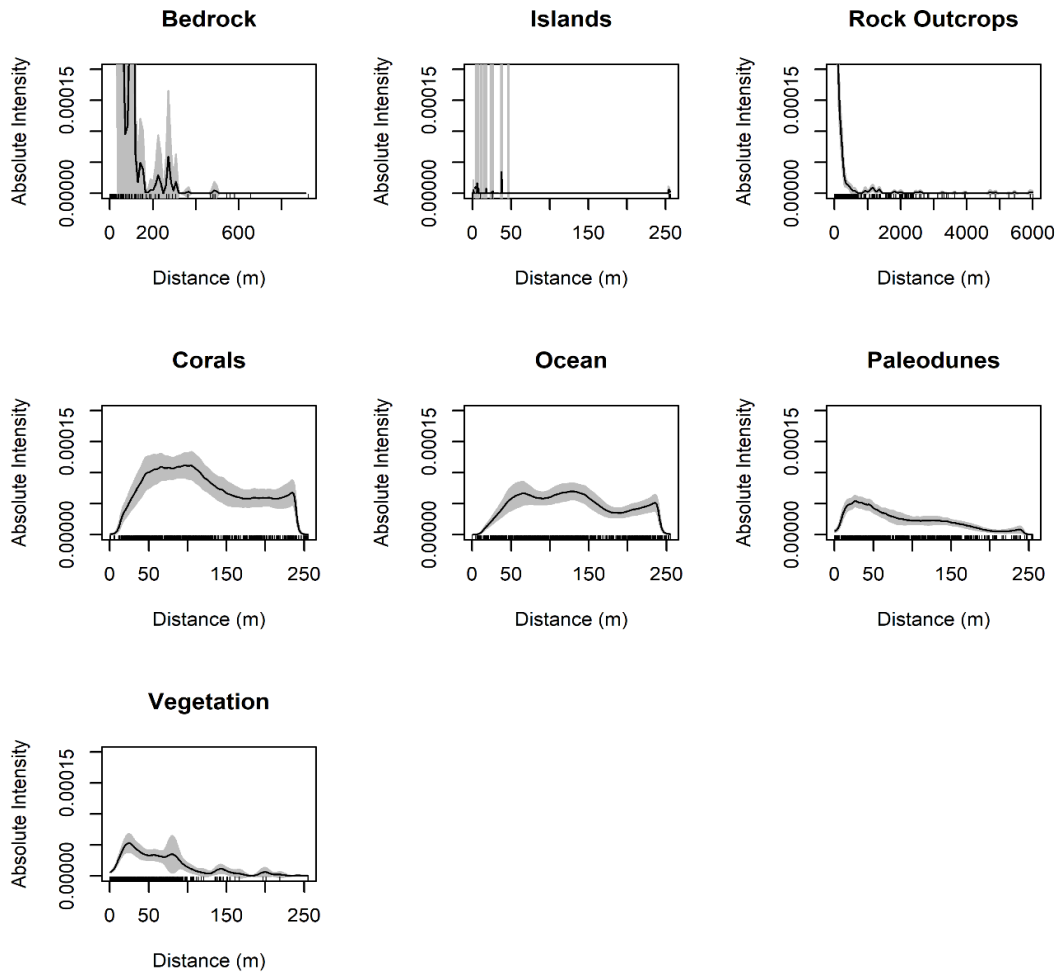


Figure 5-5: First order intensity of archaeological deposits (per m²) weighted by artifact counts as a function of different environmental variables using nonparametric smoothing (rho-hat test). Likewise to the unweighted rho-hat tests, bedrock, islands, and rock outcrops have the highest absolute intensity values, while dunes and vegetation have the lowest.

Figure 5-6 shows the results of K-, G-, and PC-functions that test for second-order interactions in the archaeological data. All tests indicate significant clustering between points ($p = 0.05$). To determine whether spatial intensity is influenced by the amount of material present in a location, we also run these tests using artifact counts as a weighting factor. The results appear identical between weighted and unweighted tests (using artifact

counts as a weight), suggesting that population weights are not significantly influencing the results (also see Supplemental File). As such, we proceed with PPMs that weight each point evenly in terms of artifact counts.

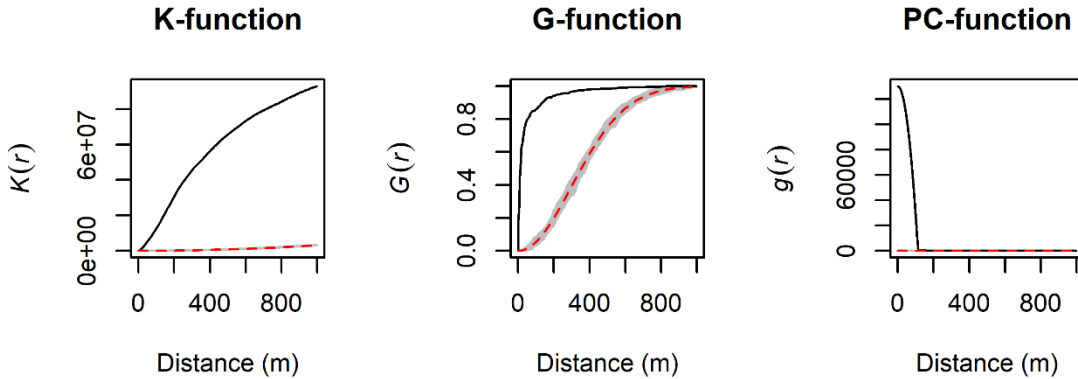


Figure 5-6: Results of testing for second-order interaction using K-, G-, and PC-functions compared to 39 simulated realizations of CSR. Black line is the empirical function for archaeological deposits, the red-dashed lines is the theoretical expectation under the null model of CSR, the grey shaded region is the simulation envelope (equivalent to $p = 0.05$).

Point Process Modeling of First-Order Properties

Table 5-2 shows the results of comparing different inhomogeneous Poisson PPMs. The multi-model selection resulted in mixed results, with AIC indicating PPM3 and BIC indicating PPM4 were the best fitting models. The difference between PPM3 and PPM4 is the inclusion of vegetation in PPM4. To decide on the best fitting model, we assessed the relative fit of PPM3 and PPM4 with PPM1 (the original Davis et al. (Davis, Andriankaja, et al. 2020) model) using residual plots (Figure 5-7). We find that PPM3 and PPM4 are very similar, and both are better models for archaeological settlement distribution than the Davis et al. (Davis, Andriankaja, et al. 2020) model in terms of first-order properties.

Table 5-2: Results of comparing the different inhomogeneous Poisson point process models using ΔAIC , ΔBIC , and their associated weights. PPM3 and PPM4 were the best fitting models according to stepwise model selection using BIC and AIC, respectively. We

chose PPM3 (bold text) because it is the simpler of the two models PPM1 (italicized) represents the Davis et al. (Davis, Andriankaja, et al. 2020) model. Df = degrees of freedom; W_i = information criterion weight value.

Model	Variables	Df	ΔAIC	W_i	ΔBIC	W_i
PPM3	coral, water, islands, rocky shoreline, depth to bedrock	6	1.13	0.256	0	0.848
PPM4	vegetation, coral, water, islands, rocky shoreline, depth to bedrock	7	0	0.452	3.55	0.143
PPM2	vegetation, dunes, coral, water, islands, rocky shoreline, depth to bedrock	8	0.88	0.292	9.12	0.009
<i>PPM1</i>	<i>vegetation, dunes, coral, water, islands</i>	6	3486.97	0	3485.84	0
PPM0	Complete spatial randomness (Poisson Process)	1	6074.78	0	6050.20	0

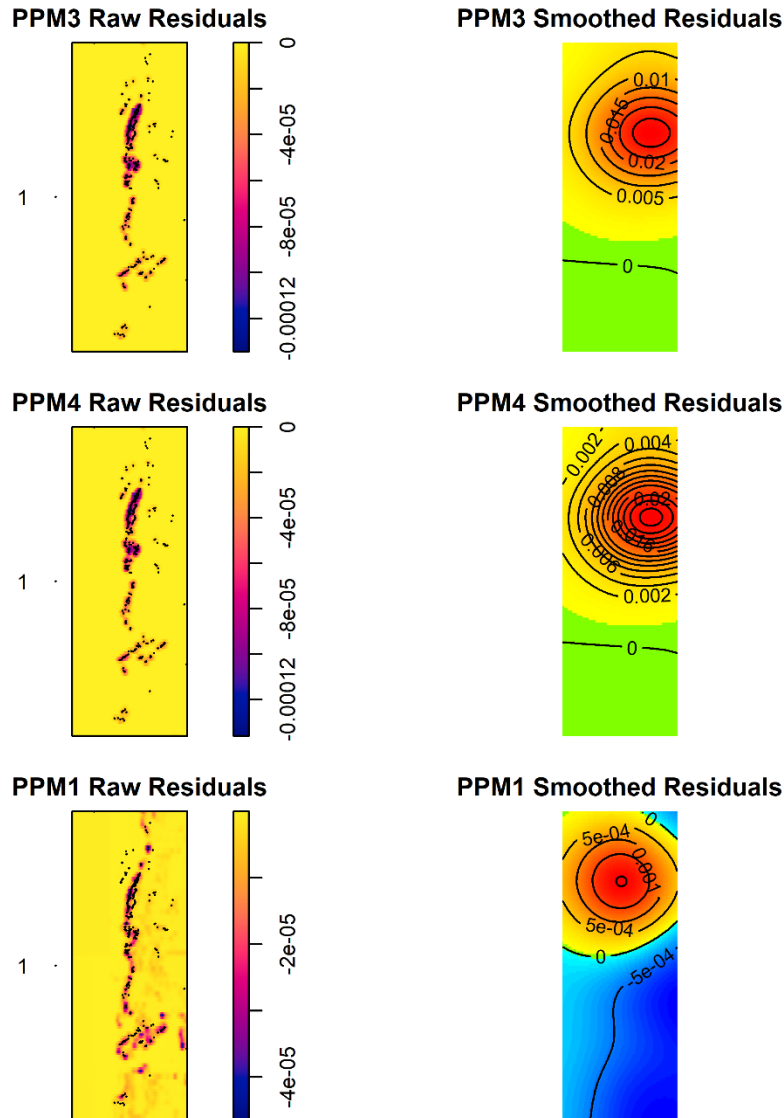


Figure 5-7: Map of raw and kernel-smoothed Pearson residual values of PPM3, PPM4, and PPM1. Note that the smoothed Pearson residuals for PPM3 and PPM4 contain more values of 0 (indicating a better fit), while PPM1 has more values greater than and less than 0, indicating more over- and under-fitting. Archaeological points are overlaid on top of the raw residual maps (black dots).

Finally, we assess PPM3 and PPM4 with PPM1 in terms of second-order properties using residual K- and G-functions. Figure 5-8 shows that both PPM3 and PPM4 are negligible in their difference and both perform better (i.e., are a better fit to the

archaeological data) than PPM1. Nonetheless, both PPM3 and PPM4 underestimate second-order clustering in the data. As such, we chose PPM3 because it is a simpler model (BIC selection chooses the simplest best performing model), we proceed with PPM3 with a $\Delta AIC=1.13$ and $W_i=0.256$ and $\Delta BIC=0$ and $W_i = 0.848$. Table 5-3 shows the covariate estimates for PPM3.

Table 5-3: Results of the chosen best fitting model (PPM3), including the parameter estimates and standard errors with a 95% confidence interval for each covariate. S.E. = standard error. CI95 = 95% confidence interval.

	Estimate	S.E.	CI95 low	CI95 hi	Ztest	Zval
Intercept	-10.3513	0.24798	-10.8373	-9.865255	<0.0001	-41.7427
Coral	-0.0118	0.00133	-0.014358	-0.0092	<0.0001	-8.8633
Water/Ocean	0.0112	0.001354	0.008508	0.0138	<0.0001	8.2433
Offshore Islands	0.0043	0.000952	0.002429	0.0062	<0.0001	4.5132
Rocky outcrops	-0.0004	0.000061	-0.000504	-0.0003	<0.0001	-6.3179
Depth to Bedrock	-0.0205	0.001075	-0.022596	-0.0184	<0.0001	-19.0557

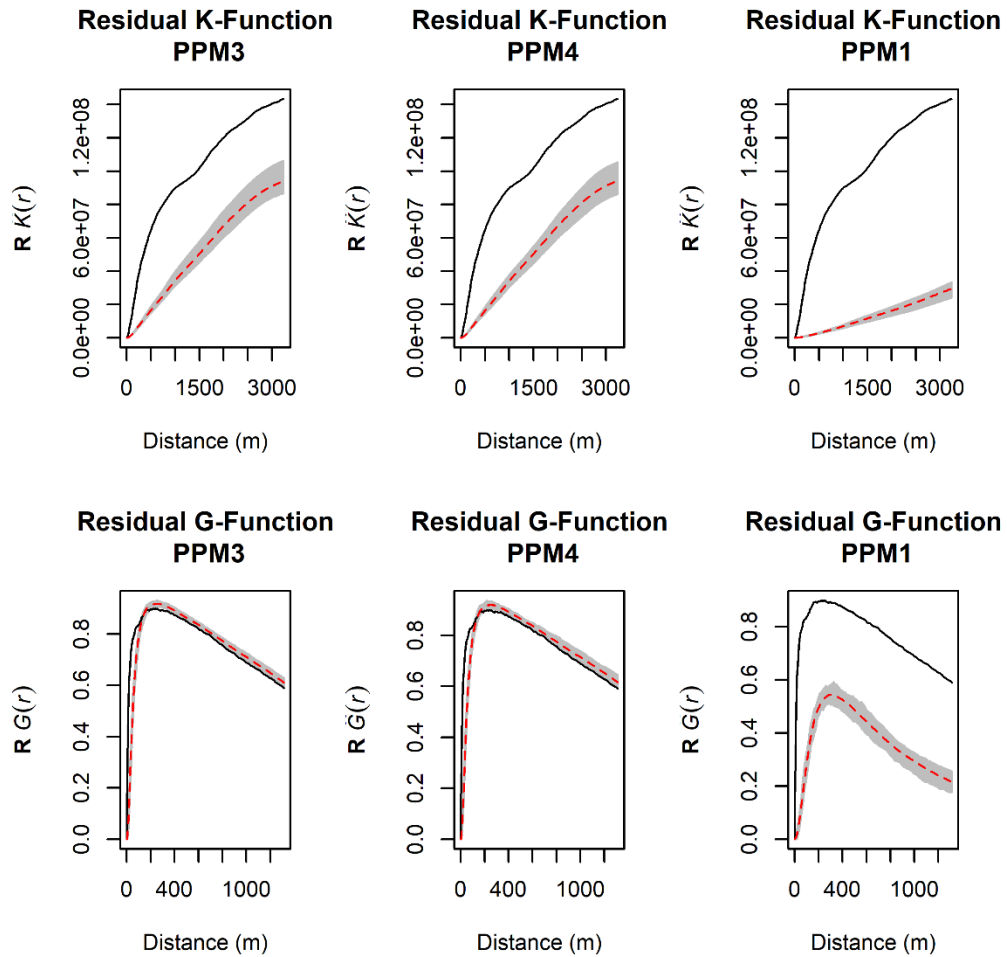


Figure 5-8: Results of the residual K- and G-function tests on PPM1 (the Davis, Andriankaja, et al. (2020) model) and best fitted models PPM3 and PPM4. Both PPM3 and PPM4 perform better than the Davis et al. algorithm, but still overestimate clustering between points at some distances.

GIS Analysis

We re-create the exact PPM developed in R (PPM2) in ArcGIS, where all variables are evenly weighted. The following formula (1) is used in the raster calculator to create the Unweighted Model:

$$P_{arch} = \left(\frac{1}{D_{pth_{BR}} + D_{RO} + D_i + D_C + D_w} \right) \quad (1)$$

Where P_{arch} = the archaeological probability value, D_{pthBR} = depth to bedrock, D_{RO} = distance to rock outcrops, D_i = distance to offshore islands, D_w = distance to water/ocean, D_c = distance to coral.

Next, we create a predictive raster with weights for each of the variables (see Table 5-4). Because the unweighted raster produced fewer true positives than the original Davis et al. (Davis, Andriankaja, et al. 2020) model, we turn to ethnohistoric records and reincorporate paleodunes and vegetation (measured by SAVI), which are known to be important for defense and terrestrial resource acquisition (Koechlin 1975; Langley 2006; Yount et al. 2001). Paleodunes were ranked the lowest by coefficient estimation and rho-hat intensity metrics, and so we weighted all variables based on their relative difference in intensity and coefficient estimates compared to dunes (the lowest ranking variable). As such, paleodunes were weighted at 1, and bedrock was 2.5 (because its coefficient estimates are strongest and rho-hat estimations show that the maximum intensity of bedrock is 2.5-3 times greater than that of paleodunes).

We find that Weighted Model 3 (which has differentially weighted variables) yields more true positive detections than the unweighted model (PPM4) and the original Davis et al. (Davis, Andriankaja, et al. 2020) model (Table 5-4). We also find that by increasing paleodune weights (Weighted Model 4) the results do not change in terms of overall true and false positive detections when compared to Weighted Model 3.

We also assess the quantitative raster probability values assigned at each location of recorded archaeological deposits ($n=1030$) to assess how well individual materials are predicted by the model. The better the model performs, the higher the probability values will be at locations of archaeological deposits. Table 5-5 shows that Weighted Models 1 and 3 achieve the highest predicted values in known locations of archaeological activity, and therefore perform best.

Finally, we create a PPM using Weighted Model 3 as the sole covariate. Model selection indicates that the weighted model is a better fit than the best-fitting unweighted model (PPM3; Table 5-6). We use Weighted Model 3 because it resulted in the greatest number of true positives when assessing 2019 survey results and had the highest average point values (see Tables 5-4 and 5-5). Nonetheless, second-order properties are excluded from this model, and exploratory analysis indicates that second-order properties are influencing the point pattern (Figure 5-6).

Point Process Modeling of Second-Order Properties

Adding a second-order area interaction process into the models produces a substantially better fit (Table 4-6). The best-fitting model combines Weighted Model 3 with an area interaction component (PPM8), with ΔAIC and ΔBIC of 0 and w_i of 1. The unweighted model with area interaction (PPM7) is worse at predicting archaeological patterns than PPM8, with ΔAIC and ΔBIC of >500 and w_i of 0. Weighted Model 3 without area interaction (PPM5) performs substantially worse than PPM8, with ΔAIC and ΔBIC of >2300 and w_i of 0. The residual K-function indicates that the best fitting model (PPM8) still underestimates second-order clustering at distances ≥ 1500 m (Figure 5-9).

Table 5-4: The formulas and respective covariate weights for each predictive model and the results of ground tested results in relation to each modified algorithm. The best performing model (bolded) produces the most true positives and highest overall values in areas with confirmed archaeological deposits (Table 5-5). D_v = distance to vegetation (measured by SAVI), and D_d = distance to paleodunes.

Algorithm	Formula	True Positive (#) ¹	False Positive (#) ¹	# Artifacts (High Prob.)	#Artifacts (Medium Prob.)	# Artifacts (Low Prob.)
Davis et al. (Davis, Andriankaja, et al. 2020)	$P_{arch} = \left(\frac{1}{D_v + D_i + D_c + D_w + D_d} \right)$	29	7	654	332	141
Unweighted Model	$P_{arch} = \left(\frac{1}{D_{pth_{BR}} + D_{RO} + D_i + D_c + D_w} \right)$	28	3	886	102	160
Weighted Model 1	$2.5 \left(\frac{1}{D_{pth_{BR}}} \right) + 2 \left(\frac{1}{D_{RO}} \right) + 2 \left(\frac{1}{D_v} \right) + 1.75 \left(\frac{1}{D_i} \right) + 1.75 \left(\frac{1}{D_c} \right) + 1 \left(\frac{1}{D_w} \right) + 1 \left(\frac{1}{D_d} \right)$	31	7	955	144	49
Weighted Model 2	$3 \left(\frac{1}{D_{pth_{BR}}} \right) + 2.5 \left(\frac{1}{D_{RO}} \right) + 2 \left(\frac{1}{D_v} \right) + +2 \left(\frac{1}{D_c} \right) 1.75 \left(\frac{1}{D_i} \right) + 1 \left(\frac{1}{D_w} \right) + 1 \left(\frac{1}{D_d} \right)$	23	2	813	136	199
Weighted Model 3	$2.5 \left(\frac{1}{D_{pth_{BR}}} \right) + 2 \left(\frac{1}{D_{RO}} \right) + 1.75 \left(\frac{1}{D_v} \right) + 1.5 \left(\frac{1}{D_i} \right) + 1.5 \left(\frac{1}{D_c} \right) + 1 \left(\frac{1}{D_w} \right) + 1 \left(\frac{1}{D_d} \right)$	32	7	957	138	53
Weighted Model 4	$2.5 \left(\frac{1}{D_{pth_{BR}}} \right) + 2 \left(\frac{1}{D_{RO}} \right) + 1.75 \left(\frac{1}{D_v} \right) + +1.75 \left(\frac{1}{D_d} \right) 1.5 \left(\frac{1}{D_i} \right) + 1.5 \left(\frac{1}{D_c} \right) + 1 \left(\frac{1}{D_w} \right)$	32	7	957	138	53

¹ True and false positives are based on “high” probability values (i.e., where the algorithm expects the most material to be found). Medium and low probability values are not considered in these calculations (i.e., the algorithm expects that you might find material, but you might not, thus it cannot be counted as a “true” positive or negative). Qualitative probability scores were derived from a natural breaks method (Jenks 1967) on the generated quantitative values.

Table 5-5: Descriptive statistical values for raster probability values at known archaeological deposit locations (n=1030) for each created predictive model.

Model	Total Average	Median	Mode	Standard Error
Unweighted	0.00924	0.00243	0.00038	0.00024
Weighted 1	0.04769	0.03150	0.01762	0.001486
Weighted 2	0.03182	0.01487	0.00106	0.000992
Weighted 3	0.04769	0.03150	0.01762	0.001486
Weighted 4	0.04467	0.03148	0.01762	0.001392
Weighted 5	0.02545	0.01189	0.00085	0.000793

Table 5-6: Results of comparing 6 PPMs using ΔAIC , ΔBIC , and their associated weights. Four PPMs (5, 6, 7, and 8) are comprised of predictive rasters created in ArcGIS. The other two (PPM0 and PPM9) represent CSR and area interaction processes without environmental covariates. The weighted model with area interaction (a second-order property) performs better than all other models. Df = degrees of freedom; W_i = information criterion weight value.

Model	Variables	Df	ΔAIC	W_i	ΔBIC	W_i
PPM8	Area interaction, Weighted Model 3*	3	0	1	0	1
PPM7	Area interaction, Unweighted Model**	3	507.96	0	508.12	0
PPM5	Weighted Model 3*	2	2376.92	0	2371.23	0
PPM6	Unweighted Model Raster**	2	3230.97	0	3225.28	0
PPM9	Area interaction, CSR	2	7632.29	0	7627.76	0
PPM0	Complete Spatial Randomness (CSR)	1	13174.52	0	13164.1 4	0

* Raster composed of the following variables (weight in parentheses): Bedrock ($w = 2.5$), rocky outcrops ($w = 2$), vegetation (SAVI) ($w = 1.75$), islands ($w = 1.5$), coral ($w = 1.5$), ocean ($w = 1$), paleodunes ($w = 2$).

** Raster composed of the following variables: coral, water, islands, rocky shoreline, depth to bedrock.

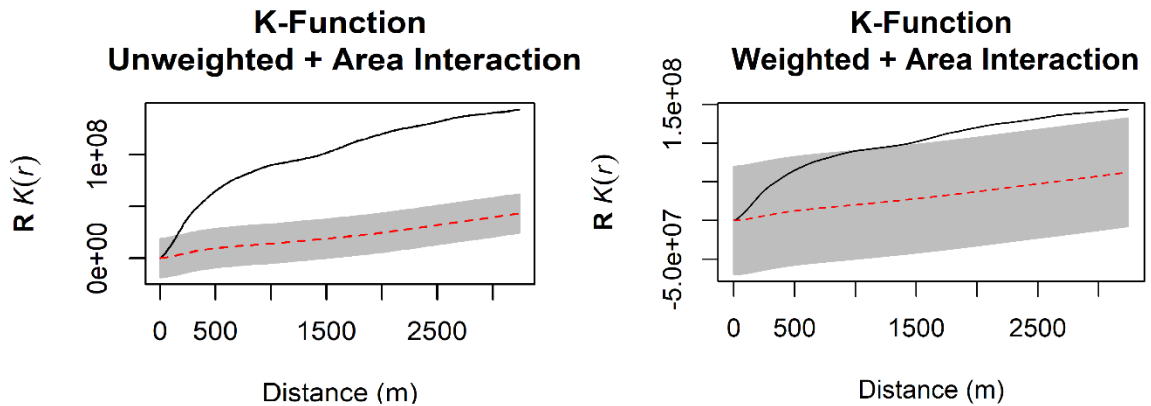


Figure 5-9: Residual K-function test of the best-fitting unweighted PPM with an area interaction parameter and the best-fitting weighted PPM with an area interaction parameter. Both models performed better with area interaction than without, and the weighted model yields the best results.

Discussion

Results of the exploratory analyses indicate that certain environmental variables (e.g., depth to bedrock and rocky outcrops) are strongly influencing the intensity of the archaeological point pattern (i.e., the distributional pattern of past populations) and that second-order clustering is also contributing to the distributional patterns of archaeological deposits. K- and G-tests show clustering at distances up to 800 m while the PC-function indicates clustering up to 100 m. This suggests that there may be multiple scales of clustering.

The PPMs demonstrate that the inclusion of variables related to freshwater and defensive strategies (i.e., depth to bedrock and rocky outcrops) improve the Davis et al. (Davis, Andriankaja, et al. 2020) predictive model. Moreover, the incorporation of differential weights for environmental covariates (derived from exploratory spatial analyses and ethnohistoric records) results in a substantial improvement in the predictive accuracy. The weighted model yields more true positive results and is a better fit to the archaeological data (based on model selection criteria) than the unweighted model. This suggests that covariates do not equally influence “suitability” of locations in the study area.

Instead, freshwater resources and defensible areas are highly important, while vegetation appears less important for settlement choice.

While these first-order models perform well, they underestimate the empirical distribution of archaeological deposits in some portion of the study region, suggesting the influence of some kind of second-order process on the settlement pattern. The addition of a second-order clustering process (i.e., area interaction) results in a substantial improvement to the models, decreasing model selection criteria values by thousands compared to models without second-order properties (Table 5-6). Combined with differential weights for environmental covariates, the settlement pattern in southwest Madagascar is best explained by environmental variables related to freshwater availability and defense, followed by marine resource access, and inter-point clustering between archaeological points at some scales (Figure 5-9).

This conclusion fits well with ethnohistoric data for coastal Vezo communities in Southwest Madagascar (Astuti 1995; Iida 2005; Koechlin 1975; Langley 2006) and provides further support of an Allee-effect distribution (as suggested by (Davis, Andriankaja, et al. 2020)). Thus, we find that PPMs—and second-order properties specifically—are critical for developing and refining predictive models for landscape-scale archaeological research in this area. Nevertheless, the best fitting model is still not a perfect explanation for settlement patterns in this area, as the residual K-function shows higher rates of clustering between points at distances of ≥ 1500 m. This suggests that some additional factor (e.g., land governance, kinship or social networks, etc.) not accounted for by the best-fitting model is causing aggregation in archaeological materials at distances greater than 1500 m. One possibility is that foraging took place by some communities at larger distances from a primary residence, which has been demonstrated ethnographically in this region (Iida 2005; Koechlin 1975).

Our results also contribute, more specifically, to the interpretation of Madagascar's archaeological record. Results in Table 5-4 suggest that archaeological settlement conforms to an ideal-free distribution (either IFD or IFD-Allee) based on the proportion of artifacts recovered from high suitability areas relative to medium and low suitability locations. This supports similar conclusions by Davis et al. (Davis, Andriankaja, et al. 2020). The IFD predicts that as population densities increase in a given habitat, the overall resource quality in that region will decrease (Fretwell and Lucas 1969). This degraded habitat quality, in turn, lowers the suitability of the area for future populations.

In Chapter 4 (Davis, Andriankaja, et al. 2020) we found correspondence between the archaeological settlement of the study region and an alternative model known as IFD-Allee. This model predicts that individuals sometimes benefit by settling less suitable habitats, either socially by attracting others to follow (which offsets predation and increases chances of group survival), or ecologically due to an economy of scale by modifying the surrounding area to increase its resource abundance (e.g., agriculture) (Angulo et al. 2018; Bliege Bird et al. 2020; Winterhalder et al. 2010). In an IFD-Allee distribution, population density can decrease in higher suitability locations and increase in mid-level suitability areas (Winterhalder et al. 2010). Assuming that the same distribution of artifacts throughout the landscape exists as documented in Davis et al. (Davis, Andriankaja, et al. 2020) (i.e., a possible IFD-Allee), a much greater number of materials and archaeological deposits should be detected when applying the predictive model(s) developed here to new surveys in this area. This in turn will help to record at-risk cultural heritage along the coasts of Madagascar, and better understand the archaeology of coastal populations in this region. While our case study focuses on coastal Madagascar, our approach can be applied to other areas as well, as long as the particular covariates included in the model are adjusted for these new contexts.

In terms of the local populations within the study region, there may be very different settlement patterns that our current models do not capture. For example, the new unweighted model (PPM6) suggests that inland dwelling groups may prioritize different resources, creating a series of “higher” suitability zones in areas currently ranked as “low” suitability. This is evidenced by the drop in artifact counts in “medium” probability areas and an increase in artifact counts in “low” probability areas (Table 5-4). This could also be evidence of resource control by certain populations, forcing larger populations into less suitable locations (e.g., IDD (Bell and Winterhalder 2014; Jazwa et al. 2017; Summers 2005).

Additionally, it has been suggested that where subsistence strategies change, environmental proxies for habitat suitability will require modification (Plekhhov and Levine 2020; Vernon et al. 2020b). This is because the variables associated with “suitability” (and their relative importance) change as subsistence strategies shift (e.g., fishing communities will value marine resources more than pastoralists living inland [e.g., (Iida 2005; Koechlin 1975; Yount et al. 2001)]. As such, the differential weights of covariates within a model are likely different across time and space and between scales of interaction. Because the southwest of Madagascar contains a diverse range of foraging strategies (Iida 2005; Langley 2006; Tucker et al. 2010; Yount et al. 2001), this pattern of artifact counts based on suitability could reflect the varied subsistence base in this region (and by extension the fluidity of how “suitability” is defined). This may help explain why the best fitting model (PPM8) still underestimates clustering at larger distances: other local contexts may differ significantly from the overall regional pattern because of fundamental differences in their social or subsistence strategies.

Therefore, defining what constitutes a “suitable” or “unsuitable” location for settlement requires additional information. One important way this can be achieved is by

engaging with local histories and ethnographic research (e.g., Douglass, Morales, et al. 2019; Gallivan et al. 2011; Green et al. 2003; Moser et al. 2002). Our current project provides a good illustration of how such anthropological research methods can improve our knowledge of the past by integrating local knowledge, human behavioral ecology, and spatially explicit modeling approaches. Additionally, such strategies permit for studies of human-environment interaction that go beyond correlation, whereby formalized hypotheses are tested to evaluate associations between different variables (Contreras 2016; Davis 2020a; DiNapoli et al. 2019; Eve and Crema 2014; d'Alpoim Guedes et al. 2016).

One limitation of our study is that our model uses modern environmental data and does not currently include paleoenvironmental information. Numerous studies have demonstrated that environmental and climate conditions have fluctuated in Madagascar over the past several-thousand years (Burney 1999; Godfrey et al. 2019; Hixon et al. 2018; Virah-Sawmy et al. 2010). As such, some of our variables (i.e., depth to bedrock), are likely to have been quite similar several thousand years ago while others (i.e., vegetative index values, paleodune features) were potentially quite different. Paleodunes contain many archaeological deposits, today, and so they are a direct proxy for past cultural activity, but vegetative health is potentially more problematic. Future work should thus focus on better integration of paleoclimate proxies matching the temporal placement of the archaeological materials identified. In the meantime, however, our results still provide a successful method for improving detection rates of archaeological deposits, even in the absence of paleoenvironmental data.

A second limitation is that we currently lack temporal information pertaining to the archaeological materials used for our analysis. Work is ongoing to acquire chronological data for these areas, but without this information we cannot extend our analysis to

investigating changes in resource use over time. This will form the basis of our future work. Currently, we can specify that some of the earliest archaeological deposits in this region (that have associated radiocarbon data) date to ~2000-3000 B.P. (Douglass 2016). More information is needed, however, to fully understand settlement chronologies of this region.

A final limitation is that we make no distinctions between artifact classes within the point pattern. Different artifact types (e.g., ceramics versus shell tools) may alter the best fitting PPM and provide insight into how specific activities differ across the study area. In the same vein, differences in site function (e.g., permanent settlement, seasonal foraging camp, etc.) will likely affect results of spatial analyses, as peoples' considerations will differ based upon the nature of what they plan to do (and how long they plan to stay) in a given location. Despite these limitations, the method presented here proves useful for planning fieldwork with respect to choosing areas for archaeological survey. Furthermore, our study provides a template of how predictive modeling and landscape archaeology can be improved using an iterative process of investigating the past.

Conclusions

Predictive modeling in archaeology has a long history, and has resulted in great improvements in archaeological settlement studies around the world (Altschul 1988; Green 1973; Hamer et al. 2019; Jochim 1976; Judge and Sebastian 1988; Kvamme 1983; van Leusen et al. 2005; Parker 1985; Plog and Hill 1971). Spatial statistical models can improve predictive algorithms and aid in survey projects, whereby the most probable locations for discovering archaeological deposits can be targeted. PPMs are one such spatial method that can substantially improve predictive modeling efforts for archaeological fieldwork given their ability to more fully characterize the fundamental properties of point patterns.

Our results led to the creation of several new archaeological predictive models, some of which resulted in a reduction of false positives during field assessment. Depending upon the purpose of the research, these models may be preferred. Aerial recording of Madagascar's archaeological landscape remains limited, and this results in researchers not having a firm understanding of where many archaeological materials are located (Davis, Andriankaja, et al. 2020). For this reason, we chose the model that resulted in the greatest number of true positives. It stands to reason that a few more false detections are a good tradeoff for a large increase in true detections when the goal is to detect as many new cultural materials as possible. In other research programs it very well might be more beneficial to reduce false positives at the expense of true positives, as false positives and negatives can assist in re-evaluating prior hypotheses pertaining to archaeological settlement patterns. Given the nature of our analysis, however, evaluating false negatives is difficult, as there are no definitive locations where the model predicts a total absence of archaeological materials. Nonetheless, researchers who utilize this method (or similar approaches) should investigate "low" probability locations with the same rigor as "high" probability areas to ensure that surveys are not biased based on initial model assumptions, which, as we demonstrate here, sometimes require adjustments.

Our study also demonstrates how the importance of different variables can be incorporated as weights within a predictive model using the results of spatial modeling procedures. By integrating ethnohistoric data with statistical model-selection, we improve our understanding of what constitutes a "suitable" environment (*sensu* HBE expectations from an IFD model) and increase the number of true positive identifications of archaeological materials during fieldwork. As such, we argue that archaeological survey procedures can be greatly enhanced by replicating the methods developed here. To

facilitate this, all code required for performing the necessary spatial statistical tests are provided as supplemental files.

Ultimately, this study can serve as a template for future settlement pattern analyses using an iterative archaeological assessment. We combine robust statistical analyses, landscape scale data (via remote sensing), and traditional knowledge with explicit theoretical frameworks to account for fundamental aspects of archaeological settlement distributions. The use of PPMs allows researchers to investigate important second-order properties that are often ignored by other predictive modeling efforts. The procedure we advocate here (Figure 5-2) allows for a continuous learning process whereby archaeologists can evaluate different hypotheses and subsequently refine those hypotheses to improve our understanding of the past. We hope that future archaeologists find this process useful for framing future landscape scale studies of past human behavior.

Note: Supplemental files for this chapter are available in Appendix C and at: <https://doi.org/10.3390/geosciences10080287>.

Chapter 6: Remote Sensing Reveals Lasting Legacies of Land-Use by Small-Scale Communities in the southwestern Indian Ocean⁷

Among archaeologists, the identification and quantification of feedbacks between past human activities and landscape-scale transformations have historically focused on economies of scale that generate highly visible changes to landscapes (e.g., monumental architecture, intensive agriculture, shifts from forests to grasslands, etc.). In contrast, activities associated with small-scale mobile foraging economies have generally been portrayed as “low impact” (Smith 2001; Stephens et al. 2019). In regions around the world, like the Amazon, this line of thought has been compounded by legacies of settler colonialism and the processes of industrialization of land and resource use, resulting in narratives that downplay, obscure, or erase earlier (and subtler) traces of human landscape use (Douglass and Cooper 2020; Heckenberger and Neves 2009). Uses of remote sensing technology (i.e., satellite images) in such contexts have successfully identified these “low-impact” signatures of human action on large geographic scales (Lombardo and Prümers 2010). While predictive models have been used around the world to narrow the search for ephemeral archaeological deposits (Davis, Andriankaja, et al. 2020; Kirk et al. 2016; McMichael et al. 2014), the use of automated remote sensing in archaeology remains skewed toward landscape modifications that are easy to identify because of their lasting marks and effects (Davis 2021; Tarolli et al. 2019).

Prior remote sensing analyses on Madagascar have focused on the drivers of settlement and mobility (e.g., resource availability and social aggregation) using predictive models based on satellite-derived environmental information and statistical modeling (Davis et al. 2020; Davis, DiNapoli, and Douglass 2020). To fully understand settlement

⁷ Davis, D. S., & Douglass, K. (2021). Remote Sensing Reveals Lasting Legacies of Land-Use by Small-Scale Communities in the southwestern Indian Ocean. *Frontiers in Ecology and Evolution*, 9, 689399. DOI: 10.3389/fevo.2021.689399.

patterns, however, we must also look at the ecological effects of human occupation (Figure 6-1). Therefore, in this paper, we focus on identifying and characterizing legacies of forager activities and coastal settlement on the landscape of the Velondriake Marine Protected Area of southwest Madagascar, a region with a history of coastal foraging that extends back at least to 2000 cal. year BP (Figure 6-2; Douglass et al. 2019). The climate of southwest of Madagascar is defined by a wet season and a dry season. The region is extremely arid, receiving less than 50cm of rainfall annually, and is home to highly endemic flora and fauna which varies according to the underlying geology (Douglass and Zinke 2015). The Velondriake region sits on a Quaternary dune system composed of sandy-shell and limestone coastal rock outcrops, while further inland the geology is characterized by Pleistocene and Eocene geological systems (Besairie 1964). Vegetation in Velondriake is largely xerophytic and classified as a “spiny thicket” ecoregion, which contains some of the highest levels of endemic flora on the island (Gautier and Goodman 2003). The people living in coastal Velondriake today primarily identify as *Vezo* (roughly translated as “to paddle”) and center their livelihood on the sea (Astuti 1995). The area has been inhabited for thousands of years by communities practicing foraging and fishing, as well as agropastoralism over the past several hundred years (Douglass et al. 2018; Hixon, Douglass, et al. 2021).

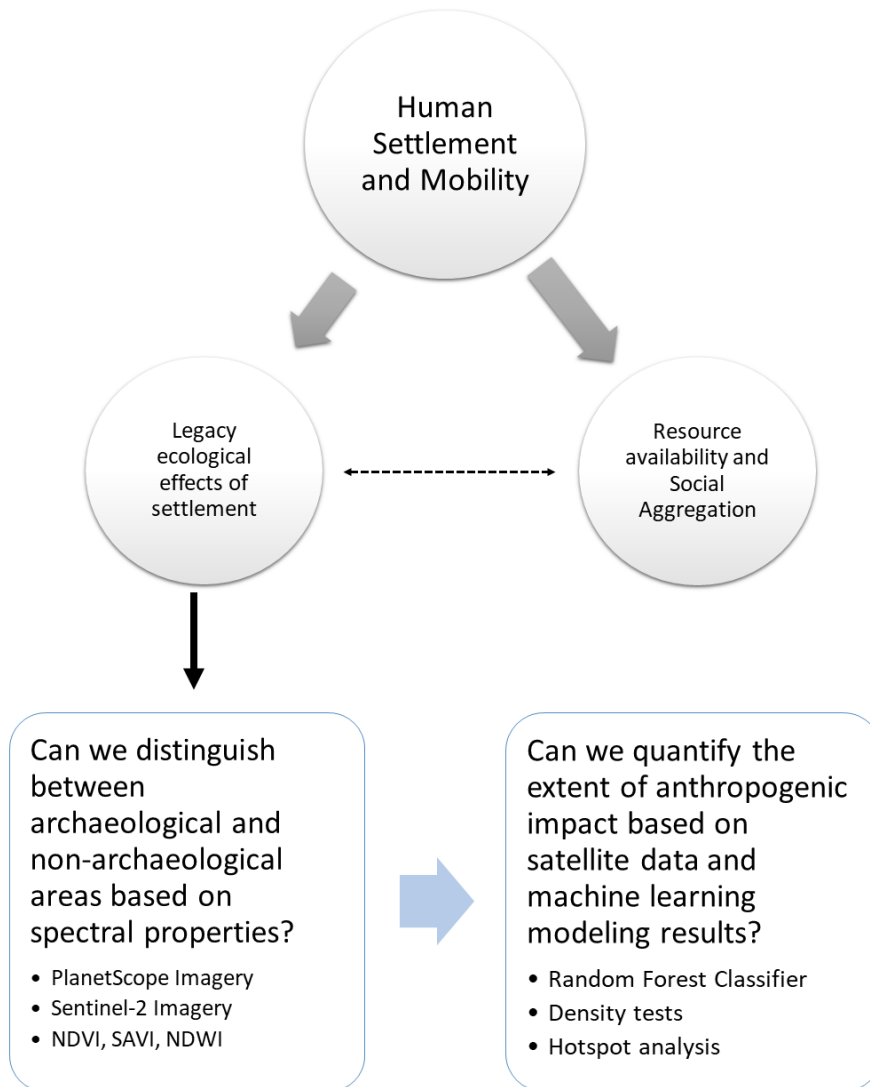


Figure 6-1: Illustrates the methodological workflow presented in this article. The central question of human settlement and mobility patterns is investigated in Chapter’s 1 and 2 (Davis et al. 2020; Davis, DiNapoli, and Douglass 2020) as a consequence of resource availability and social aggregation. The results of this prior work feed directly into this article, and vis versa (indicated by dashed arrow). Within this paper we evaluate whether we can distinguish between archaeological and non-archaeological areas recorded in our previous work based on spectral properties (including vegetative indices). Then, we use these results to train a machine learning classifier to quantify the extent of anthropogenic impacts.

In this article, we investigate whether the ancient communities inhabiting the Velondriake region in southwest Madagascar significantly modified their landscape in ways that persist into the present. Specifically, we hypothesize that lasting changes in vegetative communities and soil chemistry are legacies of fitness-enhancing activities that

have landscape-scale effects. We further demonstrate that these legacies can be systematically characterized using remote sensing and machine learning techniques. Machine learning, specifically probability-based methods (e.g., Breiman 2001; Malley et al. 2012), allow us to systematically evaluate the likelihood of anthropogenic disturbance across large geographic spaces based on the geophysical properties identified in remotely sensed data. We look at geophysical properties of vegetation and soil as a palimpsest resulting from movement, settlement, and resource use over thousands of years. We then compare these landscape signatures between locations with and without material culture surface scatters to assess cumulative anthropogenic effects on the landscape. Our expectation is that places where people settled or engaged in sustained land-use will exhibit significantly different patterns in vegetative and soil properties when compared to locations with no evidence of archaeological settlement.

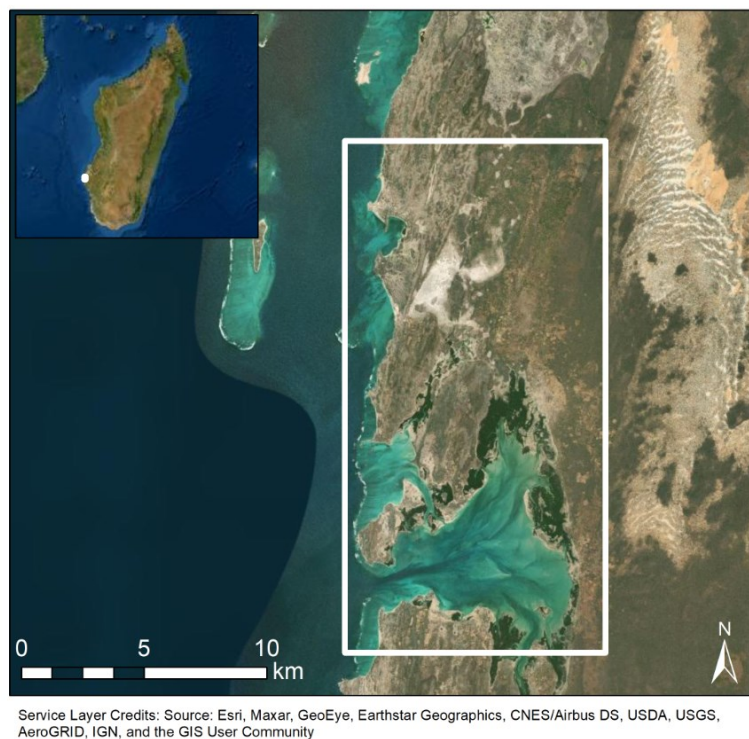


Figure 6-2: Map of the study region (white box).

While the exact timing of the initial peopling of Madagascar is hotly debated (e.g., Anderson et al. 2018; Douglass et al. 2019; Hansford et al. 2020; Mitchell 2020), coastal foraging has a long history on the island (e.g., Barret 1985; Douglass 2016; Douglass et al. 2018; Dewar et al. 2013; Rakotozafy 1996), and predates evidence for the introduction of farming and herding lifeways (Domic et al. In Review; Godfrey et al. 2019; Hixon, Douglass, et al. 2021). The debate over Madagascar's human settlement has been central to questions of anthropogenic impact on the island, notably via activities that may have contributed to the extinction of endemic fauna (Godfrey and Douglass in press). Theories regarding anthropogenic drivers of extinction include potential overhunting, habitat modification, and forms of direct or indirect competition between endemic and introduced animals (Burney 1997, 1999; Dewar 1984, 1997; Godfrey et al. 2019; Hixon et al. 2018). Teasing apart drivers of extinction requires further clarification of anthropogenic landscape change, including in regions with long histories of foraging and the management of wild resources. Madagascar is also known for its long history of climatic variability (e.g., Douglass and Zinke 2015; Dewar and Richard 2007). As climate change impacts intensify today, studies of how past populations modified landscapes to mitigate the impacts of resource scarcity and climate variability are vital for promoting sustainability (Douglass and Cooper 2020; Douglass and Rasolondrainy 2021; Razanatsoa et al. in press). However, most archaeological sites that retain information about resource use and adaptation by early mobile communities of foragers and herders consist of ephemeral artifact surface scatters and are actively disappearing due to erosion and development (Davis, DiNapoli, and Douglass 2020; Parker Pearson 2010). Innovative approaches are thus particularly needed to clarify human-environment dynamics during the earliest phases of Madagascar's human settlement and in regions vulnerable to loss or erosion of cultural landscapes.

Niche Construction and the Legacy of Land-Use Practices

Anthropologists interested in the effects that humans have on their environment and the two-way feedbacks in socio-ecological systems have productively integrated Niche Construction Theory (NCT) (Fuentes 2016; Laland and O'Brien 2010; Zeder 2016). NCT, which stems from evolutionary biology, stresses that organisms actively modify the selective pressures in their environment in order to increase their fitness. In doing so, all organisms contribute to feedbacks that influence and alter the niches of other organisms that share those same spaces (Laland and O'Brien 2010; Odling-Smee, Laland, and Feldman 2003). It should be emphasized that many of the concepts of NCT borrow from related concepts previously described by evolutionary biologists (see Spengler 2021), such as environmental engineering (e.g., Jones, Lawton, and Shachak 1994; Jones et al. 2010) – central to the work presented here. NCT has guided investigations of how “low impact” human activities create niches by altering the distribution and abundance of flora and fauna in ways that enhance human livelihoods (Rowley-Conwy and Layton 2011). Prior work shows that many such niche construction activities are identifiable through soil changes (Smith 2001) and alterations to vegetation (e.g., modification of trees) (Mobley and Eldridge 1992; Oliver 2007). Investigations of cultural landscapes further demonstrate how humans intentionally manipulate soil chemistry and vegetative growth patterns (Lightfoot et al. 2013). Such niche construction activities have landscape-scale effects that are difficult to assess using site-based approaches alone. Furthermore, taphonomic processes and other destructive forces can disproportionately affect the remains of ephemeral sites (i.e., foraging camps) and evidence for landscape management by “low impact” communities with high levels of mobility (Iovita et al. 2021; Smith 2001). Applications of NCT and related evolutionary frameworks to landscapes shaped by foraging economies have also revealed feedbacks between human use of fire, biodiversity, and resilience to climate change (Bliege Bird et al. 2008, 2020; Bliege Bird

and Bird 2020; Bird et al. 2016). This work demonstrates the vast spatial extent and persistence through time of legacies of landscape management by foragers, including through innovative use of historical aerial photographs that permit landscape-scale analysis of the effect of previous fire regimes on contemporary settlement and land-use patterns (Bliege Bird et al. 2020).

Our paper aims to build on this previous work by combining archaeological satellite-based remote sensing and innovative computational automation approaches to reveal legacies of forager land-use in coastal Madagascar. Prior remote sensing studies of archaeological foraging societies (and recently paleoanthropological sites) have taken place around the world, and many have relied on unsupervised land-cover classifications and environmental proxies to narrow down survey areas to where ephemeral cultural deposits are likely to exist (Coelho, Anemone, and Carvalho 2021; Davis et al. 2020; Keeney and Hickey 2015; Lim et al. 2021). Here, we attempt to use multispectral satellite data to directly pinpoint ecological changes associated with archaeological activity. Innovating and expanding the use of approaches that can effectively reveal “low-impact” signatures of human-environment dynamics is critical for developing more holistic understandings of the contributions of diverse communities—including highly mobile foraging communities—to shaping landscapes (Crumley 1979).

In leveraging NCT, we are also engaging principles of relocation and perturbation (Figure 6-3), wherein relocation refers to the movement of certain ideas and resources, and perturbation refers to the subsequent adaptation and changes to both human populations and environments over time (Odling-Smee, Laland, and Feldman 2003; Quintus and Cochrane 2018). Signatures of a modified niche include changes to biotic, abiotic, and artifactual components of the environment, and must be related to intentional, non-random processes (Odling-Smee et al. 2013; also see Jones et al. 2010). In order for

remote sensing tools to identify niche construction, we must be able to recognize instances of both perturbation (to quantify landscape modifications, themselves) and relocation (to identify different kinds of niche construction and the potential movement of people across a landscape). Relocation and perturbation should be traceable via similarities in material culture between sites, but also via patterns in vegetative and soil properties; i.e., archaeological niche construction will display perturbations in the form of distinct geophysical characteristics related to vegetative and soil characteristics and these differences will be relocated as communities migrate between places.

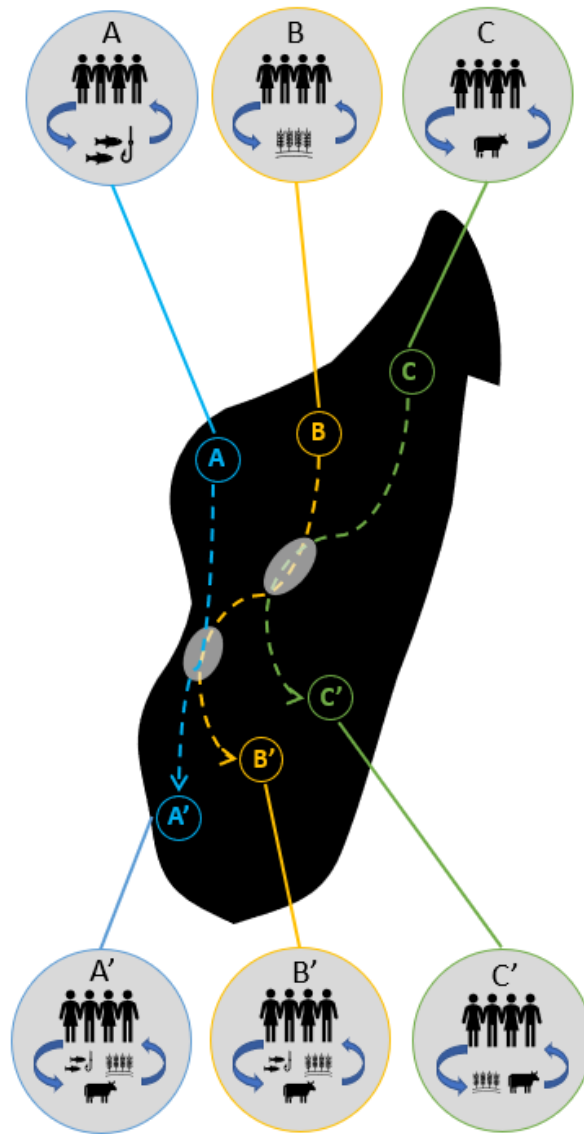


Figure 6-3: Illustration of perturbation and relocation components of NCT. Each population (A – C) performs specific activities which create feedbacks (blue arrows) between themselves and their surrounding environments. This constitutes a cultural “niche”. Relocation is represented by the dashed arrows, in which people move throughout a landscape and take their practices with them. In addition, ideas and adaptations can be spread from one community to another (gray circles) when different groups overlap in time and space, leading to the adoption of new behaviors and the formation of new niches (A’ – C’).

In this study, we focus primarily on perturbation effects. Relocation will be the focus of future work and will require a robust radiocarbon dataset to evaluate settlement chronologies and temporal shifts in settlement. Nonetheless, our present study has

ramifications for how archaeologists reconstruct and understand the impacts of foraging societies on a global scale, as the methods proposed here can be widely applied. It also contributes new insights into longstanding questions regarding the consequences of human colonization of the unique insular environments of the southwestern Indian Ocean, and Madagascar specifically.

Methods

Previous studies, using traditional ground-based and remote sensing survey (Davis, Andriankaja, et al. 2020; Davis, DiNapoli, and Douglass 2020; Douglass 2016), have expanded our understanding of Late Holocene (~3,000 cal year B.P.) settlements on Madagascar's southwest coast. This work assessed whether settlement was affected by resource availability and used satellite-derived information about environmental factors (e.g., proximity to important resources) to generate a probability model to locate archaeological settlements. This work documented hundreds of new archaeological deposits and indicated that freshwater availability, marine resources, and defensibility are among the primary drivers of settlement choice and mobility in this region since the Late Holocene. Additionally, this work suggested the presence of Allee effects, or positive density dependence, wherein settlement actively modifies surrounding environments and results in improvements to habitat suitability (Angulo et al. 2018; Fretwell and Lucas 1969).

In this paper, we are addressing whether ecological legacies of landscape modification exist and whether these constructed niches—primarily in the form of soil and vegetative properties—can allow us to predict ancient settlement locations and provide insight as to the extent of anthropogenic landscape modifications (Figure 6-1). In order to do this, we must first determine whether available satellite data have the spectral resolution needed to discern between known archaeological sites and places that do not

contain material culture deposits (Figure 6-1). We use high-resolution PlanetScope satellite imagery (Planet Team 2020) with 3m spatial resolution and multispectral capabilities to calculate vegetative productivity and soil moisture content in surveyed areas with known archaeological sites (n = 340). In total, we averaged 6 PlanetScope images taken between 2018 and 2020 during the wet and dry seasons to create a 3-year average of the study region (Appendix D Supplemental Table D-1). The years chosen experienced climatic conditions within the typical range for the region (Andavadoaka Monthly Climate Averages, n.d.). We supplemented PlanetScope images with multispectral bands available from Sentinel-2 to provide additional assessment of moisture retention properties of soils and vegetation (see below). We then compared these values with ground-tested locations without any evidence of archaeological materials based on absence of surface deposits (i.e., ceramics, shells, charcoal, etc.; n = 80). Sites in this region tend to feature single occupation horizons and relatively shallow cultural deposits that are typically indicated by the presence of surface scatters (Douglass 2016). All archaeological and non-archaeological datapoints were recorded during systematic survey operations between 2011 and 2020 (Chapter 4; Douglass 2016).

Machine Learning Algorithm

We used PlanetScope imagery and compiled 3-year averages for the dry and wet seasons between 2018 and 2020. Seasonal differences are extreme in this region (Jury 2003), and thus we need to account for these variations and how they affect our ability to discern archaeological materials in satellite data. As such, we conducted a pixel-by-pixel comparison in R (R Core Team 2020) between the 3-year averaged PlanetScope images to highlight differences in environmental geophysical properties between the wet and dry season using the equation:

$$\Delta_r = D - W$$

Where Δ_r = difference between images, D = the dry season image, and W = the wet season image.

Next, we assessed the spectral characteristics of a sample of known archaeological (n = 340) and non-archaeological (n = 80) deposits throughout the study area to determine their degree of separability between different image bands. Some prior studies have chosen non-archaeological sites randomly, but here we used ground-tested locations to alleviate potential errors in sample creation (Sonnemann et al. 2017). We drew 10m buffers around each data point and the average value for each band was calculated in R (R Core Team 2020). Then we statistically compared archaeological and non-archaeological sites using different bands of PlanetScope imagery (see Supplemental Files).

Next, we used Google Earth Engine (GEE; Gorelick et al. 2017), following Orengo et al. (2020), to train a random forest (RF) probability algorithm to identify archaeological deposits in southwest Madagascar. Because the archaeological deposits in this area are primarily ephemeral artifact scatters, high resolution data are required to attempt any sort of automated identification. We ran a RF probability algorithm using 128 trees and three iterations (which were deemed optimal for archaeological purposes by Orengo et al. (2020)) to locate artifact scatters (code can be found in the supplemental documents). The RF procedure outputs a raster of values ranging from 0-1, wherein 1 is a perfect match to an archaeological deposit. To evaluate accuracy and performance of this model, we withheld 40 archaeological points and 17 non-archaeological points (~12% of the training data) for validation. Then we calculated the precision (Equation 1), recall (Equation 2), and F1 (Equation 3) scores for the training and test data using thresholds of 0.60, 0.65, and 0.70.

$$Precision = \frac{True\ Positives}{True\ Positives+False\ Positives} \quad (1)$$

$$Recall = \frac{True\ Positives}{True\ Positives+False\ Negatives} \quad (2)$$

$$F1 = \frac{2 \times Precision \times Recall}{Precision+Recall} \quad (3)$$

A perfect result would have precision, recall, and F1 scores of 1.

Vegetative Indices

To evaluate ecological signatures between archaeological and non-archaeological areas, we used vegetative indices, which are mathematical formulas that provide indications of biomass and plant health/stress. First, we measured vegetative productivity using normalized difference (NDVI) and soil adjusted (SAVI) vegetative indices (Jensen 2007). NDVI is calculated using the formula:

$$NDVI = \frac{NIR - RED}{NIR + RED}$$

SAVI is calculated using the formula:

$$SAVI = \frac{NIR - RED}{NIR + RED + L} * (1 + L)$$

Where L is a soil adjustment factor. An optimal value for L has been demonstrated at L=0.5 and was used here (Huete 1988).

NDVI is one of the most commonly employed vegetative indices and measures vegetation based on a ratio of reflectance values in the near infrared (NIR) and Red wavelengths. However, NDVI has accuracy issues when faced with ecologically and geologically heterogeneous areas and high soil reflectance. The SAVI is an adjusted version of NDVI which corrects for reflectance caused by soil diversity, making it useful for geographically expansive studies with high rates of ecological diversity (Huete 1988). Both NDVI and SAVI relay information pertaining to water absorption and retention in

vegetation. After calculating vegetative index values, we extracted the average values from a 20m buffer around each archaeological and non-archaeological datapoint used for training the RF algorithm (discussed above). Then we assessed the difference between archaeological and undisturbed locations using non-parametric tests of association (see supplemental file). We conducted all calculations in R v. 4.0.2 (R Core Team 2020) using the *raster* (Hijmans 2019) and *rgdal* (Bivand et al. 2019) packages.

Next, we evaluated Sentinel-2 imagery, which contains short-wave infrared (SWIR) bands, in the same manner as described above. We compiled 5 years of Sentinel-2 imagery by month using GEE (Gorelick et al. 2017; also see Supplemental Files). SWIR has increased sensitivity to moisture content and can be used to distinguish mineral compositions of soils (Davis 2017; Thabeng et al. 2020). One limitation of the Sentinel-2 data is that it has much lower spatial resolution (20m). The only high-resolution SWIR satellite currently available is Maxar's Worldview-3 satellite (which has shown promise for archaeological purposes, see Davis 2017). We did not have access to these particular data, however. To improve the utility of the Sentinel-2 SWIR, we used a pansharpening procedure – a form of data fusion whereby lower-spatial resolution imagery is enhanced using a higher-resolution dataset (Garzelli et al. 2004) – to resample the SWIR data from 20m to 3m using PlanetScope imagery (see Appendix D Supplemental Figure D-1). Pansharpening followed a principle-component analysis (PCA) method using the RStoolbox package in R (Leutner et al. 2019). PCA pansharpening is appropriate because PlanetScope imagery is spectrally compatible with Sentinel-2 sensors (Ichikawa and Wakamori 2018).

Using this pansharpened SWIR data, we calculated a Normalized Difference Water Index (NDWI; Gao 1996), which is a vegetative index that reflects the biochemical metrics of plants (Sun et al. 2019). Such metrics can be used to distinguish different taxa, in addition to assessing the water content of leaves (Gao 1996; Sun et al. 2019). NDWI

uses the NIR and SWIR spectrum to measure the liquid water molecules contained within vegetative canopies (Gao 1996). It is calculated using the formula:

$$NDWI = \frac{NIR - SWIR1}{NIR + SWIR1}$$

Where NIR is the near-infrared band and SWIR1 corresponds to the first shortwave-infrared band of Sentinel 2 (1610 nm).

Finally, to assess the potential bias in our samples of archaeological and non-archaeological points, we generated 1000 random points within the study area and compared vegetative index and SWIR reflectance values between them and our ground-tested data (Appendix D Supplemental Figure D-2). If people have fundamentally changed the geophysical and/or geochemical properties of the landscape, we hypothesized earlier that the random locations will express different vegetative and soil properties than areas with archaeological surface scatters. Conversely, if people merely settled in areas with specific geochemical characteristics that are distributed throughout the landscape, random locations should show some similarities with archaeological areas.

Spatial Analysis

In order to quantify the impact of niche construction on different parts of the study area, we ran several spatial analyses to determine the amount of land area impacted by legacy effects and the distribution of niche construction activities across the landscape. Settlements in this region are non-randomly distributed (Davis, DiNapoli, and Douglass 2020), as are niche construction activities more generally (Odling-Smee et al. 2013). Thus, anthropogenic niche construction on Madagascar should also be non-random, and likely clusters in particular places that have been used repeatedly over time. After assessing the results of the RF algorithm, the locations identified as archaeological sites with the threshold with the highest accuracy scores were converted to polygons. We calculated the

area of these polygons to generate an assessment of the extent of archaeological activity within the study region. Next, we analyzed the spatial distribution of these points using the Getis-Ord General G test to compare the distribution of areas identified as archaeological by the RF algorithm with random patterns (Getis and Ord 1992). Then we converted the polygons of anthropogenic locations into points and computed kernel density estimations for these locations. We conducted all spatial tests in in ArcGIS 10.7.1 (ESRI 2020).

Results

Assessments of training datasets and PlanetScope imagery resulted in clear distinctions between archaeological and non-archaeological points in all four electromagnetic bands (Blue, Green, Red, NIR; Figure 6-4b). The differences between the samples are also statistically significant (see code in Appendix D). The RF classifier was trained using 300 archaeological points and 63 non-archaeological points and resulted in strong performance on both the training data and test data (see Table 6-1; Figure 6-4).

Table 6-1: Accuracy assessment of random forest algorithm.

Threshold	Precision (Validation)	Recall (Validation)	F1 (Validation)	Precision (Training)	Recall (Training)	F1 (Training)
0.7	0.972	0.875	0.921	0.976	0.963	0.969
0.65	0.973	0.900	0.935	0.977	0.973	0.975
0.6	0.947	0.900	0.922	0.964	0.977	0.970

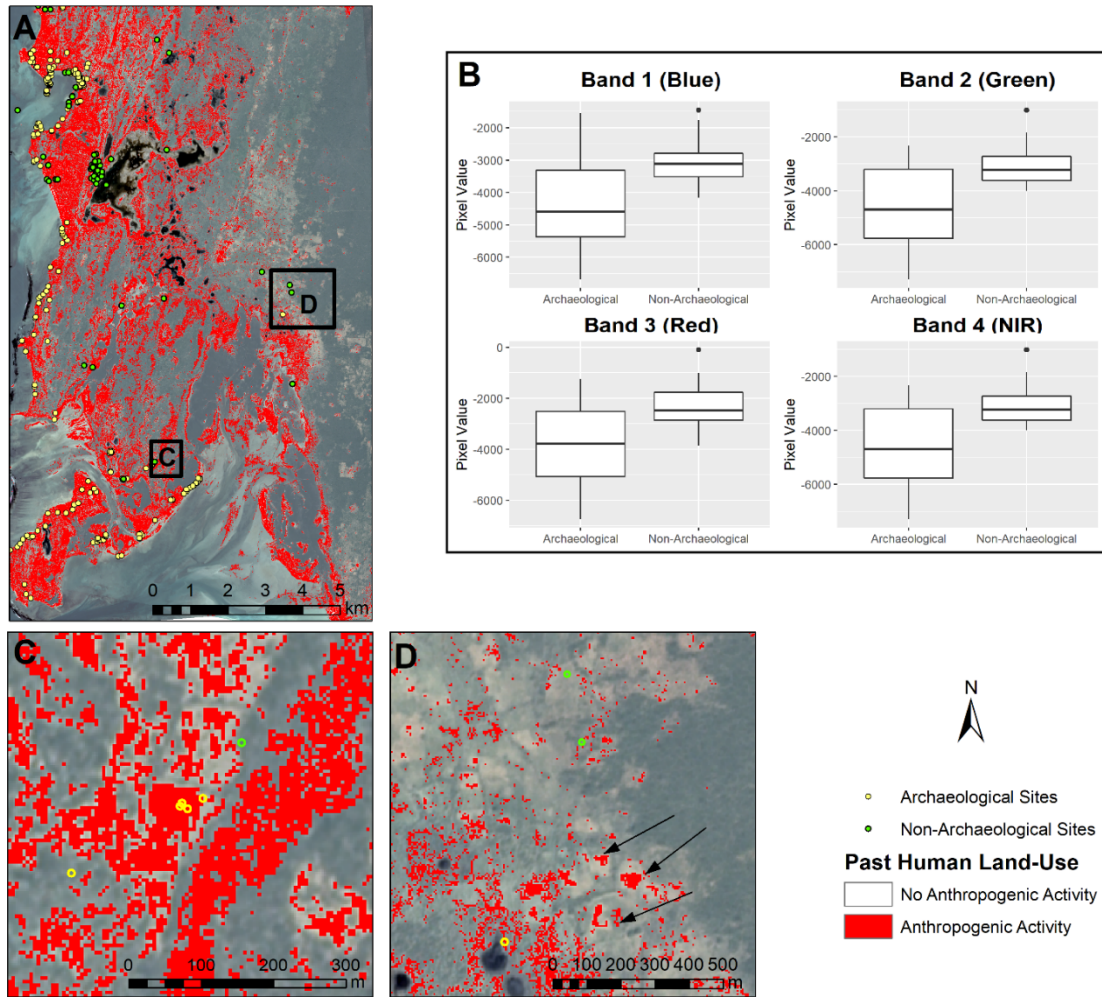


Figure 6-4: Results of RF algorithm (red) using a threshold of 0.7 compared with known archaeological deposits (yellow circles) and non-archaeological areas (green circles). B: Visualization of band separability between archaeological and non-archaeological training data. C: Close up of known archaeological and non-archaeological sites. All but one are correctly identified. D: Another area with anthropogenic activity (forest clearings indicated by arrows) and known archaeological sites. Imagery © 2020 Planet Labs. Inc.

Analyses of annually averaged NDVI and SAVI show a significant difference ($W = 8639$, $p < 0.05$) between vegetation in archaeological and non-archaeological contexts, where archaeological sites have higher mean vegetative index values than locations without archaeological activity (Figure 6-5; mean of -0.02 and -0.03, respectively). NDWI results show the same pattern ($W = 8468$, $p\text{-value} = 0.042$). This suggests that archaeological sites exhibit vegetative index values that are distinct from non-

archaeological areas. Furthermore, archaeological sites are noticeably different in their vegetative index value distribution from randomly generated points throughout the study region (see Appendix D Supplemental Figures. D2 – D5).

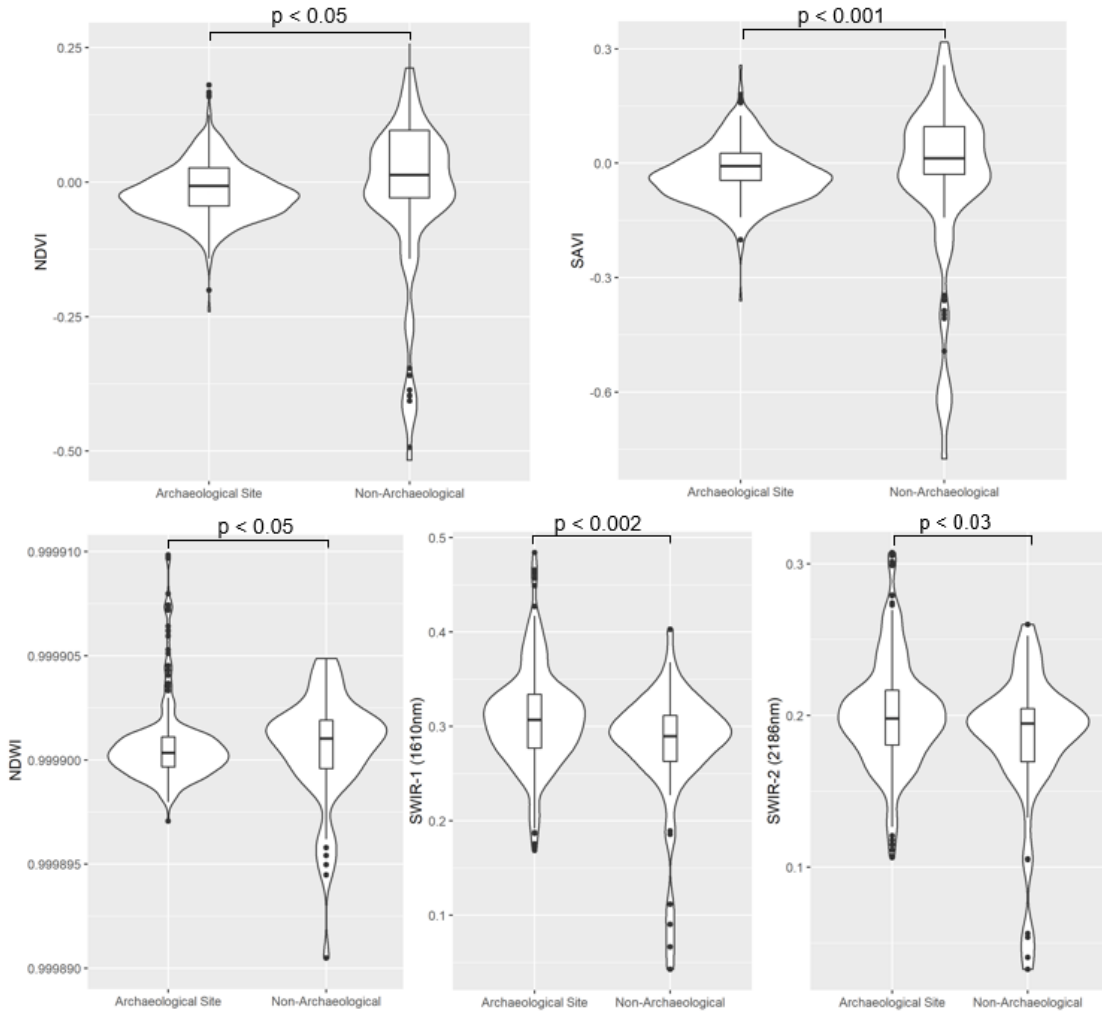


Figure 6-5: Vegetation index values for archaeological and non-archaeological locations. NDVI and SAVI are annual averages over 3 years of PlanetScope imagery (Planet 2020). NDWI uses the annually averaged PlanetScope and Sentinel-2 SWIR bands.

SWIR analysis indicates that there is a tendency for areas surrounding archaeological sites to have slightly higher reflectance values in the SWIR spectrum (SWIR1: $W = 12713$, $p\text{-value} > 0.002$; SWIR2: $W = 11999$, $p\text{-value} = 0.024$). Most archaeological deposits express higher reflectance in the SWIR spectrum, indicating

mineralogical differences and vegetation that might be distinct from surrounding non-archaeological areas.

Seasonally, we find that NDVI and SAVI values during the wet season, show a significant difference ($W = 8282$, $p < 0.02$) between vegetation in archaeological and non-archaeological contexts, where archaeological sites have higher mean vegetative index values than locations without archaeological activity (mean of -0.005 and -0.008 respectively; see Appendix D Supplemental Figure D-2). During the dry season, however, there is no significant difference ($W = 10230$, $p = 0.925$) between locations.

Using the RF results with a threshold of 0.65 , we calculated the area of all identified potential archaeological deposits within the study region. Approximately 38.6 km^2 ($\sim 17\%$) of the study region exhibits differences in soil and vegetative properties which are likely linked to human activities. Spatial analyses demonstrate that anthropogenic areas are clustered and non-randomly distributed throughout the landscape ($p > 0.0001$; Appendix D Supplemental Figure D-6). The density of anthropogenic areas appears highest 3-5km

inland from the coast (Figure 6-6), where there are known to be an abundance of seasonal freshwater ponds.

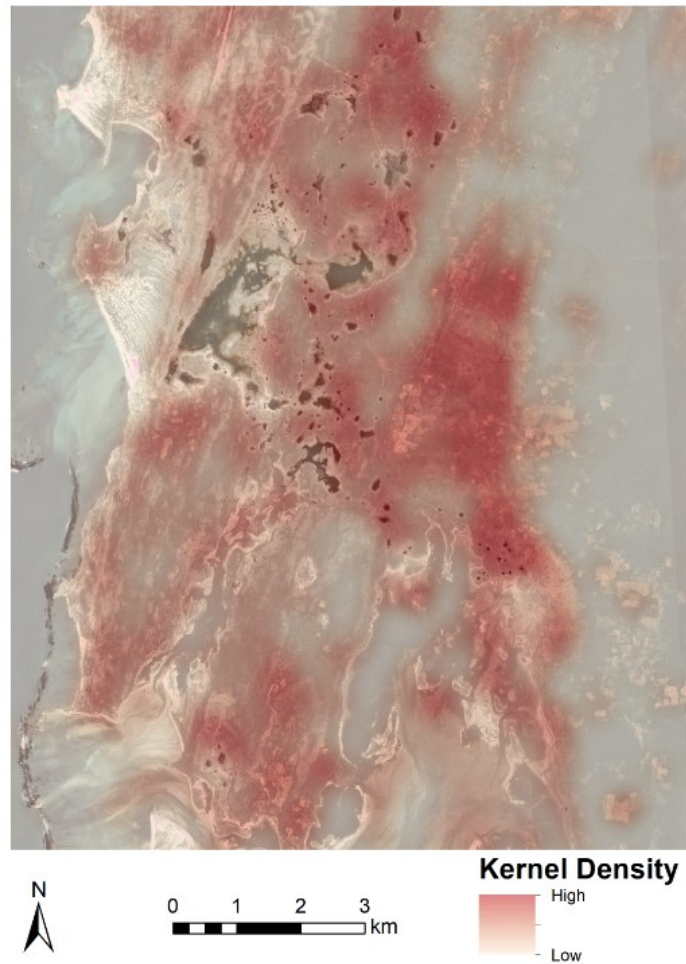


Figure 6-6: Density of anthropogenic modifications within the study region identified by the machine learning algorithm. Imagery © 2020 Planet Labs. Inc.

Discussion & Conclusions

The results of this analysis suggest that ancient coastal communities in southwest Madagascar – including highly mobile foraging and herding populations – have contributed to shaping the modern landscape in important ways. Our previous work contributed directly to this present study by allowing us to investigate settlement patterns and landscape change from two different, but complementary, angles. Our prior investigations

focused on the factors that influence settlement choice (e.g., resource availability and social cohesion), while this study focuses on the long-lasting, landscape-scale effects of settlement. In fact, prior work (Chapter's 4 and 5) indicated the presence of Allee effects, which suggests that ancient communities actively modified their ecological surroundings in ways that increased the suitability of previously settled areas. Here, we used machine learning and vegetative indices to further investigate the possibility that Allee effects were present in coastal Madagascar and resulted in legacy effects via cultural niche construction. The results of this study largely complement earlier investigations, pinpointing specific areas that contain landscape modifications, many of which overlap with previous predictive modeling results (Figure 6-7). Archaeological deposits exhibit significantly different spectral characteristics when compared to non-archaeological locations. While the potential of multispectral and hyperspectral imagery has long been established for archaeology, the detection of scant artifact scatters is not the norm (c.f., Orenge and Garcia-Molsosa 2019). Rather, most literature focuses on the detection of highly visible landscape modifications, like architecture and remains of intensive agricultural activity (e.g., Tarolli et al. 2019; also see Davis 2021). As such, this work suggests that the development of machine learning and cloud-based computational processing provides the ability to detect even the most ephemeral archaeological deposits and use these to reveal patterns of human activity and impact on the wider landscape.

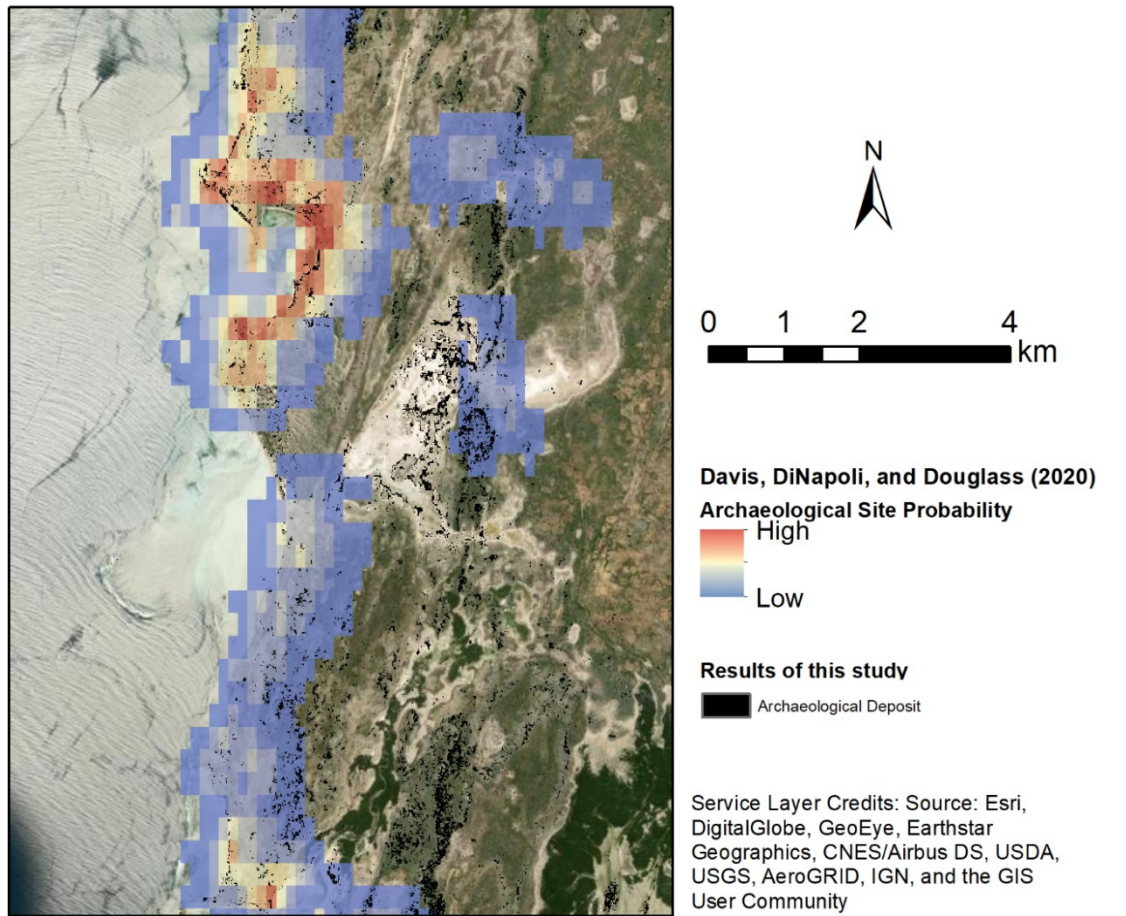


Figure 6-7: Comparison between predictive modeling results of Davis, DiNapoli, and Douglass (2020) and this study. The previous study investigated settlement distribution via environmental and social drivers, while this study looked at long-term ecological effects of settlement activity. Notice that both models detect or predict archaeological activity in many of the same locations. The areas ranked with the highest likelihood by Davis, DiNapoli, and Douglass (2020) also contain some of the oldest recorded evidence of human occupation in this region (~2500-3000 cal year B.P.).

Our analysis shows that the overall health and abundance of extant vegetation (defined by vegetative index scores) on and around archaeological deposits exhibits a statistically significant difference when compared to areas lacking any archaeological materials. The exact difference is not clear, however, as assessments of median values suggest vegetative values are higher in non-archaeological locations while evaluations of mean values suggest that vegetative values are higher in archaeological locations. The contrast between these two averages may be indicative of the wide range of

environmental contexts within the study area and could suggest that non-archaeological localities exhibit wider range of environments while archaeological areas are more limited in their vegetative diversity. This, itself, could be the result of active settlement choices or the effects of human landscape modification. This hypothesis is supported by Figure 6-5, which shows a larger range of values among non-archaeological areas compared with archaeological locations.

The difference in vegetative index scores is statistically significant in the wet season ($p = 0.01$). Additionally, the SWIR wavelength displays differences in the soils around archaeological sites and non-archaeological locations, suggesting that there are underlying differences in the mineralogical composition and moisture retention properties between areas with and without archaeological surface materials. NDWI index assessments further demonstrate that areas with archaeological materials have vegetation with different water retention properties than non-archaeological or random locations. This may signal healthier vegetation, overall, or might relate to the presence of introduced taxa that are not xerophytic and thus retain more water than endemic taxa. Because this region is arid and rainfall is highly variable (Jury 2003), even small increases in vegetation moisture content could have significant implications for human livelihoods and the biota that sustain them. This, coupled with spatial tests of identified archaeological deposits, indicates the presence of a distinctive human niche on Madagascar resulting from a variety of economic activities – ranging from foraging to pastoralism and agriculture – since the Late Holocene. The inland areas of the study area may have been preferred by pastoralists who have been present for the past several hundred years (Parker Pearson 2010), and the anthropogenic signatures found here may therefore reflect the activities of pastoral and foraging community activities. While the precise geochemical composition of soils requires further ground-based studies, human activity has likely played a role in changing these components of the landscape.

Some caution is necessary in interpreting these results, however. While it is possible that these distinctive differences between archaeological and non-archaeological locations are due to human activities (e.g., Storozum et al. 2021), it is also possible that these soils were inherently different prior to human occupation. Our prior work demonstrates that human settlement choice is not random in this region (Davis, Andriankaja, et al. 2020; Davis, DiNapoli, and Douglass 2020), and thus communities may have chosen areas already possessing specific soil and vegetation properties. To definitively establish the nature of human impact on soil chemistry, and to understand the feedbacks between soil and vegetation dynamics in this region, future studies will need to evaluate stratigraphic and geochemical changes in soil composition through time at archaeological and non-archaeological localities. This will involve ground-based survey as well as a program of radiometric dating to improve settlement chronologies.

Nonetheless, based on this analysis, we can definitively state that archaeological deposits in southwest Madagascar have distinct geophysical and vegetation profiles compared with non-archaeological locations. Likewise, the difference in vegetation between archaeological and non-archaeological areas is inherently linked to the geochemical properties of these locations, as well as to modern ecological variables. Because the primary difference between our study locations is the presence or absence of archaeological deposits, vegetative differences are likely linked to human activity (Bennett et al. 2012; Lasaponara and Masini 2007). Furthermore, our results indicate that ephemeral archaeological deposits composed of artifact scatters can be distinguished from surrounding environments using high-resolution multispectral imagery and machine learning. Thus, we can conclude that underlying differences in geophysical properties of the landscape and vegetative composition are impacted by a legacy of human landscape use over the past several thousand years. The results presented here demonstrate that archaeological sites dated to as early as ca. 3000 cal year B.P. by Douglass (2016) are

identifiable based on their ecological impact. However, a robust settlement chronology for the study region is needed to investigate whether the age of archaeological deposits impacts their signature or detectability via multispectral remote sensing.

More broadly, we demonstrate how a focus on areas with “low-impact” human activities can facilitate greater understanding of the extent of human occupation and land-use on a landscape shaped by diverse socioeconomic systems and exhibiting an ephemeral archaeological record (Douglass and Zinke 2015; Parker Pearson 2010). The impacts of early communities of foragers on Madagascar’s diverse ecosystems is widely debated, but more evidence of the (in)direct effects of human settlement are needed (Davis, Andriankaja, et al. 2020; Domic et al. In Review; Douglass, Hixon, et al. 2019). The same can be said for many regions around the world where the availability and quality of archaeological data is lower for periods of time when foraging was the dominant livelihood strategy shaping landscapes (Stephens et al. 2019). By extending our focus to these understudied components we can re-evaluate and more fully appreciate the extent to which diverse peoples have modified the Earth’s environments.

A shift in research attention toward understanding the environmental impacts of small-scale and mobile subsistence communities can also fundamentally change how we approach sustainability and conservation. One of anthropology’s longstanding goals has been to understand the dynamics between human and environmental systems (Davis 2020; Steward 1955; Carneiro 1970; Steward and Setzler 1938). Long-term perspectives on human-environment dynamics offered by archaeology provide context for understanding contemporary land-use and sustainability issues. A goal of historical ecology and ecological anthropology is to derive lessons from these long-term perspectives and eco dynamics to inform present and future management decisions (Altschul et al. 2017, 2020; Rick and Sandweiss 2020). By viewing anthropogenic landscape modifications at multiple scales and levels of intensity, as well as via a range

of (in)direct impacts, we can improve our understanding of human niche construction in diverse societies, ranging from small-scale, mobile communities to large urban centers.

This paper makes contributes to Malagasy archaeology by illuminating the scale and extent of human traces on the landscape, in a way that is time and cost-effective, allowing us to lay the critical foundation needed for further work on coupled human-natural systems. The archaeological data contained within this space has implications for our understanding of human niche construction on Malagasy landscapes over time. Beyond Madagascar, this study also holds importance for studying the ecological legacies of foraging societies and detecting ephemeral archaeological sites in semi-arid environments using high resolution satellite images and machine learning techniques.

Note: Supplemental Files (including code) associated with this chapter are available in Appendix D and at Penn State's ScholarSphere Repository: <https://doi.org/10.26207/zmsr-tc92>.

Chapter 7: Evidence for extensive social networks as risk-mitigation strategies on Southwest Madagascar⁸

As the contemporary climate crisis intensifies, understanding the interactions between climate and social network structure is increasingly important (Pisor and Jones 2021). Environmental archaeological research has long focused on identifying behavioral strategies that enhance human fitness in hypervariable climates (Davis 2020a; Dewar and Richard 2007b; Douglass and Rasolondrainy 2021; Petrie et al. 2017). Regions with long records of climatic change, like Madagascar, provide ideal opportunities to assess relationships between climate and shifts in social network structure (Pisor and Jones 2021).

Sociality and resilience in the face of external pressures

Complex systems theory (CST) is a framework that has significant potential to address human-environmental systems relationships. CST is particularly adept at explaining dynamics at different scales of interaction between people, communities, and environmental/climatic events (Preiser et al. 2018). Using CST, researchers have evaluated multifaceted and interwoven relationships across diverse human and environmental systems (e.g., d'Alpoim Guedes et al. 2016; Penny et al. 2018).

Network studies provide one way to investigate complex systems dynamics pertaining to social connectivity and resilience (Janssen et al. 2006). For example, using network analysis, Baggio et al. (2016) found that community resilience in the face of environmental stress was most closely related to cultural ties and key households within those cultural networks, but not (as the authors expected) to a decline in natural resources.

⁸ Davis, D. S., Rasolondrainy, T., Manahira, G., Hixon, S. W., Andriankaja, V., Hubertine, L., Justome, R., Lahiniriko, F., Léonce, H., Roi, R., Victorian, F., Clovis, M. B. J., Voahirana, V., Carina, T. L., Yves, A. J., Chrisostome, Z. M., Manjakahery, B., & Douglass, K. (In Review). Evidence for extensive social networks as risk-mitigation strategies on Southwest Madagascar. *Antiquity*.

A network approach is particularly useful for archaeology because it: 1) defines the structure of social systems and their interactions with external forces; and 2) provides a semantically consistent manner by which interactions can be described (i.e., nodes and links); see Janssen 2006), which is pivotal for scientific research (*sensu* Davis 2020b).

Studies of social networks during periods of stress indicate that external pressure (i.e., influences from outside of human social systems) can result in networks contracting and transforming to a structure of very close ties between a select few parties (Romero et al. 2019), rather than a reliance on “weak” ties (Granovetter 1973) that are often associated with intercommunity communication. However, different levels of connectivity come with their own sets of advantages and drawbacks, and the exact adaptive response of a network will vary based on its specific context (see Janssen et al. 2006). For instance, densely clustered networks often form as a risk-mitigation strategy (Pisor and Jones 2021), but can also result in an “overconnected” system that is prone to collapse from changes at varying scales (Redman and Kinzig 2003; also see Mills et al. 2013). On Rapa Nui, for example, communities managed to thrive despite a paucity of land and natural resources by adopting a nested social structure that relied on different scales of interaction (Lipo et al. 2021).

Centrality, or the structural importance of a given node within a broader network, is another useful measure of network connectivity. Networks with high centrality benefit from greater centralization and control, but are also disadvantaged from this centralization as it can create hierarchical concentrations of power. Furthermore, node removal from the network can destabilize the entire system (Janssen et al. 2006). Indeed, there are many instances of societies consciously preventing highly centralized network organization in favor of less-hierarchical social structures (Graeber and Wengrow 2021). In contrast, low connectivity makes the network more robust in the face of node removal and prevents

hierarchical power centralization, but comes at the cost of decreased control over connections.

Past Social Networks in SW Madagascar

Inferring past social interactions from archaeological remains can be challenging. Ceramics offer an invaluable source of information about social functions and connections (e.g., Braun 1983; David et al. 1988; Skibo et al. 1989). Among the many uses for ceramic materials is the tracing of cultural exchange between communities across time and space (Rice 2015). On Madagascar, different ceramic decorative styles have been linked to diverse cultural groups throughout the island (Dewar and Wright 1993), and a history of global interaction with Madagascar is recorded in the exchange of goods like ceramics and beads (Beaujard 2007; Buffa et al. in review). Oral histories and archaeology suggest that pottery styles indicate cultural affiliation and can be used to trace trade between regions (e.g., Verin 1971). Work conducted by Douglass (2016) established a relative chronology for the ceramics of southwest Madagascar based on decorative patterns corresponding to different dated archaeological contexts (Figure 7-1). Some decorative trends (e.g., burnishing) are commonly recorded in ceramics from all time periods, while others (e.g., incising, combing, punctation) vary through time and may reflect shared production practices (Douglass 2016). This information can help archaeologists understand social connections and their organization over time.




Time Period	Key Diagnostic Characteristics	Photographic Examples
Early (1150 – 450 BP)	<ul style="list-style-type: none"> • Round Punctation • Rectangular Punctation • Incising (wavy/zig-zag) 	
Middle (450 – 250 BP)	<ul style="list-style-type: none"> • Triangular Punctation • Incising (parallel) 	
Late (250 – 50 BP)	<ul style="list-style-type: none"> • Shell Combing 	

Figure 7-1: Ceramic characteristics and their relative chronology. The Early Period extends from 1150-450 BP, with most sherds dating between 950-450 BP.

Stressors and Expectations

Paleoclimate proxies from southwest Madagascar, particularly records of $\delta^{18}\text{O}$ which serve as proxies for precipitation and evidence dry and wet periods, indicate a highly variable climate over the past millennium, including a series of extreme drought events (Figure 7-2; Faina et al. 2021; Hixon et al. 2021; Razanatsoa 2019). These changes overlap with megafaunal extinction events (e.g., Li et al. 2020; Virah-Sawmy et al. 2010) and landscape-scale ecological shifts, some of which are directly related to changes in human subsistence practices meant to cope with such environmental instability (Crowley et al. 2017; Godfrey et al. 2019).

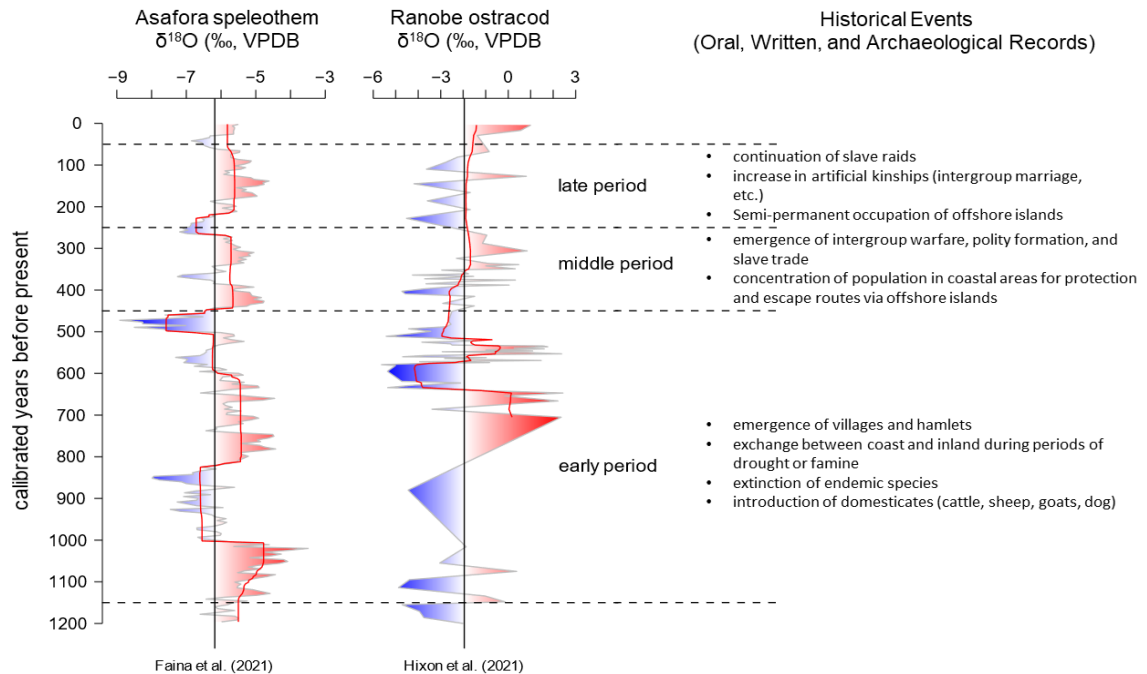


Figure 7-2: Historical events and precipitation/aridity levels based on $\delta^{18}\text{O}$ data (grey lines) from the carbonate of a speleothem collected from Asafora Cave (Faina et al. 2021) and from ostracods (*Bradleystrandesia* cf. *fuscata*) collected in laminated lake sediments at Ranobe (Hixon, Curtis, et al. 2021). Mean $\delta^{18}\text{O}$ values are given as vertical black lines, and climate shifts inferred through Bayesian change point analysis (BCPA) are illustrated by red lines. Approximate correspondence with ceramic chronological periods are indicated along with dry (red) and wet (blue) periods. BCPA is not applied to the Ranobe record before 700 cal BP due to the relative scarcity of data.

Ethnohistoric data from southwest Madagascar suggest that people responded to aridity and changes in resource availability through increased mobility and the adoption of a variety of subsistence strategies (Kelly 2005; Yount et al. 2001). Recent archaeological work further suggests that settlement distributional patterns in this area are largely the result of resource distributions and social ties (Davis, DiNapoli, and Douglass 2020).

Here, we conduct a social network analysis using a ceramic assemblage consisting of 5,221 archaeological sherds from the Velondriake region of southwest Madagascar (Figure 7-3). We then compare the results of our analysis with regional paleoclimate records from Asafora Cave (Faina et al. 2021) and Ranobe Lake (Hixon, Curtis, et al. 2021) and oral historical records to provide additional context for the patterns

observed in these network analyses (Figure 7-2). Our goal is to explore the changes in social network organization in southwest Madagascar to understand how they correlate with sociopolitical and climatological shifts in this region over the past millennium.

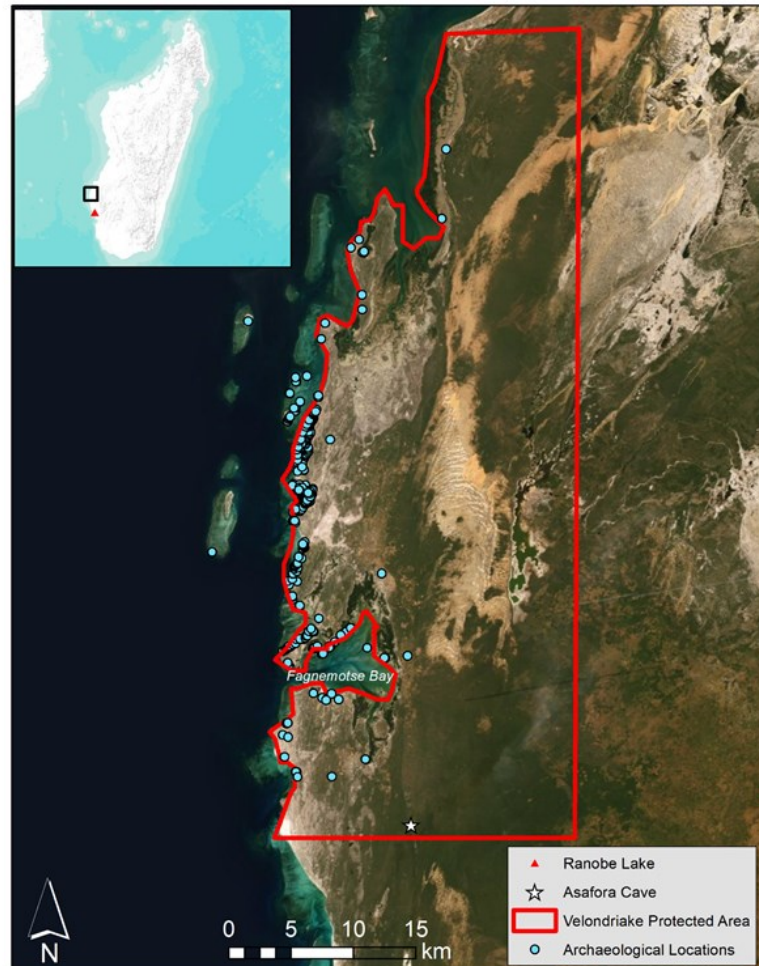


Figure 7-3: Map of the study region, showing locations where archaeological ceramics and paleoclimate data were recovered.

We address three main questions: 1) What is the level of community connectivity and the geographic extent of social networks in the study region through time, as reflected by decorative characteristics in the ceramic assemblage? And 2) Do changes in the form of these networks coincide with notable climatic and sociopolitical events? We assume that far-reaching social connections would have generated widespread ceramic stylistic similarities (e.g., decorative attributes) that persist over time. We expect that alternating

dry and wet intervals throughout the past millennium incentivized mobility and consequently generated well-integrated and extensive pottery networks. However, we expect that the relatively persistent dry conditions during the Middle and Late Periods favored spatial shifts in social/ceramic networks as inland communities moved to exploit coastal areas with relatively abundant resources, less directly influenced by changes in precipitation (Douglass and Rasolondrainy 2021). We also expect that sociopolitical instability during the Middle Period (e.g., slave raids, violent conflict, etc.) further constrained the geographic extent of social networks as groups adopted defensive strategies for security and resource access (Jazwa et al. 2017). Such instability (particularly 18th-19th century slavery) could have also constrained social interactions and the movement of pottery during the Late Period. However, movement within relatively large states (e.g. Sakalava Kingdom) may have been less restricted at this time.

Materials and Methods

We analyzed ceramics recovered during surface surveys in Velondriake between 2017 and 2020. We recorded descriptive attributes pertaining to decorative treatment (burnishing, shell-combing, punctation [rectangular, triangular, and square], and incising) for each sherd. Next, we calculated frequencies of ceramic attributes (edges) by survey location (nodes) in R (R Core Team 2020) and compiled a new CSV file containing all ceramic decorative attributes and geographic locations. Next, we divided the data by survey location and temporal period using relative chronologies developed by Douglass (2016) for Velondriake ceramics (Figure 1). Using these data, we ran a series of network analyses in R (R Core Team 2020) following a protocol developed by Peeples (2017).

Network Analysis

The incomplete nature of archaeological data holds significant challenges for the implementation of SNA methods for understanding the past (Brughmans 2013; Mills 2017;

Peeples 2017; Roberts et al. 2021). Various solutions have been proposed, but the common theme is the use of statistical validation to assess possible biases or errors in the data being analyzed (Östborn and Gerding 2014; Peeples and Roberts 2013). Östborn and Gerding (2014) discuss the need for statistical rigor in network analyses in archaeology, and advocate for a random permutation approach to randomly reshuffle data to evaluate observed patterns from randomly dispersed datasets.

Brughmans (2013) argues that there are two major problems with many recent implementations of SNA in archaeology: (1) a general unawareness of the history and diversity of formal network methods and their archaeological suitability has resulted in a very limited scope of SNA applications; and (2) most applications of SNA in archaeology are not driven by research questions, but rather a limited number of popular models and techniques. Brughmans (2013) suggests that framing studies of archaeological SNA applications using complex systems theory can help alleviate some of the limitations.

Central tenets of SNA are that: 1) Actors and their actions are viewed as interdependent; 2) Ties or linkages between actors are channels for the transfer of resources; 3) Network models view the network structural environment as providing opportunities for or constraints on individual action; and 4) Network models conceptualize structure (social, economic, political, and so forth) as lasting patterns of relations among actors (Brughmans 2013; Wasserman and Faust 1994).

We tested three commonly used comparative indices, including co-presence, Brainerd-Robinson (BR) similarity (Brainerd 1951; Robinson 1951), and chi-square distance. Co-presence is a simple similarity metric that establishes connections on the basis of the presence of particular categories of data at multiple sites (Brughmans 2010). Following Peeples (2017), co-presence is calculated as:

$$P = A \times A^T$$

Where P is the number of overlapping categories between sites, A is the incidence matrix of categories, and A^T is the transposed matrix of those categories. We generated co-presence networks using a threshold of 50% similarity. This threshold was chosen based on trial-and-error, whereby 50% provided the best visualization of network connections.

BR similarity calculates similarity between nodes as a proportion of the representation of the total number of categories present within the data. This is a commonly applied similarity metric, and is calculated, following Peeples (2017), using the equation:

$$S = \frac{2 - \sum c|x_c - y_c|}{2}$$

Where S is the BR similarity score, c represents all the categories of data, x is the proportion of c in the first data assemblage, y is the proportion of c in the second assemblage.

Lastly, Chi-Square (X^2) distance is a measurement used to assess similarities between datasets by placing higher weight on rarer data categories (Dodge 2008). Chi-square distance is calculated using the equation:

$$X_{nc} = \sqrt{\sum \frac{1}{a_n} (x_n - y_n)^2}$$

Where n is the proportional abundance of the n th element of the average row profile in the data, and x and y represent the row profiles for the two sites being compared. Chi-square distances are useful for accounting for rare attributes in the formation of data connections (Peeples and Roberts, 2013).

Assessment of sampling error on network results

To assess the effects that sampling error may have on our results, we calculated centrality metrics (degree, eigenvector, and betweenness) using 1000 bootstrap simulations to re-sample our data (following Mills et al. 2013; also see Roberts et al. 2021) and evaluate changes between randomized samples and our original dataset. Increased variability indicates higher risk of sampling error. Degree centrality for a node is defined as the total number of direct connections in which that node is involved (Peeples, 2017; Peeples and Roberts, 2013). In other words, it is a measure of a node's overall importance in a network based on how many connections it has. Betweenness centrality is defined as the number of shortest paths between pairs of nodes in a network involving the target node divided by the total number of shortest paths in the network as a whole (Peeples, 2017; Peeples and Roberts, 2013). In other words, it measures how closely connected a single node is to other nodes in the network. Eigenvector centrality is a measure of a node's importance in a network defined in relation to other nodes to which it is connected (Peeples, 2017; Peeples and Roberts, 2013; Roberts et al., 2021).

Next, we re-assess these networks for their resilience to sampling biases using 1000 bootstrap simulations to subsample the data into 10% intervals and calculate the rank-order correlation (Spearman's ρ) of the overall sample and each sub-sample (Costenbader and Valente 2003; Peeples 2017). We also assessed these biases using fewer numbers of simulations (100, 200, 500), and results remained largely identical. This allows us to evaluate the errors in the dataset that may arise from sampling issues (see Appendix E). This procedure is performed to account for missing nodes and edges in the dataset, which often plague archaeological investigations.

Then, we assess the stability of individual nodes and edges in the network by using 1000 bootstrapped simulations of our network data to create sub-sampled datasets. This

allows us to compare the original dataset with sub-sampled components for agreement or divergence.

Ceramic Chronologies

Relative chronologies for ceramics follow the typologies described in Douglass (2016). Based upon prior observations and studies (e.g., Douglass 2016; Hixon, Curtis, et al. 2021; Parker Pearson et al. 2010; Wright et al. 1996), ceramics decorated with triangular punctation and incising were associated with the oldest archaeological contexts, spanning from the 9th century AD to between the 13th and 16th centuries AD. Circular and square punctations appear slightly later (around the 11th century), and the most recent decorative style is shell-combing, which becomes prevalent around the 18th – 20th centuries. Using these decorative characteristics, we constructed the relative chronology used in this analysis.

Paleoclimate Assessment using Bayesian Change Point Analysis (BCPA)

Finally, to interpret the potential relationships between social networks and external pressures, we compared the results of our network analysis with paleoclimate datasets (Figure 1; Faina et al. 2021, Hixon, Curtis, et al. 2021) and oral history data collected by the Morombe Archaeological Project team led by Roger Samba between 2017-2018.

In tropical zones, surface water $\delta^{18}\text{O}$ values are sensitive to the ratio of evaporation to precipitation (with high E/P leaving surface water enriched in ^{18}O), and these values influence the $\delta^{18}\text{O}$ values of carbonates that are preserved over long-time scales (Lachniet 2009). The Asafora speleothem $\delta^{18}\text{O}$ record comes from the southeastern part of Velondriake and documents relative changes in moisture availability with sub-decadal temporal resolution. The Ranobe ostracod $\delta^{18}\text{O}$ record comes from ~90 km south of Asafora Cave and also documents significant changes in the ratio of evaporation to

precipitation in the study region (Hixon, Curtis, et al. 2021). We use Bayesian Change Point Analysis (Erdman and Emerson 2008) to compare potential relationships between shifts in social network configurations and climate. BCPA is a statistical modelling approach that uses Markov Chain simulation to identify splits in a sequence of datapoints that can be approximated reasonably with a single mean value. We conduct BCPA in *R* (R Core Team 2021) using the *bcp* package (Erdman and Emerson 2008).

Results

Sensitivity analyses showed that the X^2 distance index was least prone to sampling bias. When interpreting X^2 networks, distance refers to the level of connectivity between two nodes, with lower distances having higher connectivity. X^2 networks reveal extensive connections between archaeological sites in the Velondriake area that shift over time. During the Middle Period, these networks shift southward and offshore, and then further southward and northward during the Late Period (Figure 7-4). Stylistic attributes of ceramics exhibit a number of connections between large numbers of archaeological sites, as well as several smaller networks of interaction between smaller numbers of sites (Figure 7-4). The highest X^2 distances are found among those sites with the greatest number and variability in ceramics, while lower values are found among sites with fewer ceramics (Table 7-1).

Table 7-1: X²-similarity scores and associated ceramic assemblages among select sites surveyed in 2019. Higher scores are associated with greater assemblage diversity.

Site ID	Average X ² Distance	Total Ceramics	Burnished Interior	Burnished Exterior	Shell-combing Exterior	Shell-combing Interior	Rectangular Punctuation	Square Punctuation	Triangular Punctuation	Incised
G58	0.31 (Late Period)	12	6	7	1	0	0	0	0	0
G89	0.38 (Early Period)	5	0	0	0	0	1	0	0	0
G130	0.62 (Early Period)	70	25	19	23	1	2	0	0	0
G134	0.43 (Late Period)	61	44	31	20	4	0	0	0	0
	0.50 (Late Period)									

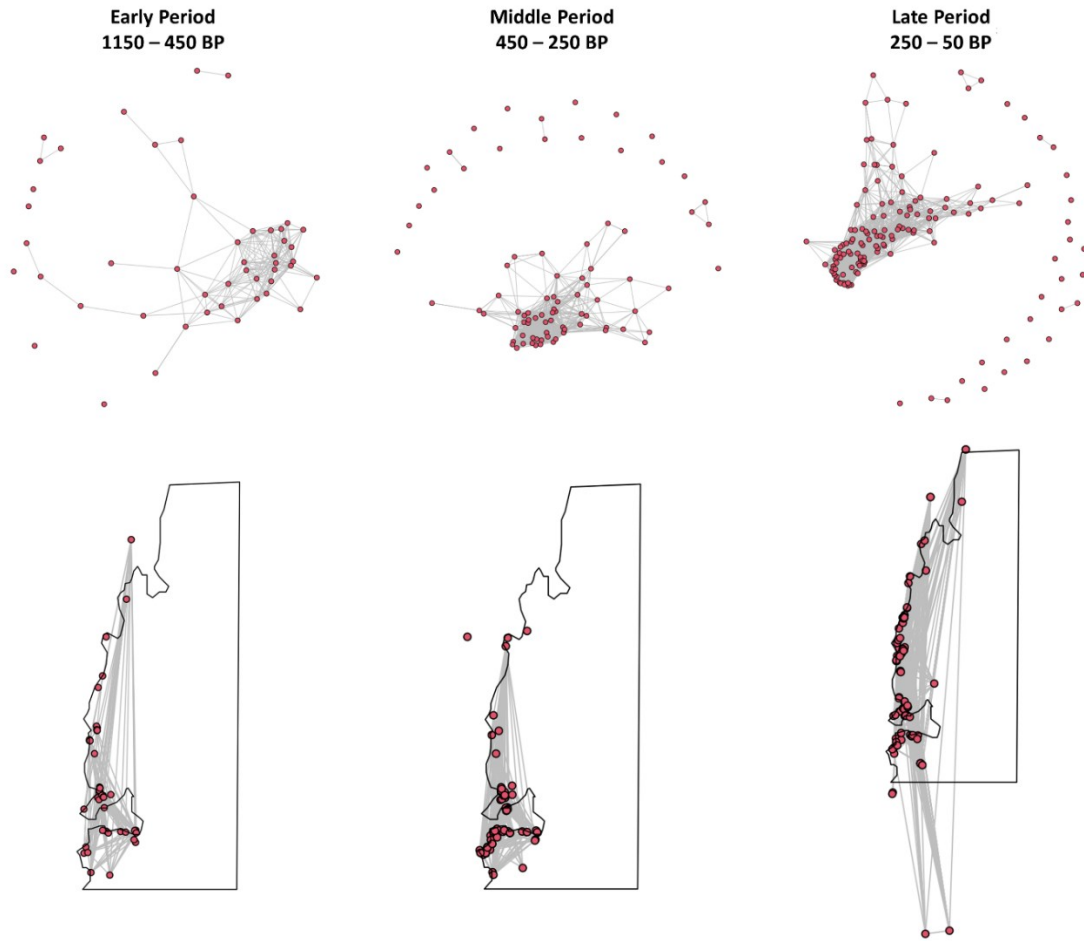


Figure 7-4: X^2 Distance network of ceramic attributes over time.

Stylistic elements like burnishing are widespread throughout most sites in this area, but incising and triangular punctations are rare, only appearing in a few select locations. Yet, these rarer elements are found both in the north and south ends of the study region.

We also find evidence of community mobility and spatial changes in social networks when analyzing centrality measurements of different archaeological sites (Table 7-2). The eigenvector and degree centrality measurements, quantifying the number of connections and relative importance of specific nodes in a network, show a decrease during the Middle Period, and then an increase during the Late Period.

Table 7-2: Average Centrality Metrics for Decorative Networks.

X² Network	Average Distance Score	SD of Distance Score	Degree	Eigenvector	Betweenness
Early Period	0.460	0.210	8.583	0.719	21.521
Middle Period	0.318	0.178	16.186	0.703	21.919
Late Period	0.303	0.180	28.192	0.713	57.781

Discussion

We find evidence of spatially extensive, densely clustered social networks in this area over the past 1200 years that fluctuate through time. We observe spatial contractions of networks around resource rich areas and defensible locations during periods of climatic and sociopolitical instability, which is consistent with our expectations. Trends in average X² distance scores between locations suggest that community organization is consistent with a core-periphery model (Gondal and McLean 2013), which can help reduce risk by balancing redundancy and diversity in social structure. Ethnographically, communities in this area demonstrate a mix of strong and weak social relationships that give flexibility when coping with hypervariable climatic conditions (Douglass and Rasolondrainy 2021).

Locations with low X² distance scores appear to have higher ceramic abundance and variability than sites with higher scores, suggesting that these sites were central nodes for community connection that were likely occupied for longer timeframes. We find that the strongest connectivity between sites occurs between locations surrounding Fagnemotse Bay, which may reflect stable food sources and/or increased defensibility of this region (Figure 7-3). Geographical shifts in social connections may indicate mobility among communities through time, which is a well-established lifeway strategy in Velondriake, historically (e.g., Koechlin 1975; Deschamps 1959). We know from previous archaeological investigations that settlement and mobility patterns are driven by resource availability and social aggregation (Davis, Andriankaja, et al. 2020).

Over the last millennium, there appears to be a series of contractions and expansions of social networks (Figure 7-4). Looking at historical and paleoclimate records, we can evaluate the degree to which different socio-environmental and sociopolitical contexts may have impacted social networks.

Early Period Network (1150-450 BP)

The earliest ceramic network is characterized by gradual fluctuations in precipitation that persist over 100-200 years and represent both the wettest and driest intervals of the last millennium (Figure 7-2). This period is defined by initially drier conditions, followed by 400 years of fluctuation between wet and dry periods. During this time period social networks expand for most of the Velondriake coastline, including the offshore island of Nosy Ve. Apart from this main network, there appears to have been a subset of the population that participated in its own distinct social network, defined by connections between several coastal sites that were disconnected from this central hub of interaction (Figure 7-4).

Archaeology and oral history help to elucidate what influenced the structure of this early ceramic network. Archaeological research suggests that villages and hamlets started to emerge in the southwest during this period (Douglass 2016). Potsherds encountered in the Velondriake area dating to the Early Period resemble an inland assemblage dating between 600-800 BP from the site of Asambalahy (Vérin 1971). Oral history, although for later periods, mentions long traditions of people in the Velondriake area exchanging marine goods with agricultural products and pottery vessels from the middle valley of the Mangoky River (where the site of Asambalahy is located) during lean seasons or droughts. This suggests that while climate stresses started to affect livelihoods in the Velondriake area during the last four centuries of this period and sociopolitical insecurity was still low, communities relied on trade/barter with other regions to alleviate the impacts of climate

challenges. Therefore, communities likely relied on trade and kinship relationships with other communities to acquire goods.

Middle Period Network (450-250 B.P.)

In the Middle Period, fluctuations in climatic conditions appear more temporally concentrated, with shifts occurring multiple times within 200 years. These shifts include a pronounced drought identified in other proxies ca. 400 BP (Razanatsoa 2019). These dry conditions could have contributed to the spatial contraction of settlements that we see in ceramic assemblages and our network analysis. The number of nodes disconnected from the bay area increases to 23, and a third subnetwork consisting of two node connections is established, perhaps from a breakdown of the larger social network. 102 of 121 oral historians in the Velondriake region mentioned an increase in aridification and rainfall unpredictability over time. According to historians, this unpredictability of rainfall pushed herders and agriculturists to abandon inland activities and adopt marine subsistence strategies along the Velondriake coast. As they were still new to a maritime subsistence, migrants to the coast described a preference for exploiting near shore resources (e.g., gathering shellfish, gleaning octopuses, and net-fishing in the near shore (*tarikaky*)) (Douglass and Rasolondrainy 2021). Places like Fagnemotse Bay would have been ideal for exploiting near shore resources, potentially explaining the concentration of nodes around the bay during periods of stress. All 35 oral historians living in villages around this bay confirmed their ancestors used to be farmers, herders, and foragers, but converted to maritime fishing to exploit the bay's resources.

This period also saw the emergence of intergroup warfare, polity formation, and the slave trade in southwest Madagascar (Grandidier and Grandidier 1903, 1904). 58 of 121 oral historians mentioned slave and cattle raiders attacking their former villages. Most of these attacks happened inland rather than along the coast. The concentration of

populations along the Velondriake coast may therefore indicate increased sociopolitical stability due to the emergence of Sakalava polities who were more interested in cattle raids and grabbing pastureland and farmland than in attacking fishing villages (Lombard 1988). Oral historians also reported that slave raids conducted along the Velondriake coast mostly failed because Vezo fishers avoided confrontations by moving to offshore islands that inland slave raiders could not access.

Late Period Network (250-50 B.P.)

In the Late Period, climatic conditions appear more stable and consistently drier (Figure 7-2). This climate coincides with expanded social networks northward and southward along the coast of Velondriake, and even beyond the Velondriake region. The number of nodes disconnected from Fagnemotse Bay increases from 23 to 29. The return of spatially extensive network connections, including settlements on offshore islands, suggests increased sociopolitical insecurity, but also possibly demographic increase due to the arrival of new groups seeking refuge.

During this period, archaeology demonstrates an increase in number and size of habitation sites, along with shorter occupation horizons (Douglass 2016), while oral history records mention an increase in artificial kinships (such as intergroup marriage, *ziva*, and blood brotherhood) between natives and newcomers. Meanwhile, both historical documents (Grandidier and Grandidier 1906, 1907) and oral history provide evidence of ongoing raids and slave trading during this period, which people in Velondriake often avoided by temporarily moving to offshore islands. During this later period, however, the nature of archaeological sites suggests (semi)permanent habitations on offshore islands. The expansion of social networks during this period may be related to the establishment of the Sakalava Kingdom, which may have brought some level of stability to the Velondriake region. However, the continuation of sociopolitical instability and violence

coupled with climate-induced resource scarcity could explain the geographic expansion of community networks. Throughout these periods, communities seem to have maintained higher levels of connectivity through their natural and artificial kinships. Maintaining these ties is indeed crucial in terms of resource access, especially in the face of climate unpredictability (Douglass and Rasolondrainy 2021). There is evidence from oral history records that climate change influenced how people tried to acquire resources by maintaining higher levels of community connectivity across larger geographic distances. Future work can seek to disentangle this relationship via chronology construction and causality testing.

Conclusion

Our analysis demonstrates that communities living in the Velondriake area over the past millennium maintained widespread social networks, which have contracted and expanded over time. We find that the shifts in network structure coincide with changes in climatological conditions and sociopolitical instability, suggesting that these external factors influenced social connectivity. We offer the following questions for future work in light of our results which should be assessed using causality testing and additional data collection: 1) shifts in climatological conditions impacted food procurement, leading to migrations of communities to a centralized location that was resilient to changes in marine and terrestrial climate; and 2) periods of sociopolitical unrest (e.g., slave raids, community conflict, war and conquest) resulted in community dispersal across a broader geographic area, including offshore islands, and a reorganization of social networks. By establishing comprehensive chronologies for the sites explored in this study and the generation of highly resolved climatic and environmental reconstructions for this region, we can further assess these hypotheses.

Chapter 8: Refining the settlement chronology of SW Madagascar: Results of new excavations in the Velondriake Marine Protected Area⁹

Over the past three years the Morombe Archaeological Project (MAP) has been involved in a landscape scale analysis of the settlement history of the Velondriake Marine Protected Area in Southwest Madagascar. Using a mix of remote sensing and ground-based survey strategies, over 1000 km² of area was systematically investigated for archaeological materials and several hundred new sites were recorded (Davis, Andriankaja, et al. 2020). Based on earlier surveys, we conducted targeted excavations at locations throughout Velondriake to refine chronological information about the timing and nature of settlement in this region (Figure 8-1).

Between 2020 and 2021, a total of 8 excavation units were uncovered at 7 different sites across the study area. These sites all displayed evidence of human occupation (e.g., ceramics, marine shell tools, beads, etc.) based on surface surveys conducted prior to excavation (see Davis et al. 2020). This article describes the material culture recovered from these excavations as well as a chronology of the region's settlements. In what follows, we present a brief synopsis of the excavation units at each location, the materials recovered, and a short interpretation of the age and use of each of these sites. Further investigation and analysis of recovered materials is necessary and will constitute future work.

⁹ Davis, D. S., Manahira, G., Domic, A. I., Lahiniriko, F., Andriankaja, V., Carnat, T. L., Clovis, M. B. J., Colombe, C., Fenomanana, F., Hubertine, L., Justome, R., Léonce, H., Yves, A. J., Roi, R., Victorian, F., Voahirana, V., & Douglass, K. (In Preparation). Refining the settlement chronology of SW Madagascar: Results of new excavations in the Velondriake Marine Protected Area.

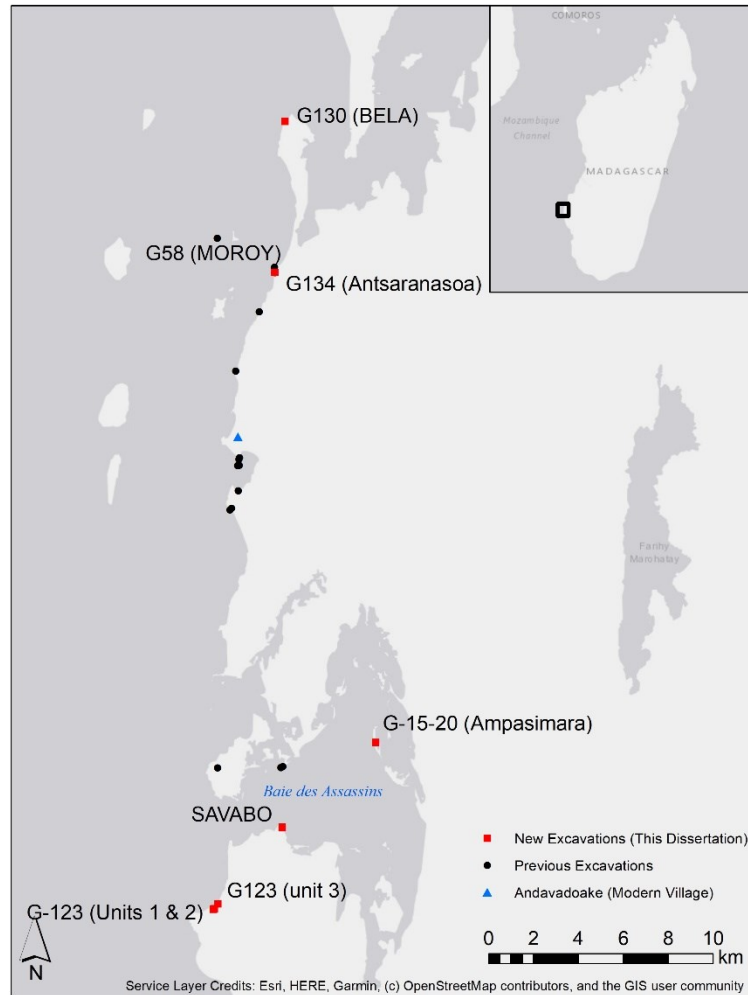


Figure 8-1: Map of excavated locations reported in this chapter alongside prior Morombe Archaeological Project excavation work (2011-2017) in the Velondriake Marine Protected Area.

Regional Background

The climatic conditions in the southwest of Madagascar are demarcated by a wet (monsoon) season and a dry season. Overall, the southwest of the island is extremely arid, accumulating less than 50cm of rainfall per year (Faina et al. 2021; Jury 2003; Razanatsoa 2019). The Velondriake region, specifically, contains an underlying geology composed of limestone and sandy-shell, and sits on a Quaternary dune system (Besairie 1964). The area is home to highly endemic flora and fauna which varies according to the underlying geology (Douglass and Zinke 2015), and vegetative species are largely

xerophytic and comprise the “spiny thicket” ecoregion (Gautier and Goodman 2003). Further inland from Velondriake, Pleistocene and Eocene deposits define the geological system (Besairie 1964).

The Velondriake Marine Protected Area consists of a total area of approximately 800 km² and is the home to over 10,000 people (Harris 2007). The area’s northernmost boundary is located ~20km south of the city of Morombe and its southernmost boundary is ~130km north of the city of Toliara in SW Madagascar’s Toliara Province. Velondriake is home to a variety of marine ecosystems, including coral reefs, mangroves, seagrass beds, and intertidal estuaries. The inhabitants of Velondriake consist primarily of Vezo fishers, communities whose livelihood strategies revolve primarily around marine resource exploitation (Astuti 1995), as well as Mikea and Masikoro communities, whose livelihood strategies revolve around forest resources, agriculture, and pastoralism (Yount et al. 2001). Today, Velondriake consists of over 32 different villages, and the marine protected status of the region was established by these communities to aid in marine resource conservation efforts (Cripps and Harris 2009).

The archaeology of the Velondriake region of Madagascar is a recent development, with the first comprehensive investigation taking place starting in 2011 by Douglass (2016). Douglass’ work focused on regional survey and the excavation of six different open air and rock shelter sites occupied between 3000 B.P. and the present (Table 8-1; Douglass 2016, 2017; Douglass et al. 2019). She conducted a more targeted analysis of contexts dated between 1400 – 100 BP (Douglass et al. 2018). The region appears to have an extensive history of marine resource exploitation by human inhabitants, including resource acquisition in a range of habitats extending from coral reefs, mangroves, and intertidal zones, among others (Davis, DiNapoli, and Douglass 2020; Douglass 2017). Recent surveys of the area reveal a settlement system driven by

environmental and sociopolitical resources and a closely connected social network of permanent and semipermanent communities (Davis, Andriankaja, et al. 2020; Davis et al. *In Review*).

Table 8-1: Previous Radiocarbon Dates from Excavations in the Velondriake Marine Protected Area.

Lab ID	Sample Description	Site/Context	¹⁴ C Age	Error	Calibrated Date B.P. (2σ or 95.4%)	Calibration Curve	Reporting Publication
D-AMS-012442	Worked Marine Shell	NSS2, Velondriake	3086	±32	3375-3214	Marine20*	Douglass 2017
D-AMS-012441	Worked Marine Shell	Antsaragnangny, Velondriake	1954	±27	1987-1820	Marine20*	Douglass 2017
D-AMS-012440	Charcoal	Antsaragnangny, Velondriake	915	±25	911-742	SHCAL20	Douglass 2017
D-AMS-001950	Charcoal	Tony, Velondriake	1179	±21	1178-1004	SHCAL20	Douglass 2017
D-AMS-001951	Charcoal	Tony, Velondriake	196	±26	301-0	SHCAL20	Douglass 2017
D-AMS-001949	Charcoal	Antsaragnasoa, Velondriake	279	±22	430-159	SHCAL20	Douglass 2017
OxA 34215	Avian eggshell	Tony, Velondriake	2012	±37	2004-1883	SHCAL20	Douglass et al. 2019
OxA 34216	Avian eggshell	Tony, Velondriake	2004	±37	2000-1832	SHCAL20	Douglass et al. 2019
OxA-34274	Avian eggshell	Tony, Velondriake	1677	±27	1588-1426	SHCAL20	Douglass et al. 2019
OxA-34217	Avian eggshell	Tony, Velondriake	8470	±75	9545-9149	SHCAL20	Douglass et al. 2019
OxA-34640	Avian eggshell	Tony, Velondriake	2010	±25	1999-1837	SHCAL20	Douglass et al. 2019

* Calibrated using Marine20 marine curve (Heaton et al. 2020) with estimated δR of 200 years ±50 (following Douglass 2017).

Overall, most chronological information available for Velondriake, to date, comes from ceramic data, with only a small number of absolute radiocarbon dates. Thus, our purpose in this study is to acquire a better understanding of the timeframe of human occupation of the Velondriake area using absolute dating and a regional approach to excavation.

Methods

Excavations were conducted with trowels, and soils were screened using a 2mm mesh. We excavated using natural stratigraphic changes as level breaks. Soil was described using the Munsell soil color chart.

Ceramics were analyzed in the field by the MAP team following the protocol established by Douglass (2016). All sherds wider than 1cm were included in the analysis and were weighed using a digital scale and measured with mechanical calipers. Sherd interior, exterior, and paste colors were described using the Munsell soil color chart, and all decorative elements and surface treatments were recorded and described. Ceramic rims were drawn, in addition to sherds representing unique decorative styles. We used hand magnifying glasses with 10x magnification to record macro inclusions and firing atmosphere was described for each ceramic sherd.

Faunal remains were analyzed using a species code developed by Douglass (2017) which includes the scientific names and how these animals were gathered, processed, disposed of, and used. An in-depth analysis of faunal material is not the focus of this article, however, and will constitute a future project.

Charcoal materials excavated in situ from each excavation unit were analyzed at Penn State's Olo Be Taloha African Environmental Archaeology Laboratory (see Supplemental Table F-1). All charcoal was photographed using a Keyence VK-X1100

(violet) laser scanning microscope at 40x, 80x, 100x, and 150x magnification. Samples were identified using a reference collection of modern macrocharcoal from southwestern Madagascar housed at the Olo Be Taloha African Archaeology Laboratory and the Inside Wood Database (<https://insidewood.lib.ncsu.edu/>). A total of 65 charcoal pieces were recovered from across all the excavations reported here. All well-preserved, identifiable samples with stratigraphically secure contexts were selected for AMS analysis, following chronometric hygiene procedures (Figure 8-2; see Napolitano et al. 2019; Spriggs 1989; Wilmshurst et al. 2011). All selected samples were pretreated using an acid-base-acid (ABA) decontamination protocol to remove humates from the charcoal. ABA consisted of washes with 1N HCl and 1N NaOH for 20-minute intervals at 70°C. Pretreatment and graphitization were conducted in the PSU Stable Isotope Geochemistry Laboratory. AMS was conducted at Penn State's Energy and Environmental Sustainability Laboratories Radiocarbon Facility and dates are reported using accepted standards (Stuiver and Polach 1977). We conducted AMS calibrations using the SHCAL20 calibration curve (Hogg et al. 2020) within the *rcarbon* package in R (Crema and Bevan 2021; R Core Team 2021).

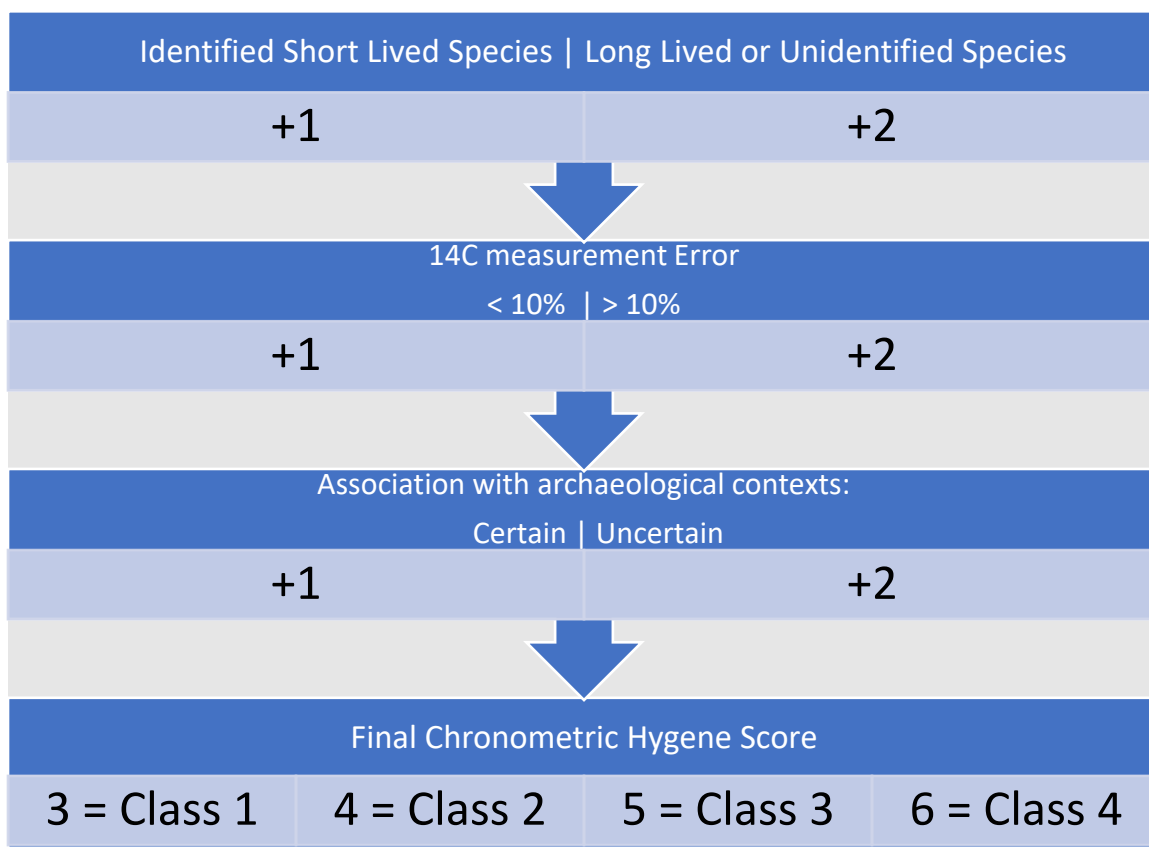


Figure 8-2: Illustration of chronometric hygiene procedure, following previous protocols by Wilmhurst et al. (2011) and Douglass et al. (2019).

For site G134, which yielded an abundance of radiocarbon dates, we generated a Bayesian age-depth estimation for the site using the *rbacon* package in R (Blaauw et al. 2021; R Core Team 2020) (see Appendix F Supplemental Code). Bacon is a method of age-depth estimation that uses Bayesian statistics to construct accumulation models using ¹⁴C dates and other prior information (Blaauw and Christen 2011). Bacon divides a deposit into vertical sections and estimates soil accumulation/sedimentation rates using millions of Markov Chain Monte Carlo (MCMC) iterations for each of these sections. These accumulation rates are then combined with estimated starting dates and other prior information (see Supplemental Code) about the deposit to form the age-depth model. This allows us to understand depositional histories and estimate ages of artifacts found in

between charcoal samples. Below we describe the results of each of the excavations and provide a basic site description for each location.

Results

We excavated eight 1x1m units and one 1x2m unit throughout the Velondriake. Within five of these units, charcoal material was recovered (Table 8-2). Most charcoal dates were attributed as class 1 or 2, which are the most reliable (Table 8-3). Below, we present these newly acquired chronological data and provide a descriptive report of materials recovered from each excavation.

Table 8-2: Radiocarbon dates from charcoal recovered from excavation units reported in this study. All calibrations use the SHCAL20 calibration curve (Hogg et al. 2020) unless otherwise indicated.

PSUAMS#	Sample ID	Description	F ¹⁴ C	±	D ¹⁴ C (‰)	±	Species	¹⁴ C age (BP)	±	Cal BP (2σ)
10424	BELA1	G130 (BELA) Unit 1 Level 1 Charcoal #1. 13cm.	1.1911	0.0021	191.1	2.1	Tree	200	15	283-107
10425	BELA2	G130 (BELA) Unit 1 Level 1 Charcoal #2. 20cm.	0.9878	0.0016	-12.2	1.6	Tree	200	15	283-107
10426	BELA3	G130 (BELA) Unit 1 Level 1 Charcoal #3. 18cm.	0.9847	0.0016	-15.3	1.6	Tree	205	15	283-141
10427	BELA4	G130 (BELA) Unit 1 Level 1 Charcoal #4. 21cm.	0.9974	0.0017	-2.6	1.7	Tree	125	20	253-0
10428	BELA5	G130 (BELA) Unit 1 Level 2 Charcoal #5. 20cm.	0.9866	0.0017	-13.4	1.7	Tree	155	15	262-0
10429	G123-5	G123. Unit 3 Level 2 Charcoal #2. 20cm.	0.9897	0.0018	-10.3	1.8	Wood	415	15	495-331
10430	G123-4	G123. Unit 3 Level 1 Charcoal #1. 16.5cm.	0.9333	0.0018	-66.7	1.8	Tree	555	20	549-509
10431	G123-3	G123. Unit 2 Level 1 Charcoal #3. 22cm.	0.9499	0.0017	-50.1	1.7	<i>Cf. Adansonia</i>	85	15	132-26
10432	G123-2	G123. Unit 2 Level 1 Charcoal #2. 16cm.	0.9755	0.0017	-24.5	1.7	<i>Cf. Adansonia</i>	110	15	242-23
10433	G123-1	G123. Unit 2 Level 1 Charcoal #1. 14cm.	0.9753	0.0017	-24.7	1.7	Wood	20	15	58-27
10434*	AMP1	Ampasimara. Unit 1 Level 1 Charcoal #1. 8cm.	0.9746	0.0017	-25.4	1.7	Wood	-1400	15	-9 – -38
10435	AMP2	Ampasimara. Unit 1 Level 1 Charcoal #2. 26cm.	0.9844	0.0019	-15.6	1.9	Tree	100	15	239-25
10436	AMP3	Ampasimara. Unit 1 Level 2 Charcoal #3. 27cm.	0.9810	0.0016	-19.0	1.6	Tree	125	15	252-5
10437	G134-1	G134. Unit 1 Level 1 Charcoal #1. 21cm.	0.9868	0.0016	-13.2	1.6	Wood	105	15	240-24
10438	G134-2	G134. Unit 1 Level 1 Charcoal #2. 20cm.	0.9903	0.0017	-9.7	1.7	Tree	80	15	129-26

10439	G134-3	G134. Unit 1 Level 1 Charcoal #3. 19cm.	0.9855	0.0017	-14.5	1.7	Tree	120	15	251-7
10440	G134-4	G134. Unit 1 Level 1 Charcoal #4. 34cm.	0.9848	0.0017	-15.2	1.7	Tree	125	15	252-5
10441	G134-5	G134. Unit 1 Level 1 Charcoal #5. 38cm.	0.9935	0.0015	-6.5	1.5	Tree	55	15	59-26
10442	G134-6	G134. Unit 1 Level 1 Charcoal #6. 38cm.	0.9918	0.0018	-8.2	1.8	Tree	65	15	125-27
10443	G134-7	G134. Unit 1 Level 1 Charcoal #7. 43cm.	0.9852	0.0017	-14.8	1.7	Unidentified	120	15	251-7
10463	G134-8	G134. Unit 1 Level 1 Charcoal #8. 40cm.	0.9882	0.0018	-11.8	1.8	Tree	95	15	256-33
10444	G134-10	G134. Unit 1 Level 2 Charcoal #10. 43.5cm.	0.9788	0.0016	-21.2	1.6	Possible tuber	170	15	272-0
10445	G134-11	G134. Unit 1 Level 2 Charcoal #11. 47cm.	0.6988	0.0016	-	1.6	Tree	2880	20	3062- 2867
10446	G134-13	G134. Unit 1 Level 2 Charcoal #13. 50cm.	0.9857	0.0016	-14.3	1.6	Possible shrub	115	15	246-22
10447	G134-14	G134. Unit 1 Level 2 Charcoal #14. 50cm.	0.9870	0.0022	-13.0	2.2	Possible shrub/cactus	105	20	251-7
10448	G134-F1	G134. Unit 1 Level 3 Feature 1 Charcoal #1. 57cm.	0.9777	0.0019	-22.3	1.9	Tree	180	20	279-0
10449	G134-F2	G134. Unit 1 Level 3 Feature 2 Charcoal #1. 65cm.	0.9866	0.0017	-13.4	1.7	Possible Tuber	110	15	242-23
10450	G134-15	G134. Unit 1 Level 4 Charcoal #15. 68cm.	0.9854	0.0018	-14.6	1.8	Possible shrub	120	15	251-7
10451	G134-16	G134. Unit 1 Level 4 Charcoal #16. 66cm.	0.9858	0.0017	-14.2	1.7	Cf. <i>Adansonia</i>	115	15	246-22
10452	G134-17	G134. Unit 1 Level 4 Charcoal #17. 68cm.	0.9832	0.0016	-16.8	1.6	Tree	135	15	253-0
10453	G134-18	G134. Unit 1 Level 4 Charcoal #18. 68cm.	0.9799	0.0019	-20.1	1.9	Tree	165	20	273-0
10464	G134-19	G134. Unit 1 Level 4 Charcoal #19. 68cm.	0.9846	0.0019	-15.4	1.9	Tree	125	20	268-14
10465	G134-20	G134. Unit 1 Level 4 Charcoal #20. 69cm.	0.9806	0.0018	-19.4	1.8	Possible shrub/cactus	160	15	283-0
10466	G134-23	G134. Unit 1 Level 4 Charcoal #23. 71cm.	0.9875	0.0017	-12.5	1.7	Possible shrub	100	15	256-33
10467	G134-24	G134. Unit 1 Level 4 Charcoal #24. 71cm.	0.9836	0.0018	-16.4	1.8	Tree	135	15	270-10

10468	G134-26	G134. Unit 1 Level 4 Charcoal #26. 73.5cm.	0.9860	0.0018	-14.0	1.8	Possible Palm Tree	115	15	259-30
10469	G134-27	G134. Unit 1 Level 5 Charcoal #22. 76cm.	0.9768	0.0020	-23.2	2.0	Possible shrub	190	20	291-0
10470	G134-28	G134. Unit 1 Level 5 Charcoal #23. 72cm.	0.9800	0.0019	-20.0	1.9	Possible shrub	160	20	284-0
10471	G134-30	G134. Unit 1 Level 5 Charcoal #25a. 82cm.	0.9885	0.0019	-11.5	1.9	Tree	95	20	257-33
10472	G134-31	G134. Unit 1 Level 5 Charcoal #25b. 82cm.	0.9768	0.0017	-23.2	1.7	Shrub	190	15	290-0
10473	G134-32	G134. Unit 1 Level 5 Charcoal #26. 77cm.	0.9786	0.0019	-21.4	1.9	Unidentified	175	20	289-0
10474	G134-33	G134. Unit 1 Level 5 Charcoal #27. 79cm.	0.9836	0.0017	-16.4	1.7	Unidentified	135	15	270-10
10475	G134-34	G134. Unit 1 Level 5 Charcoal #28. 78cm.	0.9739	0.0019	-26.1	1.9	Tree	210	20	303-0
10476	G134-35	G134. Unit 1 Level 5 Charcoal #29. 84cm.	0.9760	0.0018	-24.0	1.8	Tree	195	20	293-0
10477	G134-36	G134. Unit 1 Level 5 Charcoal #30. 82cm.	0.9776	0.0018	-22.4	1.8	Tree	180	15	286-0
10478	G134-37	G134. Unit 1 Level 6 Charcoal #31. 85cm.	0.9694	0.0019	-30.6	1.9	Tree	250	20	422-151
10479	G134-38	G134. Unit 1 Level 6 Charcoal #32. 81cm.	0.9818	0.0017	-18.2	1.7	Tree	145	15	278-6
10480	G134-39	G134. Unit 1 Level 6 Charcoal #33. 90cm.	0.9846	0.0018	-15.4	1.8	Tree	125	15	265-22
10481	G134-40	G134. Unit 1 Level 6 Charcoal #34. 90cm.	0.9807	0.0019	-19.3	1.9	Tree	155	20	283-0
10482	G134-41	G134. Unit 1 Level 6 Charcoal #35. 92cm.	0.9765	0.0018	-23.5	1.8	Tree	190	15	290-0
10483	G134-42	G134. Unit 1 Level 6 Charcoal #36. 89cm.	0.9772	0.0018	-22.8	1.8	Not Euphorbiaceae	185	20	290-0
10484	G134-43	G134. Unit 1 Level 6 Charcoal #37. 96cm.	0.9718	0.0016	-28.2	1.6	Cf. Euphorbiaceae	230	15	207-151
10485	G134-44	G134. Unit 1 Level 6 Charcoal #38. 87cm.	0.9853	0.0018	-14.7	1.8	Not Euphorbiaceae	120	15	263-26
10486	G134-45	G134. Unit 1 Level 6 Charcoal #39. 96cm.	0.9725	0.0018	-27.5	1.8	Tree	225	20	309-0
10487	G134-47	G134. Unit 1 Level 7 Charcoal #41. 110cm.	0.9766	0.0018	-23.4	1.8	Tree	190	15	290-0

10488	G134-48	G134. Unit 1 Level 7 Charcoal #42. 115cm.	0.9794	0.0018	-20.6	1.8	Tree	165	15	285-0
10489	G134-49	G134. Unit 1 Level 8 Charcoal #43. 129cm.	0.9769	0.0017	-23.1	1.7	Tree	190	15	290-0
10490	G134-50	G134. Unit 1 Level 8 Charcoal #44. 144cm.	0.8983	0.0019	- 101.7	1.9	Cf. <i>Adansonia</i>	860	20	792-722

* Calibrated using BOMB21 SH1 2 curve (Hua et al. 2021).

Table 8-3: Chronometric Hygiene of charcoal samples processed via AMS. For specific details, see Supplemental Table F-1.

Site ID	# of Charcoal Samples Processed	Class #1	Class #2	Class #3	Class #4
G58 (MOROY)	0	-	-	-	-
G123 Unit 1	0	-	-	-	-
G123 Unit 2	3	0	0	3	0
G123 Unit 3	2	0	2	0	0
G130 (BELA)	5	0	4	1	0
G134	45	6	17	22	0
G-15-2020 (Ampasimara)	3	0	1	2	0
SAVABO	0	-	-	-	-
TOTAL	58	6	24	28	0

Radiocarbon Chronology of Human Presence in Velondriake, Madagascar

¹⁴C dates from the excavations reported here vastly expand our chronological record for the archaeology of Velondriake (Figure 8-3). In the south, charcoal from site G123 Unit 2 provides evidence of occupation between 240 and 27 cal. BP. Moving northward, G123 Unit 3 indicates human occupancy between 550 and 330 cal. BP. To the northeast of G123, Ampasimara (G-15-20) has evidence of human occupancy as early as 252 cal. BP up to the present day (-37 cal. BP). The northernmost site of G130 (BELA) demonstrates human occupation between 280 cal. BP and the present.

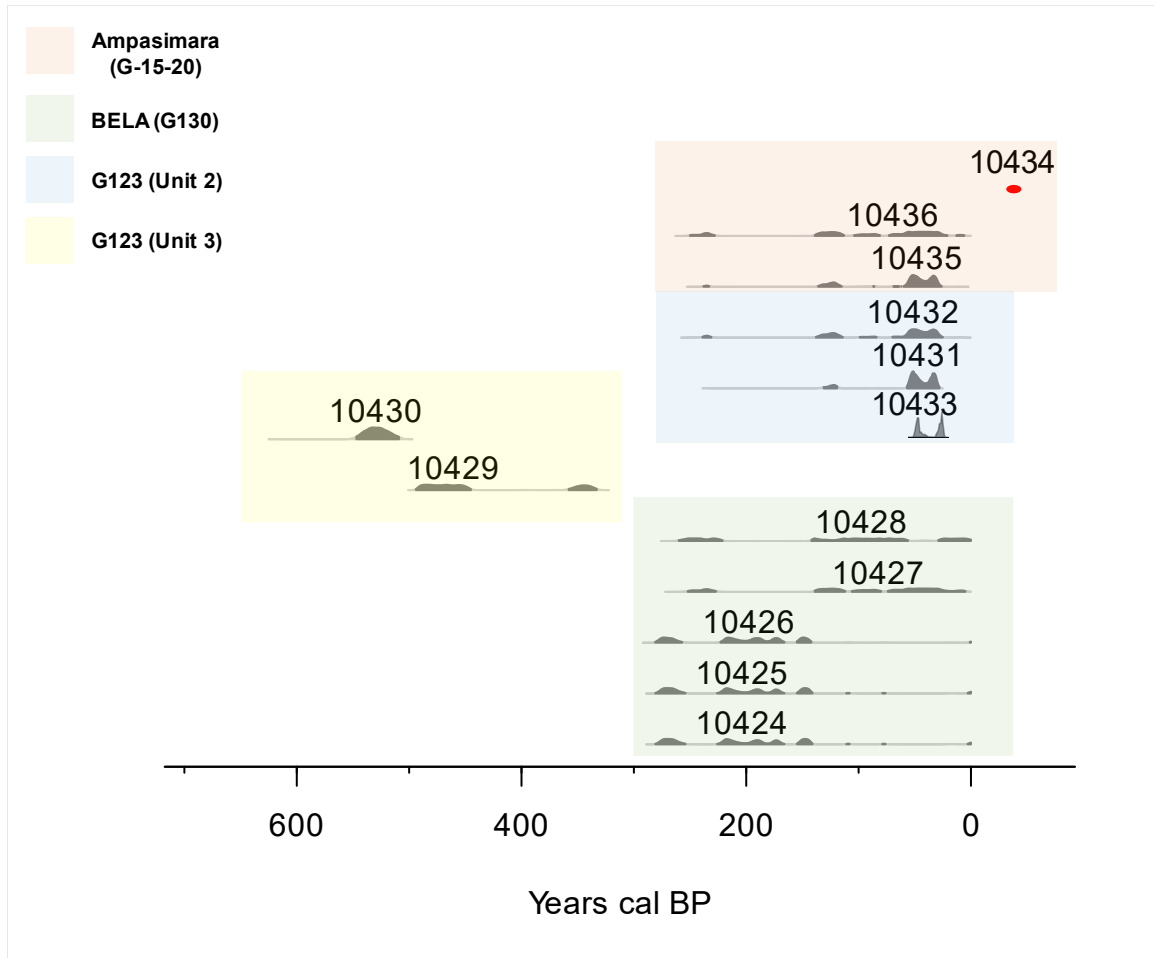


Figure 8-3: Radiocarbon data for all excavations in Velondriake conducted in this study except G134. Red dot represents calibration for PSUAMS#10434 which contained bomb carbon from post-1950.

G134 presents the largest continuous sequence of carbon dates for the entire Velondriake region, to date, with a total of 45 charcoal dates. We generate a Bayesian age-depth estimation (Figure 8-4) for the site using the *rbacon* package in R (Blaauw et al. 2021; R Core Team 2020). We constructed our model using the following parameters: [accumulation rate (acc.mean) = 2 year cm^{-1} , shape distribution of accumulation rate (acc.shape) = 1.5, memory mean (mem.mean) = 0.5, memory strength (mem.strength) = 10, depths of hiatuses (hiatus.depths) = c(130, 140, 150), maximum hiatus length in years (hiatus.max) = 100] (see Appendix F). We assume the presence of three hiatus periods around 130cm, 140cm, and 150cm based on the age difference between a charcoal date

from 129cm (185 median cal. BP) and the charcoal date from 144cm (756 median cal. BP) coupled by an absence of in situ artifacts recovered between 130 and 135 cm, 139 and 143 cm, and 149 and 153cm. Based on the distance between these two dates, we use a maximum hiatus length of 100 years as our starting assumption for the model. Longer lengths of time were also tested (e.g., 200) but resulted in poorer fitting models. All ^{14}C dates were included in the model except for PSUAMS#10445, which was an extreme outlier. Based on this age depth model, lithic material (discussed below) recovered at a depth of 166cm likely dates to between 728 and 1235 cal. BP (CI = 95%, median = 982 cal. BP). We also ran another model using only class 1 and 2 dates with the same parameters and results were comparable (Supplemental Figure F-1).

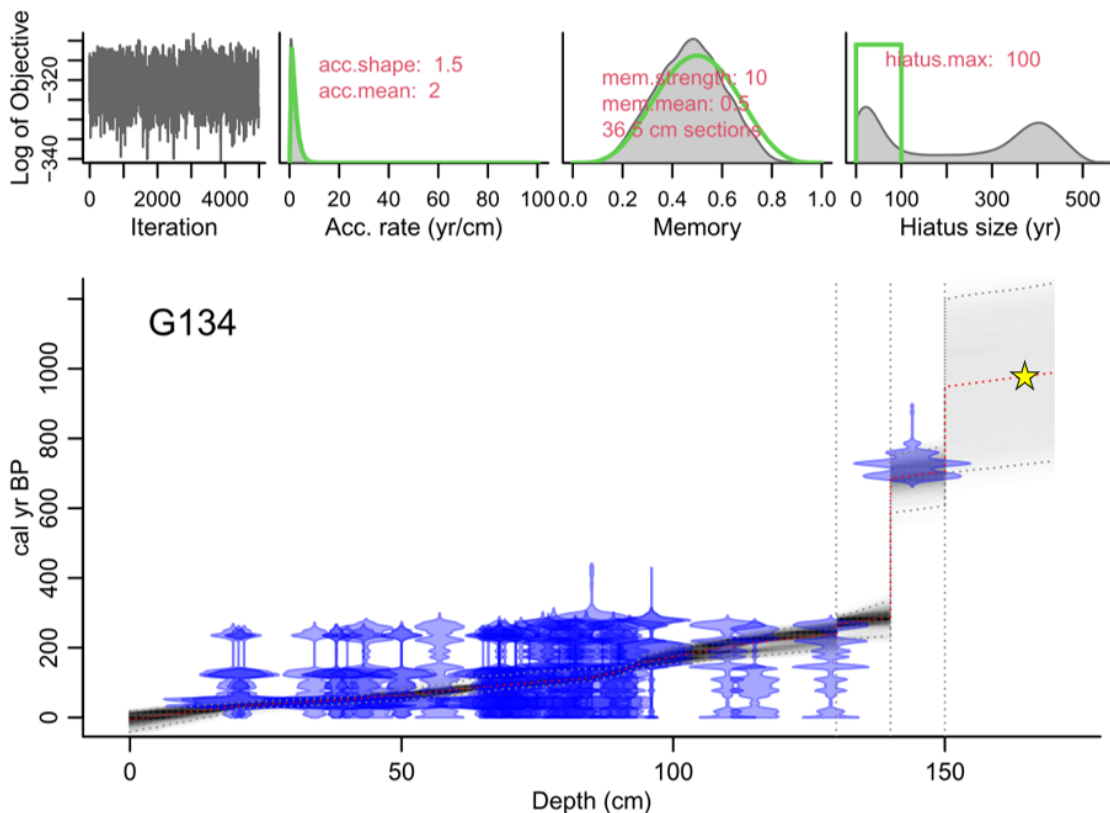


Figure 8-4: Bayesian age depth estimation model. **Top:** MCMC iterations of the modeling simulation (left plot). Good runs show stationary distributions with little structure between neighboring iterations (Blaauw and Christien 2013). The prior (green curve) and posterior (grey histogram) distributions of the accumulation rate (top left-middle plot), memory (top right-middle plot), and hiatus size (top right). **Bottom:** plot shows ^{14}C dates (transparent

blue) calibrated using SHCAL20 (Hogg et al. 2020) and the age-depth model, where darker grey areas indicate higher likelihood ages. Horizontal grey dotted lines represent 95% confidence intervals, and the red dotted line is the best-fit model based on a weighted mean. Vertical grey lines represent hiatuses added to the model at 130, 140, and 150cm based on absences of cultural materials recovered between 130-135, 139-144, and 145-153cm. Depth of recovered lithic (166cm) is indicated by the yellow star.

Site Descriptions

G-123 Units 1 and 2: The site lies approximately 50m southeast from the coastline of a small bay located approximately 1 km south of the modern village of Andavadoaka. Initial ground survey of the area identified dozens of artifacts consisting of ceramics, marine shells, shell beads, and burnt stones, indicating that there was a likelihood of finding the remnants of a foraging campsite in this area with further investigation.

In 2021, three 1m X 1m excavation units were opened at G123 by members of the MAP Team (Figure 8-5). Unit 1 yielded three stratigraphic levels of cultural material extending to a depth of 90cm, including an abundance of bones from marine species (Table 8-4, Supplemental Figure F-2). The unit was subsampled within the third stratigraphic level due to a significant decrease in the density of cultural material recovered. This unit includes a circular concreted feature that appears in the second level and continues past the third excavation level (Figure 8-5). It is located at about 50cm in depth near the northern edge of the excavation unit. The feature itself might represent a hearth or fire-pit, given its darker color (10YR 6/4) from the surrounding soil (10YR 7/2) and hardened components that may be remnants of firing activity.

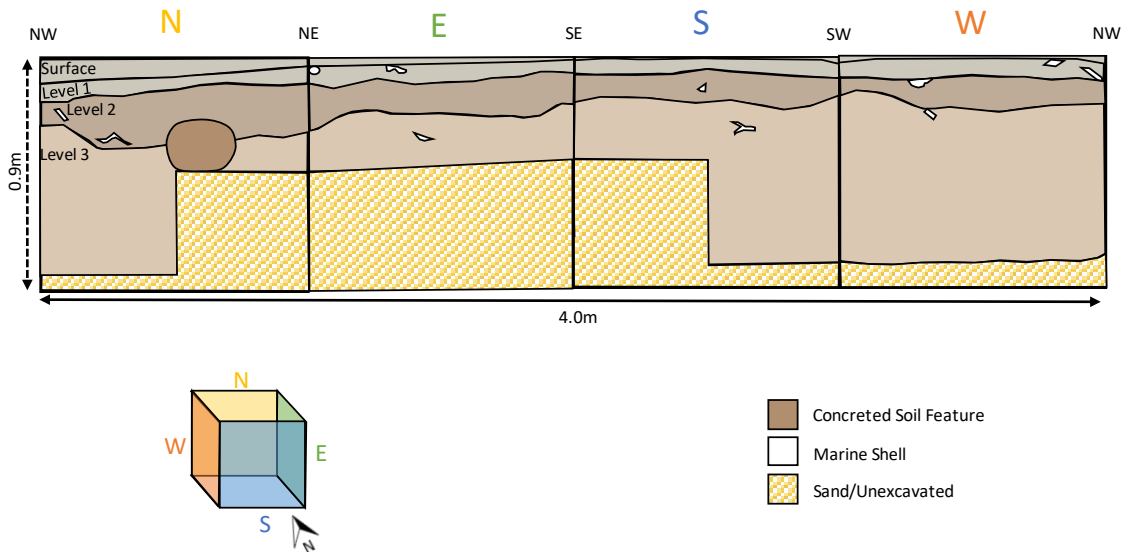


Figure 8-5: Profile wall drawings of G123 Unit 1. Colors correspond with munsell color codes recorded during excavation (Surface and Level 1 = 5Y 8/1; Level 2 = 10YR 7/2; Level 3 = 10YR 8/2; Concreted Feature = 10YR 6/4). 3D box shows dimensions of excavation unit and colored directional abbreviations correspond with sections of the drawing.

Table 8-4: G123 Unit 1 Marine Shell Material

Level	Family	Species	Food (Y/N)	Intact	Broken	Burned	Total	Weight
Surface	Strombidae		N		1	1	1	10
Surface	Turbinidae	<i>Turbo coronatus</i>	Y		2		2	7
Surface	Fascioliariidae	<i>Fasciolaria trapezium</i>	Y					
Level 1	Turbinidae	<i>Turbo coronatus</i>	Y					
Level 1	Fascioliariidae	<i>Fasciolaria trapezium</i>	Y		1		1	75
Level 1	Fascioliariidae	<i>Fasciolaria trapezium</i>	Y	1	1		1	140
Level 1	Turbinidae	<i>Turbo coronatus</i>	Y		1		1	7
Level 1	Strombidae	<i>Lambis lambis</i>	N		1		1	8
Level 1	Unknown				1		1	48
Level 1	Achatinidae	<i>Achatina achatina</i>	N	9	1		10	22
							1	
Level 2	Neritidae	<i>Nerita albicilla</i>	N	1			1	5
Level 2	Buccinidae		N	1	1		1	0
Level 2	Neritidae	<i>Nerita undae</i>	Y (starvation)*	1			1	0
Level 2	Achatinidae	<i>Achatina achatina</i>	N	12	4		16	27

*Starvation foods refer to taxa which are generally only consumed in times of stress or poverty when preferred sources are unavailable.

Unit 2 is located 35m to the southwest of Unit 1 and consists of two stratigraphic levels of cultural activity (Figure 8-6). The surface is defined by the presence of faunal remains (crab bones), worked shell, and charcoal fragments. The first layer of excavation revealed 17 in situ marine shell tools and three pieces of charcoal. Level 2 contained 7 more in situ worked marine shells as well as several crab bones and charcoal material. Marine shells consist of similar species to those recovered in Unit 1 (Table 8-5; Supplemental Figure F-3). Charcoal recovered from this unit indicates human occupation between 258 and 27 cal. BP. Heavy fractions of soil were taken from the surface and layer 1.

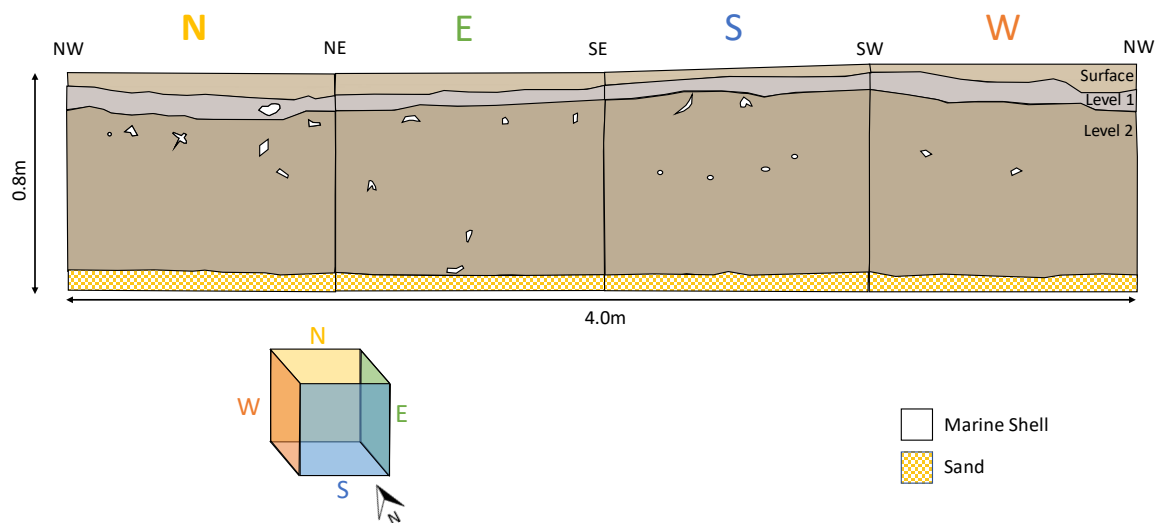


Figure 8-6: Profile wall drawing of G123 Unit 2. Colors correspond with munsell color codes recorded during excavation (Surface = 2.5Y 8/2; Level 1 = 2.5Y 8/1; Level 2 = 2.5Y 7/2). 3D box shows dimensions of excavation unit and colored directional abbreviations correspond with sections of the drawing.

Table 8-5: G123 Unit 2 Marine Shell Materials

Level	Family	Species	Food (Y/N)	Intact	Broken	Burned	Total	Weight
Surface	Fascioliariidae	<i>Fasciolaria trapezium</i>	Y					
Surface	Potamididae	<i>Terebralia palustris</i>	Y	2	2	2	2	22
Surface	Turbinidae	<i>Turbo coronatus</i>	Y					
Surface	Cypraeidae	<i>Cypraea annulus</i>	Y	1			1	0
Surface	Neritidae	<i>Nerita undae</i>	Y (starvation)					5
Surface	Turbinidae		Y	4	1	1	5	4
Surface	Chitonidae	<i>Onithochiton literatus</i>	Y	8	2	1	10	5
Surface	Glycymeridae	<i>Glycymeris connollyi</i>	Y		2		2	6
Surface	Mytilidae	<i>Mytilus galloprovincialis</i>	Y		2		2	0
Surface	Achatinidae	<i>Achatina achatina</i>	N	1			1	0
1	Fascioliariidae	<i>Fasciolaria trapezium</i>	Y		4	1	20	315
1	Potamididae	<i>Terebralia palustris</i>	Y	4	7		8	135
1	Chitonidae	<i>Onithochiton literatus</i>	Y	18	2		20	11
1	Achatinidae	<i>Achatina achatina</i>	N	1			1	3
1	Murex	<i>Chicoreus austramosus</i>	Y	1	4		4	267
1	Strombidae	<i>Lambis lambis</i>	N		1		1	22
1	Mytilidae	<i>Mytilus galloprovincialis</i>	Y	1			1	4
1	Lucinidae (types)		Unknown					7
1	Turbinidae	<i>Turbo coronatus</i>	Y		1		1	18
1	Mytilidae	<i>Mytilus galloprovincialis</i>	Y		1		1	0
1	Naticidae		Y					54
2	Fascioliariidae	<i>Fasciolaria trapezium</i>	Y		2		2	201

2	Potamididae	<i>Terebralia palustris</i>	Y	1	4	4	124
2	Murex	<i>Chicoreus austramosus</i>	Y				
2	Chitonidae	<i>Onithochiton literatus</i>	Y	52	1	67	46
2	Neritidae	<i>Nerita undae</i>	Y (starvation)				72
2	Littorinidae		N		1	5	10
2	Muricidae	<i>Purpura panama</i>	N		1	1	23
2	Turbinidae	<i>Turbo coronatus</i>	Y	2	3	4	68
2	Buccinidae		N	2		2	5
2	Muricidae	<i>Purpura panama</i>	N				18
2	Littorinidae		N	15	7	22	48
2	Strombidae	<i>Lambis lambis</i>	N				63

G123 Unit 3:¹⁰ Unit 3 is located 250m to the Northeast of G123 Unit 1 and contained three stratigraphic levels of cultural material (Figure 8-7). This unit was subsampled after level 2 due to a substantial decrease in material culture density. The surface contained a few small marine shells, and a heavy fraction of soil was taken as a sample. Level 1 revealed a myriad of faunal remains, including fish bones and marine shells, as well as charcoal, which dates to 549-509 cal. BP. Marine shells represent a variety of species, some of which are edible and others of which are not used as food sources. Additionally, there was a circular feature at the north-central boundary of the excavation unit that was defined by extremely compact soil with a darker brown color (10YR 5/3) (Figure 8-8). Two soil samples were taken from the compacted area.

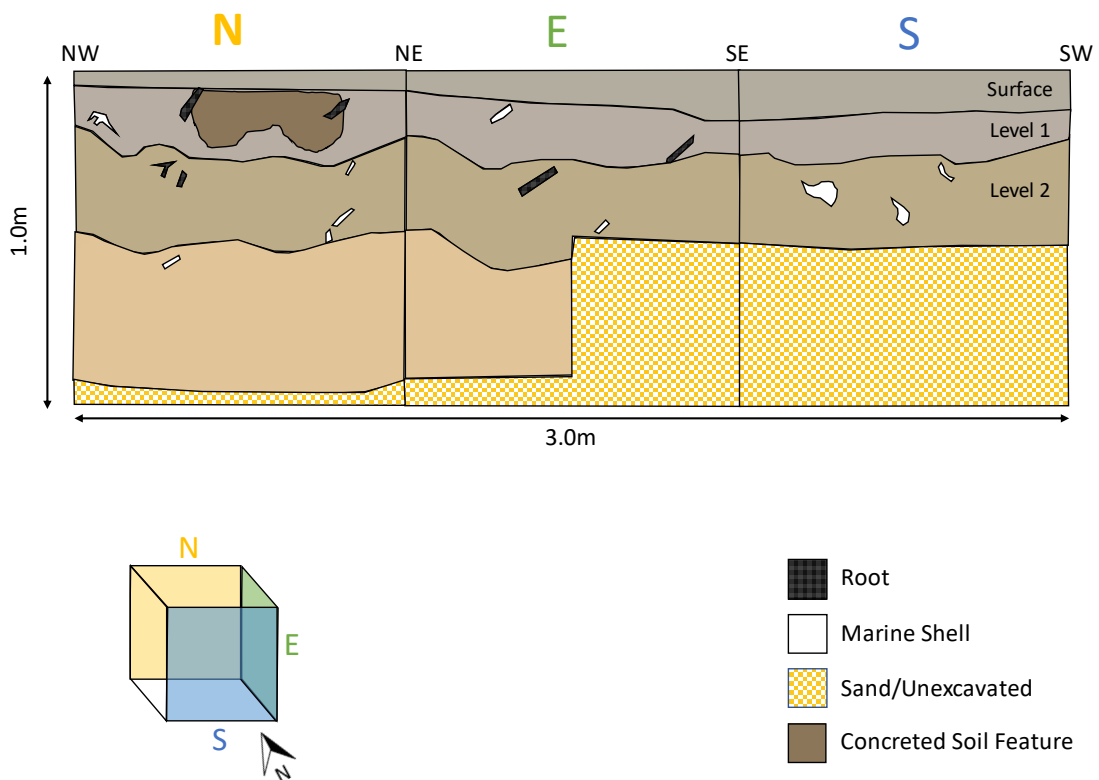


Figure 8-7: Profile wall of G123 Unit 3. Colors correspond with munsell color codes recorded during excavation (Surface = 2.5Y 7/1; Level 1 = 10YR 7/1; Level 2 = 10YR

¹⁰ This unit was originally surveyed as site G-90, which was identified as high likelihood of containing archaeological deposits by Davis et al. (2020).

7/3; Level 3 = 2.5Y 8/4). 3D box shows dimensions of excavation unit and colored directional abbreviations correspond with sections of the drawing.



Figure 8-8: Photo of concreted soil layer found in G123 Unit 3.

Level 2 of the excavation unit revealed three more in situ marine shells that comprise both food and non-food sources, including several *Nerita undae* shells which are edible but not a preferred food source in the region today (Table 8-6; Supplemental Figure F-4). Charcoal recovered from this excavation level dates to 495-331 cal. BP and a heavy fraction of soil was taken. Level 3 contains five more marine shells, of which four are edible species (one of which is *Nerita undae*). Additionally, some crab bones were recovered, and the total number of cultural materials drops significantly. We concluded the excavation once cultural materials were no longer present.

Table 8-6: G123 Unit 3 Marine Shell Materials

Level	Family	Species	Food (Y/N)	Intact	Broken	Burned	Total	Weight
Surface	Fascioliariidae	<i>Fasciolaria trapezium</i>	Y		1		1	67
Surface	Chitonidae	<i>Onithochiton literatus</i>	Y	5			5	3
Surface	Turbinidae	<i>Turbo coronatus</i>	Y		2		2	20
Surface	Neritidae	<i>Nerita undae</i>	Y (starvation)					6
1	Neritidae	<i>Nerita undae</i>	Y (starvation)	4			4	78
1	Strombidae	<i>Lambis lambis</i>	N		1		1	107
1	Cassidae	<i>Cypraecassis rufa</i>	N		2		2	109
1	Turbinidae	<i>Turbo coronatus</i>	Y		7		7	75
1	Fissurellidae (types)		N	1			1	0
1	Achatinidae	<i>Achatina achatina</i>	N	3	1		5	16
1	Chitonidae	<i>Onithochiton literatus</i>	Y	44	2		48	35
1	Unknown		Unknown		2	1	2	183
1	Bursidae (types)		Y	2	3		3	407
1	Murex	<i>Chicoreus austramosus</i>	Y		1		1	93
1	Fascioliariidae	<i>Fasciolaria trapezium</i>	Y		2		2	333
2	Bursidae (types)		Y		3		3	76
2	Achatinidae	<i>Achatina achatina</i>	N	12	4		16	24
2	Strombidae	<i>Lambis lambis</i>	N					10
2	Chitonidae	<i>Onithochiton literatus</i>	Y	21			21	15
2	Neritidae	<i>Nerita undae</i>	Y (starvation)	5	2		7	30
2	Neritidae	<i>Nerita albicilla</i>	N	1	2		3	7
3	Achatinidae	<i>Achatina achatina</i>	N	13	3		16	31

3	Neritidae	<i>Nerita undae</i>	Y (starvation)	3	2	5	17
3	Turbinidae	<i>Turbo coronatus</i>	Y	1	1	1	14
3	Chitonidae	<i>Onithochiton literatus</i>	Y	5	1	6	4
3	Murex	<i>Chicoreus austramosus</i>	Y				7

G130 (BELA): This site lies on top of coastal sand dunes that are ~30m from the beach and ~80m from the shoreline to the immediate SW of the village of Belavenoka. The surface of the site was littered with ceramics and marine shells, along with smaller quantities of faunal materials, coral, metal, and burnt stones.

In 2020, one 1m X 1m excavation unit was opened in the surveyed area which extended to a depth of 89cm and consisted of three stratigraphic layers (Figure 8-9). The first level of the excavation revealed dozens of in situ artifacts, including ceramic sherds, marine shells, metal, charcoal, elephant bird eggshells, and faunal materials. This level contained the greatest number of artifacts. The second excavation level yielded more ceramics, faunal remains, marine shell, elephant bird eggshell, and charcoal. The third and final excavation level produced only marine shell. Soil samples were taken from each level of the unit.

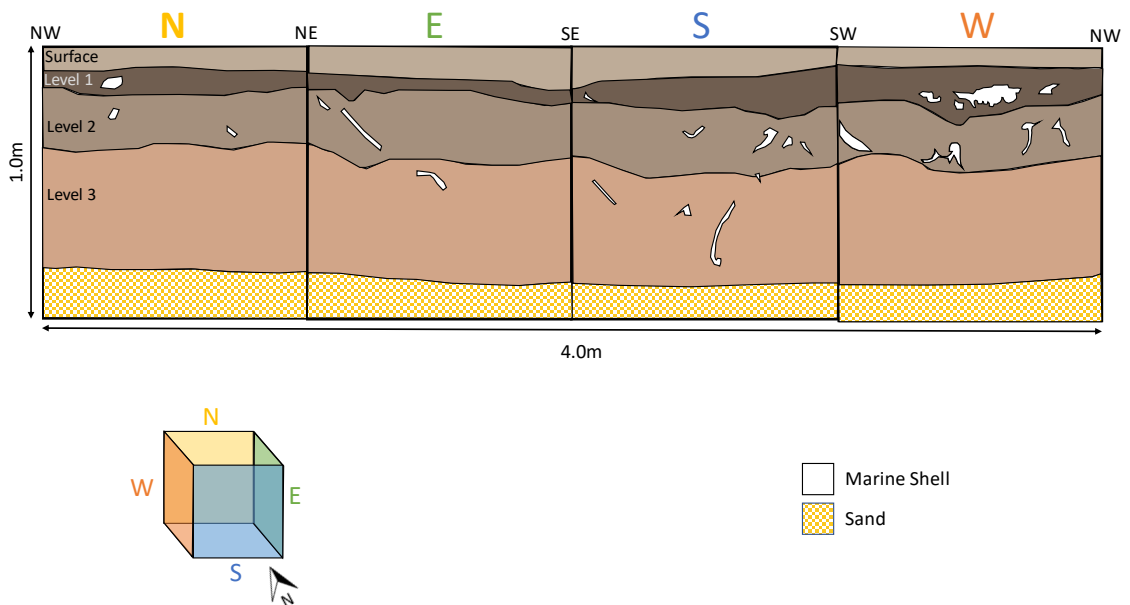


Figure 8-9: Profile wall drawing of G130. Colors correspond with munsell color codes recorded during excavation (Surface = 10YR 7/2; Level 1 = 10YR 4/2; Level 2 = 10YR 6/2; Level 3 = 7.5YR 7/4). 3D box shows dimensions of excavation unit and colored directional abbreviations correspond with sections of the drawing.

Charcoal from this site dates to between 283-0 cal. BP, with a mean age estimation of occupancy between 100 and 180 cal. BP. The people who occupied this site appear to have relied on fishing and marine resources. Given its proximity to the modern village of Belavenoka, it speaks to the persistence of human presence in this region for the past several hundred years with similar subsistence strategies and environmental exploitation patterns as practiced today.

G58 (MOROY): This site is located on a thin strip of coastal beach that sits adjacent to a dense mangrove forest to the east (Figure 8-1). The surface was littered with materials, primarily elephant bird eggshells and shell beads (see Appendix B Supplemental Table 1). A single 1m X 1m excavation unit was opened on an area where we recovered numerous surface materials, including shell beads and ceramics. Roots were present throughout the unit (Figure 8-10). The first stratigraphic level revealed cultural materials, including: ceramics, faunal material, and marine shells. The second (and final) level was limited to elephant bird eggshell. Some of the faunal and eggshell material was burned, potentially evidence of human consumption.

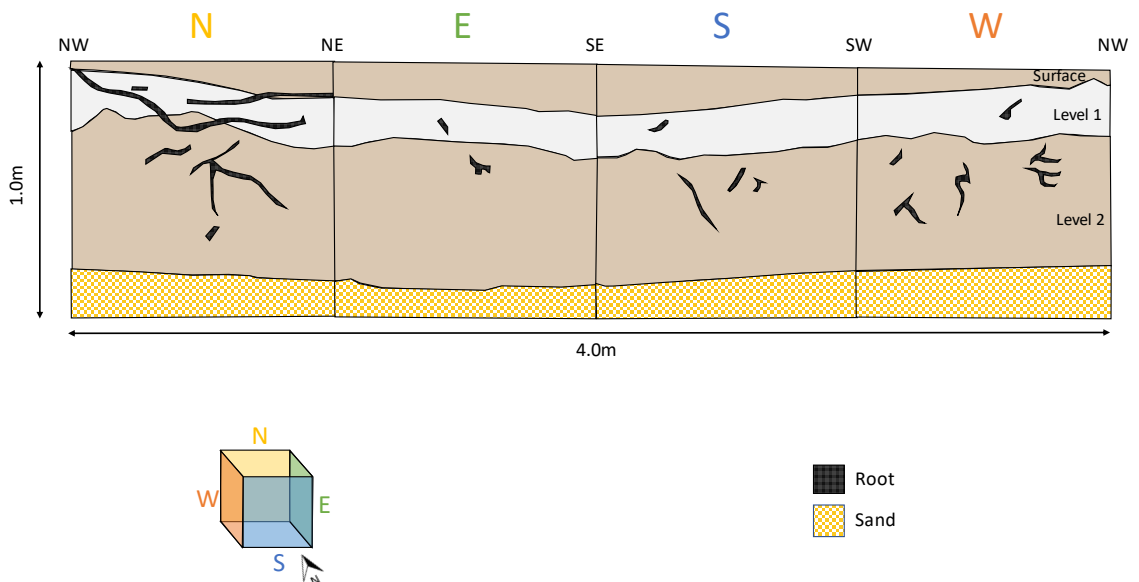


Figure 8-10: Profile wall drawing of G58. Colors correspond with munsell color codes recorded during excavation (Surface = 10YR 8/2; Level 1 = 2.5Y 2/8 (white); Level 2 =

10YR 8/2). 3D box shows dimensions of excavation unit and colored directional abbreviations correspond with sections of the drawing.

Based upon the surface deposit context, it is possible that the area served as a nesting site for elephant birds (*Aepyornithidae* sp.) and was later occupied by human communities at some point during the last 1500-2000 years. The length of occupation is uncertain; however, given the number of shell beads identified during surface surveys of areas adjacent to the excavation unit (see Davis et al. 2020), it is possible that the area was a site of moderate-to-long-term occupation. Additional excavation units in adjacent areas might help elucidate this question.

G134 (Antsaranasoa): This site yielded the greatest number of excavation levels, totaling 1.8m in depth (Figure 8-11). A 1m X 2m unit was opened at one location of the site that contained numerous surface deposits consisting of ceramics and marine shells.

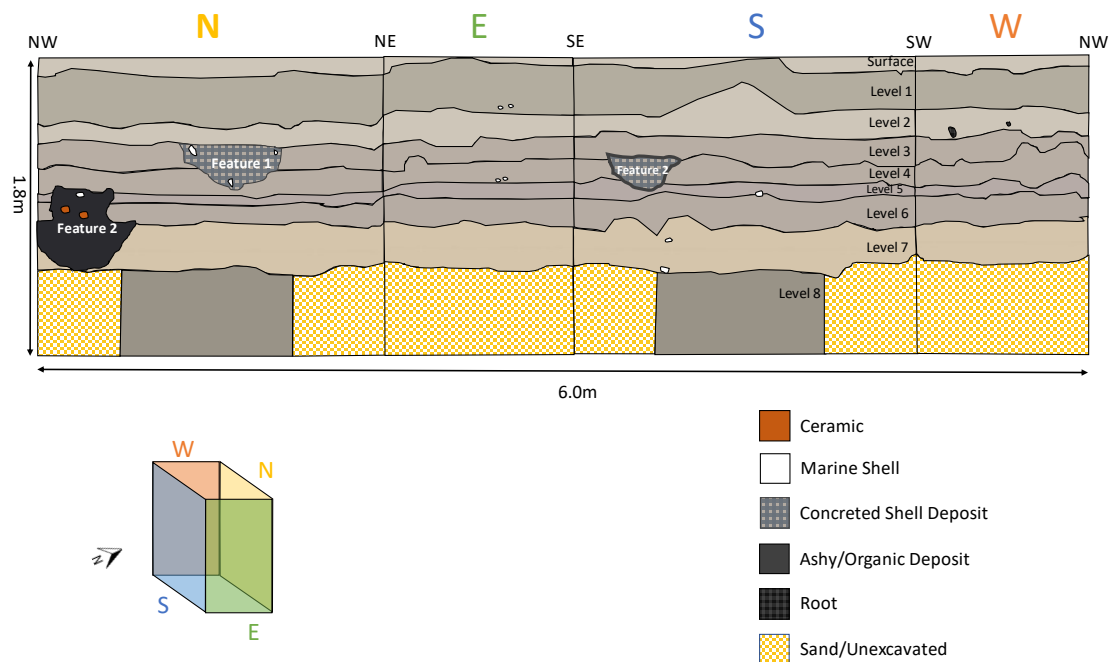


Figure 8-11: Profile wall drawing of G134. Drawing was created using field photographs but not during the excavation due to wall collapse. Colors correspond with munsell color codes recorded during excavation (Surface = 2.5Y 8/1; Level 1 = 2.5Y 7/1; Level 2 = 2.5Y 8/1; Level 3 = 10YR 7/1; Level 4 = 10YR 7/1; Level 5 = 2.5 YR 7/1; Level 6 = 7.5YR 7/1; Level 7 = 2.5Y 8/2; Level 8 = 2.5Y 6/1). 3D box shows dimensions of excavation unit and colored directional abbreviations correspond with sections of the drawing.

Level 1 of the excavation contained a lot of root activity, which was largely confined to the top of the level. An abundance of artifacts were recovered, including ceramic sherds, animal bones (marine and terrestrial fauna), marine shell, metal, and charcoal. All ceramics recovered from this level were undecorated body sherds. Nine charcoal pieces were recovered in situ from level 1, all of which indicate a median occupation period of between 40 and 120 cal. BP.

Level 2 of the unit is defined by the same soil matrix and undecorated ceramics, metal, fishbones, marine shells, and charcoal were recovered. A soil sample and 5 pieces of charcoal were recorded in situ throughout the unit level. Charcoal suggests a median occupation time of between 104 and 188 cal. BP, with one exception of a sample that dates to 3000 – 2800 cal. BP. This is an extreme outlier, however, and should not be trusted as an accurate age of this context.

Level 3 begins to transition to a darker matrix (10YR 7/1) and is the start of two features with a darker coloration. Feature 1 (10YR 6/1) appears at a depth of 57cm, and Feature 2 (10YR 5/1) appears at 65cm in depth (Figure 8-12). These two features are defined by a mass of marine shells and concreted sediment, Feature 1 in the center of the unit, and Feature 2 spans most of the level, with clusters near the SE and NW corners. Both features appear to be related to cooking activities and are likely remnants of a fire pit or hearth. Charcoal was recovered from each of these features. The top of Feature 1 has a mean age of 185 cal. BP, and the top of Feature 2 has a mean age of 108 cal. BP. Ceramics recovered from level 3 display shell combing, including body and rim sherds.



Figure 8-12: Surface of Feature 1 (Left) and Feature 2 (Right) which are defined by concreted and burnt shell material. Outlines of each feature indicated by dotted white line.

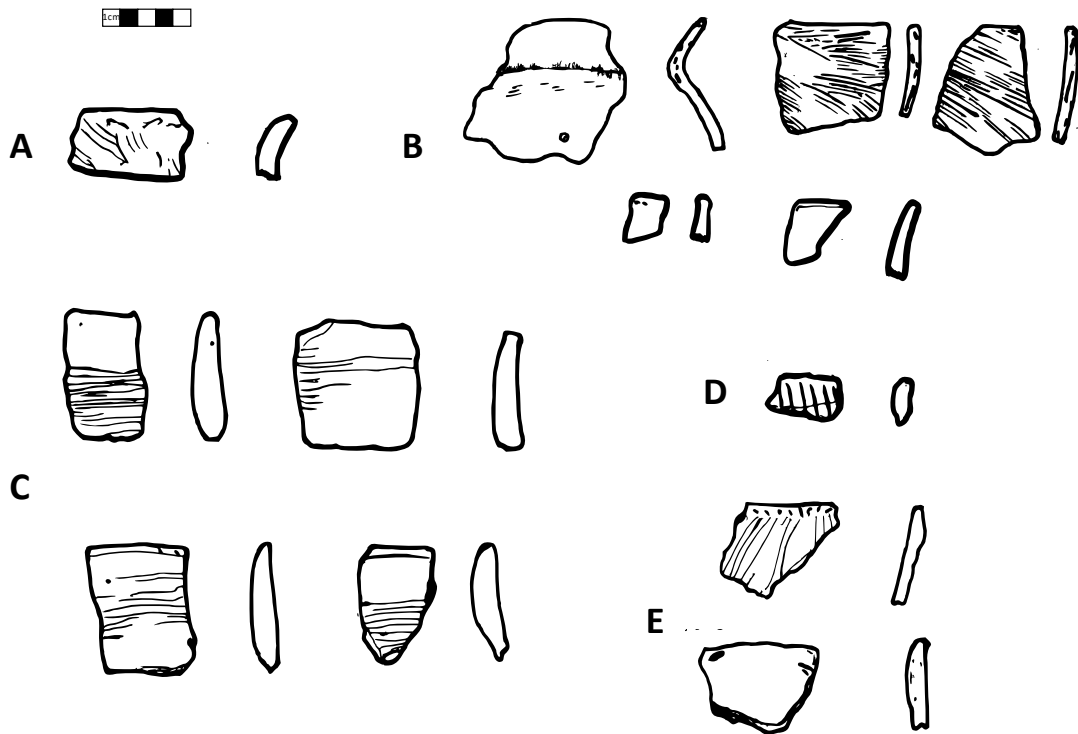


Figure 8-13: Drawings of ceramic rim sherds recovered from G134. A: shell combed sherds recovered from Level 3. B: incised and shell combed sherds recovered from Level 5. C: incised and punctated sherds recovered from Level 6. D: incised sherd recovered from Level 7. E: punctated and incised sherds recovered from Level 8.

Level 4 produced a large quantity of fishbones, as well as some ceramics, metal, marine shells, and charcoal. Ceramics are all body sherds and display burnishing and surface treatments, as well as some decorative shell combing and various mineral and marine shell inclusions. Feature 2 continues on the NW corner of the unit. Charcoal dates this level to a median age of between 102 and 185 cal. BP.

Level 5 contains ceramics, fishbones, and marine shells, as well as charcoal, but no metal is recovered from this point. 10 pieces of charcoal were recovered in situ from this level. Ceramics consist of shell combed style as well as some parallel incising, indicating earlier occupation periods (~16th-18th centuries; Figure 8-13b). This aligns with radiocarbon dates obtained from charcoal in this level, which have a median age of between 104 and 187 cal. BP. Ceramics also display a variety of manufacturing methods including land-shell and mineral inclusions. Feature 2 continues at this level and begins to transition to a darker, ashy deposit.

Level 6 contains a continuation of Feature 2, which includes burned fishbones and ceramics. Ceramics are also found on the NW wall of the unit. Ceramics include a variety of styles, and consist of shell combing, incising, and circular punctations (Figure 8-13c). The level itself is likely a multicomponent layer consisting of material spanning several hundred years, as shell combing persists from the 18th-20th centuries, but incising and circular punctation persists from the 9th-18th centuries. Eight charcoal pieces were recovered in situ from this level, and they date to a median age of between 102 and 296 cal. BP.

Level 7 contained ceramic sherds, fishbones and unidentified terrestrial faunal remains, and marine shells. Ceramics consist of circular punctations, incising, and shell combing decorative styles (Figure 8-13d). Inclusions include red, white, and yellow minerals, coral, sand and terrestrial shell. Feature 2 concludes on the NW corner of unit.

Only two pieces of charcoal were recovered from this level (significant decrease from previous levels) and yield median dates between 185-187 cal. BP.

Level 8 is the last level excavated in this unit and contained numerous ceramics, bones, marine shell, and charcoal. We also recovered a lithic blade, in situ at the very bottom (166 cm) of this excavation level (Figure 8-14). The object appears to be composed of brown chert, with thinner parts of the blade becoming somewhat translucent. Its composition appears similar to other lithics recovered in the northern parts of the island (see Dewar et al. 2013). Ceramics consist of circular punctation, incising, and combing (Figure 8-13e). Two in situ charcoal pieces were recovered. The first, recovered at 129cm, has a median date of 185 cal. BP. The second, recovered at 144cm, has a median date of 756 cal. BP. Cultural material becomes scarcer between these two charcoals and there is a possibility that there are hiatuses in cultural activity from this point on in the unit, suggesting periods of time when humans did not occupy this site between ca. 200 – 800 cal. BP. Our Bayesian age-depth accumulation model (Figure 8-4) estimates that the lithic recovered at 166cm dates to between 728 and 1235 cal. BP (Figure 8-15). Before beginning excavation on Level 9, the wall of the unit collapsed, and we suspended work at this unit. We later returned to the site and excavated Level 9 and no cultural materials were recovered.



Figure 8-14: Bayesian age estimation of the depth where the lithic blade was recovered from Level 8 of G134 Unit 1.

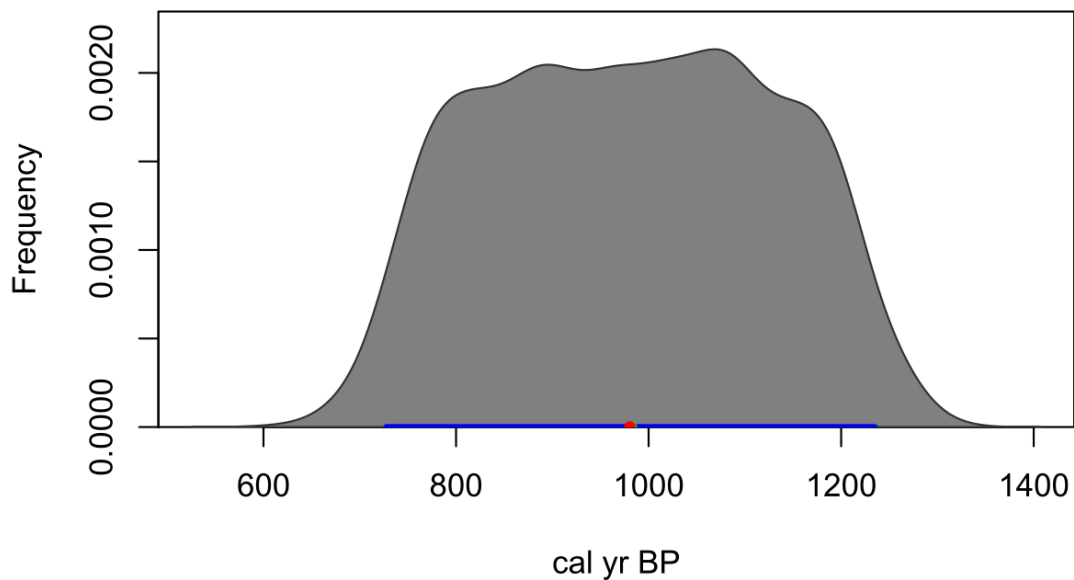


Figure 8-15: Shows the distribution of age estimates for a depth of 166cm based on the Bayesian age-depth estimation model reported above (Figure 8-4). Blue line shows the 95% confidence range, green dot shows the median age estimation (982 cal. BP), and red dot shows the mean age estimation (981 cal. BP).

Overall, G134 was likely a fishing village that was consistently occupied for the last 250 years. Prior to 300 cal. BP, there appears to have been more infrequent, but still extensive human presence that was interrupted by a series of hiatuses that lasted

between 30 and 300 years each (between 270-300 cal. BP, 340-590 cal. BP, and 700-950 cal. BP). The exact nature of these later occupations and hiatuses is uncertain given the scarcity of radiocarbon dates from these levels, but nevertheless, the site appears to be an area that saw extensive, long-term occupation that partially predates ceramic use on Madagascar.

Ampasimara (G-15-2020): The site is located just inland from the coast between the Fagnemotsy Bay [Baie des Assassins] (to the west) and a mangrove forest (to the east) (Figure 8-1). During ground surveys of the area a ceramic sherd and an abundance of worked marine shells were recovered. We excavated one 1m X 1m unit at this site (Figure 8-16). We subsampled the unit beginning in level 4 due to a significant decline in the density of recovered material culture.

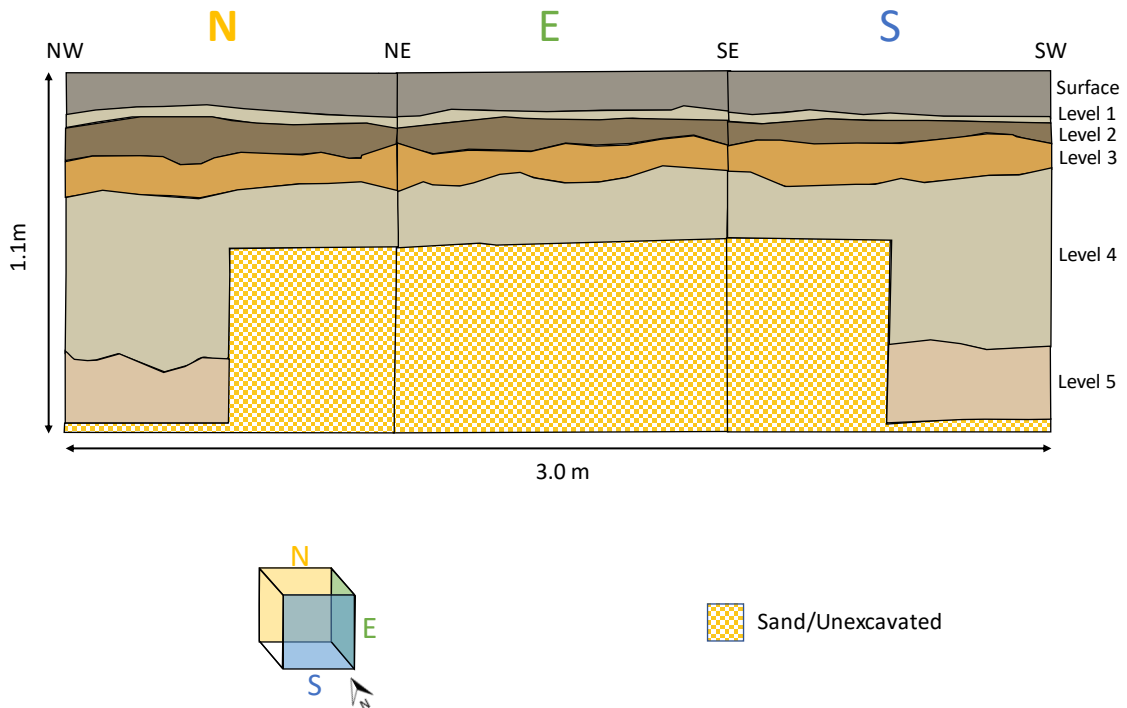


Figure 8-16: Profile wall drawing of G-15-20. (Surface = 2.5Y 6/1; Level 1 = 7.5YR 7/2; Level 2 = 2.5Y 5/3; Level 3 = 10YR 7/8; Level 4 = 5Y 8/2; Level 5 = 10YR 8/3). 3D box shows dimensions of excavation unit and colored directional abbreviations correspond with sections of the drawing.

The site resides adjacent to the shoreline, and its surface contained two in situ marine shell tools, one made from Nassariidae (which is not used as a source of food) and the other made from Turbinidae (which is used as a food source among modern and historic populations in this region) (Table 8-7). The diversity and number of marine shells increases at each level (Supplemental Figure F-5). In Level 1, six worked marine shells were recovered, as well as two burnt shells from mangrove species known to be food sources (*Terebralia palustris*). In Level 2, we recovered (in situ) 3 pieces of charcoal, 1 undecorated ceramic sherd, fishbones, and 14 marine shells, including a higher abundance of these burnt mangrove shellfish remains (*Terebralia palustris*). Three additional stratigraphic levels were excavated (3, 4, and 5) which produced no cultural materials. Based on this evidence, it appears that G-15-2020 was a fishing camp, likely a seasonal occupation that has a mean occupation date between 113 cal. BP and the present. With proper marine reservoir corrections, burnt shell material may provide a useful means of acquiring additional radiometric dates.

Table 8-7: G-15-2020 marine shell materials.

Level	Family	Species	Food Source (Y/N)	Intact	Broken	Burned	Total	Weight (g)
Surface	Nassariidae		N	3	1		4	1
Surface	Turbinidae		Y				2	1
Level 1	Turbinidae	<i>Turbo coronatus</i>	Y	4	1	1	5	45
Level 1	Potamididae	<i>Terebralia palustris</i>	Y		5		5	100
Level 1	Veneridae	<i>Tivela compressa</i>	Y				1	1
Level 1	Achatinidae	<i>Achatina achatina</i>	N				1	1
Level 1	Fascioliariidae		N				1	1
Level 1	Turbinidae		Y		2	1	6	3
Level 2	Turbinidae	<i>Turbo coronatus</i>	Y	4	2	1	6	68
Level 2	Potamididae	<i>Terebralia palustris</i>	Y		2		2	74
Level 2	Arcidae	<i>Barbatia foliata</i>	Y		1		1	43
Level 2	Turbinidae		Y	6			6	6
Level 2	Neritidae	<i>Nerita albicilla</i>	N				1	1
Level 2	Littorinidae		N		3		3	1
Level 2	Carditida(types)		Y		1		1	7

SAVABO: This site is located approximately 30m from the modern shoreline, and about 700m northwest of the modern village of Tampolove. This location was investigated by MAP in previous years, and this exact location was ranked as highly likely to contain archaeological materials by Davis et al. (2020). We excavated two 1m X 1m units (Figures 8-17 and 8-18). Both units were subsampled in their lower levels due to significant decreases in recovered cultural material density.

Unit 1: The surface of unit 1 contained marine shell material and burnt rock. In level 1, numerous ceramics, marine shell tools, fishbones, and charcoal material were recovered, in addition to more burnt rocks. Level 2 produced more ceramics and a substantial amount of faunal remains and worked marine shells. Additionally, charcoal was recovered in situ along with elephant bird eggshell and burnt rocks. Level 3 produced far less material, consisting of faunal remains and marine shell. Level 4 contained no cultural artifacts. All ceramics recovered are undecorated and soil samples were taken from all excavation levels.

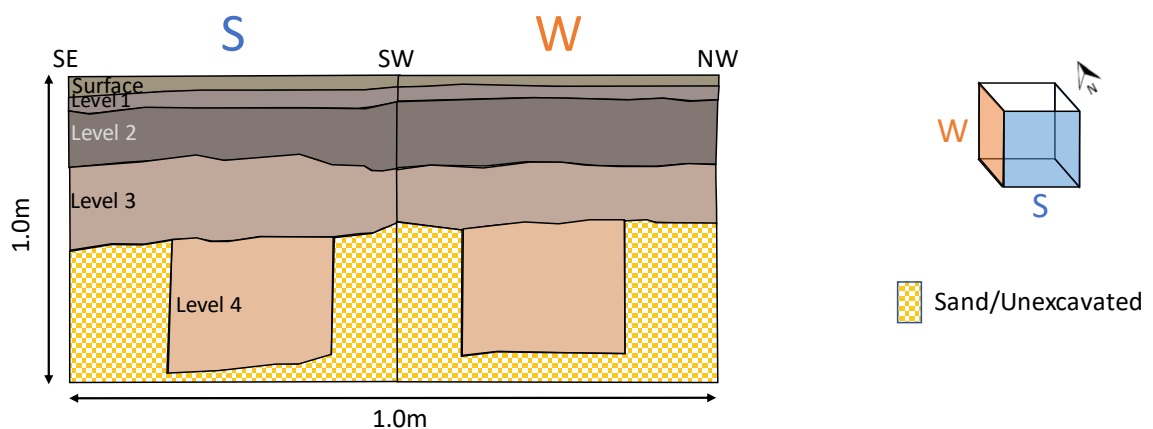


Figure 8-17: Wall profile for SAVABO Unit 1. Colors correspond with munsell color codes recorded during excavation (Surface = 5Y 6/2; Level 1 = 10R 6/1; Level 2 = 2.5YR 5/1; Level 3 = 5YR 7/2; Level 4 = 7.5YR 8/4). 3D box shows dimensions of excavation unit and colored directional abbreviations correspond with sections of the drawing.

Unit 2: Unit 2 is located ~22m south of Unit 1. The first layer of the excavation produced ceramics, faunal, and marine shell artifacts, and three worked marine shells were recovered in situ. Level 2 unveiled more faunal and marine shell material, in addition to charcoal. Level 3 only produced a few marine shell artifacts and Level 4 was devoid of cultural material. Soil samples were taken from each level of the unit. Like Unit 1, all recovered ceramics were undecorated.

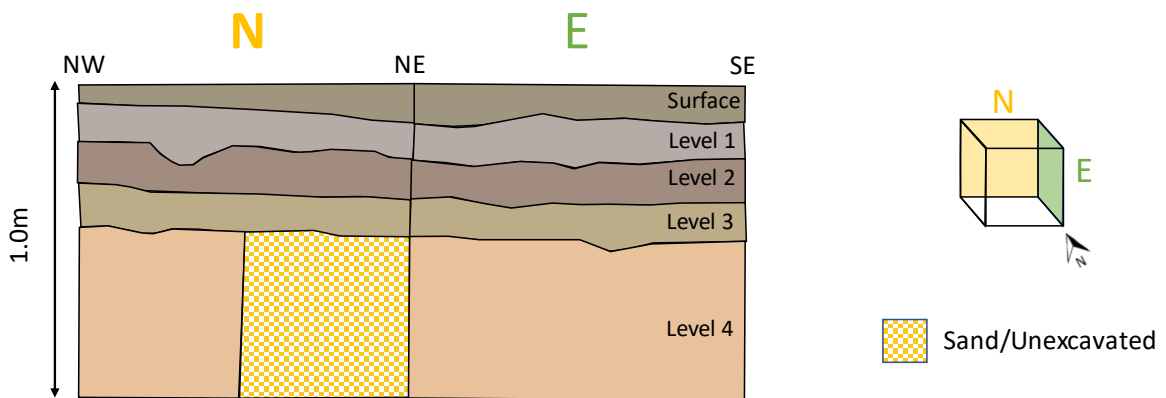


Figure 8-18: Wall profile for SAVABO Unit 2. Colors correspond with munsell color codes recorded during excavation (Surface = 5Y 6/2; Level 1 = 2.5YR 7/1; Level 2 = 7.5YR 6/2; Level 3 = 10YR 7/3; Level 4 = 10YR 8/4). 3D box shows dimensions of excavation unit and colored directional abbreviations correspond with sections of the drawing.

It appears that this site was an earlier extension of the present-day village of Tampolove that is situated just to the southeast of this area. There is evidence of burning activity which is likely related to subsistence on marine and terrestrial foodstuffs.

Discussion

Excavations reported above demonstrate a widespread and long-lived occupation of the Velondriake area dating back to approximately 700-1200 BP. Most archaeological deposits found in southern Madagascar are quite shallow, extending only 20-30cm in depth before sterile soil and date within the last 200-300 years (e.g., G-15-20, SAVABO). However, several areas excavated here contain evidence of human presence from earlier

periods (e.g., G123 Unit 3) and longer-lived occupations (e.g., G134). One radiocarbon date from G134 produced an age ca. 3000 cal. BP, but this is an extreme outlier and should not be trusted as an accurate age of this context.

The presence of potential starvation foods (i.e., foodstuffs primarily consumed during times of stress) at sites like G123 may speak to food shortages caused by erratic climatic conditions. During Unit 3's occupation (ca. 550 – 330 cal. BP), the climate in this region was in a state of transition from wetter to drier conditions (Faina et al. 2021; also see Chapter 7, Figure 7-2). Within Unit 1 and Unit 2, starvation foods are even more abundant. While we do not have radiocarbon dates for G123 Unit 1, it is located directly adjacent to Unit 2 and may contain contexts that are contemporaneous with Unit 2 which dates to between 240 and 30 BP. This period also overlaps with drier climatic conditions (Faina et al. 2021) which could have disrupted terrestrial resources and subsequent reliance on marine environments for subsistence. A great deal of historical ecological work can derive from the assemblages reported here, and future studies will seek to establish a robust understanding of environmental resource usage patterns over time and their correlation with climate change.

Material culture recovered from these excavations can provide the basis for several important future studies of the Velondriake region. There remains ample work to identify faunal materials present from archaeological contexts on Madagascar, and Danielle Buffa is currently developing a digital reference collection for zooarchaeological analysis for this area (Buffa 2019). Likewise, a great deal of work has been done by Kristina Douglass (2017; also see Douglass, Morales, et al. 2019) on developing a similar reference for marine assemblages from SW Madagascar, and the materials generated by these excavations can be incorporated into a regional analysis of marine environmental exploitation patterns over the past several centuries.

The ceramic assemblage within G134 gives us additional insight to ceramic chronologies for this region and provides evidence of a diverse collection of decorative styles ranging from punctations and incising in the earlier phases of the site to shell combing in the latter phases of the site's occupation. ^{14}C dates from contexts with shell combed support prior research (Douglass 2016) suggesting these decorative styles date to the last 200-300 years. ^{14}C dates from contexts with punctated and incised ceramics further support the determination that these decorative styles predate shell combing (Douglass 2016). The ceramics recovered here and elsewhere in the Velondriake area will subsequently enhance our understanding of cultural exchanges, population movements, and social networks in this region and their changes over time (e.g., Davis et al. *in review*; Chapter 7).

The discovery of lithic material from G134 is especially significant, as there have been no other stone-tools recovered from the SW of Madagascar – with the exception of gunflints that likely date to the 18-20th centuries (Douglass 2016). The recovered object appears to be a blade scraping tool. There is a possibility of it being a spearpoint, but the fracturing appears too rectangular to have worked well in this capacity (Kenneth Hirth, *pers. comm.* 2021). Given that no other debitage was recovered (i.e., flakes, cores, etc.), it seems unlikely that the site represents a lithic manufacturing area.

Stone tools have been discovered in only two other sites on Madagascar, both from the northeastern coast (Dewar et al. 2013). Debate proceeds on the antiquity of the lithics found in the northeast of Madagascar (e.g., Anderson 2019). The lithic identified in this dissertation appears to predate all recovered ceramics within site G134 based on its stratigraphic placement. Bayesian Accumulation Age-Depth modeling dates the lithic's context to a median age of 982 cal. B.P. (Figure 8-15). A secondary model constructed using only the highest quality ^{14}C dates (class 1 and 2) provided a similar result (median

age of 970 cal. BP; Supplemental Figure F-1). This period overlaps with stone-tool traditions recovered in Northwest Madagascar at Lakaton'i Anja and Ambohiposa (Dewar et al. 2013). Further study is needed to verify this age-depth estimation and to determine the source of the Velondriake lithic and its relation to Northwestern Malagasy stone tool traditions. Regardless, the discovery of lithic material in the southwest of Madagascar provides more evidence of stone-tool traditions on Madagascar.

Conclusion

This report outlines the results of a series of excavations conducted in the Velondriake Marine Protected Area in Southwest Madagascar between 2020 and 2021. The results presented here expand our understanding of the chronology of human occupation of the region and give insight into lithic traditions that existed in the south of Madagascar almost 1000 years ago. Chronological information suggests that the Velondriake region was densely populated over the last 300 years, but lower densities of occupation persisted for at least 700-800 years in open air villages and campsites. Evidence from prior excavations in this region indicates human presence as early as 3000 B.P., with the oldest dates coming from rock shelter sites. This study reports only on open air sites, which tend to be younger based on prior work in this region, but still demonstrates human occupations that stretch back approximately 1000 years. In the future, the materials excavated by this study can serve to expand our knowledge of dietary patterns, resource exploitation, migration, trade, stone-tool use, and social networks throughout the Velondriake region. Furthermore, it can help to improve our understanding of Velondriake within the broader context of Madagascar's archaeological record.

Chapter 9: Conclusion

The archaeology of the southwest of Madagascar was recently described by Parker Pearson et al. (2010:542) as an “archaeological desert”, and much remains to be understood about early human settlement here and elsewhere on the island. Douglass (2016) provided some of the first evidence for chronologies of human occupation in the Velondriake region where this dissertation centers. This dissertation has built on this prior work by developing new methods and theoretical frameworks to expand archaeological understanding of the Velondriake Marine Protected Area (VMPA). The approaches presented carry great potential to be applied in other regions of Madagascar. In this short chapter, I will summarize the most significant findings of this research and present a roadmap of future work that remains to address questions of human settlement in this region.

Theoretical and Practical Contributions

The study of settlement patterns has been a long-lasting point of inquiry within archaeological investigations for over a century (see Kowalewski 2008), and a great deal of theoretical and methodological work has helped advance this area of study throughout the years. Within this dissertation, I put forth a new approach to holistically investigate settlement patterns in the archaeological record. I approach the question of settlement distribution from a perspective of feedback/cause-and-effect loops and use both ecological drivers and consequences of human activity to identify and understand settlement distributional patterns on landscape scales. It is important, in my view, to understand not only *why* people choose to leave or stay in an area, but also what the long-term consequences of those choices have on environmental systems beyond our species. To place humans within a broader Earth-systems context, it is vital that we approach our species as one part of a connected environmental system, one in which we function within

– and not separated from – the rest of the natural world (Ellis 2021; Ellis et al. 2021). This ontological position will allow archaeological studies of human settlement behavior to better inform pivotal questions concerning human-environment dynamics and their role in sustainability issues, resource conservation, and societal impacts of climate change.

By using this conceptual framework, this dissertation was able to generate a multiproxy dataset that permitted for a robust interpretation of the geographic and temporal patterns of settlement and mobility strategies within the VMPA, as well as their proximal drivers and long-term effects on the ecological systems of southwest Madagascar. Each individual chapter presents novel methodological contributions to answer one or more parts of this complex issue, but only by combining the results of each of these investigations (i.e., spatial statistical models, remote sensing, survey and excavation, paleoclimate records, radiocarbon dates, and network analysis) do we produce a holistic picture of human-environment dynamics.

The theoretical innovation put forth by this dissertation has also resulted in significant methodological advances. The spatial modeling and remote sensing protocols developed here have rapidly expanded archaeological survey and prospection efforts to locate cultural heritage sites and interpret settlement distribution patterns. As demonstrated in Chapters 4 and 6, the use of each approach separately performs well, and by looking at places predicted by both approaches, we find the greatest success. Furthermore, by approaching archaeological prospection projects from an explicit theoretical framework, this dissertation contributes significantly to archaeological remote sensing, which has long been challenged by a disconnect between methods and theoretical perspectives (e.g., Davis and Douglass 2020; Thompson et al. 2011).

Settlement History of the Velondriake Region of Southwest Madagascar

The results of this dissertation program have greatly expanded our understanding of the human occupancy of the VMPA in southwest Madagascar, as well as the human history of the island as a whole. Remote sensing techniques have allowed for rapid assessment of over 1000 km² of land area in southwest Madagascar, leading to the documentation of hundreds of new archaeological deposits throughout the VMPA. Furthermore, we now have a better grasp on the driving forces behind human decision making in this region for the last several millennia. In addition to environmental constraints, social connectivity and community defense were significant contributing factors to the decisions of southwest Malagasy communities about where to situate themselves on the landscape. The remote sensing and spatial analyses conducted here further reveal the long-term ecological consequences of prolonged human occupation, consisting of altered vegetation and soil properties throughout much of the study area.

Excavations carried out at select locations provided valuable information pertaining to the nature and duration of human occupancy in the southwest of Madagascar. The excavations cover a broad swath of the Velondriake region, consisting of open-air village sites from the northern, central, and southernmost reaches of the study area. Evidence provided from charcoal and zooarchaeological assemblages document an extensive use of trees as fuel sources for cooking, extensive marine resource exploitation, especially of mangrove species, and the use of tubers, cacti, and shrubs in dietary contexts, as charred remnants of such taxa were recovered at numerous excavated locations, including within fire-pit features (e.g., G134).

The presence of starvation foods (e.g., *Nerita undae*) at sites like G123 signify potential responses to periods of environmental downturn. Climatological conditions during occupation phases of G123 Unit 3 demonstrate shifts from very wet conditions (ca.

550 – 450 cal. BP) towards drought conditions (ca. 450 – 300 cal. BP). G123 Unit 2 overlaps with a similar shift from wetter to drier conditions (ca. 240 – 0 cal. BP). Such climatological contexts may have reduced the availability of other marine resources and caused food shortages. By examining these zooarchaeological assemblages in closer detail we can learn a great deal about the diets of different communities in Velondriake over the past several hundred years. This will constitute a future research project.

Excavations also provided rare evidence of stone-tool use in the southwest of Madagascar. A lithic blade recovered from the bottom of the excavation unit at G134 is located more than 10 cm below any other cultural materials (e.g., ceramics) and likely constitutes an early presence of foragers in the Velondriake region that predates the earliest AMS dates for the site (792-722 cal. BP). Bayesian age-depth modeling suggests that the context of the lithic dates to between 728 and 1235 cal. BP. This discovery is especially significant in light of the ongoing debate over when humans first arrived on Madagascar and the nature of these populations. The presence of a lithic tradition in the southwest with some similarities to a stone-tool tradition found in the north of Madagascar dating to between 1000 and 4400 B.P. (see Dewar et al. 2013) adds to evidence of sustained and widespread human occupancy on the island for the past several millennia (e.g., Douglass, Hixon et al. 2019).

Finally, based on spatial statistical and social network analyses, we have evidence to support the possibility that Malagasy communities in the Velondriake region developed social networks that were resilient to a slew of environmental and sociopolitical shifts over the past millennium. As such, the nature of settlement patterns and mobility strategies among coastal foragers has served as an adaptive mechanism to risk posed by external pressures like climate change, resource availability, and political violence. This holds important implications for future efforts towards sustainability and resilience in the face of

increasing climate-change related impacts to coastal communities on Madagascar and elsewhere. By integrating traditional methods of mobility-based livelihood strategies into conservation policies, resource use can be better managed in ways that aid biodiversity efforts while minimizing the impact to Malagasy communities who rely on these resources for survival.

Future Research Avenues

The findings of this project provide new insight into the timing, drivers, impacts, and placement of ancient coastal settlement of Malagasy communities along the SW coast of Madagascar. Our knowledge of the archaeological record in this region has been greatly expanded due to the work conducted thus far, and this opens the door for new and exciting avenues of research that can build upon or make use of the data generated by this study.

For example, in addition to in-depth analyses of faunal assemblages recovered from excavations conducted here, such materials can also enhance our ability to derive chronological information from archaeological contexts. Research is warranted to establish marine reservoir corrections for marine shells in Velondriake, which comprise a portion of nearly every archaeological site in the area. Hopefully, this dissertation will allow for future scholars to undertake such investigations to further our understanding of Malagasy history and archaeology. It is clear that the methods deployed in this dissertation have aided in the discovery of significant cultural contexts that will help to shape our understanding of Malagasy history. As several studies suggest, the timeline for human occupation of Madagascar is likely longer than previously assumed (Douglass, Hixon, et al. 2019).

Among the many avenues for continued investigation, there are two major projects underway: one consists of a paleoclimate reconstruction program, and the other focuses on land-use comparisons between different socioeconomic groups.

Understanding the relationship between climatic change and human mobility using high-resolution paleoclimate proxies

Within this dissertation, I have laid the groundwork for future studies of human-environmental interaction by generating a robust and systematic archaeological dataset of past settlement locations in the Velondriake region. Such datasets are crucial for understanding landscape scale dynamics of human-environment interaction, but also require highly resolved paleoclimatic records to model the effects of environmental change on human behavior (d'Alpoim Guedes et al. 2016; Davis 2019b). Extensive paleoclimate work has been conducted on Madagascar and its surrounding regions (e.g., Burney 1999; Crowley et al. 2017; de Boer et al. 2014; Dewar and Richard 2007b; Douglass and Zinke 2015; Godfrey et al. 2019; Grove et al. 2012; Hixon et al. 2018; Kull 2000; Kull et al. 2012; Scroton et al. 2017; Virah-Sawmy et al. 2009, 2010; Voarintsoa et al. 2017; Zinke et al. 2004). However, no studies on Madagascar have yet applied marine paleoclimate records to archaeological data. For coastal populations, marine records are likely to be more important for understanding environmental effects on human mobility patterns, as discontinuity between terrestrial and marine proxies can occur (Piermattei et al. 2017). Additionally, there are few studies which make use of multiple proxies simultaneously (e.g., Voarintsoa et al. 2017). Multiple proxy sets (e.g., multiple isotopes or multiple material types) have improved environmental and climatological reconstruction (García-Granero et al. 2015; Hausmann et al. 2011; Kar et al. 2016; Li et al. 2010; Mügler et al. 2010).

In ongoing work funded by the National Science Foundation and the National Geographic Society, I am working with colleagues on Madagascar and in the U.K. to create a multiproxy paleoenvironmental dataset from fossil corals. Corals can provide seasonal, annual, and decadal records of precipitation, temperature, and land-use via stable isotopes and trace element signatures contained in these organisms (Grove et al.

2013, 2012; Hennekam et al. 2018). Furthermore, ancient, fossilized corals present in some regions may allow for these records to extend back thousands of years (Douglass and Zinke 2015).

During this dissertation project, I helped to lead and conduct marine surveys for living and fossil *Porites* corals located along the coastline surrounding Andavadoaka, a village at the center of the study area. A total of 9 corals have been identified as targets for an upcoming coring operation which are located in close proximity to the study region and known archaeological deposits (Figure 9-1).

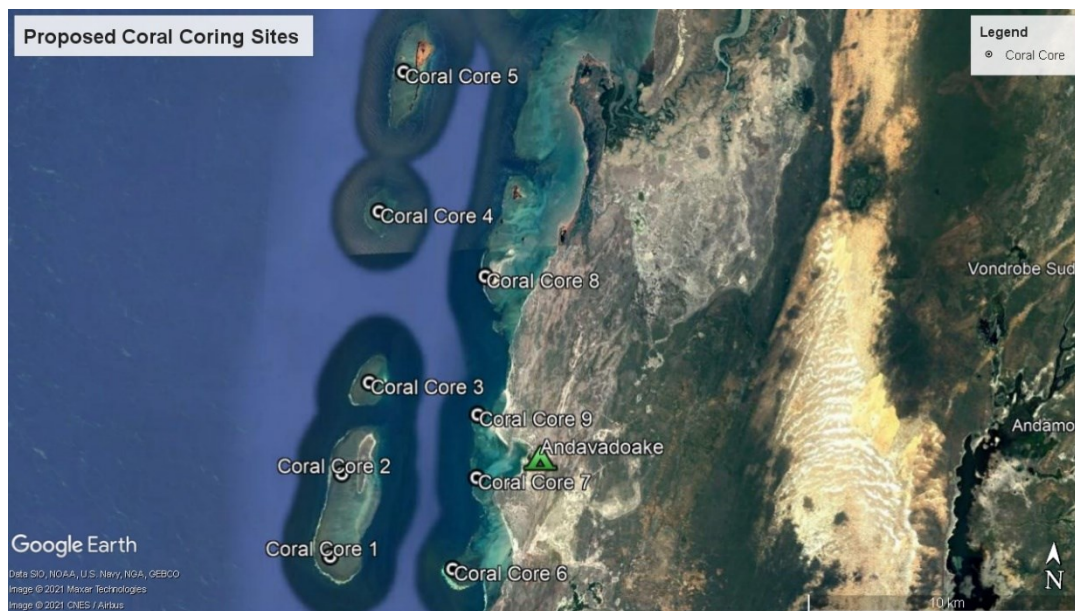


Figure 9-1: Map of corals identified for coring along the coast of Velondriake.

Fossil *Porites* boulders will provide snapshots of seasonality for several decades over the Late Holocene. With funding provided by National Geographic, our team will conduct a coral coring operation to collect necessary samples for isotope and trace element analysis. Fossil coral data generated here will provide researchers the ability to investigate long- and short-term environmental events, the effects of human land-use on ecological systems, and the effects of environmental fluctuation on biodiversity through time. As such, this project will produce data that is of use to Africanists across many

disciplines focused on environmental research questions. Subsequently, these data will improve our understanding of human-climate dynamics over a long timescale, placing us in a better position to evaluate modern day climate events and their potential societal consequences.

The legacy of ancient niche construction among foragers, herders, and farmers in southwest Madagascar

A secondary ongoing project that will build off this dissertation focuses on niche construction activities (i.e., ecosystem engineering and landscape modification) and their long-term effects on landscapes, building directly off the work of Chapter 7 (Davis and Douglass 2021). This project, funded by the Spatial Archaeometry Research Collaborations (SPARC), an NSF funded program at the University of Arkansas, is focused on the legacy ecological effects of pastoralism in the Namonte Basin, located inland from Velondriake (Figure 9-2).



Figure 9-2: Map of the Namonte Basin in southwest Madagascar. The red box shows the extent of the study area covered by the SPARC funded project, encompassing ~100 km² of the Namonte Basin region.

The project specifically aims to investigate landscape-scale environmental modifications resulting from pastoralist activities using multispectral remote sensing methods. Specifically, this project aims to understand the landscape as a system, rather than a collection of distinct anthropogenic features. As such, this research seeks to develop a novel remote sensing method that is tied explicitly to archaeological theory pertaining to landscape use, niche construction, and settlement distributions (*sensu* Davis and Douglass 2021; Chapter 7). By using a landscape approach, the project aims to explore the relationships between human populations and their surroundings at multiple scales and changes in human behavior over time and space (Anschuetz et al. 2001; Green

and Petrie 2018), thereby providing insight into land-use practices and their larger ecological effects over the past several hundred years.

This ongoing work seeks to address several key questions, including identifying where pastoralist activities have been predominant and how they have impacted ecological systems in the past and present within southwest Madagascar over the past 400 years. Additionally, the project will aim to compare niche construction activities and their geophysical signatures between different socioeconomic societies, including foraging and fishing communities, pastoralist herders, and agriculturalists.

Final Thoughts

Environmental archaeology has a long and rich history. One fundamental limitation of much of this prior literature, however, has been in the development of high-resolution datasets at the necessary scale to address central archaeological questions concerning human-environment dynamics (Davis 2020a). Today, with the global climate crisis that threatens the livelihoods of hundreds-of-millions of people, questions concerning human-environmental interactions are even more significant (IPCC 2021). Archaeology, thus, has a major role to play in developing long-term solutions to environmental and climatic deterioration.

As I discuss in an article published in *Environmental Archaeology*, “the future of environmental archaeological studies involves development of techniques and methods for reconstructing past environmental conditions... [as well as] creating a deeper understanding of processes that increase and inhibit resilience of human populations in times of environmental uncertainty” (Davis 2020a:375). This dissertation provides one such attempt to push towards this goal by developing geospatial methods for recording and interpreting past socioenvironmental systems. By so doing, the data generated here

can be coupled by future work to reconstruct past socioenvironmental contexts and their roles in shaping human communities.

Appendix A: IRB Protocols Pertaining to Geophysical Data Collection at Penn State

22.1 Which of the following identifiers will be recorded for the research project? Check all that apply. If none of the following identifiers will be recorded, do not check any of the boxes.

	Hard Copy Data	Electronic Stored Data
Names and/or initials (including on signed consent documents)	<input type="checkbox"/>	<input type="checkbox"/>
All geographic subdivisions smaller than a State, including street address, city, county, precinct, zip code, and their equivalent geocodes,	<input type="checkbox"/>	<input type="checkbox"/>
All elements of dates (except year) for dates directly related to an individual, including birth date, admission date, discharge date, date of death; and all ages over 89 and all elements of dates (including year) indicative of such age, except that such ages and elements may be aggregated into a single category of age 90 or older	<input type="checkbox"/>	<input type="checkbox"/>
Telephone numbers	<input type="checkbox"/>	<input type="checkbox"/>
Fax numbers	<input type="checkbox"/>	<input type="checkbox"/>
Electronic mail addresses	<input type="checkbox"/>	<input type="checkbox"/>
Social security numbers	<input type="checkbox"/>	<input type="checkbox"/>
Medical record numbers	<input type="checkbox"/>	<input type="checkbox"/>
Health plan beneficiary numbers	<input type="checkbox"/>	<input type="checkbox"/>
Account numbers	<input type="checkbox"/>	<input type="checkbox"/>
Certificate/license numbers	<input type="checkbox"/>	<input type="checkbox"/>
Vehicle identifiers and serial numbers, including license plate numbers	<input type="checkbox"/>	<input type="checkbox"/>
Device identifiers and serial numbers	<input type="checkbox"/>	<input type="checkbox"/>
Web Universal Resource Locators (URLs)	<input type="checkbox"/>	<input type="checkbox"/>
Internet Protocol (IP) address numbers	<input type="checkbox"/>	<input type="checkbox"/>
Biometric identifiers, including finger and voice prints	<input type="checkbox"/>	<input type="checkbox"/>
Full face photographic images and any comparable images	<input type="checkbox"/>	<input type="checkbox"/>
Any other unique identifying number, characteristic, or code (such as the pathology number)	<input type="checkbox"/>	<input type="checkbox"/>
Study code number with linking list	<input type="checkbox"/>	<input type="checkbox"/>
Genomic sequence data	<input type="checkbox"/>	<input type="checkbox"/>
State ID numbers	<input type="checkbox"/>	<input type="checkbox"/>
Passport numbers	<input type="checkbox"/>	<input type="checkbox"/>
Driver's license numbers	<input type="checkbox"/>	<input type="checkbox"/>

22.2 If storing paper records of research data, answer the following questions:

22.2.1 Where will the paper records, including copies of signed consent forms, associated with this research study will be stored?
[redacted]

22.2.2 How will the paper records be secured?
[redacted]

22.2.3 How will access to the paper records be restricted to authorized project personnel?
[redacted]

22.3 If storing electronic records of research data, indicate where the electronic data associated with this research study will be stored. Check all that apply.

Penn State-provided database application. Check which of the following database applications are being used (check all that apply):

Penn State REDCap

Other – Specify - provided and approved database application:
[redacted]

Penn State, College, or Department IT file server

Box.psu.edu (Apply for a Box NPA here: <https://box.psu.edu/non-person-account/>)

Web-based system provided by the sponsor or cooperative group - Specify URL and contact information:
[redacted]

Other – Specify the database application or server:
[redacted]

Provide details about the data security features or attach security documentation provided by sponsor or group:
[redacted]

If there is a list/key that links indirect identifiers (code numbers, participant IDs, etc.) to direct identifiers, that list must not be comingled (i.e., stored in the same location) as the identifiable data, including copies of signed informed consent forms. Additionally, access to that list/key must be restricted to authorized project personnel.

22.4 Is there a list/key that links code numbers to identifiers?

Yes - explain how the list that links the code to identifiers is stored separately from coded data:
[redacted]

Not applicable, there is no list that links code numbers to identifiers. Skip to section 22.6.

22.5 Is there a list of people who have access to the list/key?

Yes – explain how access to that list is restricted and why certain persons require access.

- 22.7 Will any research data (such as survey data) be collected on a mobile device, such as an electronic tablet, cell phone, or wireless activity tracker?**
- No
 Yes - answer the following questions:
- 22.7.1 Specify the provider of the mobile device(s)**
- Supplied by the sponsor
 Penn State owned device
 A personal device
 Other – Please specify source:
- 22.7.2 Specify the type(s) of mobile device(s) that will be used to capture data and all identifiers captured on the mobile device(s). Please list all devices, and if more than one, the identifiers to be collected on each.**
-
- 22.7.3 Specify the type of data collected on the mobile device(s).**
-
- 22.7.4 Specify the application or website used to collect the data from the mobile device, if applicable.**
-
- 22.7.5 Describe the measures taken to protect the confidentiality of the data collected on mobile device(s). Please address physical security of the device(s), electronic security, and secure transfer of data from device(s) to the previously indicated data/file storage location provided in section 22.3.**
-

The use of online survey tools and email to collect or send research data containing identifiers that represent more than minimal risk to subjects must be approved by the Office of Information Security. Before completing this section, please contact security@psu.edu.

- 22.8 Will any research data be directly entered/sent by subjects over the internet or via email (e.g., data capture using on-line surveys/questionnaires, surveys via email, observation of chat rooms or blogs)?**
- No
 Yes - answer the following questions:
- 22.8.1 Specify the identifiers collected over the internet or via email (including IP addresses if IP addresses will be collected).**
-
- 22.8.2 Specify the type of data collected over the internet or via email.**
-
- 22.8.3 Describe the measures taken to protect the confidentiality of the data collected?**
-
- 22.8.4 Describe how the research team will access the data once data collection is complete.**
-

22.8.5 If the research involves online surveys, list the name(s) of the service provider(s) that will be used for the survey(s) (e.g., REDCap, Penn State licensed Qualtrics, Survey Monkey, Zoomerang)? (Note: The IRB strongly recommends the use of REDCap for online surveys that obtain sensitive identifiable human subjects data.)

- Penn State REDCap,
- Penn State Qualtrics (de-identified data only)
- Other - Please specify:
Application:
URL (if applicable):

22.8.6 If the answer above is "Other" contact security@psu.edu for approval of an alternative data capture method

Depending on the nature of the subject matter involved, certain security requirements must be in place for the audio and/or video recording or photographing of subjects. If the subject matter presents more than minimal risk to the subjects, then, before completing the section below, please contact the Office of Information Security at security@psu.edu to confirm whether these requirements are required.

22.9 Will any type of recordings (e.g., audio or video) or photographs of the subjects be made during this study?

- No - skip to section 22.10
- Yes - answer the following questions:

22.9.1 What will be used to capture the audio/video/images? Give a brief description of content.

- Audio – Describe the intended content of the audio recording:
- Video – Describe the intended content of the video recording:
- Photographs of the subjects – Describe the intended content of the photographs:
- 3-D Images – Describe the intended content of the of 3-D images:
- Other - Specify:

22.9.2 How will the recordings/photographs/images be stored (electronically or physically)?

22.9.3 Where will the recordings/photographs/images be stored?

22.9.4 Who will have access to the recordings/photographs/images?

22.9.5 Will any of the recordings be transcribed?

- Not applicable
- No
- Yes – indicate who will be doing the transcribing?

22.9.6 Will the recordings/photographs be used for purposes other than this research study?

- No
- Yes - specify purpose(s) (e.g., publication, presentations, educational training, future undetermined research):

Appendix B: Supplemental Data for Chapter 4

Supplemental Table B-1: Shows list of surveyed grid locations during the summer of 2019 and materials collected from each area. Probability is given as a qualitative ranking (Low, Medium, High, or Null), which relates to the quantitative measurements given in Table 1 in the text.

Grid #	Probability	Charcoal	Eggshell	Marine Shell	Faunal	Ceramics	Beads	Other	Total
9	Medium	0	0	2	0	0	0		2
11	Null	0	0	0	0	0	0		0
15	Low	0	9	0	0	0	0		9
16	Medium	0	0	0	0	0	0		0
18	Low	0	0	1	0	0	0		1
23	Medium	0	0	0	0	0	0		0
24	Medium	0	7	2	0	0	0		9
25	Low	0	13	0	0	0	0		13
26	Low	0	6	0	0	0	0		6
30	Low	0	8	5	0	0	0		13
31	Medium	0	16	10	0	3	0		29
32	Medium	0	26	3	0	4	0		33
52	High	0	0	0	0	0	0		0
53	High	0	3	2	0	0	0		5
54	High	0	8	7	0	0	0		15
55	High	0	0	0	0	0	0		0
56	Medium	0	1	3	0	0	0		4
57	High	0	11	11	1	10	4	Burnt Stone (1)	39
58	High	0	68	6	0	3	7		84
61	Null	0	0	5	0	0	0		5
62	High	0	12	0	0	0	0		12
63	Low	0	1	0	0	0	0		1
64	High	0	0	0	0	0	0		0
67	High	0	0	0	0	0	0		0
68	High	0	0	0	0	0	0		0
69	High	0	0	3	0	0	0		3
70	Null	0	0	2	0	0	0		2
71	Medium	0	5	0	0	0	0		5
72	High	0	0	0	2	0	0	Burnt stone (1)	3
73	Low	0	0	1	0	0	0		1
74	Medium	0	0	0	0	0	0		0
75	Low	0	0	0	0	0	0		0

76	High	0	2	0	0	0	0		2
88	Low	0	0	8	0	11	0		19
89	Medium	0	0	20	0	5	1		26
90	High	3	5	6	1	1	1		17
91	High	0	0	4	0	0	0		4
92	High	0	10	4	0	0	0		14
100	Low	0	5	10	0	0	0		15
101	High	0	0	0	0	0	0		0
103	Null	0	0	0	0	0	0		0
104	Medium	0	0	0	0	2	0		2
105	High	0	0	8	2	5	0		15
106	Medium	0	0	5	4	1	0		10
107	High	0	0	0	0	1	0		1
108	High	0	0	0	0	1	0		1
109	Low	0	2	7	0	1	0		10
110	Null	0	0	0	1	0	0		1
111	Null	0	0	1	0	0	0		1
113	High	0	0	1	0	0	0		1
114	Medium	0	0	0	0	0	0		0
115	High	0	0	0	0	0	0		0
116	Low	0	0	0	0	0	0		0
117	High	0	0	2	0	0	0		2
118	High	0	50	32	15	40	8	Burnt stones (2)	149
119	High	0	3	2	0	7	0		12
120	Medium	0	23	24	0	15	2	Glass (1), Burnt Stone (1)	66
121	Low	1	10	0	5	3	0		19
122	High	0	0	0	0	0	0		0
123	High	0	0	21	0	8	2	Burnt Stone (2)	41
124	Medium	0	1	0	0	0	0		1
125	High	0	1	3	0	1	0		5
126	High	0	0	6	0	0	0		6
127	High	0	0	2	0	0	0		2
128	High	0	2	22	0	12	1		37
129	Null	0	0	5	0	0	0		5
130	High	0	3	44	1	69	0	Coral (1), Burnt	121

								Stone (2), Metal (1)	
133	High	2	0	8	3	24	0		37
134	Medium	1	0	11	0	62	0		75
136	Low	0	0	9	0	24	0		34
138	Low	0	0	0	0	0	0		0
139	High	1	9	14	0	5	0		31
144	High	0	0	2	0	11	0		13
145	Medium	0	0	22	2	37	0		61

Supplemental Code: Archaeological Distributional Analysis

This R Markdown details the distributional analysis of archaeological data discussed in the text. The goal of this analysis was to ascertain the conformity of the data to different continuous distributional functions to provide evidence to support or reject an ideal free distribution. This document also contains confidence envelopes (95%) for the archaeological data and each simulated dataset.

```
library(stats)
library(readxl)

## Warning: package 'readxl' was built under R version 3.5.3

library(emdbook)

## Warning: package 'emdbook' was built under R version 3.5.3

library(sfsmisc)

## Warning: package 'sfsmisc' was built under R version 3.5.3

##
## Attaching package: 'sfsmisc'

## The following object is masked from 'package:emdbook':
##
##   lseq

library(rmarkdown)

## Warning: package 'rmarkdown' was built under R version 3.5.3

setwd("C:/Users/Dylan/Documents/School-Work/Dissertation/RS_project")

#Load excel file containing artifact probability values

prob <- read_excel("Survey_results_probability.xlsx", sheet = "Material
_Prob_Scores_R")
```

```

#create random sample of uniformly distributed values

set.seed(1)

unif_prob <- runif(245, min = 0, max = 23)

#K-S distribution test between archaeological data and uniform distribu
tion with same max and min values
ks.test(prob$Prob, unif_prob)

## Warning in ks.test(prob$Prob, unif_prob): p-value will be approximat
e in
## the presence of ties

##
## Two-sample Kolmogorov-Smirnov test
##
## data: prob$Prob and unif_prob
## D = 0.13469, p-value = 0.02348
## alternative hypothesis: two-sided

#create random sample of normally distributed values

set.seed(1)

norm_dist <- rnorm(245)

#K-S distribution test between archaeological data and normal distribut
ion data

ks.test(prob$Prob, norm_dist)

## Warning in ks.test(prob$Prob, norm_dist): p-value will be approximat
e in
## the presence of ties

##
## Two-sample Kolmogorov-Smirnov test
##
## data: prob$Prob and norm_dist
## D = 0.83673, p-value < 2.2e-16
## alternative hypothesis: two-sided

##create gamma distributed data

set.seed(1)

gamma_dist <- rgamma(n=246, shape = 1)

ks.test(prob$Prob, gamma_dist)

```

```

## Warning in ks.test(prob$Prob, gamma_dist): p-value will be approxima
te in
## the presence of ties

##
## Two-sample Kolmogorov-Smirnov test
##
## data: prob$Prob and gamma_dist
## D = 0.7879, p-value < 2.2e-16
## alternative hypothesis: two-sided

##poisson distributed data
set.seed(1)

pois_dist <- rpois(n=246, lambda = 1)

ks.test(prob$Prob,pois_dist)

## Warning in ks.test(prob$Prob, pois_dist): p-value will be approximat
e in
## the presence of ties

##
## Two-sample Kolmogorov-Smirnov test
##
## data: prob$Prob and pois_dist
## D = 0.80823, p-value < 2.2e-16
## alternative hypothesis: two-sided

##create sample of logarithmically distributed values (using emdbook li
brary)
set.seed(1)
log_dist <- lseq(0.1, 24, 245)

##K-S distribution between archaeological data and log distribution dat
a

ks.test(prob$Prob, log_dist)

## Warning in ks.test(prob$Prob, log_dist): p-value will be approximate
in the
## presence of ties

##
## Two-sample Kolmogorov-Smirnov test
##
## data: prob$Prob and log_dist
## D = 0.5102, p-value < 2.2e-16
## alternative hypothesis: two-sided

##plotting KS distribution tests

```

```

##KS test with UNIFORM DIstribution

U_group <- c(rep(prob$Prob, length(prob$Prob)), rep(unif_prob, length(unif_prob)))

U_dat <- data.frame(KSD = c(prob$Prob, unif_prob), group=U_group)

# create ECDF of data

U_cdf1 <- ecdf(prob$Prob)
U_cdf2 <- ecdf(unif_prob)

# find min and max statistics to draw line between points of greatest distance
U_minMax <- seq(min(prob$Prob, unif_prob), max(prob$Prob, unif_prob), length.out=length(prob$Prob))
U_x0 <- U_minMax[which( abs(U_cdf1(U_minMax) - U_cdf2(U_minMax)) == max(abs(U_cdf1(U_minMax) - U_cdf2(U_minMax))) )]
U_y0 <- U_cdf1(U_x0)
U_y1 <- U_cdf2(U_x0)

##Plot distribution curves without ggplot

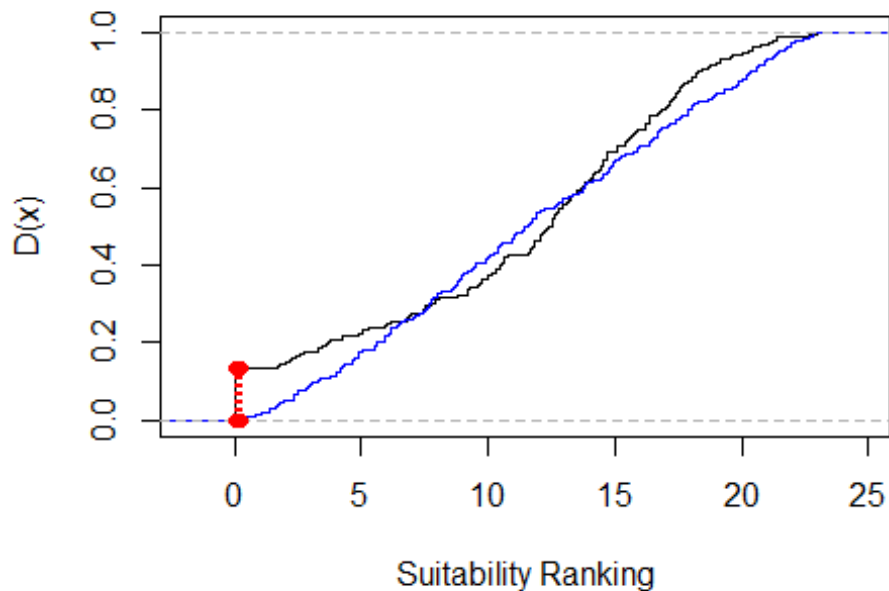
plot(U_cdf1, verticals=TRUE, do.points=FALSE, col="black", main = "K-S Test of Uniform Distribution", xlab="Suitability Ranking", ylab="D(x)")
plot(U_cdf2, verticals=TRUE, do.points=FALSE, col="blue", add=TRUE)

## creates line for maximum difference between both datasets

points(c(U_x0, U_x0), c(U_y0, U_y1), pch=16, col="red")
segments(U_x0, U_y0, U_x0, U_y1, col="red", lty="dotted")

```

K-S Test of Uniform Distribution



```
##TEST WITH NORMAL DISTRIBUTION

N_group <- c(rep(prob$Prob, length(prob$Prob)), rep(norm_dist, length(norm_dist)))

N_dat <- data.frame(KSD = c(prob$Prob, norm_dist), group=N_group)

# create ECDF of data

N_cdf1 <- ecdf(prob$Prob)
N_cdf2 <- ecdf(norm_dist)

# find min and max statistics to draw line between points of greatest distance
N_minMax <- seq(min(prob$Prob, norm_dist), max(prob$Prob, norm_dist), length.out=length(prob$Prob))
N_x0 <- N_minMax[which( abs(N_cdf1(N_minMax) - N_cdf2(N_minMax)) == max(abs(N_cdf1(N_minMax) - N_cdf2(N_minMax))) )]
N_y0 <- N_cdf1(N_x0)
N_y1 <- N_cdf2(N_x0)

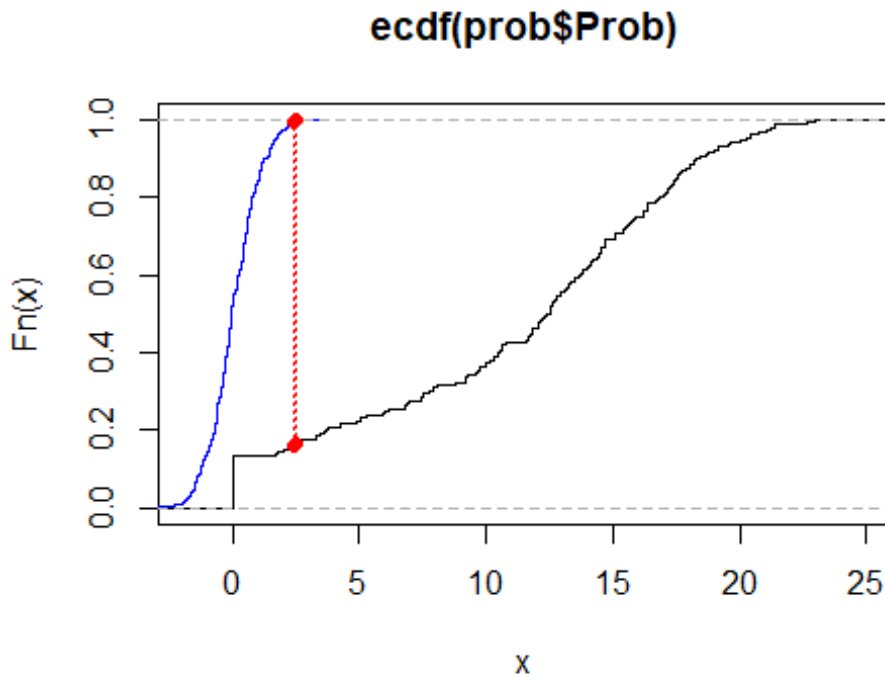
##PLOT

plot(N_cdf1, verticals=TRUE, do.points=FALSE, col="black")
plot(N_cdf2, verticals=TRUE, do.points=FALSE, col="blue", add=TRUE)
```

```

# draw line between points of greatest distance
points(c(N_x0, N_x0), c(N_y0, N_y1), pch=16, col="red")
segments(N_x0, N_y0, N_x0, N_y1, col="red", lty="dotted")

```



```

#####TEST WITH GAMMA DISTRIBUTION

##plotting KS distribution tests

G_group <- c(rep(prob$Prob, length(prob$Prob)), rep(gamma_dist, length(
gamma_dist)))

# create ECDF of data

G_cdf1 <- ecdf(prob$Prob)
G_cdf2 <- ecdf(gamma_dist)

# find min and max statistics to draw line between points of greatest d
istance
G_minMax <- seq(min(prob$Prob, gamma_dist), max(prob$Prob, gamma_dist),
length.out=length(prob$Prob))
G_x0 <- G_minMax[which( abs(G_cdf1(G_minMax) - G_cdf2(G_minMax)) == max
(abs(G_cdf1(G_minMax) - G_cdf2(G_minMax))) )]
G_y0 <- G_cdf1(G_x0)
G_y1 <- G_cdf2(G_x0)

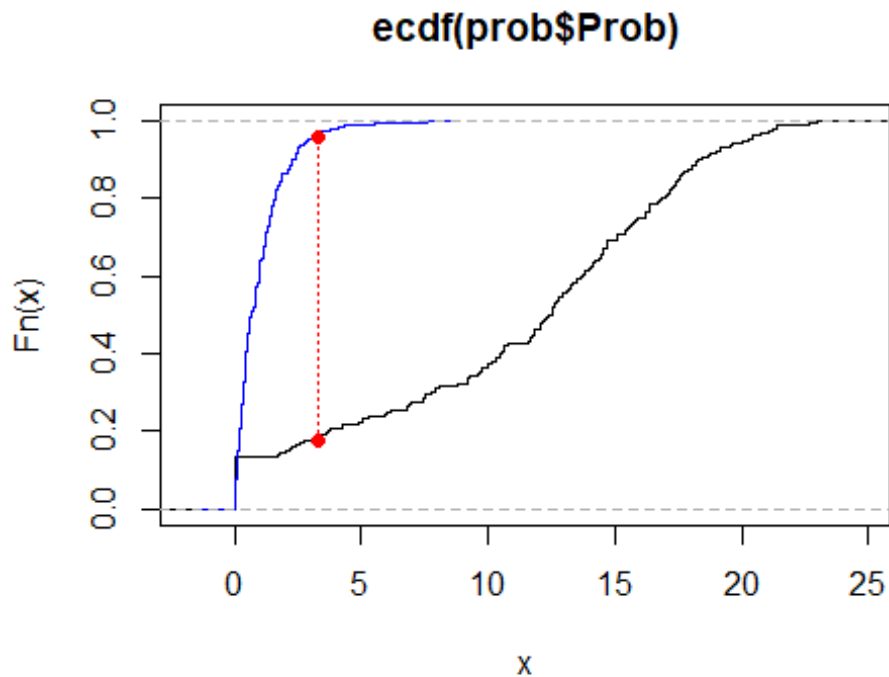
```

```
##PLOT

plot(G_cdf1, verticals=TRUE, do.points=FALSE, col="black")
plot(G_cdf2, verticals=TRUE, do.points=FALSE, col="blue", add=TRUE)

# draw line between points of greatest distance

points(c(G_x0, G_x0), c(G_y0, G_y1), pch=16, col="red")
segments(G_x0, G_y0, G_x0, G_y1, col="red", lty="dotted")
```



```
#####TEST WITH POISSION DISTRIBUTION
##plotting KS distribution tests

P_group <- c(rep(prob$Prob, length(prob$Prob)), rep(pois_dist, length(pois_dist)))

# create ECDF of data

P_cdf1 <- ecdf(prob$Prob)
P_cdf2 <- ecdf(pois_dist)

# find min and max statistics to draw line between points of greatest distance
P_minMax <- seq(min(prob$Prob, pois_dist), max(prob$Prob, pois_dist), length.out=length(prob$Prob))
```

```

P_x0 <- P_minMax[which( abs(P_cdf1(P_minMax) - P_cdf2(P_minMax)) == max
(abs(P_cdf1(P_minMax) - P_cdf2(P_minMax))) )]
P_y0 <- P_cdf1(G_x0)
P_y1 <- P_cdf2(G_x0)

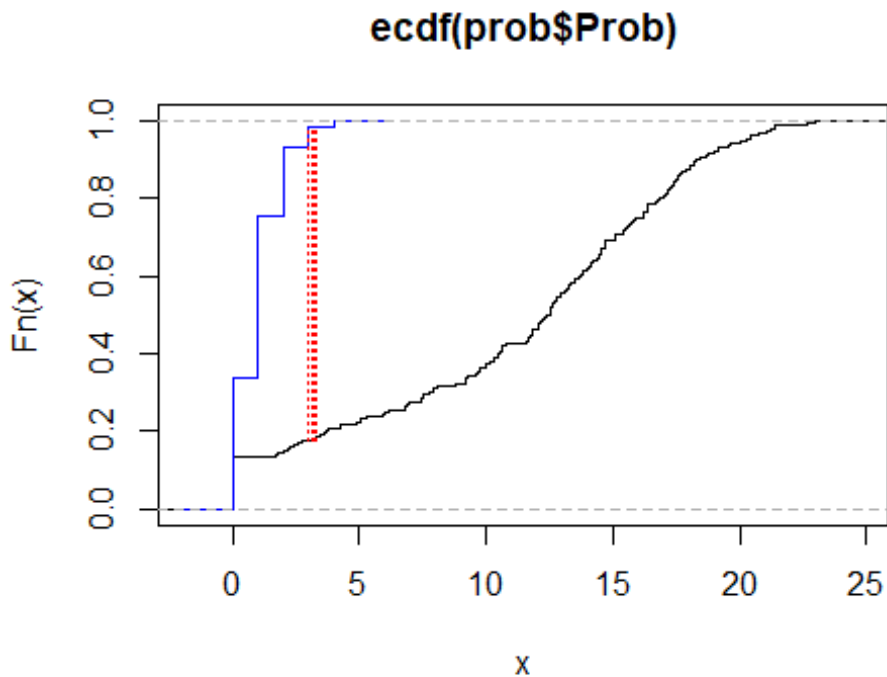
##PLOT

plot(P_cdf1, verticals=TRUE, do.points=FALSE, col="black")
plot(P_cdf2, verticals=TRUE, do.points=FALSE, col="blue", add=TRUE)

# draw line between points of greatest distance

segments(P_x0, P_y0, P_x0, P_y1, col="red", lty="dotted")

```



```

##CREATE PANNELED FIGURE
# 4 figures arranged in 2 rows and 2 columns

attach(mtcars)

## The following object is masked from package:ggplot2:
##
##   mpg

par(mfrow=c(2,2))

```



```

#UNIFORM
plot(U_cdf1, verticals=TRUE, do.points=FALSE, col="black",
     main = "K-S Test of Uniform Distribution", xlab="Suitability Ranki
ng", ylab="D(x)")
plot(U_cdf2, verticals=TRUE, do.points=FALSE, col="blue", add=TRUE)
points(c(U_x0, U_x0), c(U_y0, U_y1), pch=16, col="red")
segments(U_x0, U_y0, U_x0, U_y1, col="red", lty="dotted")

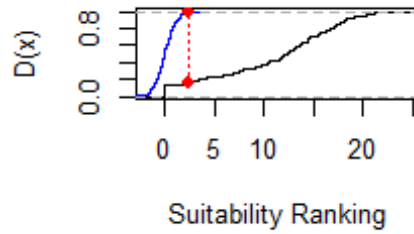
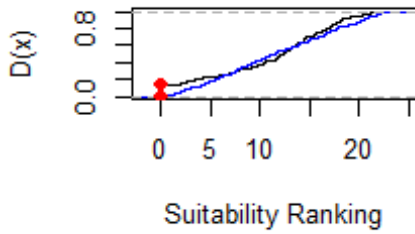
#NORMAL
plot(N_cdf1, verticals=TRUE, do.points=FALSE, col="black",
     main = "K-S Test of Normal Distribution", xlab="Suitability Rankin
g", ylab="D(x)")
plot(N_cdf2, verticals=TRUE, do.points=FALSE, col="blue", add=TRUE)
points(c(N_x0, N_x0), c(N_y0, N_y1), pch=16, col="red")
segments(N_x0, N_y0, N_x0, N_y1, col="red", lty="dotted")

#GAMMA
plot(G_cdf1, verticals=TRUE, do.points=FALSE, col="black",
     main = "K-S Test of Gamma Distribution", xlab="Suitability Rankin
g", ylab="D(x)")
plot(G_cdf2, verticals=TRUE, do.points=FALSE, col="blue", add=TRUE)
points(c(G_x0, G_x0), c(G_y0, G_y1), pch=16, col="red")
segments(G_x0, G_y0, G_x0, G_y1, col="red", lty="dotted")

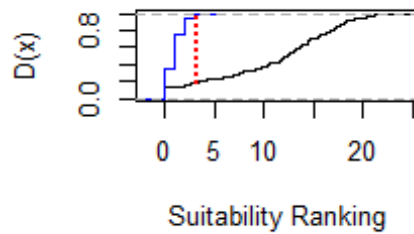
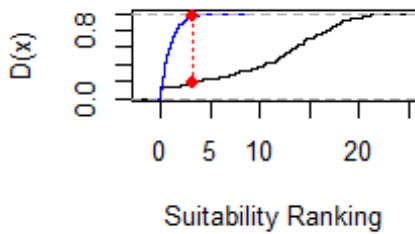
#POISSON
plot(P_cdf1, verticals=TRUE, do.points=FALSE, col="black",
     main = "K-S Test of Poisson Distribution", xlab="Suitability Ranki
ng", ylab="D(x)")
plot(P_cdf2, verticals=TRUE, do.points=FALSE, col="blue", add=TRUE)
segments(P_x0, P_y0, P_x0, P_y1, col="red", lty="dotted")

```

K-S Test of Uniform Distributi **K-S Test of Normal Distributi**

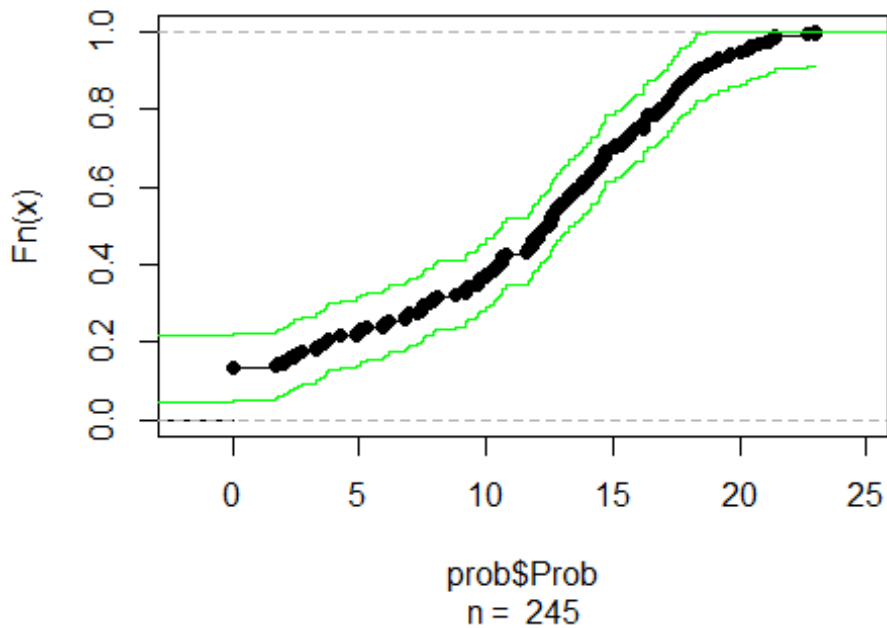


K-S Test of Gamma Distributi **K-S Test of Poisson Distributi**

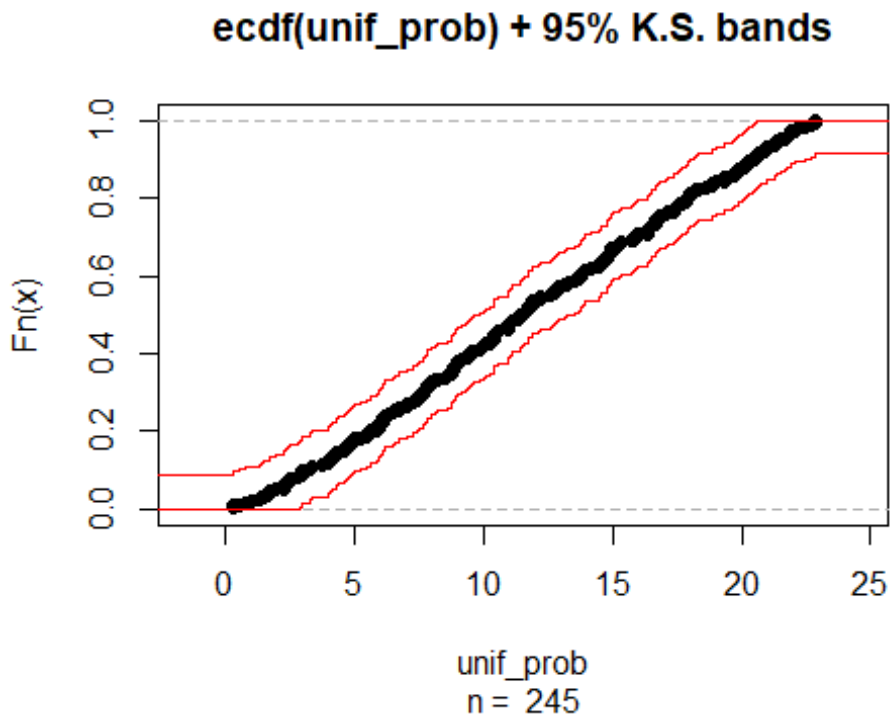


```
##CONFIDENCE ENVELOPES FOR KS, ECDF distribution (uses sfsmisc package)
ecdf.ksCI(prob$Prob, ci.col = "green")
```

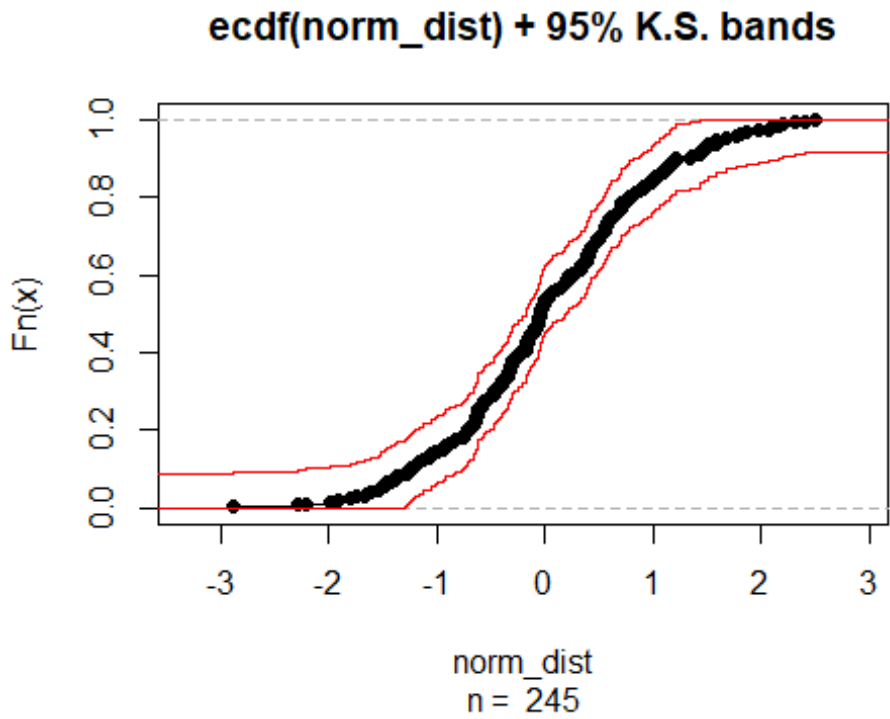
ecdf(prob\$Prob) + 95% K.S. bands



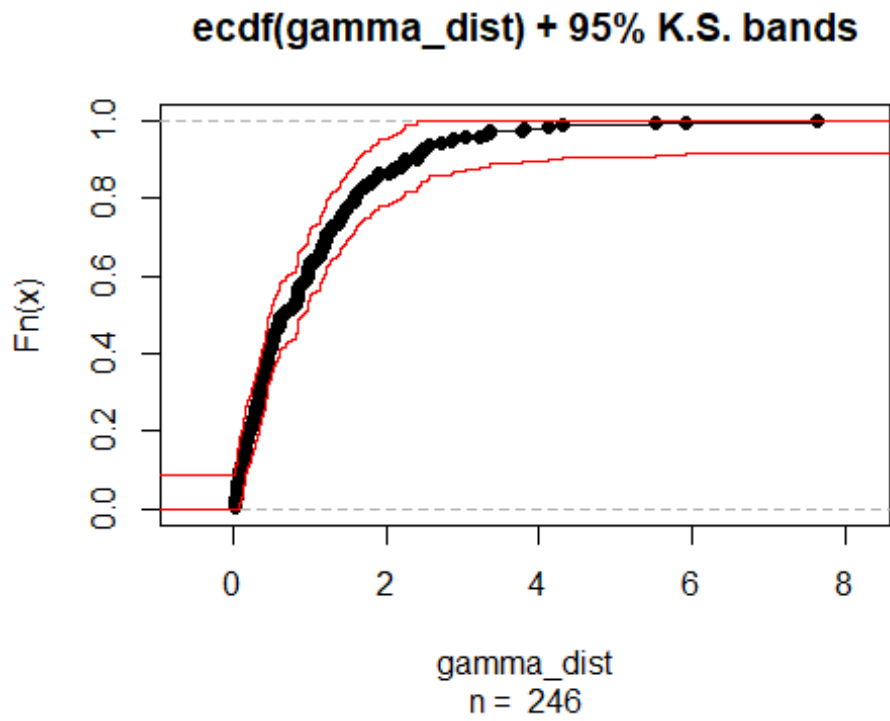
`ecdf.ksCI(unif_prob)`



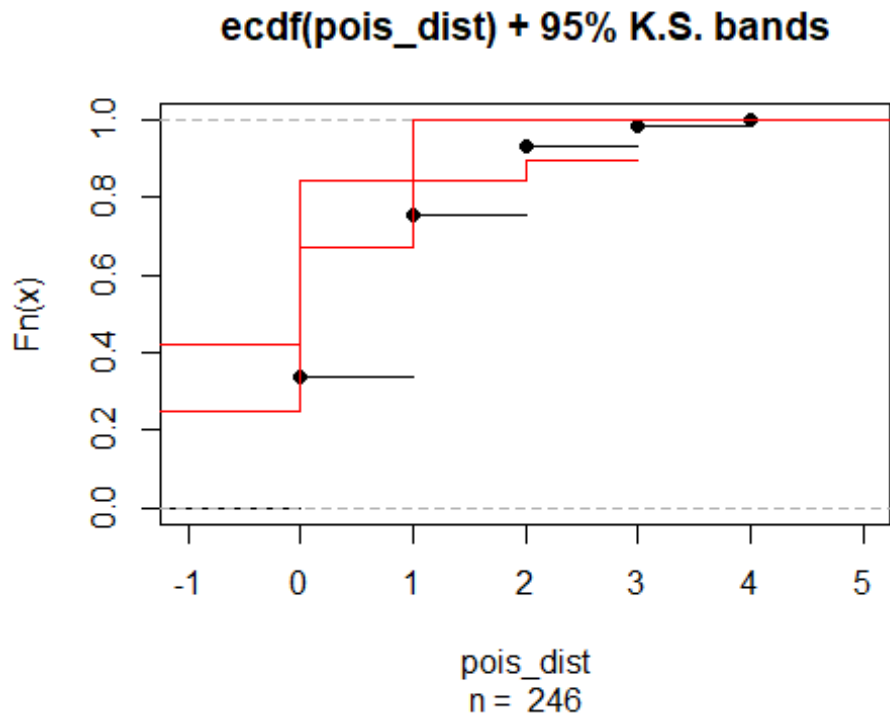
`ecdf.ksCI(norm_dist)`



```
ecdf.ksCI(gamma_dist)
```



```
ecdf.ksCI(pois_dist)
```



Appendix C: Supplemental Information from Chapter 5

This R Markdown shows the development of a point process modeling procedure to evaluate archaeological predictive models. This code reflects the methods discussed in the text of the manuscript.

Load Libraries

```
library(spatstat)
## spatstat 1.63-0      (nickname: 'Space
camouflage') ## For an introduction to spatstat,
type 'beginner' library(maptools) library(raster)
library(rgdal)
## rgdal: version: 1.4-8, (SVN revision 845)

library(rgeos)
## rgeos version: 0.5-2, (SVN revision 621)
## GEOS runtime version: 3.6.1-CAPI-1.10.1
## Linking to sp version: 1.3-2

library(sp)
library(MuMIn)
library(MASS)
library(here)

##
## Attaching package: 'MASS'

## The following objects are masked from 'package:raster':
##
##   area, select

## The following object is masked from
'package:spatstat': ##
##   area
library(graphics)
```

Setup workspace for spatial analysis

```
setwd(here())

#Bounding window data
win_ext <- readOGR(dsn="AOI_boundary.shp")
```

Load Archaeological Points and Environmental Datasets

```
Arch <- readOGR(dsn = "TOTAL_POINT_artifWGS_2019.shp")
veg_index <- mask(raster("SAVI_35_dist_p5_9.tif"), win_ext)
dunes <- mask(raster("dune_dist_p5_9.tif"), win_ext)
water <- mask(raster("water_dist_p5_9.tif"), win_ext)
coral <- mask(raster("coral_dist_p5_9.tif"), win_ext)
islands <- mask(raster("island_dist_p5_9.tif"), win_ext)
rocks <- mask(raster("rock_dist_5_91.tif"), win_ext)
bedrock <- mask(raster("bedrk_120dst.tif"), win_ext)
```

Convert data to PPM format for spatstat analysis

```
b_win <- as.owin(win_ext)
#creates coordinate matrix
arch_pp <- matrix(NA, nrow = nrow(Arch),
ncol = 2) arch_pp[,1] <- Arch$coords.x1
#Long arch_pp[,2] <- Arch$coords.x2 #Lat
#converts CM to PPP (spatstat format)
ppparch_points <- ppp(x=arch_pp[,1], y=arch_pp[,2],
window = owin(bbox(arch_pp)[1,],
bbox(arch_pp)[2,]))
```

```
## Warning: data contain duplicated points #there are no duplicated points, but some points are too close together for spatstat to recognize. We use rjitter to correct this.
```

```
ppparch <- rjitter(ppparch_points, 0.001) #to rectify duplicated point issue
```

```
SAVI_pp <- as.im(veg_index)
```

```
pppwater <- as.im(water)
```

```
pppdunes <- as.im(dunes)
```

```
pppcoral <- as.im(coral)
```

```
pppisland <- as.im(islands)
```

```
ppprocshor <- as.im(rocks)
```

```
ppp_bedrock <- as.im(bedrock)
```

Exploratory Analysis

```
#First-order Trends using rho-hat estimation with 95% confidence bands
```

```
#Unweighted Rho-hat tests
```

```
SAVI_rh_nw <- rhohat(ppparch, SAVI_pp)
```

```
dune_rh_nw <- rhohat(ppparch, pppdunes)
```

```
water_rh_nw <- rhohat(ppparch, pppwater)
```

```
coral_rh_nw <- rhohat(ppparch, pppcoral)
```

```
island_rh_nw <- rhohat(ppparch, pppisland)
```

```
rock_rh_nw <- rhohat(ppparch, ppprocshor)
```

```
bedrock_rh_nw <- rhohat(ppparch, ppp_bedrock)
```

```
bedrock_rh_nw
```

```
#The following code creates Figure 5-4.
```

```

par(mfrow=c(3,3))
par(mar=c(2,2,1.5,1.5))

plot(bedrock_rh_nw, main= "Bedrock", legend=F, ylim=c(0,0.00002),
xlab="Distance (m)", ylab="Absolute Intensity")# highest y-Limit
(0.00009)plot(island_rh_nw, main= "Islands", legend=F,
ylim=c(0,0.00002), xlab="Distance (m)", ylab="Absolute Intensity")
#very high y-Limit (0.1)plot(rock_rh_nw, main= "Rock Outcrops",
legend=F, ylim=c(0,0.00002), xlab="Distance (m)", ylab="Absolute
Intensity") #high limit (0.00004)plot(coral_rh_nw, main= "Coral",
legend=F, ylim=c(0,0.00002), xlab="Distance
(m)", ylab="Absolute Intensity")
plot(water_rh_nw, main= "Ocean", legend=F, ylim=c(0,0.00002),
xlab="Distance
(m)", ylab="Absolute Intensity")
plot(dune_rh_nw, main= "Paleodunes", legend=F, ylim=c(0,0.00002),
xlab="Distance (m)", ylab="Absolute Intensity")
plot(SAVI_rh_nw, main= "Vegetation", legend=F, ylim=c(0,0.00002),
xlab="Distance (m)", ylab="Absolute Intensity")

dev.off()

par(mfrow=c(1,1))

#First-order rho-hat intensity tests using weights (by artifact count)

SAVI_rh <- rhohat(ppparch, SAVI_pp, weights = Arch$Total_Mate)
dune_rh <- rhohat(ppparch, pppdunes, weights = Arch$Total_Mate)

water_rh <- rhohat(ppparch, pppwater, weights = Arch$Total_Mate)

coral_rh <- rhohat(ppparch, pppcoral, weights = Arch$Total_Mate)

island_rh <- rhohat(ppparch, pppisland, weights = Arch$Total_Mate)

rock_rh <- rhohat(ppparch, ppprocshor, weights = Arch$Total_Mate)
bedrock_rh <- rhohat(ppparch, ppp_bedrock, weights = Arch$Total_Mate)

#The following code creates Figure 5-5.

par(mfrow=c(3,3))
par(mar=c(2,2,1.5,1.5))

plot(bedrock_rh, main="Bedrock", legend=F, ylim=c(0,0.0002),
xlab="Distance
(m)", ylab="Absolute Intensity")#highest y-Limit (0.002)

```



```

plot(island_rh, main="Islands", legend=F, ylim=c(0,0.0002),
xlab="Distance
(m)", ylab="Absolute Intensity") #very Low y-Limit (0.00002)
plot(rock_rh, main="Rock Outcrops", legend=F, ylim=c(0,0.0002),
xlab="Distance (m)", ylab="Absolute Intensity")#third highest y-
Limit, everything else visible from this point
plot(coral_rh,
main="Corals", legend=F, ylim=c(0,0.0002), xlab="Distance
(m)", ylab="Absolute Intensity")
plot(water_rh, main="Ocean", legend=F, ylim=c(0,0.0002), xlab="Distance
(m)", ylab="Absolute Intensity")
plot(dune_rh, main="Paleodunes", legend=F, ylim=c(0,0.0002),
xlab="Distance
(m)", ylab="Absolute Intensity")
plot(SAVI_rh, main="Vegetation", legend=F, ylim=c(0,0.0002),
xlab="Distance (m)", ylab="Absolute Intensity")

par(mfrow=c(1,1))
dev.off()

```

Second-Order Tests: Summary Distribution Functions

#Unweighted

```

K_test <- envelope(ppparch, fun=Kest, nsim=39, fix.n=T,
correction="translation", global=F)

```

```

G_test <- envelope(ppparch, fun=Gest, nsim=39, fix.n=T,
correction="best", global=F)

```

```

PCFtest <- envelope(ppparch, fun=pcf, nsim=39,
fix.n=T, correction="translation", global=F,
divisor="d") par("mar") #check dimensions of
image plots #The following code creates Figure 5-
6

```

```

par(mfrow=c(1,3)) par(mar=c(2,2,2,2)) plot(K_test, main="K-
function",xlim=c(0,1000), legend=F, xlab="Distance (m)") plot(G_test,
main="G-function",xlim=c(0,1000), legend=F, xlab="Distance
(m)")
plot(PCFtest, main="PC-function",xlim=c(0,1000), legend=F,
xlab="Distance
(m)")

```

#Weighted model functions (by artifact count)

```

K_test_w <- envelope(ppparch, fun=Kest, nsim=39, fix.n=T,
wght=Arch$Total_Mate, correction="translation", global=F)

```

```

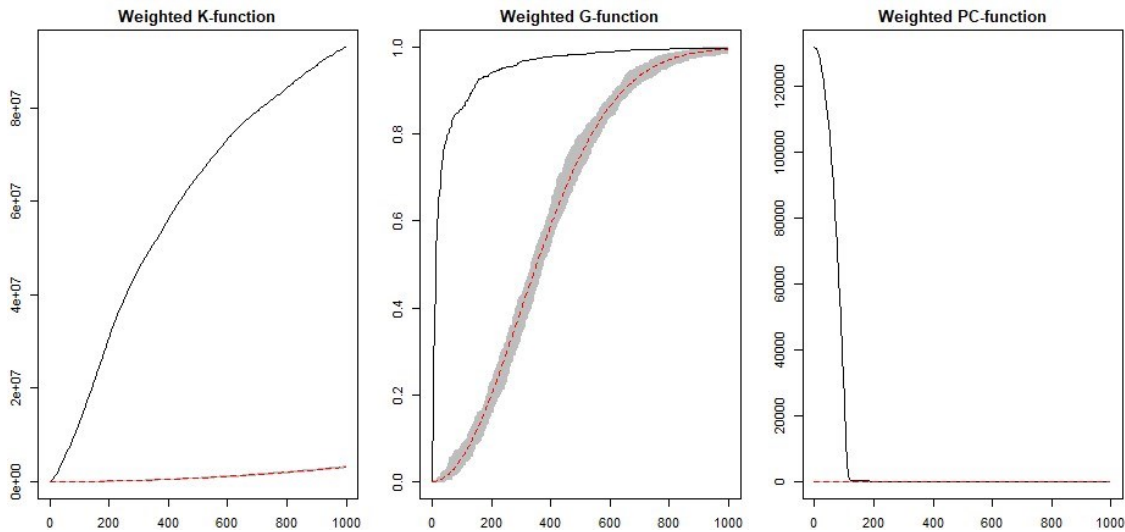
G_test_w <- envelope(ppparch, fun=Gest, nsim=39, fix.n=T,
wght=Arch$Total_Mate, correction="best", global=F)

```

```
PCFtest_w <- envelope(ppparch, fun=pcf, nsim=39, fix.n=T,
wght=Arch$Total_Mate, correction="translation", global=F, divisor="d")

#Creates figure below (weighted summary distribution functions)
par(mfrow=c(2,2)) par(mar=c(2,2,2,2)) plot(K_test_w, main="Weighted K-
function",xlim=c(0,1000), legend=F) plot(G_test_w, main="Weighted G-
function",xlim=c(0,1000), legend=F) plot(PCFtest_w, main="Weighted PC-
function",xlim=c(0,1000), legend=F)

par(mfrow=c(1,1))
```



Point Process Modeling of First-Order Properties

```
#PPM_0 - null model using complete spatial randomness (CSR)

ppm0 <- ppm(ppparch, ~1, correction="translation")

#Point Process model of Davis et al. (2020) predictive algorithm

ppm1 <- ppm(ppparch, ~SAVI_pp+pppdunes+pppcoral+pppwater+pppisland,
correction = "translation")

#New algorithm including all environmental
covariates ppm2 <- ppm(ppparch,
~SAVI_pp+pppdunes+pppcoral+pppwater+pppisland+ppprocshor+ppp_b
edrock, correction = "translation") ppm2
```

```

## Nonstationary Poisson process
##
## Log intensity: ~SAVI_pp + pppdunes + pppcoral + pppwater +
pppisland + ## ppprocshor + ppp_bedrock
##
## Fitted trend coefficients:
## (Intercept) SAVI_pp pppdunes pppcoral
pppwater ## -1.023702e+01 -1.300368e-03 5.448134e-04 -1.149442e-02
1.092304e-02
## pppisland ppprocshor
ppp_bedrock ## 3.847663e-03 -3.899362e-
04 -2.019069e-02 ##
## Estimate S.E. CI95.lo CI95.hi
Ztest
## (Intercept) -1.023702e+01 2.560448e-01 -1.073886e+01 -9.7351829007
***
## SAVI_pp -1.300368e-03 8.236907e-04 -2.914772e-03 0.0003140365
## pppdunes 5.448134e-04 5.105335e-04 -4.558138e-04 0.0015454407
## pppcoral -1.149442e-02 1.335140e-03 -1.411124e-02 -0.0088775922
***
## pppwater 1.092304e-02 1.360987e-03 8.255550e-03 0.0135905213
***
## pppisland 3.847663e-03 9.748846e-04 1.936924e-03 0.0057584013
***
## ppprocshor -3.899362e-04 6.091072e-05 -5.093190e-04 -0.0002705534
*** ## ppp_bedrock -2.019069e-02 1.094142e-03 -2.233517e-02 -
0.0180462133 *** ##
Zval
## (Intercept) -39.981372
## SAVI_pp -1.578709
## pppdunes 1.067145
## pppcoral -8.609151
## pppwater 8.025818
## pppisland 3.946788
## ppprocshor -6.401767
## ppp_bedrock -18.453449

```

Covariate Model Selection

#Model Selection between CSR, the original Davis et al. (2020) model, and model with new covariates

```
MS_AIC <- model.sel(ppm0, ppm1, ppm2, rank = AIC)
MS_AIC
```

```
## Model selection table
##                               trend df      logLik      AIC  delta
weight
## ppm2 S_pp+pppd+pppc+pppw+ppps+pppr+  8 -8394.182 16804.4   0.0
1
## ppm1      S_pp+pppd+pppc+pppw+ppps  6 -10139.231 20290.5 3486.1
0 ## ppm0                               1 -11438.133 22878.3 6073.9
0 ## Abbreviations:
## trend: = '~1',
##      S_pp+pppd+pppc+pppw+ppps =
'~SAVI_pp+pppdunes+pppcoral+pppwater+pppisland',
##      S_pp+pppd+pppc+pppw+ppps+pppr+ =
'~SAVI_pp+pppdunes+pppcoral+pppwater+pppisland+ppprocsh
or+' ## Models ranked by AIC(x)
```

```
MS_BIC <- model.sel(ppm0, ppm1, ppm2, rank = BIC)
MS_BIC
```

```
## Model selection table
##                               trend df      logLik      BIC  delta
weight
## ppm2 S_pp+pppd+pppc+pppw+ppps+pppr+  8 -8394.182 16841.9   0.00
1
## ppm1      S_pp+pppd+pppc+pppw+ppps  6 -10139.231 20318.6 3476.72
0 ## ppm0                               1 -11438.133 22883.0 6041.08
0 ## Abbreviations:
## trend: = '~1',
##      S_pp+pppd+pppc+pppw+ppps =
'~SAVI_pp+pppdunes+pppcoral+pppwater+pppisland',
##      S_pp+pppd+pppc+pppw+ppps+pppr+ =
'~SAVI_pp+pppdunes+pppcoral+pppwater+pppisland+ppprocsh
or+' ## Models ranked by BIC(x)
```

#Assess best fitting model (PPM2) using stepwise selection
stepAIC(ppm2)

```
## Start: AIC=16804.36
## ~SAVI_pp + pppdunes + pppcoral + pppwater + pppisland +
ppprocshor + ##      ppp_bedrock
```

```
##           Df  AIC
## - pppdunes  1 16804
## <none>      1 16804
## - SAVI_pp   1 16805
## - pppisland 1 16821
```

```

## - ppprocshor 1 16856
## - pppwater 1 16882
## - pppcoral 1 16898
## - ppp_bedrock 1 19366

## Step: AIC=16803.49
## ~SAVI_pp + pppcoral + pppwater + pppisland + ppprocshor +
ppp_bedrock

##          Df    AIC
## <none>      16804
## - SAVI_pp    1 16805
## - pppisland  1 16822
## - ppprocshor 1 16854
## - pppwater   1 16882
## - pppcoral   1 16898
## - ppp_bedrock 1 19504

## Nonstationary Poisson process
##
## Log intensity: ~SAVI_pp + pppcoral + pppwater + pppisland +
ppprocshor + ## ppp_bedrock
##
## Fitted trend coefficients:
## (Intercept)      SAVI_pp      pppcoral      pppwater
pppisland
## -1.023407e+01 -1.410127e-03 -1.149096e-02  1.092652e-02
3.993073e-03 ##      ppprocshor      ppp_bedrock ## -3.835392e-04 -
2.009802e-02 ##
##          Estimate          S.E.          CI95.lo          CI95.hi
Ztest
## (Intercept) -1.023407e+01 2.557837e-01 -1.073540e+01 -9.7327431970
***
## SAVI_pp      -1.410127e-03 8.191544e-04 -3.015640e-03  0.0001953863
## pppcoral     -1.149096e-02 1.326391e-03 -1.409064e-02 -0.0088912848
***
## pppwater     1.092652e-02 1.353405e-03  8.273893e-03  0.0135791415
***
## pppisland    3.993073e-03 9.637460e-04  2.104166e-03  0.0058819805
***
## ppprocshor  -3.835392e-04 6.042613e-05 -5.019722e-04 -0.0002651061
*** ## ppp_bedrock -2.009802e-02 1.093286e-03 -2.224082e-02 -
0.0179552200 *** ##          Zval
## (Intercept) -40.010644
## SAVI_pp      -1.721442
## pppcoral     -8.663329
## pppwater     8.073355
## pppisland    4.143284
## ppprocshor  -6.347240

```

```

## ppp_bedrock -
18.383129 ## Problem:

stepBIC <- stepAIC(ppm2, k=log(length(Arch)))

## Start: AIC=16841.87
## ~SAVI_pp + pppdunes + pppcoral + pppwater + pppisland +
ppprocshor + ## ppp_bedrock

##           Df  AIC
## - pppdunes   1 16836
## - SAVI_pp    1 16838
## <none>       16842
## - pppisland  1 16854
## - ppprocshor 1 16889
## - pppwater   1 16914
## - pppcoral  1 16930
## - ppp_bedrock 1 19399

##
## Step: AIC=16836.31
## ~SAVI_pp + pppcoral + pppwater + pppisland + ppprocshor +
ppp_bedrock

##           Df  AIC
## - SAVI_pp    1 16833
## <none>       16836
## - pppisland  1 16850
## - ppprocshor 1 16882
## - pppwater   1 16910
## - pppcoral  1 16926
## - ppp_bedrock 1 19532

##
## Step: AIC=16832.75
## ~pppcoral + pppwater + pppisland + ppprocshor + ppp_bedrock

##           Df  AIC
## <none>       16833
## - pppisland  1 16851
## - ppprocshor 1 16878
## - pppwater   1 16910
## - pppcoral  1 16928
## - ppp_bedrock 1 20076

#New Best fitting PPM based on model selection
ppm3 <- ppm(ppparch,
~pppcoral+pppwater+pppisland+ppprocshor+ppp_bedrock, correction =
"translation") #Best fitting based on BIC

ppm4 <- ppm(ppparch,

```

```

~SAVI_pp+pppcoral+pppwater+pppisland+ppprocshor+ppp_bedrock,
correction = "translation") #Best fitting based on AIC

#Following code produces data in Table 2

MS_AIC2 <- model.sel(ppm0, ppm1, ppm2, ppm3, ppm4, rank = AIC)

## Model selection table
##                                     trend
## ppm4 S_pp+pppc+pppw+ppps+pppr+ppp_b
## ppm2 S_pp+pppd+pppc+pppw+ppps+pppr+
## ppm3      pppc+pppw+ppps+pppr+ppp_b
## ppm1      S_pp+pppd+pppc+pppw+ppps
## ppm0
##      df      logLik      AIC
## ppm4  7 -8394.744 16803.5
## ppm2  8 -8394.182 16804.4
## ppm3  6 -8396.311 16804.6
## ppm1  6 -10139.231 20290.5
## ppm0  1 -11438.133 22878.3
##      delta weight
## ppm4      0.00  0.452
## ppm2      0.88  0.292
## ppm3      1.13  0.256
## ppm1 3486.97  0.000
## ppm0 6074.78  0.000
## Abbreviations:
## trend: = '~1',
##      pppc+pppw+ppps+pppr+ppp_b =
## '~pppcoral+pppwater+pppisland+ppprocshor+ppp_bedrock',
##      S_pp+pppc+pppw+ppps+pppr+ppp_b =

```

```

## '~SAVI_pp+pppcoral+pppwater+pppisland+ppprocshor+ppp_bedrock',
##       S_pp+pppd+pppc+pppw+ppps =
## '~SAVI_pp+pppdunes+pppcoral+pppwater+pppisland',
##       S_pp+pppd+pppc+pppw+ppps+pppr+ =
## '~SAVI_pp+pppdunes+pppcoral+pppwater+pppisland+ppprocshor+'
## Models ranked by AIC(x)

MS_BIC2 <- model.sel(ppm0, ppm1, ppm2, ppm3, ppm4, rank = BIC)

## Model selection table
##                                     trend
## ppm3          pppc+pppw+ppps+pppr+ppp_b
## ppm4 S_pp+pppc+pppw+ppps+pppr+ppp_b
## ppm2 S_pp+pppd+pppc+pppw+ppps+pppr+
## ppm1          S_pp+pppd+pppc+pppw+ppps
## ppm0
##      df      logLik      BIC
## ppm3  6  -8396.311 16832.8
## ppm4  7  -8394.744 16836.3
## ppm2  8  -8394.182 16841.9
## ppm1  6 -10139.231 20318.6
## ppm0  1 -11438.133 22883.0
##      delta weight
## ppm3      0.00  0.848
## ppm4      3.55  0.143
## ppm2      9.12  0.009
## ppm1 3485.84  0.000
## ppm0 6050.20  0.000
## Abbreviations:
## trend: = '~1',
##          pppc+pppw+ppps+pppr+ppp_b =
## '~pppcoral+pppwater+pppisland+ppprocshor+ppp_bedrock',
##          S_pp+pppc+pppw+ppps+pppr+ppp_b =
## '~SAVI_pp+pppcoral+pppwater+pppisland+ppprocshor+ppp_bedrock',
##          S_pp+pppd+pppc+pppw+ppps =
## '~SAVI_pp+pppdunes+pppcoral+pppwater+pppisland',
##          S_pp+pppd+pppc+pppw+ppps+pppr+ =
##
## '~SAVI_pp+pppdunes+pppcoral+pppwater+pppisland+ppprocsh
or+' ## Models ranked by BIC(x)

```

Assess Residual Values

```

#Evaluate Residual Values for Best Fitting Model RES_PPM3 <-
residuals.ppm(ppm3, drop=T)

RES_PPM4 <- residuals.ppm(ppm4, drop=T)

```



```

RES_PPM1 <- (residuals.ppm(ppm1, drop=T))

#Following code produces Figure 5-7.

par(mfrow=c(3,2))
par(mar=c(1,3,1,3)) #reset image dimensions to 1x1

plot.msr(RES_PPM3, main="PPM3 Raw Residuals", pch=16, cex=0.25)
diagnose.ppm(ppm3, main="PPM3 Smoothed Residuals",type =
"pearson", which="smooth", cumulative = T) plot.msr(RES_PPM4,
main="PPM4 Raw Residuals", pch=16, cex=0.25)

diagnose.ppm(ppm4, main="PPM4 Smoothed Residuals",type =
"pearson", which="smooth", cumulative = T) plot.msr(RES_PPM1,
main="PPM1 Raw Residuals", pch=16, cex=0.25)

diagnose.ppm(ppm1, main="PPM1 Smoothed Residuals", type =
"pearson", which="smooth", cumulative = T) par(mfrow=c(1,1))

#Assess fit of models with second-order properties using Residual K-
and Gtests

K_sim1_ppm0 <- envelope(ppm0, Kres, nsim=39, fix.n=T,
correction="translation", global=F, divisor="d")

K_sim1_ppm1 <- envelope(ppm1, Kres, nsim=39, fix.n=T,
correction="translation", global=F, divisor="d")

K_sim1_ppm3 <- envelope(ppm3, Kres, nsim=39, fix.n=T,
correction="translation", global=F, divisor="d")

K_sim1_ppm4 <- envelope(ppm4, Kres, nsim=39, fix.n=T,
correction="translation", global=F, divisor="d")

G_sim1_ppm0 <- envelope(ppm0, Gres, nsim=39, fix.n=T,
correction="best", global=F)

G_sim1_ppm1 <- envelope(ppm1, Gres, nsim=39, fix.n=T,
correction="best", global=F)

G_sim1_ppm3 <- envelope(ppm3, Gres, nsim=39, fix.n=T,
correction="best", global=F)

G_sim1_ppm4 <- envelope(ppm4, Gres, nsim=39, fix.n=T,
correction="best", global=F)

```

#Following Code Produces Figure 5-7

```
par(mfrow=c(2,3))
par(mar=c(2,2,2,2))
plot(K_sim1_ppm3, legend=F, main="Residual K-Function\n PPM3",
xlab="Distance (m)")
plot(K_sim1_ppm4, legend=F, main="Residual K-Function\n PPM4",
xlab="Distance (m)")
plot(K_sim1_ppm1, legend=F, main="Residual K-Function\n PPM1",
xlab="Distance (m)")
plot(G_sim1_ppm3, legend=F, main="Residual G-Function\n PPM3",
xlab="Distance (m)")
plot(G_sim1_ppm4, legend=F, main="Residual G-Function\n PPM4",
xlab="Distance (m)")
plot(G_sim1_ppm1, legend=F, main="Residual G-Function\n PPM1",
xlab="Distance (m)")
```

#Coefficient Estimates of Best-fitting model (PPM3) ppm3

```
## Nonstationary Poisson process
##
## Log intensity: ~pppcoral + pppwater + pppisland +
ppprocshor + ## ppp_bedrock
##
## Fitted trend coefficients:
## (Intercept)      pppcoral      pppwater      pppisland
## -10.351284181 -0.011757903  0.011161231  0.004294965
##   ppprocshor   ppp_bedrock
## -0.000384706 -0.020488528

##              Estimate      S.E.      CI95.lo
## (Intercept) -10.351284181 2.479784e-01 -1.083731e+01
## pppcoral     -0.011757903 1.326579e-03 -1.435795e-02
## pppwater      0.011161231 1.353968e-03  8.507502e-03
## pppisland     0.004294965 9.516529e-04  2.429760e-03
## ppprocshor   -0.000384706 6.089174e-05 -5.040516e-04
## ppp_bedrock  -0.020488528 1.075191e-03 -2.259586e-02
##              CI95.hi Ztest      Zval
## (Intercept) -9.8652554468 *** -41.742685
## pppcoral     -0.0091578568 *** -8.863329
## pppwater      0.0138149591 ***  8.243349
## pppisland     0.0061601708 ***  4.513164
## ppprocshor   -0.0002653604 ***  -
6.317868 ## ppp_bedrock -0.0183811931
*** -19.055715
```

GIS Analysis

From the results of exploratory rho-hat tests and coefficient estimates from the PPMs, we take the above information into consideration to develop a series of probability rasters in ArcGIS. The Raster Calculator tool is used.

Code Creates Unweighted predictive raster using Raster Calculator Tool, following PPM2

```
Unweighted_Model =
(1/"bdrck_dpt_10m")+(1/"coral_dist_p5_9.tif")+(1/"island_dist_p5_9.tif"
)+(1/" rock_dist_5_91.tif")+(1/"water_dist_p5_9.tif")
```

Code Creates Weighted Model 1 using Raster Calculator Tool, following PPM results

```
Weighted_Model1 =
((2.5*1/"bdrck_dpt_10m"))+(1.75*(1/"coral_dist_p5_9.tif"))+(1/"dune_dis
t_p5_9
.tif")+(1.75*(1/"island_dist_p5_9.tif"))+(2*(1/"rock_dist_5_91.tif"))+(
1/"wat er_dist_p5_9.tif")+2*(1/"SAVI_35_dist_p5_9.tif"))
```

Code Creates Weighted Model 2 using Raster Calculator Tool, following PPM results

```
Weighted_Model2 =
((3*1/"bdrck_dpt_10m"))+(2*(1/"coral_dist_p5_9.tif"))+(1/"dune_dist_p5_
9.tif"
)+(1.75*(1/"island_dist_p5_9.tif"))+(2.5*(1/"rock_dist_5_91.tif"))+(1/"
water_
dist_p5_9.tif")+2*(1/"SAVI_35_dist_p5_9.tif"))
```

Code Creates Weighted Model 3 using Raster Calculator Tool, following PPM results

```
Weighted_Model3 =
((2.5*1/"bdrck_dpt_10m"))+(1.5*(1/"coral_dist_p5_9.tif"))+(1/"dune_dist
_p5_9.
tif")+1.5*(1/"island_dist_p5_9.tif"))+(2*(1/"rock_dist_5_91.tif"))+(1/"
water
_dist_p5_9.tif")+1.75*(1/"SAVI_35_dist_p5_9.tif"))
```

Code Creates Weighted Model 4 using Raster Calculator Tool, following PPM results

```
Weighted_Model4 =
((2.5*1/"bdrck_dpt_10m"))+(1.5*(1/"coral_dist_p5_9.tif"))+(1.75*(1/"dun
e_dist
_p5_9.tif"))+(1.5*(1/"island_dist_p5_9.tif"))+(2*(1/"rock_dist_5_91.tif
"))+(1 /"water_dist_p5_9.tif")+1.75*(1/"SAVI_35_dist_p5_9.tif"))
```

These rasters are assessed against one another in their ability to positively identify known areas with archaeological material. The best performing probability raster is then tested using the PPM procedure detailed above to quantitatively assess its performance against the unweighted model and the Davis et al. (2020) model (PPM1).

Assess best predictive raster against Weighted Raster

```
#Weighted Raster
w_model <- mask(raster("PPA_Datasets/Weight_Mod5_WGS.tif"), win_ext)
WMod_pp <- as.im(w_model)

ppm5 <- ppm(ppparch, ~WMod_pp, correction = "translation")

#Unweighted raster (same as PPM3)
uw_model <- mask(raster("PPA_Datasets/unweight_BIC_WGS1.tif"), win_ext)
uwMod_pp <- as.im(uw_model) ppm6 <- ppm(ppparch, ~uwMod_pp, correction =
"translation")
```

Point Process Modeling of Second-Order Properties

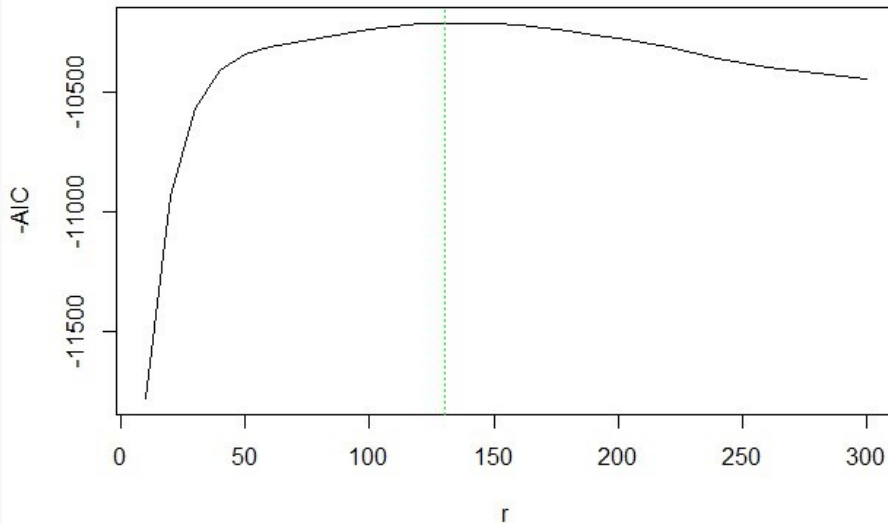
```
##Evaluate Clustering/Dispersion as Model for Settlement Distribution

#Unweighted Model with Area Interaction area_int2 <-
data.frame(r=seq(10, 300, by=10)) p1 <-
profilepl(area_int2, AreaInter, ppparch~uwMod_pp,
aic=T)

p1

## profile log pseudolikelihood
## for model: ppm(ppparch ~ uwMod_pp, aic = T, interaction =
AreaInter) ## fitted with rbord = 600
## interaction: Area-interaction process
## irregular parameter: r in [10, 300]
## optimum value of irregular parameter: r = 130
plot(p2)
```

```
ppm(ppparch ~ uwMod_pp, aic = T, interaction = AreaInter)
```



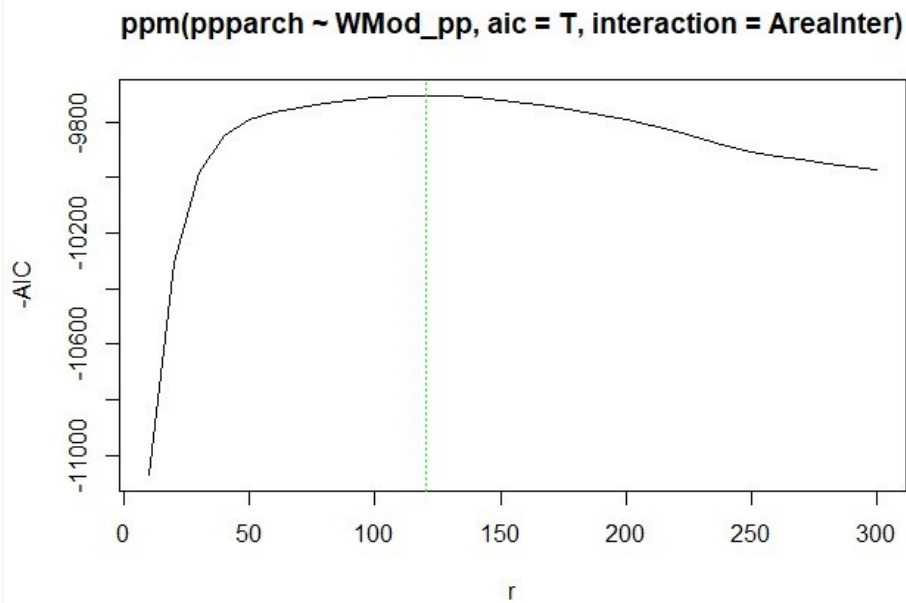
```
ppm7 <- as.ppm(p1)

#Weighted Model with Area Interaction
area_int3 <- data.frame(r=seq(10, 300, by=10))
p2 <- profilepl(area_int3, AreaInter, ppparch~wMod_pp, aic=T)

p2

## profile log pseudolikelihood
## for model: ppm(ppparch~wMod_pp,aic = T,interaction = AreaInter)
## fitted with rbord = 600
## interaction: Area-interaction process
## irregular parameter: r in [10, 300]
## optimum value of irregular parameter: r = 120(

plot(p2)
```



```
ppm8 <- as.ppm(p2)
```

#CSR with Area Interaction

```
area_int3 <- data.frame(r=seq(10, 300, by=10))
```

```
p3 <- profilepl(area_int3, AreaInter, ppparch~1, aic=T)
```

```
p3
```

```
## profile log pseudolikelihood
```

```
## for model: ppm(ppparch ~ WMod_pp, aic = T, interaction = AreaInter)
```

```
## fitted with rbord = 600
```

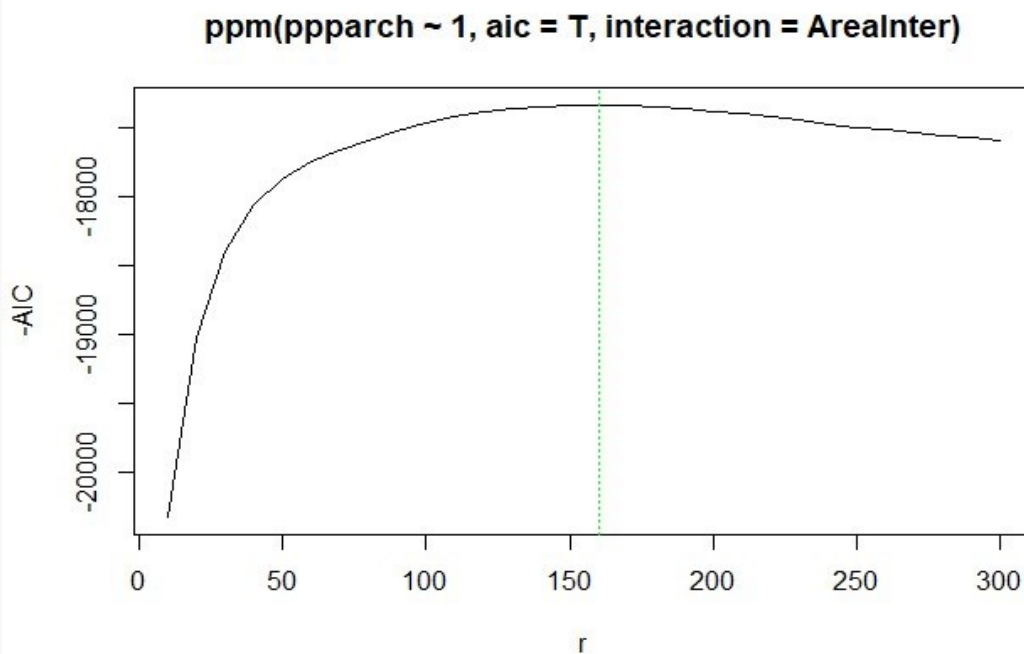
```
## interaction: Area-interaction process
```

```
## irregular parameter: r in [10, 300]
```

```
## optimum value of irregular parameter: r = 160
```

```
Ppm9 <- as.ppm(p3)
```

```
plot(p3)
```



##Evaluate Fit of Area Interaction Process Models

```
K_sim1_ppm7 <- envelope(ppm7, Kres, nsim=39, fix.n=T,
correction="translation", global=T)
```

```
K_sim1_ppm8 <- envelope(ppm8, Kres, nsim=39, fix.n=T,
correction="translation", global=T)
```

#Following code produces figure 9

```
par(mfrow=c(2,1))
```

```
plot(K_sim1_ppm7, legend=F, main="K-Function\n Unweighted + Area
Interaction", xlab="Distance (m)")
```

```
plot(K_sim1_ppm8, legend=F, main="K-Function\nWeighted+Area Interaction"
xlab="Distance (m)")
```

```
par(mfrow=c(1,1))
```

#Model Selection of secondorder PPMs

#Following code produces data in Table 6

```
MS_AIC2 <- model.sel(ppm0, ppm5, ppm6, ppm7, ppm8, ppm9,rank = AIC)
```

```

MS_AIC2
> MS_AIC2

## Model selection table
##           Q trend correction           interaction rbord df
## ppm8 ppp~W_pp                    l(Ar-int,AI,l(inf, 600 3
## ppm7 ppp~u_pp                    l(Ar-int,AI,l(inf, 600 3
## ppm5      ppp WM_pp translatin                                2
## ppm6      ppp uM_pp translatin                                2
## ppm9      ppp~1                    l(Ar-int,AI,l(inf, 600 2
## ppm0      ppp      translatin                                1
##           logLik      AIC      delta weight
## ppm8 -4849.373  9703.7      0.00      1
## ppm7 -5103.432 10211.7     507.96      0
## ppm5 -6038.332 12080.7    2376.92      0
## ppm6 -6465.358 12934.7    3230.97      0
## ppm9 -8666.598 17336.0    7632.29      0
## ppm0 -11438.133 22878.3 13174.52      0
## Abbreviations:
## Q: ppp = 'ppparch', ppp~1 = 'ppparch~1',
##     ppp~u_pp = 'ppparch~uwMod_pp',
##     ppp~W_pp = 'ppparch~WMod_pp'
## trend: = '~1', uM_pp = '~uwMod_pp', WM_pp = '~WMod_pp'
## correction: translatin = 'translation'
## interaction: l(Ar-int,AI,l(inf, = 'list(Area-
## interactionprocess,AreaInter,list(inforder,')
## Models ranked by
AIC(x)

MS_BIC2 <- model.sel(ppm0, ppm5, ppm6, ppm7, ppm8, ppm9, rank = BIC)

MS_BIC2

## Model selection table
##           Q trend correction           interaction rbord df
## ppm8 ppp~W_pp                    l(Ar-int,AI,l(inf, 600 3
## ppm7 ppp~u_pp                    l(Ar-int,AI,l(inf, 600 3
## ppm5      ppp WM_pp translatin                                2
## ppm6      ppp uM_pp translatin                                2
## ppm9      ppp~1                    l(Ar-int,AI,l(inf, 600 2
## ppm0      ppp      translatin                                1
##           logLik      BIC      delta weight
## ppm8 -4849.373  9718.8      0.00      1
## ppm7 -5103.432 10226.9     508.12      0
## ppm5 -6038.332 12090.0    2371.23      0
## ppm6 -6465.358 12944.1    3225.28      0
## ppm9 -8666.598 17346.6    7627.76      0
## ppm0 -11438.133 22883.0 13164.14      0
## Abbreviations:
## Q: ppp = 'ppparch', ppp~1 = 'ppparch~1',

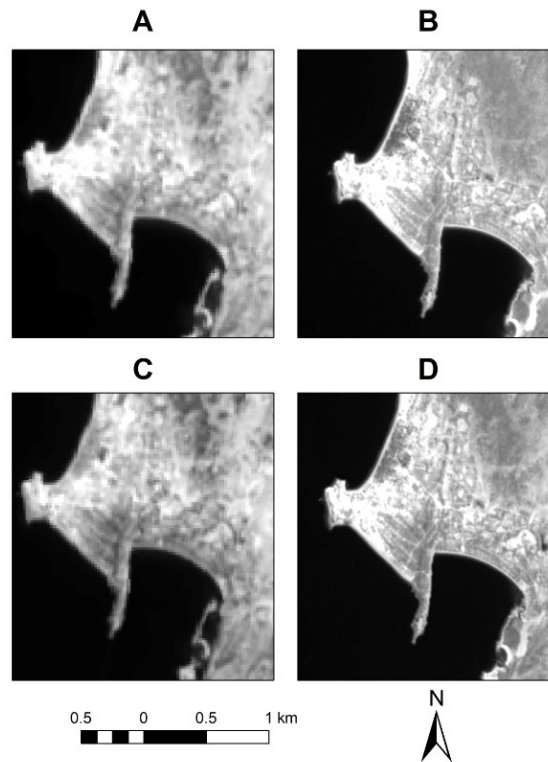
```



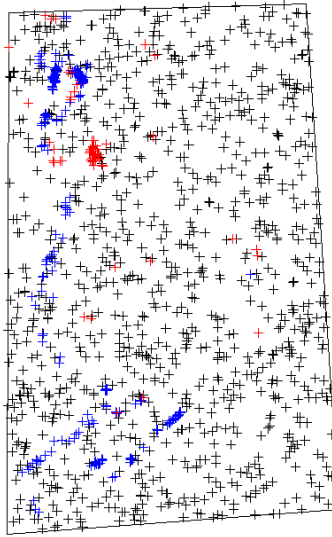
```
## ppp~u_pp = 'ppparch~uwMod_pp',  
## ppp~W_pp = 'ppparch~WMod_pp'  
## trend: = '~1', uM_pp = '~uwMod_pp', WM_pp = '~WMod_pp'  
## correction: translatin = 'translation'  
## interaction: l(Ar-int,AI,l(inf, = 'list(Area-  
## interactionprocess,AreaInter,list(inforder,'  
## Models ranked by  
BIC(x)
```

Appendix D: Supplemental Information from Chapter 6

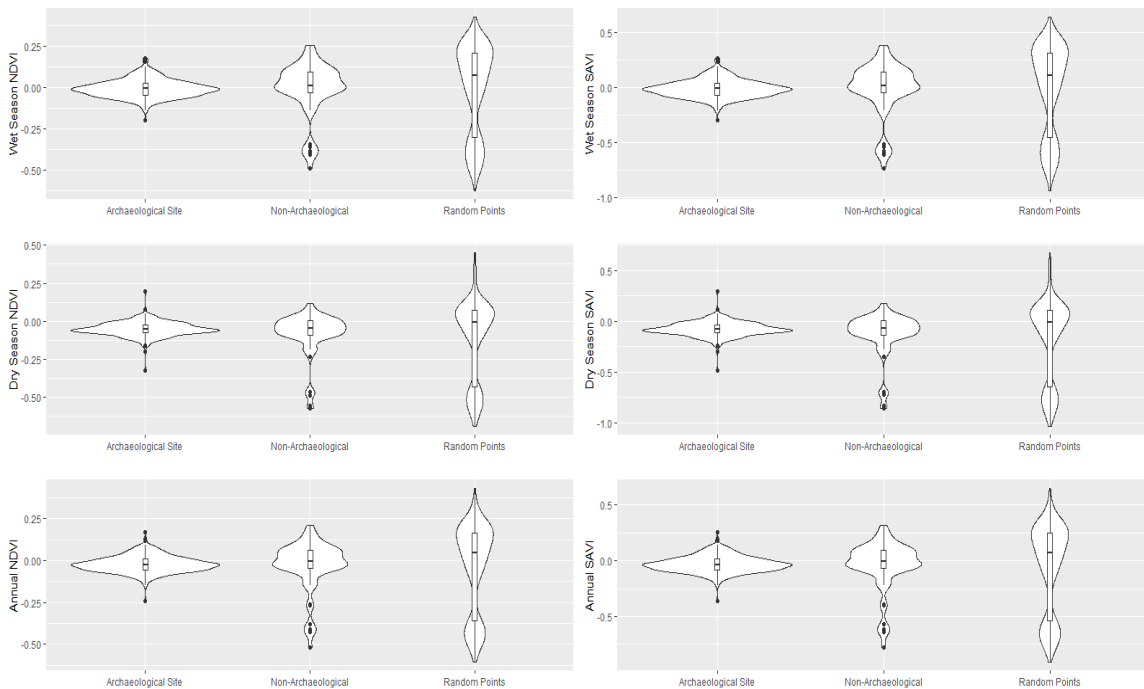
Supplementary Figures



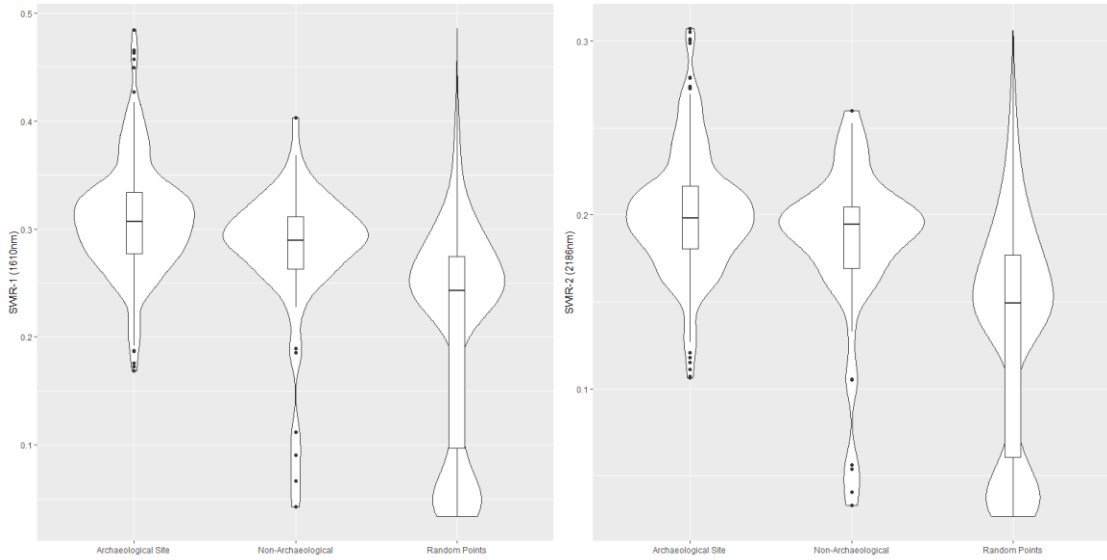
Supplemental Figure D-1: Shows results of pansharpening procedure on SWIR imagery. **A:** Unsharpened Sentinel-2 SWIR Band 1. **B:** Pansharpened Sentinel-2 SWIR Band 1. **C:** Unsharpened Sentinel-2 SWIR Band 2. **D:** Pansharpened Sentinel-2 SWIR Band 2.



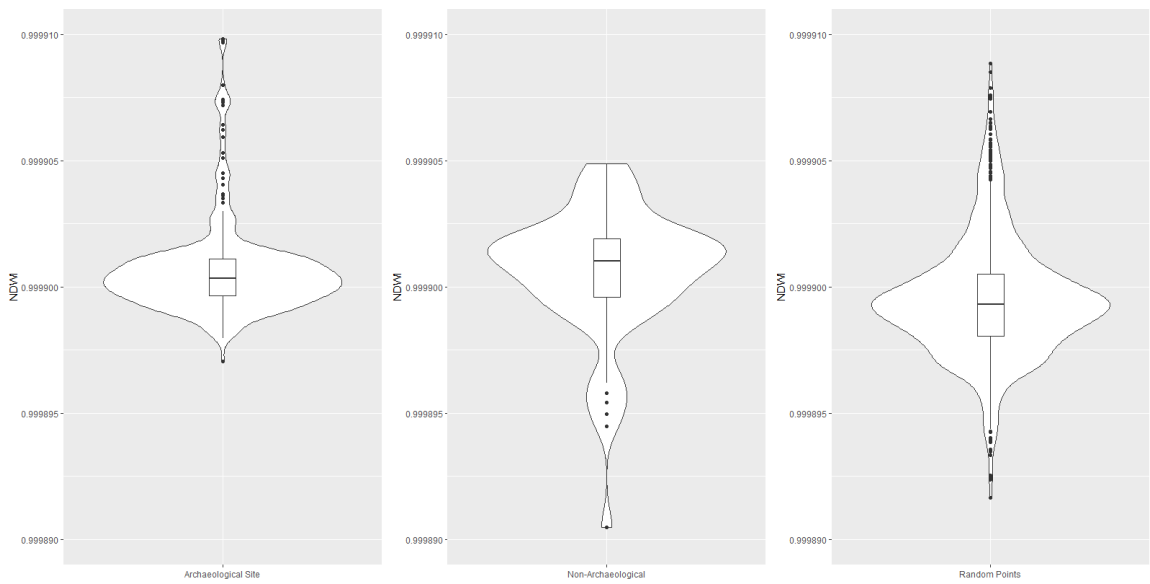
Supplemental Figure D-2: Shows the locations of ground-verified archaeological sites (blue), non-archaeological sites (red), and randomly generated test points (black) used in the analysis.



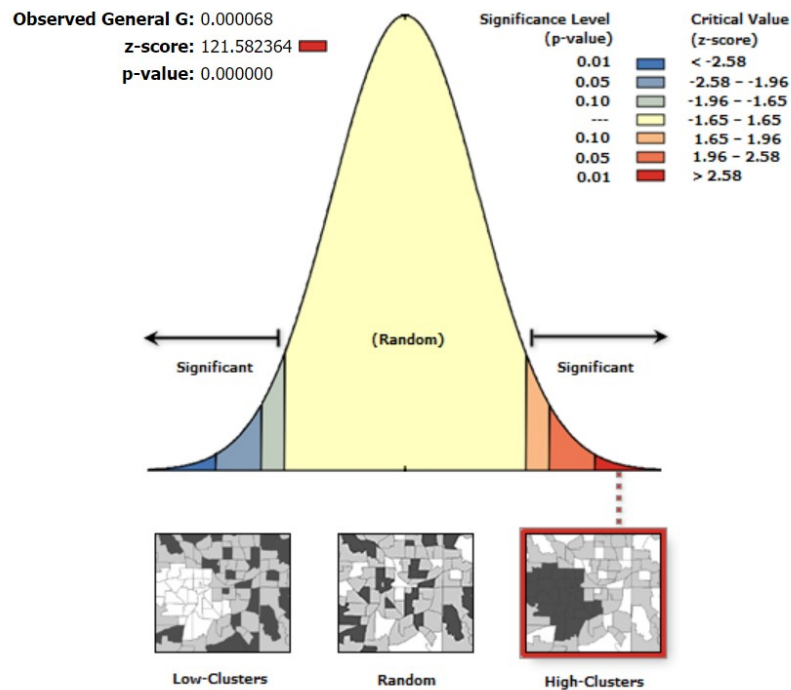
Supplemental Figure D-3: Shows violin and boxplots for annual and seasonal vegetative index values. Note that archaeological sites have a much smaller range of values, whereas non-archaeological and random points have a wider range of vegetative values.



Supplemental Figure D-4: Shows the SWIR reflectance signatures for archaeological, non-archaeological, and randomly generated points within the study area.



Supplemental Figure D-5. Shows NDWI vegetative index values for archaeological, non-archaeological, and randomly generated points within the study area.



Supplemental Figure D-6. Results of Getis-Ords General G test. Anthropogenic modifications identified by the machine learning algorithm are highly clustered and non-random in their distribution.

Supplementary Tables

Supplemental Table D-1. List of PlanetScope images used for the analyses in this paper.

Year	Planet Item ID	Season
2018	20180220_064133_103e	Dry
2018	20180220_064134_103e	Dry
2018	20180220_064136_103e	Dry
2018	20180718_064538_103d	Wet
2018	20180718_064539_103d	Wet
2018	20180718_064540_103d	Wet
2019	20190201_065143_1014	Dry
2019	20190201_065145_1014	Dry
2019	20190201_065146_1014	Dry
2019	20190201_065147_1014	Dry
2019	20190709_065822_1043	Wet
2019	20190709_065822_1_1043	Wet
2019	20190709_065823_1043	Wet

2019	20190709_065824_1043	Wet
2020	20200130_070044_0f3f	Dry
2020	20200130_070045_0f3f	Dry
2020	20200130_070046_0f3f	Dry
2020	20200130_070047_0f3f	Dry
2020	20200724_055747_0f3c	Wet
2020	20200724_055748_0f3c	Wet
2020	20200724_055749_0f3c	Wet

Code used for Analyses

R-Code. The following code replicates the analysis of image pixel value statistics of archaeological and non-archaeological training points. Band statistics for the Planet imagery were generated in ArcGIS (see Methods of main manuscript) before being imported into R v. 4.0.2 (R Core Team 2020). Analysis makes use of the raster (Hijmans 2019), rgdal (Bivand, Keitt, and Rowlingson 2019), ggplot2 (Wickham 2016), gridExtra (Auguie 2017), and RStoolbox (Leutner, Horning, and Schwalb-Willmann 2019) packages.

```
##Load Libraries

library(raster)

## Loading required package: sp

library(rgdal)

## rgdal: version: 1.5-16, (SVN revision 1050)
## Geospatial Data Abstraction Library extensions to R successfully loaded
## Loaded GDAL runtime: GDAL 3.0.4, released 2020/01/28
## Path to GDAL shared files: C:/Program Files/R/R-4.0.2/library/rgdal/gdal
## GDAL binary built with GEOS: TRUE
## Loaded PROJ runtime: Rel. 6.3.1, February 10th, 2020, [PJ_VERSION: 631]
## Path to PROJ shared files: C:/Program Files/R/R-4.0.2/library/rgdal/proj
## Linking to sp version:1.4-2
## To mute warnings of possible GDAL/OSR exportToProj4() degradation,
## use options("rgdal_show_exportToProj4_warnings"="none") before loading rgdal.

library(ggplot2)
library(gridExtra)
library(RStoolbox)

getwd()

## [1] "C:/Users/dsd40/Documents/Planet_Imagery/files"
```

```

#Set working directory
setwd("C://Users/dsd40/Documents/Planet_Imagery")

#Load AOI Boundary File

AOI <- readOGR("AOI.shp")

## OGR data source with driver: ESRI Shapefile
## Source: "C:\Users\dsd40\Documents\Planet_Imagery\AOI.shp", layer: "AOI"
## with 1 features
## It has 1 fields

setwd("C://Users/dsd40/Documents/Planet_Imagery/files")

```

Load Planet Imagery and compile seasonal rasters

```

##Load image data by band

j1B1 <- raster("20180718_064538_103d_3B_AnalyticMS_clip.tif", band = 1)
j1B2 <- raster("20180718_064538_103d_3B_AnalyticMS_clip.tif", band = 2)
j1B3 <- raster("20180718_064538_103d_3B_AnalyticMS_clip.tif", band = 3)
j1B4 <- raster("20180718_064538_103d_3B_AnalyticMS_clip.tif", band = 4)

#stack all bands together
Jul18_1 <- raster::stack(j1B1, j1B2, j1B3, j1B4)

j2B1 <- raster("20180718_064539_103d_3B_AnalyticMS_clip.tif", band = 1)
j2B2 <- raster("20180718_064539_103d_3B_AnalyticMS_clip.tif", band = 2)
j2B3 <- raster("20180718_064539_103d_3B_AnalyticMS_clip.tif", band = 3)
j2B4 <- raster("20180718_064539_103d_3B_AnalyticMS_clip.tif", band = 4)

Jul18_2 <- raster::stack(j2B1, j2B2, j2B3, j2B4)

j3B1 <- raster("20180718_064540_103d_3B_AnalyticMS_clip.tif", band = 1)
j3B2 <- raster("20180718_064540_103d_3B_AnalyticMS_clip.tif", band = 2)
j3B3 <- raster("20180718_064540_103d_3B_AnalyticMS_clip.tif", band = 3)
j3B4 <- raster("20180718_064540_103d_3B_AnalyticMS_clip.tif", band = 4)

Jul18_3 <- raster::stack(j3B1, j3B2, j3B3, j3B4)

#merge all individual images from same date into single raster
July_2018_mrg <- raster::merge(Jul18_1, Jul18_2, Jul18_3)
July_2018_clp <- crop(July_2018_mrg, AOI)

#Repeat same process above for all images

j1B1_19 <- raster("20190709_065822_1_1043_3B_AnalyticMS_clip.tif", band = 1)
j1B2_19 <- raster("20190709_065822_1_1043_3B_AnalyticMS_clip.tif", band

```

```

= 2)
j1B3_19 <- raster("20190709_065822_1_1043_3B_AnalyticMS_clip.tif", band
= 3)
j1B4_19 <- raster("20190709_065822_1_1043_3B_AnalyticMS_clip.tif", band
= 4)

Jul19_1 <- raster::stack(j1B1_19, j1B2_19, j1B3_19, j1B4_19)

j2B1_19 <- raster("20190709_065822_1043_3B_AnalyticMS_clip.tif", band =
1)
j2B2_19 <- raster("20190709_065822_1043_3B_AnalyticMS_clip.tif", band =
2)
j2B3_19 <- raster("20190709_065822_1043_3B_AnalyticMS_clip.tif", band =
3)
j2B4_19 <- raster("20190709_065822_1043_3B_AnalyticMS_clip.tif", band =
4)

Jul19_2 <- raster::stack(j2B1_19, j2B2_19, j2B3_19, j2B4_19)

j3B1_19 <- raster("20190709_065823_1043_3B_AnalyticMS_clip.tif", band =
1)
j3B2_19 <- raster("20190709_065823_1043_3B_AnalyticMS_clip.tif", band =
2)
j3B3_19 <- raster("20190709_065823_1043_3B_AnalyticMS_clip.tif", band =
3)
j3B4_19 <- raster("20190709_065823_1043_3B_AnalyticMS_clip.tif", band =
4)

Jul19_3 <- raster::stack(j3B1_19, j3B2_19, j3B3_19, j3B4_19)

j4B1_19 <- raster("20190709_065824_1043_3B_AnalyticMS_clip.tif", band =
1)
j4B2_19 <- raster("20190709_065824_1043_3B_AnalyticMS_clip.tif", band =
2)
j4B3_19 <- raster("20190709_065824_1043_3B_AnalyticMS_clip.tif", band =
3)
j4B4_19 <- raster("20190709_065824_1043_3B_AnalyticMS_clip.tif", band =
4)

Jul19_4 <- raster::stack(j4B1_19, j4B2_19, j4B3_19, j4B4_19)

#merge all individual images from same date into single raster
July_2019_mrg <- raster::merge(Jul19_1, Jul19_2, Jul19_3, Jul19_4)
July_2019_clp <- crop(July_2019_mrg, AOI)

jB1_20 <- raster("20200724_055747_0f3c_3B_AnalyticMS_clip.tif", band =
1)
jB2_20 <- raster("20200724_055747_0f3c_3B_AnalyticMS_clip.tif", band =
2)
jB3_20 <- raster("20200724_055747_0f3c_3B_AnalyticMS_clip.tif", band =

```



```

3)
jB4_20 <- raster("20200724_055747_0f3c_3B_AnalyticMS_clip.tif", band =
4)

July20_1 <- raster::stack(jB1_20, jB2_20, jB3_20, jB4_20)

j2B1_20 <- raster("20200724_055748_0f3c_3B_AnalyticMS_clip.tif", band =
1)
j2B2_20 <- raster("20200724_055748_0f3c_3B_AnalyticMS_clip.tif", band =
2)
j2B3_20 <- raster("20200724_055748_0f3c_3B_AnalyticMS_clip.tif", band =
3)
j2B4_20 <- raster("20200724_055748_0f3c_3B_AnalyticMS_clip.tif", band =
4)

July20_2 <- raster::stack(j2B1_20, j2B2_20, j2B3_20, j2B4_20)

j3B1_20 <- raster("20200724_055749_0f3c_3B_AnalyticMS_clip.tif", band =
1)
j3B2_20 <- raster("20200724_055749_0f3c_3B_AnalyticMS_clip.tif", band =
2)
j3B3_20 <- raster("20200724_055749_0f3c_3B_AnalyticMS_clip.tif", band =
3)
j3B4_20 <- raster("20200724_055749_0f3c_3B_AnalyticMS_clip.tif", band =
4)

July20_3 <- raster::stack(j3B1_20, j3B2_20, j3B3_20, j3B4_20)

July_2020_mrg <- raster::merge(July20_1, July20_2, July20_3)
July_2020_clp <- crop(July_2020_mrg, AOI) #crop merged image to the AOI

#July_2020_mrg <- setExtent(July_2020_mrg, July_2019_mrg, snap=TRUE)

####WET SEASON IMAGERY

f1B1_18 <- raster("20180220_064133_103e_3B_AnalyticMS_clip.tif", band =
1)
f1B2_18 <- raster("20180220_064133_103e_3B_AnalyticMS_clip.tif", band =
2)
f1B3_18 <- raster("20180220_064133_103e_3B_AnalyticMS_clip.tif", band =
3)
f1B4_18 <- raster("20180220_064133_103e_3B_AnalyticMS_clip.tif", band =
4)

Feb18_1 <- raster::stack(f1B1_18, f1B2_18, f1B3_18, f1B4_18)

f2B1_18 <- raster("20180220_064134_103e_3B_AnalyticMS_clip.tif", band =
1)

```

```

f2B2_18 <- raster("20180220_064134_103e_3B_AnalyticMS_clip.tif", band =
2)
f2B3_18 <- raster("20180220_064134_103e_3B_AnalyticMS_clip.tif", band =
3)
f2B4_18 <- raster("20180220_064134_103e_3B_AnalyticMS_clip.tif", band =
4)

Feb18_2 <- raster::stack(f2B1_18, f2B2_18, f2B3_18, f2B4_18)

f3B1_18 <- raster("20180220_064136_103e_3B_AnalyticMS_clip.tif", band =
1)
f3B2_18 <- raster("20180220_064136_103e_3B_AnalyticMS_clip.tif", band =
2)
f3B3_18 <- raster("20180220_064136_103e_3B_AnalyticMS_clip.tif", band =
3)
f3B4_18 <- raster("20180220_064136_103e_3B_AnalyticMS_clip.tif", band =
4)

Feb18_3 <- raster::stack(f3B1_18, f3B2_18, f3B3_18, f3B4_18)

Feb_2018_mrg <- raster::merge(Feb18_1, Feb18_2, Feb18_3)
Feb_2018_clp <- crop(Feb_2018_mrg, AOI)

f1B1_19 <- raster("20190201_065143_1014_3B_AnalyticMS_clip.tif", band =
1)
f1B2_19 <- raster("20190201_065143_1014_3B_AnalyticMS_clip.tif", band =
2)
f1B3_19 <- raster("20190201_065143_1014_3B_AnalyticMS_clip.tif", band =
3)
f1B4_19 <- raster("20190201_065143_1014_3B_AnalyticMS_clip.tif", band =
4)

Feb19_1 <- raster::stack(f1B1_19, f1B2_19, f1B3_19, f1B4_19)

f2B1_19 <- raster("20190201_065145_1014_3B_AnalyticMS_clip.tif", band =
1)
f2B2_19 <- raster("20190201_065145_1014_3B_AnalyticMS_clip.tif", band =
2)
f2B3_19 <- raster("20190201_065145_1014_3B_AnalyticMS_clip.tif", band =
3)
f2B4_19 <- raster("20190201_065145_1014_3B_AnalyticMS_clip.tif", band =
4)

Feb19_2 <- raster::stack(f2B1_19, f2B2_19, f2B3_19, f2B4_19)

f3B1_19 <- raster("20190201_065146_1014_3B_AnalyticMS_clip.tif", band =
1)
f3B2_19 <- raster("20190201_065146_1014_3B_AnalyticMS_clip.tif", band =
2)
f3B3_19 <- raster("20190201_065146_1014_3B_AnalyticMS_clip.tif", band =

```

```

3)
f3B4_19 <- raster("20190201_065146_1014_3B_AnalyticMS_clip.tif", band =
4)

Feb19_3 <- raster::stack(f3B1_19, f3B2_19, f3B3_19, f3B4_19)

f4B1_19 <- raster("20190201_065147_1014_3B_AnalyticMS_clip.tif", band =
1)
f4B2_19 <- raster("20190201_065147_1014_3B_AnalyticMS_clip.tif", band =
2)
f4B3_19 <- raster("20190201_065147_1014_3B_AnalyticMS_clip.tif", band =
3)
f4B4_19 <- raster("20190201_065147_1014_3B_AnalyticMS_clip.tif", band =
4)

Feb19_4 <- raster::stack(f4B1_19, f4B2_19, f4B3_19, f4B4_19)

Feb_2019_mrg <- raster::merge(Feb19_1, Feb19_2, Feb19_3, Feb19_4)
Feb_2019_clp <- crop(Feb_2019_mrg, AOI)

jB1_20 <- raster("20200130_070044_0f3f_3B_AnalyticMS_clip.tif", band =
1)
jB2_20 <- raster("20200130_070044_0f3f_3B_AnalyticMS_clip.tif", band =
2)
jB3_20 <- raster("20200130_070044_0f3f_3B_AnalyticMS_clip.tif", band =
3)
jB4_20 <- raster("20200130_070044_0f3f_3B_AnalyticMS_clip.tif", band =
4)

Jan20_1 <- raster::stack(jB1_20, jB2_20, jB3_20, jB4_20)

j2B1_20 <- raster("20200130_070045_0f3f_3B_AnalyticMS_clip.tif", band =
1)
j2B2_20 <- raster("20200130_070045_0f3f_3B_AnalyticMS_clip.tif", band =
2)
j2B3_20 <- raster("20200130_070045_0f3f_3B_AnalyticMS_clip.tif", band =
3)
j2B4_20 <- raster("20200130_070045_0f3f_3B_AnalyticMS_clip.tif", band =
4)

Jan20_2 <- raster::stack(j2B1_20, j2B2_20, j2B3_20, j2B4_20)

j3B1_20 <- raster("20200130_070046_0f3f_3B_AnalyticMS_clip.tif", band =
1)
j3B2_20 <- raster("20200130_070046_0f3f_3B_AnalyticMS_clip.tif", band =
2)
j3B3_20 <- raster("20200130_070046_0f3f_3B_AnalyticMS_clip.tif", band =
3)
j3B4_20 <- raster("20200130_070046_0f3f_3B_AnalyticMS_clip.tif", band =
4)

```

```

Jan20_3 <- raster::stack(j3B1_20, j3B2_20, j3B3_20, j3B4_20)

j4B4_20 <- raster("20200130_070047_0f3f_3B_AnalyticMS_clip.tif", band =
1)
j4B4_20 <- raster("20200130_070047_0f3f_3B_AnalyticMS_clip.tif", band =
2)
j4B4_20 <- raster("20200130_070047_0f3f_3B_AnalyticMS_clip.tif", band =
3)
j4B4_20 <- raster("20200130_070047_0f3f_3B_AnalyticMS_clip.tif", band =
4)

Jan20_4 <- raster::stack(j3B1_20, j3B2_20, j3B3_20, j3B4_20)

Jan_2020_mrg <- raster::merge(Jan20_1, Jan20_2, Jan20_3, Jan20_4)
Jan_2020_clp <- crop(Jan_2020_mrg, AOI)

##COMPUTE SEASONALLY AND ANNUALLY AVERAGED RASTERS
#This will take some time to run depending on your processing power and
AOI size

WS_val <- overlay(Feb_2018_clp, Feb_2019_clp, Jan_2020_clp,
  fun=function(x){
    mean(x[x!=0],na.rm=T)
  }
)

DS_val <- overlay(July_2018_clp, July_2019_clp, July_2020_clp,
  fun=function(x){
    mean(x[x!=0],na.rm=T)
  }
)

#Calculate the mean values for each band for all mosaiced images
Ann_val <- overlay(Feb_2018_clp, Feb_2019_clp, July_2018_clp,
  July_2019_clp, Jan_2020_clp, July_2020_clp,
  fun=function(x){
    mean(x[x!=0],na.rm=T)
  }
)

#Calculate Seasonal Difference Raster (For Machine Learning Process)

Diff <- (WS_val - DS_val)

#Calculate NDVI
NDVI_WS <- (WS_val[[4]] - WS_val[[3]])/(WS_val[[4]] + WS_val[[3]])
NDVI_DS <- (DS_val[[4]] - DS_val[[3]])/(DS_val[[4]] + DS_val[[3]])
NDVI_AN <- (Ann_val[[4]] - Ann_val[[3]])/(Ann_val[[4]] + Ann_val[[3]])

```

```

#Calculate SAVI
SAVI_WS <- ((WS_val[[4]] - WS_val[[3]])/(WS_val[[4]] + WS_val[[3]]+0.5)
*(1.5))
SAVI_DS <- ((DS_val[[4]] - DS_val[[3]])/(DS_val[[4]] + DS_val[[3]]+0.5)
*(1.5))
SAVI_AN <- ((Ann_val[[4]] - Ann_val[[3]])/(Ann_val[[4]] + Ann_val[[3]]+
0.5)*(1.5))

```

Calculate Band Statistics for Data

```

###CALCULATE BAND STATISTICS BETWEEN ARCHAEOLOGICAL AND NON-ARCHAEOLOGICAL SITES

```

```

setwd("C://Users/dsd40/Documents/Planet_Imagery/Shapefiles")

```

```

arch_points <- readOGR(dsn = "Arch_total_pts.shp")

```

```

non_arch_points <- readOGR(dsn = "non_arch_pts.shp")

```

```

arch_points <- crop(arch_points, AOI)

```

```

non_arch_points <- crop(non_arch_points, AOI)

```

```

#Generate Random Points to Compare with known ground-tested point Locations

```

```

set.seed(1)

```

```

rsam <- spsample(AOI,1000,"random")

```

```

#plot random points along with ground-tested points within AOI

```

```

#Creates Supplemental Figure 6-1

```

```

plot(AOI)

```

```

plot(rsam, add=T)

```

```

plot(arch_points,col='blue', add=T)

```

```

plot(non_arch_points, col='red', add=T)

```

```

#Extract raster values at each archaeological point Location

```

```

#Depending on the size of the study region and processing power

```

```

#of your computer, this can take a while to run

```

```

Comp_Img <- raster::stack(NDVI_WS, SAVI_WS, NDVI_DS, SAVI_DS, NDVI_AN,
SAVI_AN)

```

```

Arch_values=extract(Comp_Img, arch_points, buffer=20, fun=mean)

```

```

Non_Arch_values=extract(Comp_Img, non_arch_points, buffer=20, fun=mean)

```

```

random_values=extract(Comp_Img, rsam, buffer=20, fun=mean)

```

```

View(Arch_values) #views the resulting information in a table

```

```

#make data frames from each raster point table

```

```

arc_df <- data.frame(Arch_values)
NAr_df <- data.frame(Non_Arch_values)
NAr_df <- na.omit(NAr_df)
Rdm_df <- data.frame(random_values)

#add new column named "cat" (for category)
arc_df$cat <- "Archaeological Site" #archaeological points
NAr_df$cat <- "Non-Archaeological" #non-archaeological points
Rdm_df$cat <- "Random Points"
#combine both dataframes into a single dataframe
df <- rbind(arc_df, NAr_df, Rdm_df)

WS_NDVI_plot <- ggplot(df, aes(df))+
  geom_violin(aes(cat, layer.1))+
  xlab("")+
  ylab("Wet Season NDVI")+
  geom_boxplot(aes(cat, layer.1),width=0.03)
WS_SAVI_plot <- ggplot(df, aes(df))+
  geom_violin(aes(cat, layer.2))+
  xlab("")+
  ylab("Wet Season SAVI")+
  geom_boxplot(aes(cat, layer.2),width=0.03)
DS_NDVI_plot <- ggplot(df, aes(df))+
  geom_violin(aes(cat, layer.3))+
  xlab("")+
  ylab("Dry Season NDVI")+
  geom_boxplot(aes(cat, layer.3),width=0.03)
DS_SAVI_plot <- ggplot(df, aes(df))+
  geom_violin(aes(cat, layer.4))+
  xlab("")+
  ylab("Dry Season SAVI")+
  geom_boxplot(aes(cat, layer.4),width=0.03)
AN_NDVI_plot <- ggplot(df, aes(df))+
  geom_violin(aes(cat, layer.5))+
  xlab("")+
  ylab("Annual NDVI")+
  geom_boxplot(aes(cat, layer.5),width=0.03)
AN_SAVI_plot <- ggplot(df, aes(df))+
  geom_violin(aes(cat, layer.6))+
  xlab("")+
  ylab("Annual SAVI")+
  geom_boxplot(aes(cat, layer.6),width=0.03)

#plot using the gridExtra package
#Creates Supplemental Figure 6-2
grid.arrange(WS_NDVI_plot, WS_SAVI_plot, DS_NDVI_plot, DS_SAVI_plot,
             AN_NDVI_plot, AN_SAVI_plot, ncol=2, nrow=3)

```

```

#Quantitative values for NDVI
mean(arc_df$layer.1) #wet season
## [1] -0.005315107

mean(NAr_df$layer.1) #wet season
## [1] -0.008050252

mean(arc_df$layer.3) #dry season
## [1] -0.05079376

mean(NAr_df$layer.3) #dry season
## [1] -0.08240189

mean(arc_df$layer.5) #annual
## [1] -0.02056559

mean(NAr_df$layer.5) #annual
## [1] -0.03019765

#Quantitative values for SAVI
mean(arc_df$layer.2)
## [1] -0.007972707

mean(NAr_df$layer.2)
## [1] -0.01207179

mean(arc_df$layer.4)
## [1] -0.07618616

mean(NAr_df$layer.4)
## [1] -0.1235879

mean(arc_df$layer.6)
## [1] -0.03084745

mean(NAr_df$layer.6)
## [1] -0.04529075

```

Test for differences between archaeological and non-archaeological points

```

#Test for normality of data
shapiro.test(arc_df$layer.1)

```

```

##
## Shapiro-Wilk normality test
##
## data:  arc_df$layer.1
## W = 0.98468, p-value = 0.001174
shapiro.test(NAr_df$layer.1)

##
## Shapiro-Wilk normality test
##
## data:  NAr_df$layer.1
## W = 0.85266, p-value = 3.129e-06
shapiro.test(NAr_df$layer.2)

##
## Shapiro-Wilk normality test
##
## data:  NAr_df$layer.2
## W = 0.85267, p-value = 3.132e-06
shapiro.test(arc_df$layer.2)

##
## Shapiro-Wilk normality test
##
## data:  arc_df$layer.2
## W = 0.98468, p-value = 0.001174
shapiro.test(NAr_df$layer.3)

##
## Shapiro-Wilk normality test
##
## data:  NAr_df$layer.3
## W = 0.74488, p-value = 5.924e-09
shapiro.test(arc_df$layer.3)

##
## Shapiro-Wilk normality test
##
## data:  arc_df$layer.3
## W = 0.95557, p-value = 1.379e-08
shapiro.test(NAr_df$layer.4)

##
## Shapiro-Wilk normality test
##

```



```

## data:  NAr_df$layer.4
## W = 0.74493, p-value = 5.937e-09

shapiro.test(arc_df$layer.4)

##
##  Shapiro-Wilk normality test
##
## data:  arc_df$layer.4
## W = 0.95558, p-value = 1.381e-08

shapiro.test(NAr_df$layer.5)

##
##  Shapiro-Wilk normality test
##
## data:  NAr_df$layer.5
## W = 0.83913, p-value = 1.257e-06

shapiro.test(arc_df$layer.5)

##
##  Shapiro-Wilk normality test
##
## data:  arc_df$layer.5
## W = 0.98184, p-value = 0.0002861

shapiro.test(NAr_df$layer.6)

##
##  Shapiro-Wilk normality test
##
## data:  NAr_df$layer.6
## W = 0.83915, p-value = 1.259e-06

shapiro.test(arc_df$layer.6)

##
##  Shapiro-Wilk normality test
##
## data:  arc_df$layer.6
## W = 0.98184, p-value = 0.0002862

#test for normality in random test data
shapiro.test(Rdm_df$layer.1)

##
##  Shapiro-Wilk normality test
##
## data:  Rdm_df$layer.1
## W = 0.89365, p-value < 2.2e-16

shapiro.test(Rdm_df$layer.2)

```

```

##
## Shapiro-Wilk normality test
##
## data: Rdm_df$layer.2
## W = 0.89366, p-value < 2.2e-16

shapiro.test(Rdm_df$layer.3)

##
## Shapiro-Wilk normality test
##
## data: Rdm_df$layer.3
## W = 0.85715, p-value < 2.2e-16

shapiro.test(Rdm_df$layer.4)

##
## Shapiro-Wilk normality test
##
## data: Rdm_df$layer.4
## W = 0.85717, p-value < 2.2e-16

shapiro.test(Rdm_df$layer.5)

##
## Shapiro-Wilk normality test
##
## data: Rdm_df$layer.5
## W = 0.87815, p-value < 2.2e-16

shapiro.test(Rdm_df$layer.6)

##
## Shapiro-Wilk normality test
##
## data: Rdm_df$layer.6
## W = 0.87816, p-value < 2.2e-16

#ALL data are non-normal, non-parametric tests will be used

#test significance of difference in mean values
wilcox.test(arc_df$layer.1, NAr_df$layer.1) #wet season

##
## Wilcoxon rank sum test with continuity correction
##
## data: arc_df$layer.1 and NAr_df$layer.1
## W = 8282, p-value = 0.01451
## alternative hypothesis: true location shift is not equal to 0

wilcox.test(arc_df$layer.2, NAr_df$layer.2) #wet season

```

```

##
## Wilcoxon rank sum test with continuity correction
##
## data:  arc_df$layer.2 and NAr_df$layer.2
## W = 8282, p-value = 0.01451
## alternative hypothesis: true location shift is not equal to 0
wilcox.test(arc_df$layer.3, NAr_df$layer.3) #dry season

##
## Wilcoxon rank sum test with continuity correction
##
## data:  arc_df$layer.3 and NAr_df$layer.3
## W = 10230, p-value = 0.9246
## alternative hypothesis: true location shift is not equal to 0
wilcox.test(arc_df$layer.4, NAr_df$layer.4) #dry season

##
## Wilcoxon rank sum test with continuity correction
##
## data:  arc_df$layer.4 and NAr_df$layer.4
## W = 10230, p-value = 0.9246
## alternative hypothesis: true location shift is not equal to 0
wilcox.test(arc_df$layer.5, NAr_df$layer.5) #annually

##
## Wilcoxon rank sum test with continuity correction
##
## data:  arc_df$layer.5 and NAr_df$layer.5
## W = 8639, p-value = 0.04403
## alternative hypothesis: true location shift is not equal to 0
wilcox.test(arc_df$layer.6, NAr_df$layer.6) #annually

##
## Wilcoxon rank sum test with continuity correction
##
## data:  arc_df$layer.6 and NAr_df$layer.6
## W = 8639, p-value = 0.04403
## alternative hypothesis: true location shift is not equal to 0
#test significance of difference between archaeological and random data
wilcox.test(arc_df$layer.1, Rdm_df$layer.1) #wet season

##
## Wilcoxon rank sum test with continuity correction
##
## data:  arc_df$layer.1 and Rdm_df$layer.1
## W = 134910, p-value = 2.842e-08
## alternative hypothesis: true location shift is not equal to 0

```

```

wilcox.test(arc_df$layer.2, Rdm_df$layer.2) #wet season

##
## Wilcoxon rank sum test with continuity correction
##
## data: arc_df$layer.2 and Rdm_df$layer.2
## W = 134910, p-value = 2.842e-08
## alternative hypothesis: true location shift is not equal to 0

wilcox.test(arc_df$layer.3, Rdm_df$layer.3) #dry season

##
## Wilcoxon rank sum test with continuity correction
##
## data: arc_df$layer.3 and Rdm_df$layer.3
## W = 143790, p-value = 4.044e-05
## alternative hypothesis: true location shift is not equal to 0

wilcox.test(arc_df$layer.4, Rdm_df$layer.4) #dry season

##
## Wilcoxon rank sum test with continuity correction
##
## data: arc_df$layer.4 and Rdm_df$layer.4
## W = 143790, p-value = 4.044e-05
## alternative hypothesis: true location shift is not equal to 0

wilcox.test(arc_df$layer.5, Rdm_df$layer.5) #annually

##
## Wilcoxon rank sum test with continuity correction
##
## data: arc_df$layer.5 and Rdm_df$layer.5
## W = 136258, p-value = 9.746e-08
## alternative hypothesis: true location shift is not equal to 0

wilcox.test(arc_df$layer.6, Rdm_df$layer.6) #annually

##
## Wilcoxon rank sum test with continuity correction
##
## data: arc_df$layer.6 and Rdm_df$layer.6
## W = 136258, p-value = 9.746e-08
## alternative hypothesis: true location shift is not equal to 0

```

Short Wave Infrared (SWIR) Analysis

```

#Set working directory
setwd("C://Users/dsd40/Documents/Planet_Imagery/files")

##EVALUATE SOIL MINERAL COMPOSITION AND WATER RETENTION
#Load SWIR data from Sentinel-2

```

```

SWIR1 <- raster("Sent_Month_Comp.tif", band = 13)
SWIR2 <- raster("Sent_Month_Comp.tif", band = 14)

SWIR_stk <- raster::stack(SWIR1, SWIR2)
SWIR_clp <- crop(SWIR_stk, AOI)

#Pan sharpen SWIR data using Planet imagery (data fusion from 20m to 3m
)
##Uses RStoolbox package
SWIR_PS <- panSharpen(SWIR_clp, Ann_val$Annual_18_20.4, method='pca')

par(mfrow=c(2,2))

```

```

#Extract point values
Arch_Values=extract(SWIR_PS, arch_points, buffer=20, fun=mean) #with an
d without buffer, same results
NArc_values=extract(SWIR_PS, non_arch_points, buffer=20, fun=mean) #wit
h and without buffer, same result
NArc_values_cln <- na.omit(NArc_values)
random_values=extract(SWIR_PS, rsam, buffer=20, fun=mean)

#make data frames from each raster point table
S2arc_df <- data.frame(Arch_Values)
S2NAr_df <- data.frame(NArc_values_cln)
S2Rdm_df <- data.frame(random_values)

#add new column named "cat" (for category)
S2arc_df$cat <- "Archaeological Site" #archaeological points
S2NAr_df$cat <- "Non-Archaeological" #non-archaeological points
S2Rdm_df$cat <- "Random Points"
#combine both dataframes into a single dataframe
df2 <- rbind(S2arc_df, S2NAr_df, S2Rdm_df)

# Function to produce summary statistics (mean and +/- sd)
p1 <- ggplot(df2, aes(df2))+
  geom_violin(aes(cat, Sent_Month_Comp.1_pan))+
  xlab("")+
  ylab("SWIR-1 (1610nm)")+
  geom_boxplot(aes(cat, Sent_Month_Comp.1_pan),width=0.1)

p2<- ggplot(df2, aes(df2))+
  geom_violin(aes(cat, Sent_Month_Comp.2_pan))+
  xlab("")+
  ylab("SWIR-2 (2186nm)")+
  geom_boxplot(aes(cat, Sent_Month_Comp.2_pan),width=0.1)

#Create Supplemental Figure D-3

```

```
grid.arrange(p1, p2, ncol=2)
```

Test for differences in SWIR values for data

```
#Test for normality of data
shapiro.test(S2arc_df$Sent_Month_Comp.1_pan)

##
## Shapiro-Wilk normality test
##
## data:  S2arc_df$Sent_Month_Comp.1_pan
## W = 0.97472, p-value = 1.193e-05

shapiro.test(S2arc_df$Sent_Month_Comp.2_pan)

##
## Shapiro-Wilk normality test
##
## data:  S2arc_df$Sent_Month_Comp.2_pan
## W = 0.97795, p-value = 4.762e-05

shapiro.test(S2NAr_df$Sent_Month_Comp.1_pan)

##
## Shapiro-Wilk normality test
##
## data:  S2NAr_df$Sent_Month_Comp.1_pan
## W = 0.80648, p-value = 1.966e-07

shapiro.test(S2NAr_df$Sent_Month_Comp.2_pan)

##
## Shapiro-Wilk normality test
##
## data:  S2NAr_df$Sent_Month_Comp.2_pan
## W = 0.83493, p-value = 1.125e-06

#test significance of difference in mean values
wilcox.test(S2arc_df$Sent_Month_Comp.1_pan, S2NAr_df$Sent_Month_Comp.1_
pan)

##
## Wilcoxon rank sum test with continuity correction
##
## data:  S2arc_df$Sent_Month_Comp.1_pan and S2NAr_df$Sent_Month_Comp.1
_pan
## W = 12713, p-value = 0.001732
## alternative hypothesis: true location shift is not equal to 0

wilcox.test(S2arc_df$Sent_Month_Comp.2_pan, S2NAr_df$Sent_Month_Comp.2_
pan)
```

```

##
## Wilcoxon rank sum test with continuity correction
##
## data: S2arc_df$Sent_Month_Comp.2_pan and S2NAr_df$Sent_Month_Comp.2
_pan
## W = 11999, p-value = 0.02362
## alternative hypothesis: true location shift is not equal to 0

#test significance of difference between archaeological and random poin
ts
wilcox.test(S2arc_df$Sent_Month_Comp.1_pan, S2Rdm_df$Sent_Month_Comp.1_
pan)

##
## Wilcoxon rank sum test with continuity correction
##
## data: S2arc_df$Sent_Month_Comp.1_pan and S2Rdm_df$Sent_Month_Comp.1
_pan
## W = 282643, p-value < 2.2e-16
## alternative hypothesis: true location shift is not equal to 0

wilcox.test(S2arc_df$Sent_Month_Comp.2_pan, S2Rdm_df$Sent_Month_Comp.2_
pan)

##
## Wilcoxon rank sum test with continuity correction
##
## data: S2arc_df$Sent_Month_Comp.2_pan and S2Rdm_df$Sent_Month_Comp.2
_pan
## W = 278508, p-value < 2.2e-16
## alternative hypothesis: true location shift is not equal to 0

```

NDWI Analysis

```

#Calculate NDWI Index
NDWI_AN <- (Ann_val$Annual_18_20.4-SWIR_PS$Sent_Month_Comp.1_pan)/(Ann_
val$Annual_18_20.4+SWIR_PS$Sent_Month_Comp.1_pan)

#Extract point values
Arch_Values=extract(NDWI_AN, arch_points, buffer=20, fun=mean) #with an
d without buffer, same results
NArc_values=extract(NDWI_AN, non_arch_points, buffer=20, fun=mean) #wit
h and without buffer, same result
NArc_values_cln <- na.omit(NArc_values)
random_values=extract(NDWI_AN, rsam, buffer=20, fun=mean)

#make data frames from each raster point table
S3arc_df <- data.frame(Arch_Values)
S3NAr_df <- data.frame(NArc_values_cln)
S3Rdm_df <- data.frame(random_values)

```

```

#add new column named "cat" (for category)
S3arc_df$cat <- "Archaeological Site" #archaeological points
S3NAr_df$cat <- "Non-Archaeological" #non-archaeological points
S3Rdm_df$cat <- "Random Points"

p1 <- ggplot(S3arc_df, aes(S3arc_df))+
  geom_violin(aes(cat, Arch_Values))+
  xlab("")+
  ylab("NDWI")+
  geom_boxplot(aes(cat, Arch_Values),width=0.1)+
  ylim(0.99989, 0.999910)

p2<- ggplot(S3NAr_df, aes(S3NAr_df))+
  geom_violin(aes(cat, NArc_values_cln))+
  xlab("")+
  ylab("NDWI")+
  geom_boxplot(aes(cat, NArc_values_cln),width=0.1)+
  ylim(0.99989, 0.999910)

p3 <- ggplot(S3Rdm_df, aes(S3Rdm_df))+
  geom_violin(aes(cat, random_values))+
  xlab("")+
  ylab("NDWI")+
  geom_boxplot(aes(cat, random_values),width=0.1)+
  ylim(0.99989, 0.999910)

#Creates Supplemental Figure D-4
grid.arrange(p1, p2, p3, ncol=3)

#Test for normality of data
shapiro.test(S3arc_df$Arch_Values)

##
## Shapiro-Wilk normality test
##
## data: S3arc_df$Arch_Values
## W = 0.77782, p-value < 2.2e-16

shapiro.test(S3arc_df$Arch_Values)

##
## Shapiro-Wilk normality test
##
## data: S3arc_df$Arch_Values
## W = 0.77782, p-value < 2.2e-16

shapiro.test(S3NAr_df$NArc_values_cln)

```



```

##
## Shapiro-Wilk normality test
##
## data: S3NAr_df$NArc_values_cln
## W = 0.89988, p-value = 0.0001302

shapiro.test(S3Rdm_df$random_values)

##
## Shapiro-Wilk normality test
##
## data: S3Rdm_df$random_values
## W = 0.95851, p-value = 3.121e-16

#test significance of difference in mean values
wilcox.test(S3arc_df$Arch_Values, S3NAr_df$NArc_values_cln)

##
## Wilcoxon rank sum test with continuity correction
##
## data: S3arc_df$Arch_Values and S3NAr_df$NArc_values_cln
## W = 8468, p-value = 0.0418
## alternative hypothesis: true location shift is not equal to 0

#test significance of difference between archaeological and random points
wilcox.test(S3arc_df$Arch_Values, S3Rdm_df$random_values)

##
## Wilcoxon rank sum test with continuity correction
##
## data: S3arc_df$Arch_Values and S3Rdm_df$random_values
## W = 233192, p-value < 2.2e-16
## alternative hypothesis: true location shift is not equal to 0

mean(S3NAr_df$NArc_values_cln)

## [1] 0.9999005

mean(S3arc_df$Arch_Values)

## [1] 0.9999007

```

Javascript Code for Compiling Sentinel-2 Data. The following code creates a composite of Sentinel-2 data over a 5 year timeframe in Google Earth Engine (GEE). For interested readers, the code can be executed within GEE by using the following link: <https://code.earthengine.google.com/67eeee7b0e7cb49beac1237aff1f5f53>.

```

// This code borrows the method described by Orengo et al. (2020)
// Define a central point in your study area (as X,Y WGS84 decimal
degrees) and a scale,

```

```

// just for visualization purposes. Change the coordinates to center
the map in your own area

Map.setCenter(-22.086143, 43.304527, 9);

// Create a polygon delimiting the AOI.

// The user can draw their own polygon(as a geometry) delimiting a new
AOI
// using the Geometry Imports menu in the top right corner of the map
area below.
var geometry = geometry;

print('Study area', geometry.area().divide(1000 * 1000), 'km2'); //
AOI area km2 for info

////////// IMPORT & COMPOSITE SENTINEL 2 COLLECTION
//////////

// Function to mask clouds using the Sentinel-2 QA band.
function maskS2clouds(image) {

    var qa = image.select('QA60');

    // Bits 10 and 11 are clouds and cirrus, respectively.

    var cloudBitMask = 1 << 10;
    var cirrusBitMask = 1 << 11;

    // Both flags should be set to zero, indicating clear conditions.

    var mask = qa.bitwiseAnd(cloudBitMask).eq(0).and(
        qa.bitwiseAnd(cirrusBitMask).eq(0));

    // Return the masked and scaled data, without the QA bands.

    return image.updateMask(mask).divide(10000)

        .select("B.*")

        .copyProperties(image, ["system:time_start"]);
}

// Map the function over one year of data and take the median.
// Load Sentinel-2 TOA reflectance data.

var s2 = ee.ImageCollection('COPERNICUS/S2')

```

```

.filterBounds(geometry)

.filterDate('2015-6-23', '2020-07-05')

// Pre-filter to get less cloudy granules.

.filter(ee.Filter.lt('CLOUDY_PIXEL_PERCENTAGE', 20))

.map(maskS2clouds);

// Filter them by two-month periods and extract the average values
var s2_JanFeb = s2.filter(ee.Filter.dayOfYear(1,60))
  .median();
var s2_MarApr = s2.filter(ee.Filter.dayOfYear(61,120))
  .median();
var s2_MayJun = s2.filter(ee.Filter.dayOfYear(121,180))
  .median();
var s2_JulAug = s2.filter(ee.Filter.dayOfYear(181,240))
  .median();
var s2_SepOct = s2.filter(ee.Filter.dayOfYear(241,300))
  .median();
var s2_NovDec = s2.filter(ee.Filter.dayOfYear(301,360))
  .median();
// Create a multiband composite image
var s2comp = ee.Image([s2_JanFeb, s2_MarApr, s2_MayJun, s2_JulAug,
s2_SepOct, s2_NovDec])
  .clip(geometry);

// Print total Sentinel 2 images employed

print('Sentinel 2 images', s2comp);

// Select the bands of interest form the Image Collection

var s2comp_band =
s2.select(['B2', 'B3', 'B4', 'B5', 'B6', 'B7', 'B8', 'B8A', 'B11', 'B12'])

  .mean().clip(geometry);

// Reduction in the number of decimal places of the values of the
resulting raster
// This will not reduce noticeably the quality of the data but it will
reduce significantly
// the size of the resulting raster.

var Composite = ee.Image(0).expression(

  'round(img * 10000) / 10000', {

```

```

        'img': s2comp_band
    });

    print('Composite:', Composite);
    Map.addLayer(Composite);

    Export.image.toAsset({ // It is also possible to export to Google
    Drive, just select the option in the dialogue

        image: Composite,

        scale: 10,

        maxPixels: 1e12,

        region: geometry

    });

```

Javascript Code for Machine Learning Analysis. The following code replicates the analysis performed in Google Earth Engine (GEE). The code can be pasted directly into GEE's code editor and run as is to replicate the analysis performed in the manuscript. Alternatively, interested users can use the following link to run the analysis in GEE: <https://code.earthengine.google.com/99ccb498ea588d44a0b3300841163405>

```

// Define a central point in your study area (as X,Y WGS84 decimal degr
// ees) and a scale. If applying to different location, change the coor
// dinates to center the map in your new study region

Map.setCenter(-22.130350, 43.240261, 9);

// Indicate the number of iterations for the RF algorithm

var iteration = 'it03';

// Create or load composite image of Planet Imagery

var Composite = ee.Image("users/dylandavis996/Planet_2019_Dif");

// Create a polygon outlining the study area (as a geometry) using the
// Geometry Imports menu in the top right corner of the map area, below
.

// Create a polygon defining the study area.

```

```

var geometry =
  ee.Geometry.Polygon(
    [[[43.20159553966782, -22.21131419742182],
      [43.315578693964696, -22.22084927789693],
      [43.34373115978501, -22.05802855054113],
      [43.23204168734154, -22.03808254866185]]]);

print('Study area', geometry.area().divide(1000 * 1000), 'km2'); // Prints AOI area km2 in Console

```

```

//////////////////// MACHINE LEARNING RF CLASSIFIER //////////////////////

```

```

// Call training data for current iteration (in this case iteration 3).
// The user wanting to generate their own training data is prompted to
// use the geometry imports panel in the map view below to create new
// feature collections (named 'sites' and 'other' if the user wants to
// reuse the code below) with a property named 'class' and a value of 1
// and 0 respectively.

```

```

var sites = ee.FeatureCollection('users/dylandavis996/training_data/Planet_Arch_Train'),
    other = ee.FeatureCollection('users/dylandavis996/training_data/Planet_Other_Train');

```

```

// Merge training data

```

```

var trn_pols = sites.merge(other);

```

```

print(trn_pols, 'train_pols');

```

```

// Create variable for bands

```

```

var bands = ['b1','b2','b3','b4'];

```

```

// SampleRegions to extract band values for each pixel in each training polygon

```

```

var training = Composite.select(bands).sampleRegions({
  collection: trn_pols,
  properties: ['Class'],
  scale: 5
});

```

```

});

// Apply RF classifier calling mode "probability"
// To apply a standard RF classifier, call mode "CLASSIFICATION"

var classifier = ee.Classifier.randomForest({'numberOfTrees':128})
  .setOutputMode('PROBABILITY').train({
    features: training,
    classProperty: 'Class',
    inputProperties: bands
  });

// Create classified probability raster

var classified = Composite.select(bands).classify(classifier);

// Add the resulting classified layer to the Map Window below

Map.addLayer(classified, {min: 0.60, max: 1}, iteration); // It can take
several minutes to load

////////////////////// EXPORT OF RESULTING DATASETS ////////////////////////

// Data exports as assets so they can be included and visualizes in next
iterations
// You can also export to Google Drive by selecting the option in the dialog
ue box

Export.image.toAsset({
  image: classified,
  description: 'RF_128_Arch' + iteration,
  scale: 5,
  maxPixels: 1e12,
  region: geometry
});

```

Appendix E: Supplemental Information from Chapter 7

This R Markdown includes the code necessary to replicate the analysis in the associated manuscript. In what follows, code and its associated description will be provided along with the output of each component of the analysis.

The following code implements a network analysis of ceramic data from Southwest Madagascar following the protocol developed by Matt Peeples (2017). The original Script by Matt Peeples can be found at: <http://www.mattpeeples.net/netstats.html>

```
##Load libraries and necessary datasets
#Load required Libraries
library(statnet) #for network analysis

library(tnet) #for network analysis

library(rgdal) #for mapping GIS files

library(here)

#set working directory
setwd(here())

#Load data as properly formatted CSV files (See Peeples 2017 for format
ting information)

# the name of each row (site name) should be the first column in the in
put table
d_data1 <- read.table(file='Early_Period_Data.csv', sep=',', header=T,
row.names=1)
d_data2 <- read.table(file='Middle_Period_Data.csv', sep=',', header=T,
row.names=1)
d_data3 <- read.table(file='Late_Period_Data.csv', sep=',', header=T, r
ow.names=1)

#Load shapefile of study area
AOI <- readOGR(dsn='Velondriake_AOI.shp')
## OGR data source with driver: ESRI Shapefile
## Source: "C:\Users\dylan\Documents\School_Work\Dissertation\Ceramic_A
nalysis\Ceramic_Network_Data\Velondriake_AOI.shp", layer: "Velondriake_
AOI"
## with 1 features
## It has 1 fields

##Implement functions for co-presence, Brainerd-Robinson (BR) coefficient, and
chi-square distance metrics.

#Function to create a co-ocurance dataset using presence/absence
co.p <- function(x, thresh = 0.1) {
  # create matrix of proportions from ceramic data
  temp <- prop.table(as.matrix(x), 1)
  # define anything with greater than or equal to 0.1 as present (1)
```

```

temp[temp >= thresh] <- 1
# define all other cells as absent (0)
temp[temp < 1] <- 0
# matrix algebraic calculation to find co-occurrence (%*% indicates ma
trix
# multiplication)
out <- temp %*% t(temp)
return(out)
}

# run the function on the datasets
d_data1P <- co.p(d_data1) #Decoration data
d_data2P <- co.p(d_data2) #Manufacturing data
d_data3P <- co.p(d_data3)

# Function for calculating Brainerd-Robinson (BR) coefficients
# This creates a matrix of similarity values used in many SNAs
sim.mat <- function(x) {
  # get names of sites
  names <- row.names(x)
  x <- na.omit(x) # remove any rows with missing data
  x <- prop.table(as.matrix(x), 1) # convert to row proportions
  rd <- dim(x)[1]
  # create an empty symmetric matrix of 0s
  results <- matrix(0, rd, rd)
  # the following dreaded double for-loop goes through every cell in th
e
  # output data table and calculates the BR value as described above
  for (s1 in 1:rd) {
    for (s2 in 1:rd) {
      x1Temp <- as.numeric(x[s1, ])
      x2Temp <- as.numeric(x[s2, ])
      results[s1, s2] <- 2 - (sum(abs(x1Temp - x2Temp)))
    }
  }
  row.names(results) <- names # assign row names to output
  colnames(results) <- names # assign column names to output
  results <- results/2 # rescale results between 0 and 1
  results <- round(results, 3) # round results
  return(results)
} # return the final output table

# Run the BR coefficient function on our sample data
d_data1BR <- sim.mat(d_data1) #Decoration data
d_data2BR <- sim.mat(d_data2) #Manufacturing data
d_data3BR <- sim.mat(d_data3)

# Chi-square (X2) distance function
chi.dist <- function(x) {
  rowprof <- x/apply(x, 1, sum) # calculates the profile for every row

```



```

avgprof <- apply(x, 2, sum)/sum(x) # calculates the average profile
# creates a distance object of  $\chi^2$  distances
chid <- dist(as.matrix(rowprof) %*% diag(1/sqrt(avgprof)))
# return the results
return(as.matrix(chid))
}

# Run the X2 function and then create the rescaled 0-1 version
d_data1X <- chi.dist(d_data1) #Decoration data

## Warning in sqrt(avgprof): NaNs produced

d_data1X01 <- d_data1X/max(d_data1X)

d_data2X <- chi.dist(d_data2)#Manufacturing data

## Warning in sqrt(avgprof): NaNs produced

d_data2X01 <- d_data2X/max(d_data2X)

d_data3X <- chi.dist(d_data3) #Decoration data

## Warning in sqrt(avgprof): NaNs produced

d_data3X01 <- d_data3X/max(d_data3X)

###VISUALIZING NETWORKS

# create network object from co-occurrence
Pnet_d1 <- network(d_data1P, directed = F)
Pnet_d2 <- network(d_data2P, directed = F)
Pnet_d3 <- network(d_data3P, directed = F)
# Now Let's add names for our nodes based on the row names of our original
# matrix
Pnet_d1 %v% "vertex.names" <- row.names(d_data1P)
Pnet_d2 %v% "vertex.names" <- row.names(d_data2P)
Pnet_d3 %v% "vertex.names" <- row.names(d_data3P)
# Look at the results
Pnet_d1

## Network attributes:
## vertices = 48
## directed = FALSE
## hyper = FALSE
## loops = FALSE
## multiple = FALSE
## bipartite = FALSE
## total edges= 1119
## missing edges= 0

```

```

##      non-missing edges= 1119
##
## Vertex attribute names:
##      vertex.names
##
## Edge attribute names not shown

Pnet_d2

## Network attributes:
## vertices = 86
## directed = FALSE
## hyper = FALSE
## loops = FALSE
## multiple = FALSE
## bipartite = FALSE
## total edges= 3655
##      missing edges= 0
##      non-missing edges= 3655
##
## Vertex attribute names:
##      vertex.names
##
## Edge attribute names not shown

Pnet_d3

## Network attributes:
## vertices = 146
## directed = FALSE
## hyper = FALSE
## loops = FALSE
## multiple = FALSE
## bipartite = FALSE
## total edges= 10559
##      missing edges= 0
##      non-missing edges= 10559
##
## Vertex attribute names:
##      vertex.names
##
## Edge attribute names not shown

# plot network using default layout
par(mfrow = c(2, 3))
par(mar=c(0.5,1,1,0.5))

plot(Pnet_d1, edge.col = "gray", edge.lwd = 0.10, vertex.cex = 0.75, ma
in = "Co-Presence network, Early Period")
plot(Pnet_d2, edge.col = "gray", edge.lwd = 0.10, vertex.cex = 0.75, ma
in = "Co-Presence network, Middle Period")

```

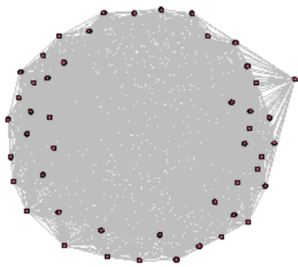
```

plot(Pnet_d3, edge.col = "gray", edge.lwd = 0.10, vertex.cex = 0.75, main = "Co-Presence network, Late Period")
# plot network spatially using geographic coordinates
plot(Pnet_d1, edge.col = "gray", edge.lwd = 0.10, vertex.cex = 0.5, main = "Spatial CP Network, Early Period", coord = d_data1[,10:11])
plot(AOI, add=T) #overlay network with coastline of study area
plot(Pnet_d2, edge.col = "gray", edge.lwd = 0.10, vertex.cex = 0.5, main = "Spatial CP Network, Middle Period", coord = d_data2[,10:11])
plot(AOI, add=T) #overlay network with coastline of study area

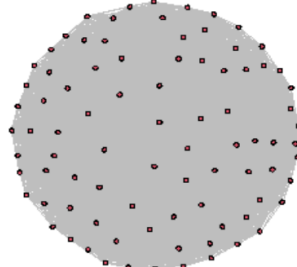
plot(Pnet_d3, edge.col = "gray", edge.lwd = 0.10, vertex.cex = 0.5, main = "Spatial CP Network, Late Period", coord = d_data3[,10:11])
plot(AOI, add=T) #overlay network with coastline of study area

```

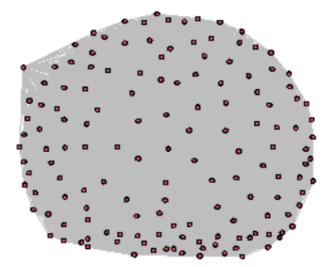
Co-Presence network, Early Period



Co-Presence network, Middle Period



Co-Presence network, Late Period



Spatial CP Network, Early Period



Spatial CP Network, Middle Period



Spatial CP Network, Late Period



```

par(mfrow = c(1, 1)) # return to single plotting mode

# Define our binary network object from BR similarity
BRnet_d1 <- network(event2dichot(d_data1BR, method = "absolute", thresh = 0.6),
                    directed = F)
BRnet_d2 <- network(event2dichot(d_data2BR, method = "absolute", thresh = 0.6),
                    directed = F)
BRnet_d3 <- network(event2dichot(d_data3BR, method = "absolute", thresh = 0.6),
                    directed = F)

# Add names for nodes based on the row names of the original matrix
BRnet_d1 %v% "vertex.names" <- row.names(d_data1BR)
BRnet_d2 %v% "vertex.names" <- row.names(d_data2BR)

```

```
BRnet_d3 %v% "vertex.names" <- row.names(d_data3BR)
# Look at the results.
```

```
BRnet_d1
```

```
## Network attributes:
## vertices = 48
## directed = FALSE
## hyper = FALSE
## loops = FALSE
## multiple = FALSE
## bipartite = FALSE
## total edges= 351
## missing edges= 0
## non-missing edges= 351
##
## Vertex attribute names:
## vertex.names
##
## No edge attributes
```

```
BRnet_d2
```

```
## Network attributes:
## vertices = 86
## directed = FALSE
## hyper = FALSE
## loops = FALSE
## multiple = FALSE
## bipartite = FALSE
## total edges= 1743
## missing edges= 0
## non-missing edges= 1743
##
## Vertex attribute names:
## vertex.names
##
## Edge attribute names not shown
```

```
BRnet_d3
```

```
## Network attributes:
## vertices = 146
## directed = FALSE
## hyper = FALSE
## loops = FALSE
## multiple = FALSE
## bipartite = FALSE
## total edges= 4068
## missing edges= 0
## non-missing edges= 4068
##
```

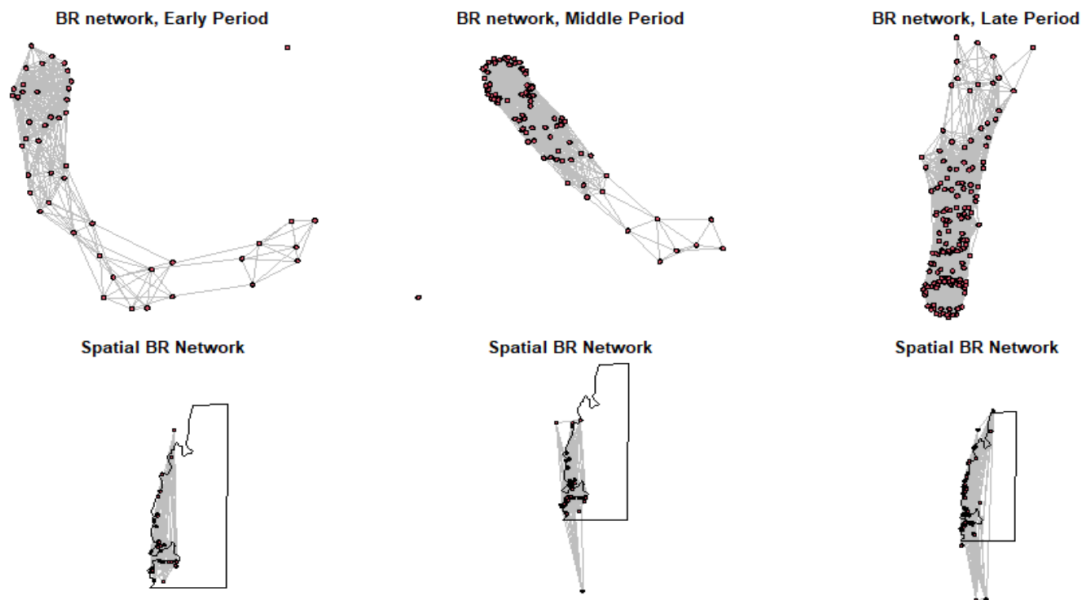
```

## Vertex attribute names:
##   vertex.names
##
## Edge attribute names not shown

# plot network using default layout
par(mfrow = c(2, 3))
par(mar=c(0.5,1,1,0.5))

plot(BRnet_d1, edge.col = "gray", edge.lwd = 0.001, vertex.cex = 0.75,
main = "BR network, Early Period")
plot(BRnet_d2, edge.col = "gray", edge.lwd = 0.001, vertex.cex = 0.75,
main = "BR network, Middle Period")
plot(BRnet_d3, edge.col = "gray", edge.lwd = 0.001, vertex.cex = 0.75,
main = "BR network, Late Period")
# plot network spatially using geographic coordinates
plot(BRnet_d1, edge.col = "gray", edge.lwd = 0.001, vertex.cex = 0.5, m
ain = "Spatial BR Network", coord = d_data1[,10:11])
plot(AOI, add=T) #overlay network with coastline of study area
plot(BRnet_d2, edge.col = "gray", edge.lwd = 0.001, vertex.cex = 0.5, m
ain = "Spatial BR Network", coord = d_data2[,10:11])
plot(AOI, add=T) #overlay network with coastline of study area
plot(BRnet_d3, edge.col = "gray", edge.lwd = 0.001, vertex.cex = 0.5, m
ain = "Spatial BR Network", coord = d_data3[,10:11])
plot(AOI, add=T) #overlay network with coastline of study area

```



```

par(mfrow = c(1, 1)) # return to single plotting mode

```

```

# Plot X2 distance similarity index
# This uses the 1 minus dataX01 calculation to convert

```

```

# X2 distance to a similarity (following Peeples 2017)
Xnet_d1 <- network(event2dichot(1 - d_data1X01, method = "quantile", th
resh = 0.8),
                directed = F)
Xnet_d2 <- network(event2dichot(1 - d_data2X01, method = "quantile", th
resh = 0.8),
                directed = F)
Xnet_d3 <- network(event2dichot(1 - d_data3X01, method = "quantile", th
resh = 0.8),
                directed = F)

# Once again add vertex names
Xnet_d1 %v% "vertex.names" <- row.names(d_data1X01)
Xnet_d2 %v% "vertex.names" <- row.names(d_data2X01)
Xnet_d3 %v% "vertex.names" <- row.names(d_data3X01)
# Look at the results
Xnet_d1

## Network attributes:
## vertices = 48
## directed = FALSE
## hyper = FALSE
## loops = FALSE
## multiple = FALSE
## bipartite = FALSE
## total edges= 206
## missing edges= 0
## non-missing edges= 206
##
## Vertex attribute names:
## vertex.names
##
## No edge attributes

Xnet_d2

## Network attributes:
## vertices = 86
## directed = FALSE
## hyper = FALSE
## loops = FALSE
## multiple = FALSE
## bipartite = FALSE
## total edges= 696
## missing edges= 0
## non-missing edges= 696
##
## Vertex attribute names:
## vertex.names

```

```

##
## No edge attributes

Xnet_d3

## Network attributes:
## vertices = 146
## directed = FALSE
## hyper = FALSE
## loops = FALSE
## multiple = FALSE
## bipartite = FALSE
## total edges= 2058
## missing edges= 0
## non-missing edges= 2058
##
## Vertex attribute names:
## vertex.names
##
## Edge attribute names not shown

# plot network using default layout
par(mfrow = c(2, 3))
par(mar=c(0.5,1,1,0.5))

plot(Xnet_d1, edge.col = "gray", edge.lwd = 0.001, vertex.cex = 0.75, m
ain = "Chi-squared network \nEarly Period")
plot(Xnet_d2, edge.col = "gray", edge.lwd = 0.001, vertex.cex = 0.75, m
ain = "Chi-squared network \nMiddle Period")
plot(Xnet_d3, edge.col = "gray", edge.lwd = 0.001, vertex.cex = 0.75, m
ain = "Chi-squared network \nLate Period")

# plot network using geographic coordinates
plot(Xnet_d1, edge.col = "gray", edge.lwd = 0.75, vertex.cex = 0.5, coo
rd = d_data1[,

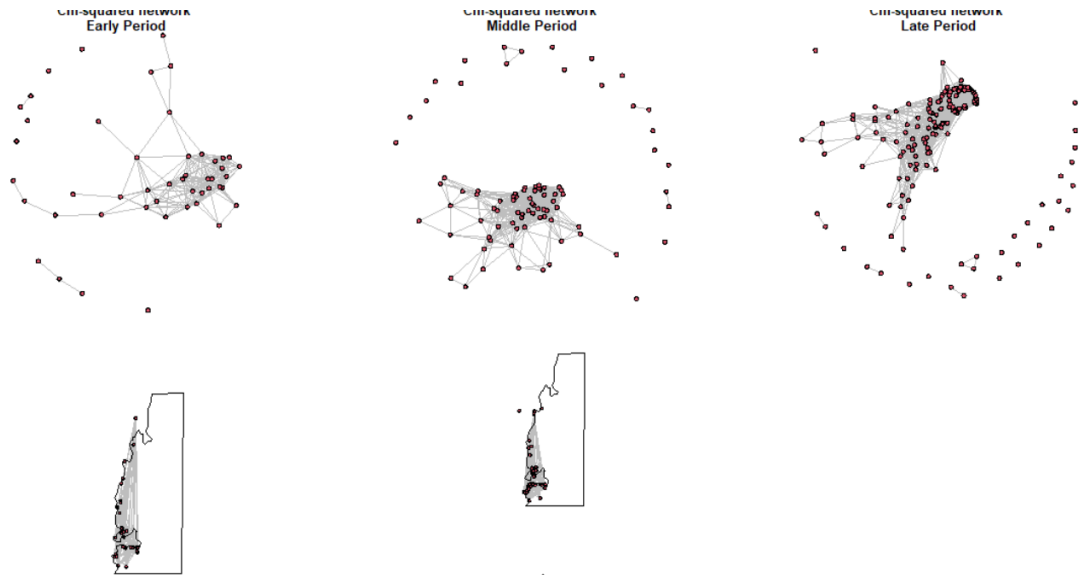
10:11])
plot(AOI, add=T) #overlay network with coastline of study area
plot(Xnet_d2, edge.col = "gray", edge.lwd = 0.75, vertex.cex = 0.5, coo
rd = d_data2[,

10:11])
plot(AOI, add=T) #overlay network with coastline of study

plot(Xnet_d3, edge.col = "gray", edge.lwd = 0.75, vertex.cex = 0.5, coo
rd = d_data3[,

10:11])
plot(AOI, add=T) #overlay network with coastline of study area

```



```
par(mfrow = c(1, 1))
```

#Peoples (2017) finds that weighted networks do not perform well with similarity or distance matrices, so we do not use them here.

Calculate Raw Data Values of Network Connectivity

```
# Calculate centrality scores for binary networks
```

```
net.stats <- function(y) {
  # calculate degree centrality
  dg <- as.matrix(sna::degree(y, gmode = "graph"))
  # calculate and scale eigenvector centrality
  eg <- as.matrix(sna::eigcent(y, use.eigen = TRUE))
  eg <- sqrt((eg^2) * length(eg))
  # calculate betweenness centrality
  bw <- sna::betweenness(y, gmode = "graph")
  # combine centrality scores into matrix
  output <- cbind(dg, eg, bw)
  rownames(output) <- rownames(as.matrix(y))
  colnames(output) <- c("dg", "eg", "bw")
  return(output)
} # return results of this function
```

```
# net stats for binary co-presence network
```

```
co.p.stats_d <- net.stats(Pnet_d1)
co.p.stats_d2 <- net.stats(Pnet_d2)
co.p.stats_d3 <- net.stats(Pnet_d3)
```

```
# net stats for binary BR similarity network
```

```
BR.stats_d <- net.stats(BRnet_d1)
BR.stats_d2 <- net.stats(BRnet_d2)
BR.stats_d3 <- net.stats(BRnet_d3)
```

```
# net stats for binary X^2 similarity network (1-distance)
```



```

X.stats_d <- net.stats(Xnet_d1)
X.stats_d2 <- net.stats(Xnet_d2)
X.stats_d3 <- net.stats(Xnet_d3)
head(X.stats_d)

##           dg           eg bw
## G-11-20    1 2.480331e-05  0
## VATO Za003 0 3.076740e-15  0
## G-48-20    2 3.797514e-04 36
## LSS_52     3 1.534534e-02 36
## GI118      2 1.528389e-02  0
## GI128      1 1.002275e-03  0

#write.csv(X.stats_d3, "X2_1700_1900_Stats.csv")

# The following function does the same calculation as above but is set
up to
# work with the output of net.stats and net.stats.wt
nsim <- 1000

samp.frac <- c("S90", "S80", "S70", "S60", "S50", "S40", "S30", "S20",
"S10")

cv.resamp.bin <- function(x) {
  # calculate all network stats for the original network
  stats.g <- net.stats(x)
  mat <- as.matrix(x)
  dim.x <- dim(mat)[1] # count number of rows (nodes)
  # define empty matrices for output
  dg.mat <- matrix(NA, nsim, 9)
  ev.mat <- matrix(NA, nsim, 9)
  bw.mat <- matrix(NA, nsim, 9)
  # add column names based on sampling fraction
  colnames(dg.mat) <- samp.frac
  colnames(ev.mat) <- samp.frac
  colnames(bw.mat) <- samp.frac

  # this double loop goes through each sampling fraction and each random
  # replicate to calculate centrality statistics and runs a Spearman's rho
  # correlation between the resulting centrality values and the original
  # sample
  for (j in 1:9) {
    for (i in 1:nsim) {
      sub.samp <- sample(seq(1, dim.x), size = round(dim.x * ((10 - j)/
10),
                                0), replace = F)
      temp.stats <- net.stats(mat[sub.samp, sub.samp])
    }
  }
}

```

```

    dg.mat[i, j] <- suppressWarnings(cor(temp.stats[, 1], stats.g[sub
.samp,
                                                                    1],
method = "spearman"))
    ev.mat[i, j] <- suppressWarnings(cor(temp.stats[, 2], stats.g[sub
.samp,
                                                                    2],
method = "spearman"))
    bw.mat[i, j] <- suppressWarnings(cor(temp.stats[, 3], stats.g[sub
.samp,
                                                                    3],
method = "spearman"))
  }
}
out.list <- list() # create list for output and populate it
out.list[[1]] <- dg.mat
out.list[[2]] <- ev.mat
out.list[[3]] <- bw.mat
return(out.list)
} # return the resulting list

cop.rs_d <- cv.resamp.bin(Pnet_d1)
cop.rs_d2 <- cv.resamp.bin(Pnet_d2)
cop.rs_d3 <- cv.resamp.bin(Pnet_d3)
BR.rs_d <- cv.resamp.bin(BRnet_d1)
BR.rs_d2 <- cv.resamp.bin(BRnet_d2)
BR.rs_d3 <- cv.resamp.bin(BRnet_d3)
X.rs_d <- cv.resamp.bin(Xnet_d1)
X.rs_d2 <- cv.resamp.bin(Xnet_d2)
X.rs_d3 <- cv.resamp.bin(Xnet_d3)

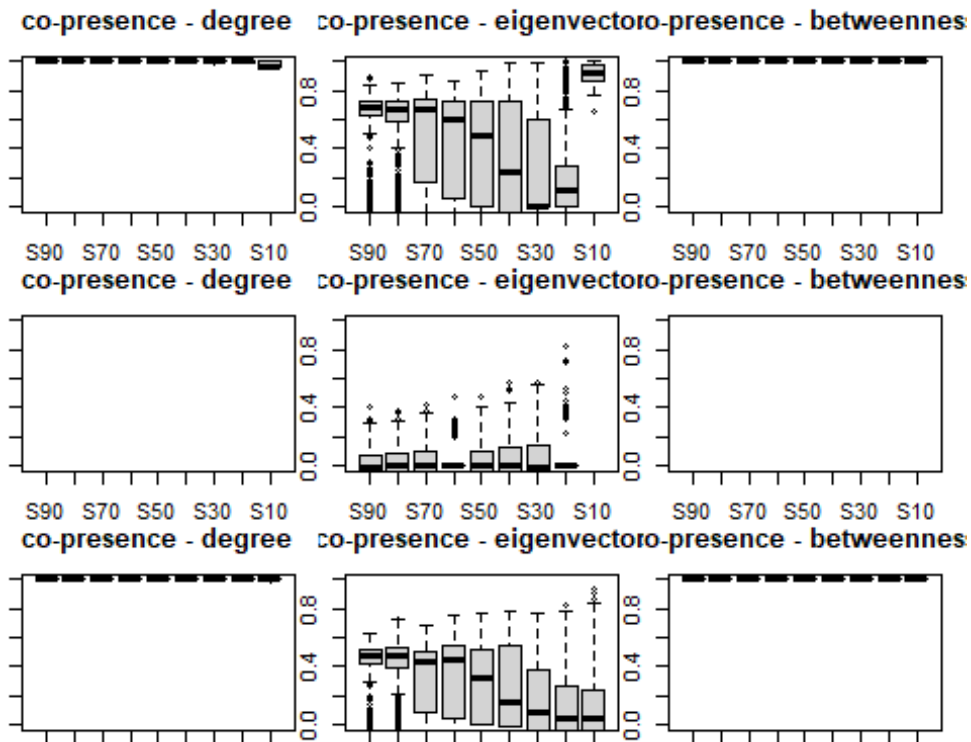
##PLOT DECORATIVE NETWORKS
par(mfrow = c(3, 3)) # set up for 3 by 3 plotting
par(mar=c(1,1,3,1))
# plot boxplots by sampling fraction for each measure and each network
type
boxplot(cop.rs_d[[1]], ylim = c(0, 1), main = "co-presence - degree", x
lab = "sampling fraction",
        ylab = "Spearman's rho")
boxplot(cop.rs_d[[2]], ylim = c(0, 1), main = "co-presence - eigenvecto
r", xlab = "sampling fraction")
boxplot(cop.rs_d[[3]], ylim = c(0, 1), main = "co-presence - betweenne
s", xlab = "sampling fraction")
boxplot(cop.rs_d2[[1]], ylim = c(0, 1), main = "co-presence - degree",
xlab = "sampling fraction",
        ylab = "Spearman's rho")
boxplot(cop.rs_d2[[2]], ylim = c(0, 1), main = "co-presence - eigenvect
or", xlab = "sampling fraction")
boxplot(cop.rs_d2[[3]], ylim = c(0, 1), main = "co-presence - betweenne
ss", xlab = "sampling fraction")

```

```

boxplot(cop.rs_d3[[1]], ylim = c(0, 1), main = "co-presence - degree",
        xlab = "sampling fraction",
        ylab = "Spearman's rho")
boxplot(cop.rs_d3[[2]], ylim = c(0, 1), main = "co-presence - eigenvector",
        xlab = "sampling fraction")
boxplot(cop.rs_d3[[3]], ylim = c(0, 1), main = "co-presence - betweenness",
        xlab = "sampling fraction")

```



```

par(mfrow = c(3, 3)) # set up for 3 by 3 plotting
par(mar=c(1,1,3,1))

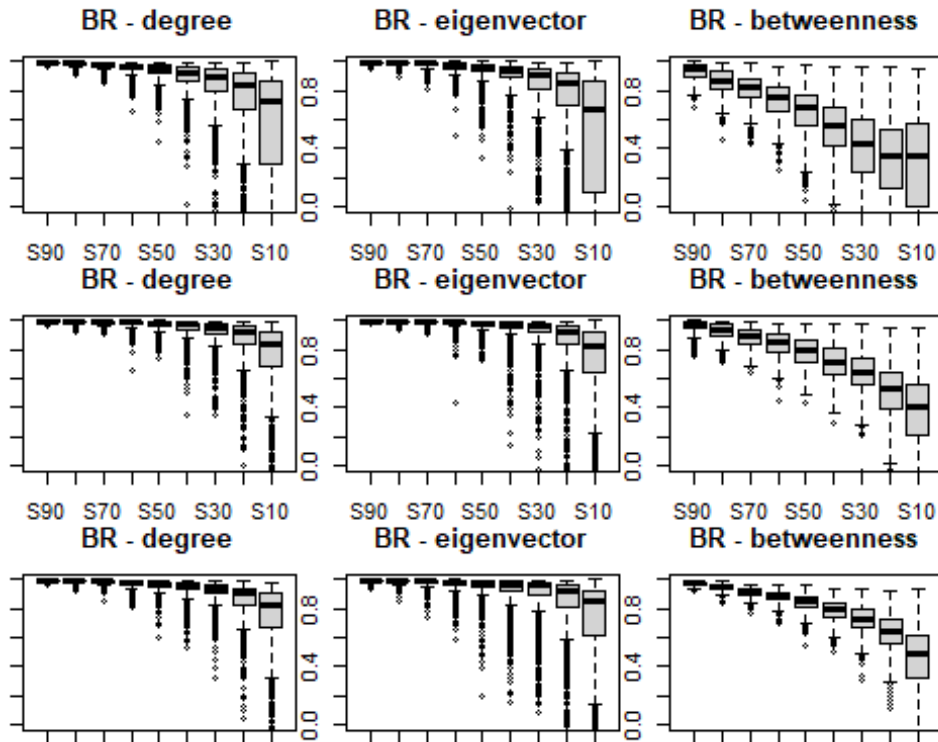
boxplot(BR.rs_d[[1]], ylim = c(0, 1), main = "BR - degree", xlab = "sampling fraction",
        ylab = "Spearman's rho")
boxplot(BR.rs_d[[2]], ylim = c(0, 1), main = "BR - eigenvector", xlab = "sampling fraction")
boxplot(BR.rs_d[[3]], ylim = c(0, 1), main = "BR - betweenness", xlab = "sampling fraction")
boxplot(BR.rs_d2[[1]], ylim = c(0, 1), main = "BR - degree", xlab = "sampling fraction",
        ylab = "Spearman's rho")
boxplot(BR.rs_d2[[2]], ylim = c(0, 1), main = "BR - eigenvector", xlab = "sampling fraction")
boxplot(BR.rs_d2[[3]], ylim = c(0, 1), main = "BR - betweenness", xlab = "sampling fraction")
boxplot(BR.rs_d3[[1]], ylim = c(0, 1), main = "BR - degree", xlab = "sampling fraction",
        ylab = "Spearman's rho")

```

```

    ylab = "Spearman's rho")
boxplot(BR.rs_d3[[2]], ylim = c(0, 1), main = "BR - eigenvector", xlab
= "sampling fraction")
boxplot(BR.rs_d3[[3]], ylim = c(0, 1), main = "BR - betweenness", xlab
= "sampling fraction")

```



```

par(mfrow = c(3, 3)) # set up for 3 by 3 plotting
par(mar=c(1,1,3,1))

boxplot(X.rs_d[[1]], ylim = c(0, 1), main = "Chi squared - degree", xla
b = "sampling fraction",
    ylab = "Spearman's rho")
boxplot(X.rs_d[[2]], ylim = c(0, 1), main = "Chi squared - eigenvector"
, xlab = "sampling fraction")
boxplot(X.rs_d[[3]], ylim = c(0, 1), main = "Chi squared - betweenness"
, xlab = "sampling fraction")
boxplot(X.rs_d2[[1]], ylim = c(0, 1), main = "Chi squared - degree", xl
ab = "sampling fraction",
    ylab = "Spearman's rho")
boxplot(X.rs_d2[[2]], ylim = c(0, 1), main = "Chi squared - eigenvector"
, xlab = "sampling fraction")
boxplot(X.rs_d2[[3]], ylim = c(0, 1), main = "Chi squared - betweenness"
, xlab = "sampling fraction")
boxplot(X.rs_d3[[1]], ylim = c(0, 1), main = "Chi squared - degree", xl
ab = "sampling fraction",
    ylab = "Spearman's rho")
boxplot(X.rs_d3[[2]], ylim = c(0, 1), main = "Chi squared - eigenvector

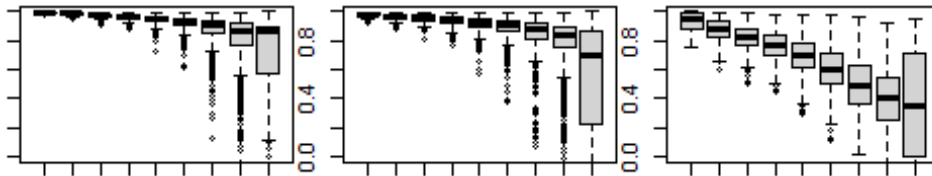
```

```

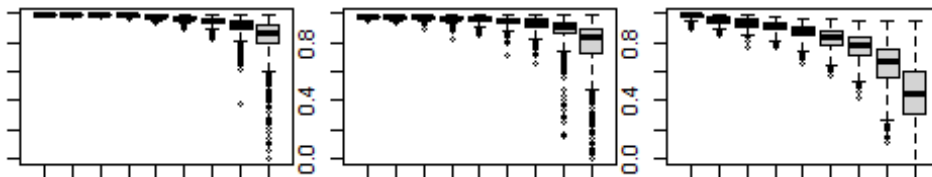
", xlab = "sampling fraction")
boxplot(X.rs_d3[[3]], ylim = c(0, 1), main = "Chi squared - betweenness",
", xlab = "sampling fraction")

```

Chi squared - degree Chi squared - eigenvector Chi squared - betweenness



Chi squared - degree Chi squared - eigenvector Chi squared - betweenness



Chi squared - degree Chi squared - eigenvector Chi squared - betweenness



```

##Assess missing nodes within dataset
#NODE ASSESSMENT
nsim <- 1000 #set number of replicates

resamp.node <- function(x, samp.frac) {
  mat <- as.matrix(x)
  dim.x <- dim(mat)[1]
  out.mat <- matrix(NA, dim.x, nsim)
  for (i in 1:nsim) {
    sub.samp <- sample(seq(1, dim.x), size = round(dim.x * samp.frac, 0),
),
                        replace = F)
    # calculate centrality statistic for a given sub-sample and put in
output
    # matrix
    temp.stats <- sna::degree(mat[sub.samp, sub.samp], gmode = "graph")
    out.mat[sub.samp, i] <- temp.stats
  }
  return(out.mat)
}
#ASSESSMENT OF DECORATIVE NETWORKS

# calculate the rank order of degree centrality in the CP network

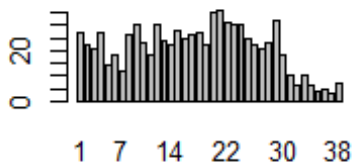
```

```

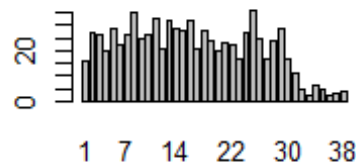
top.dg <- rank(-sna::degree(Pnet_d1), ties.method = "min")
par(mfrow = c(2, 2))
P.resamp <- resamp.node(Pnet_d1, samp.frac = 0.8) #samp.frac is 80%
# calculate the rank order of the replicates and plot the top 4 as barplots
# showing rank across all replicates
for (i in 1:4) {
  barplot(table(apply(-P.resamp, 2, rank, ties.method = "random", na.last = "keep")[order(top.dg)[i],
]), main = paste("samp.frac=80%, rank = ", top.dg[order(top.dg)[i]]))
}

```

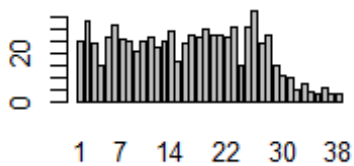
samp.frac=80%, rank = 1



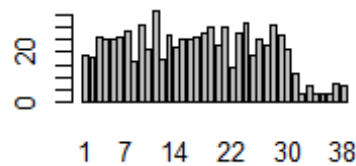
samp.frac=80%, rank = 1



samp.frac=80%, rank = 1



samp.frac=80%, rank = 1

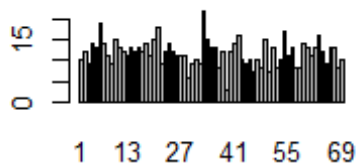


```

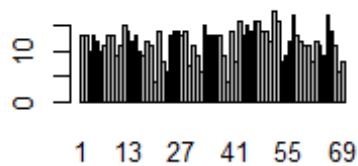
top.dg <- rank(-sna::degree(Pnet_d2), ties.method = "min")
par(mfrow = c(2, 2))
P.resamp <- resamp.node(Pnet_d2, samp.frac = 0.8) #samp.frac is 80%
# calculate the rank order of the replicates and plot the top 4 as barplots
# showing rank across all replicates
for (i in 1:4) {
  barplot(table(apply(-P.resamp, 2, rank, ties.method = "random", na.last = "keep")[order(top.dg)[i],
]), main = paste("samp.frac=80%, rank = ", top.dg[order(top.dg)[i]]))
}

```

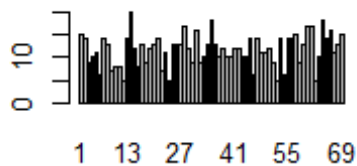
samp.frac=80%, rank = 1



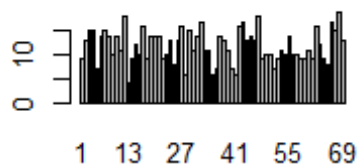
samp.frac=80%, rank = 1



samp.frac=80%, rank = 1



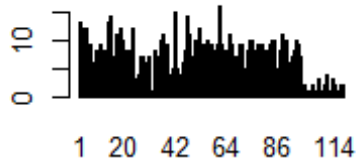
samp.frac=80%, rank = 1



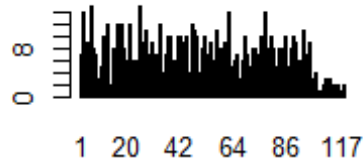
```
top.dg <- rank(-sna::degree(Pnet_d3), ties.method = "min")
par(mfrow = c(2, 2))
P.resamp <- resamp.node(Pnet_d3, samp.frac = 0.8) #samp.frac is 80%
# calculate the rank order of the replicates and plot the top 4 as barplots
# showing rank across all replicates

for (i in 1:4) {
  barplot(table(apply(-P.resamp, 2, rank, ties.method = "random", na.last = "keep")[order(top.dg)[i],
  ]), main = paste("samp.frac=80%, rank = ", top.dg[order(top.dg)[i]]))
}
```

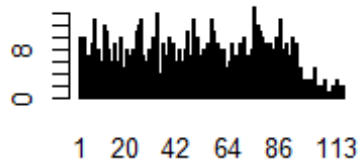
samp.frac=80%, rank = 1



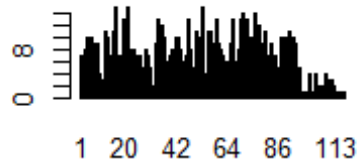
samp.frac=80%, rank = 1



samp.frac=80%, rank = 1

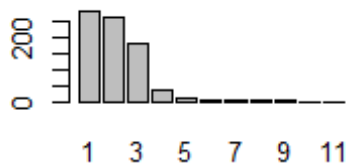


samp.frac=80%, rank = 1

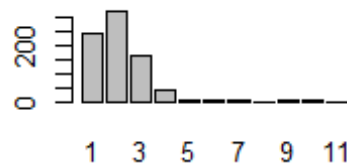


```
# calculate the rank order of degree centrality in the BR network
top.dg <- rank(-sna::degree(BRnet_d1), ties.method = "min")
par(mfrow = c(2, 2))
BR.resamp <- resamp.node(BRnet_d1, samp.frac = 0.8) #samp.frac is 80%
# calculate the rank order of the replicates and plot the top 4 as barplots
Lots
# showing rank across all replicates
for (i in 1:4) {
  barplot(table(apply(-BR.resamp, 2, rank, ties.method = "random", na.last = "keep")[order(top.dg)[i],
    ]), main = paste("samp.frac=80%, rank = ", top.dg[order(top.dg)[i]]))
}
```

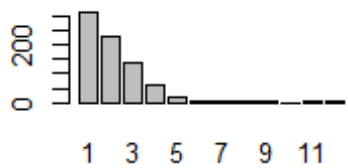

samp.frac=80%, rank = 1



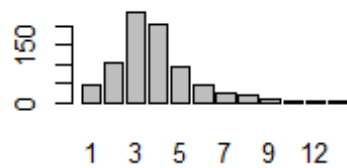
samp.frac=80%, rank = 1



samp.frac=80%, rank = 1

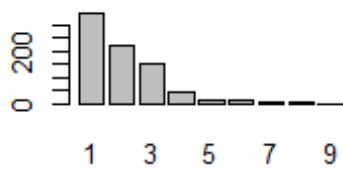


samp.frac=80%, rank = 4

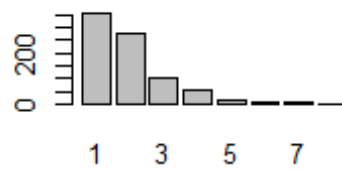


```
# calculate the rank order of degree centrality in the BR network
top.dg <- rank(-sna::degree(BRnet_d2), ties.method = "min")
par(mfrow = c(2, 2))
BR.resamp <- resamp.node(BRnet_d2, samp.frac = 0.8) #samp.frac is 80%
# calculate the rank order of the replicates and plot the top 4 as barplots
Lots
# showing rank across all replicates
for (i in 1:4) {
  barplot(table(apply(-BR.resamp, 2, rank, ties.method = "random", na.last = "keep")[order(top.dg)[i],
    ]), main = paste("samp.frac=80%, rank = ", top.dg[order(top.dg)[i]]))
}
```

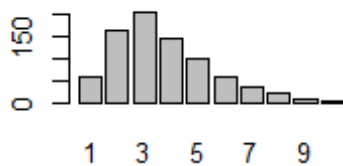
samp.frac=80%, rank = 1



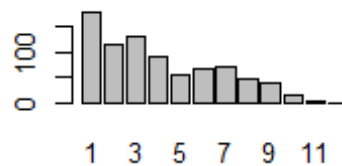
samp.frac=80%, rank = 1



samp.frac=80%, rank = 3

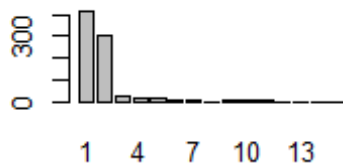


samp.frac=80%, rank = 3

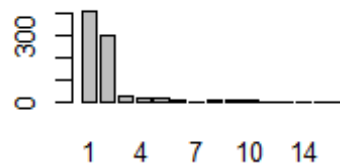


```
# calculate the rank order of degree centrality in the BR network
top.dg <- rank(-sna::degree(BRnet_d3), ties.method = "min")
par(mfrow = c(2, 2))
BR.resamp <- resamp.node(BRnet_d3, samp.frac = 0.8) #samp.frac is 80%
# calculate the rank order of the replicates and plot the top 4 as barplots
# showing rank across all replicates
for (i in 1:4) {
  barplot(table(apply(-BR.resamp, 2, rank, ties.method = "random", na.last = "keep")[order(top.dg)[i],
    ]), main = paste("samp.frac=80%, rank = ", top.dg[order(top.dg)[i]]))
}
```

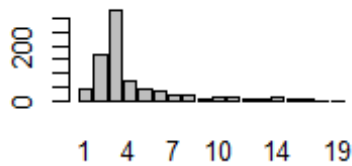
samp.frac=80%, rank = 1



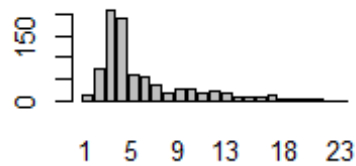
samp.frac=80%, rank = 1



samp.frac=80%, rank = 3

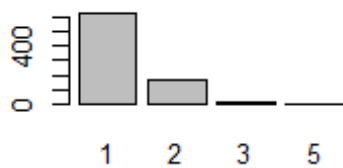


samp.frac=80%, rank = 4

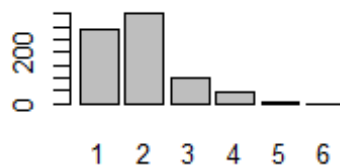


```
# calculate the rank order of degree centrality in the BR network
top.dg <- rank(-sna::degree(Xnet_d1), ties.method = "min")
par(mfrow = c(2, 2))
X.resamp <- resamp.node(Xnet_d1, samp.frac = 0.8) #samp.frac is 80%
# calculate the rank order of the replicates and plot the top 4 as barplots
Lots
# showing rank across all replicates
for (i in 1:4) {
  barplot(table(apply(-X.resamp, 2, rank, ties.method = "random", na.last = "keep")[order(top.dg)[i],
]), main = paste("samp.frac=80%, rank = ", top.dg[order(top.dg)[i]]))
}
```

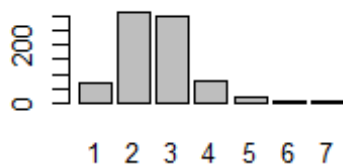
samp.frac=80%, rank = 1



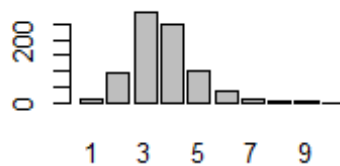
samp.frac=80%, rank = 2



samp.frac=80%, rank = 3

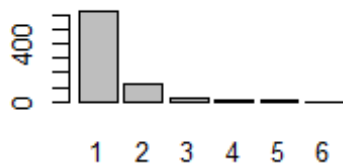


samp.frac=80%, rank = 4

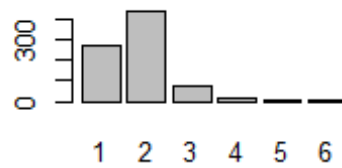


```
# calculate the rank order of degree centrality in the BR network
top.dg <- rank(-sna::degree(Xnet_d2), ties.method = "min")
par(mfrow = c(2, 2))
X.resamp <- resamp.node(Xnet_d2, samp.frac = 0.8) #samp.frac is 80%
# calculate the rank order of the replicates and plot the top 4 as barplots
Lots
# showing rank across all replicates
for (i in 1:4) {
  barplot(table(apply(-X.resamp, 2, rank, ties.method = "random", na.last = "keep")[order(top.dg)[i],
]), main = paste("samp.frac=80%, rank = ", top.dg[order(top.dg)[i]]))
}
```

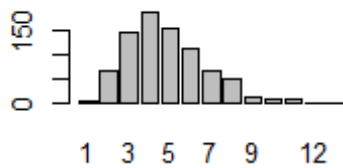
samp.frac=80%, rank = 1



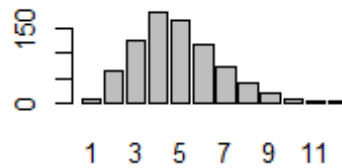
samp.frac=80%, rank = 2



samp.frac=80%, rank = 3

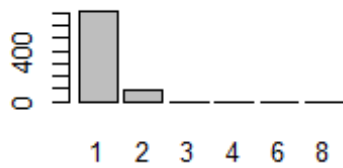


samp.frac=80%, rank = 3

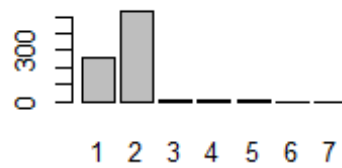


```
# calculate the rank order of degree centrality in the BR network
top.dg <- rank(-sna::degree(Xnet_d3), ties.method = "min")
par(mfrow = c(2, 2))
X.resamp <- resamp.node(Xnet_d3, samp.frac = 0.8) #samp.frac is 80%
# calculate the rank order of the replicates and plot the top 4 as barplots
# showing rank across all replicates
for (i in 1:4) {
  barplot(table(apply(-X.resamp, 2, rank, ties.method = "random", na.last = "keep")[order(top.dg)[i],
  ]), main = paste("samp.frac=80%, rank = ", top.dg[order(top.dg)[i]]))
}
```

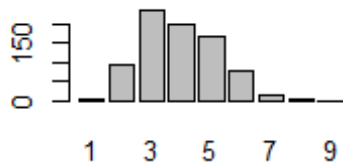
samp.frac=80%, rank = 1



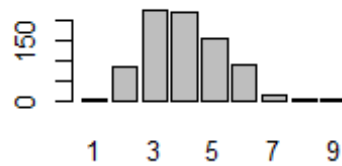
samp.frac=80%, rank = 2



samp.frac=80%, rank = 3



samp.frac=80%, rank = 3



```
##Assess missing edges in dataset
# ASSESS MISSING EDGES
# set up to work with the output of net.stats
nsim <- 1000
samp.frac <- c("S90", "S80", "S70", "S60", "S50", "S40", "S30", "S20",
"S10")

cv.resamp.edge <- function(x) {
  stats.g <- net.stats(x)
  mat <- as.matrix(x)
  dim.x <- dim(mat)[1]
  dg.mat <- matrix(NA, nsim, 9)
  ev.mat <- matrix(NA, nsim, 9)
  bw.mat <- matrix(NA, nsim, 9)
  colnames(dg.mat) <- samp.frac
  colnames(ev.mat) <- samp.frac
  colnames(bw.mat) <- samp.frac

  for (j in 1:9) {
    for (i in 1:nsim) {
      sub.samp <- sample(seq(1, network.edgecount(x)), size = round(net
work.edgecount(x) *
      (
j/10), 0), replace = F)
      temp.net <- x
      net.reduced <- network::delete.edges(temp.net, sub.samp)
      temp.stats <- net.stats(net.reduced)
    }
  }
}
```

```

    dg.mat[i, j] <- cor(temp.stats[, 1], stats.g[, 1], method = "spea
rman")
    ev.mat[i, j] <- cor(temp.stats[, 2], stats.g[, 2], method = "spea
rman")
    bw.mat[i, j] <- cor(temp.stats[, 3], stats.g[, 3], method = "spea
rman")
  }
}
out.list <- list()
out.list[[1]] <- dg.mat
out.list[[2]] <- ev.mat
out.list[[3]] <- bw.mat
return(out.list)
}

```

#ASSESS DECORATIVE NETWORKS

run the script for our three binary networks

```

cop.edge.d <- cv.resamp.edge(Pnet_d1)
BR.edge.d <- cv.resamp.edge(BRnet_d1)
X.edge.d <- cv.resamp.edge(Xnet_d1)

cop.edge.d2 <- cv.resamp.edge(Pnet_d2)

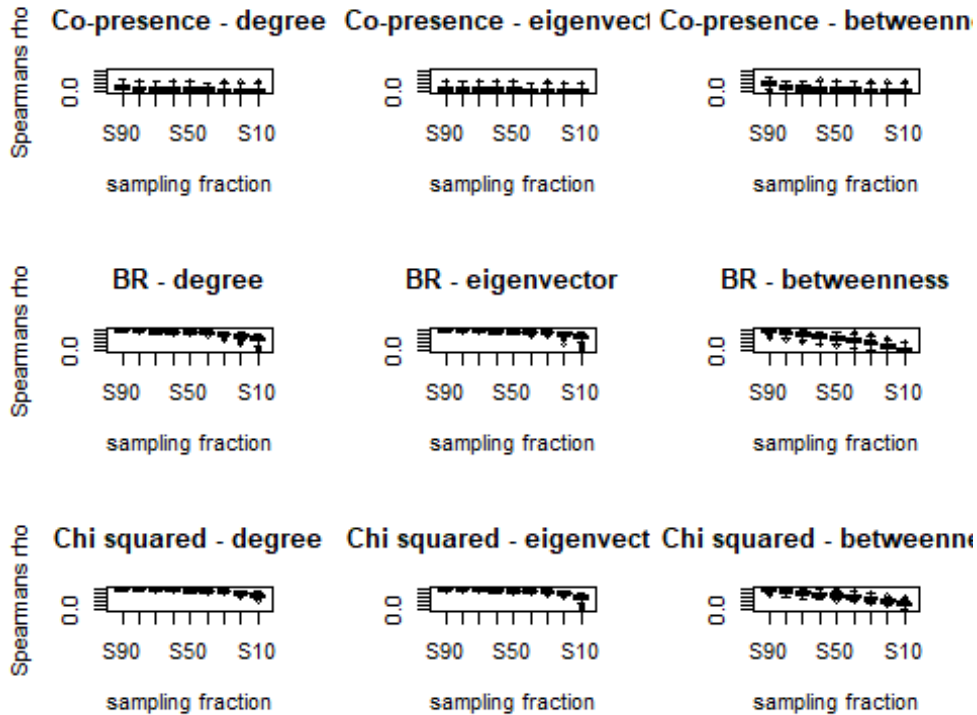
BR.edge.d2 <- cv.resamp.edge(BRnet_d2)
X.edge.d2 <- cv.resamp.edge(Xnet_d2)

cop.edge.d3 <- cv.resamp.edge(Pnet_d3)
BR.edge.d3 <- cv.resamp.edge(BRnet_d3)
X.edge.d3 <- cv.resamp.edge(Xnet_d3)

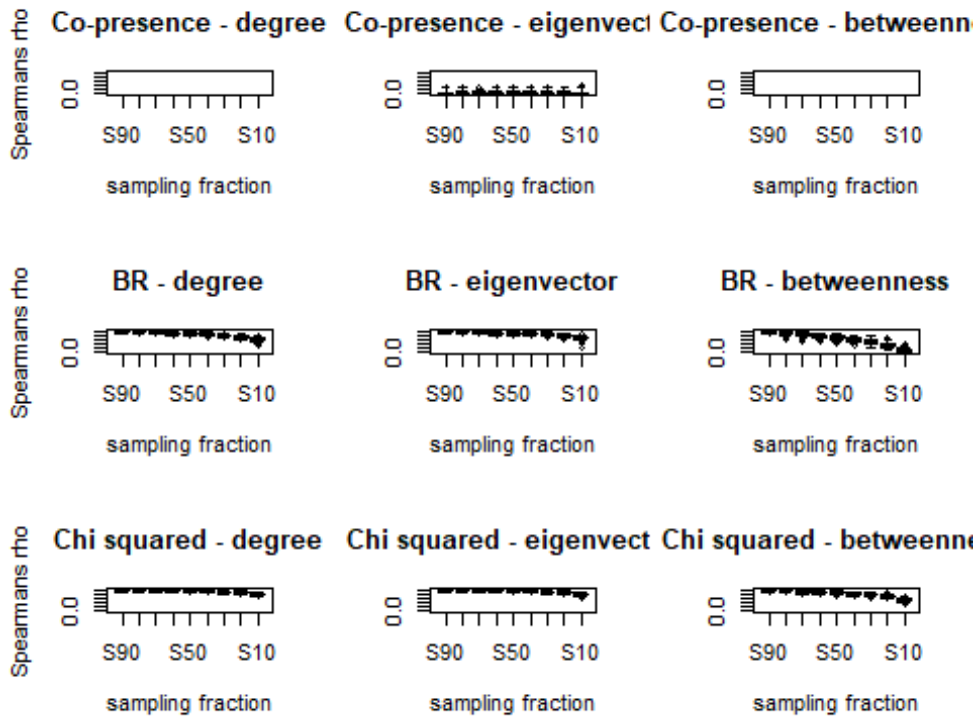
par(mfrow = c(3, 3))
boxplot(cop.edge.d[[1]], ylim = c(0, 1), main = "Co-presence - degree",
xlab = "sampling fraction",
        ylab = "Spearmans rho")
boxplot(cop.edge.d[[2]], ylim = c(0, 1), main = "Co-presence - eigenvec
tor", xlab = "sampling fraction")
boxplot(cop.edge.d[[3]], ylim = c(0, 1), main = "Co-presence - betweenn
ess", xlab = "sampling fraction")
boxplot(BR.edge.d[[1]], ylim = c(0, 1), main = "BR - degree", xlab = "s
ampling fraction",
        ylab = "Spearmans rho")
boxplot(BR.edge.d[[2]], ylim = c(0, 1), main = "BR - eigenvector", xlab
= "sampling fraction")
boxplot(BR.edge.d[[3]], ylim = c(0, 1), main = "BR - betweenness", xlab
= "sampling fraction")
boxplot(X.edge.d[[1]], ylim = c(0, 1), main = "Chi squared - degree", x
lab = "sampling fraction",
        ylab = "Spearmans rho")
boxplot(X.edge.d[[2]], ylim = c(0, 1), main = "Chi squared - eigenvecto

```

```
r", xlab = "sampling fraction")
boxplot(X.edge.d[[3]], ylim = c(0, 1), main = "Chi squared - betweenness", xlab = "sampling fraction")
```



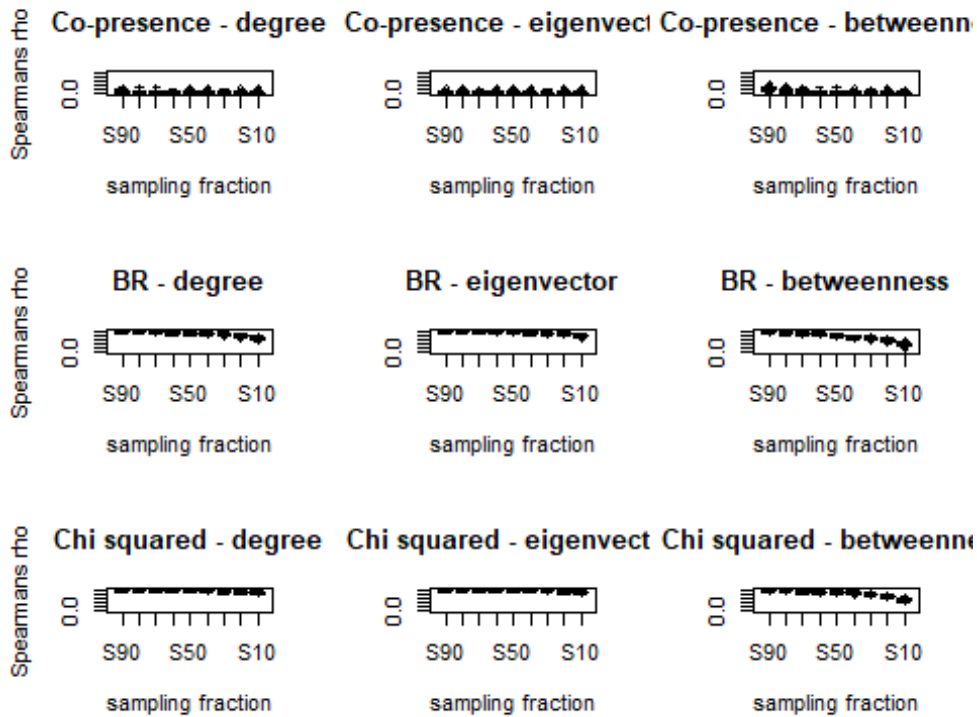
```
par(mfrow = c(3, 3))
boxplot(cop.edge.d2[[1]], ylim = c(0, 1), main = "Co-presence - degree",
, xlab = "sampling fraction",
      ylab = "Spearman's rho")
boxplot(cop.edge.d2[[2]], ylim = c(0, 1), main = "Co-presence - eigenvector", xlab = "sampling fraction")
boxplot(cop.edge.d2[[3]], ylim = c(0, 1), main = "Co-presence - betweenness", xlab = "sampling fraction")
boxplot(BR.edge.d2[[1]], ylim = c(0, 1), main = "BR - degree", xlab = "sampling fraction",
      ylab = "Spearman's rho")
boxplot(BR.edge.d2[[2]], ylim = c(0, 1), main = "BR - eigenvector", xlab = "sampling fraction")
boxplot(BR.edge.d2[[3]], ylim = c(0, 1), main = "BR - betweenness", xlab = "sampling fraction")
boxplot(X.edge.d2[[1]], ylim = c(0, 1), main = "Chi squared - degree",
xlab = "sampling fraction",
      ylab = "Spearman's rho")
boxplot(X.edge.d2[[2]], ylim = c(0, 1), main = "Chi squared - eigenvector", xlab = "sampling fraction")
boxplot(X.edge.d2[[3]], ylim = c(0, 1), main = "Chi squared - betweenness", xlab = "sampling fraction")
```

```

par(mfrow = c(3, 3))
boxplot(cop.edge.d3[[1]], ylim = c(0, 1), main = "Co-presence - degree",
        , xlab = "sampling fraction",
        ylab = "Spearman's rho")
boxplot(cop.edge.d3[[2]], ylim = c(0, 1), main = "Co-presence - eigenvector",
        xlab = "sampling fraction")
boxplot(cop.edge.d3[[3]], ylim = c(0, 1), main = "Co-presence - betweenness",
        xlab = "sampling fraction")
boxplot(BR.edge.d3[[1]], ylim = c(0, 1), main = "BR - degree", xlab = "sampling fraction",
        ylab = "Spearman's rho")
boxplot(BR.edge.d3[[2]], ylim = c(0, 1), main = "BR - eigenvector", xlab = "sampling fraction")
boxplot(BR.edge.d3[[3]], ylim = c(0, 1), main = "BR - betweenness", xlab = "sampling fraction")
boxplot(X.edge.d3[[1]], ylim = c(0, 1), main = "Chi squared - degree",
        xlab = "sampling fraction",
        ylab = "Spearman's rho")
boxplot(X.edge.d3[[2]], ylim = c(0, 1), main = "Chi squared - eigenvector",
        xlab = "sampling fraction")
boxplot(X.edge.d3[[3]], ylim = c(0, 1), main = "Chi squared - betweenness",
        xlab = "sampling fraction")

```



##Check for additional potential errors with missing data. This helps to validate our conclusions despite limited datasets

###CHECK FOR SAMPLING ERRORS AND BIASES IN DATASET

**## This code was originally written by Peeples (2017) and uses
simulations to check for sampling issues**

nsim <- 100 # we use 100 simulations due to computational limitations. We did assess the data using larger numbers of simulations (200, 500, 1000) and it provided identical results, but also occasionally crashed the computer used for analysis.

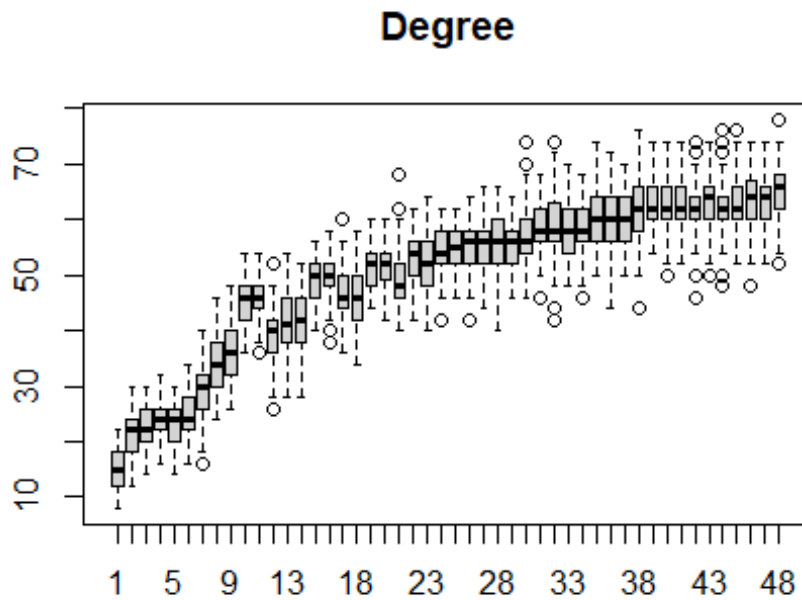
```
net.prob <- function(x) {
  x <- as.matrix(x)
  x[x < 0] <- 0 # define threshold for excluding edges
  net.list <- list()
  for (i in 1:nsim) {
    y <- x
    for (j in 1:length(x)) {
      y[j] <- rbinom(1, 1, prob = x[j])
    }
    net.list[[i]] <- network(y, directed = F)
  }
  return(net.list)
}
```

##ASSESS DECORATIVE NETWORKS

```

# Run the script on the BR similarity matrix
BRprob <- net.prob(d_data1BR)
# set up matrix and calculate eigenvector centrality for every replicat
e
dg.mat <- matrix(NA, nrow(d_data1BR), nsim)
for (i in 1:nsim) {
  dg.mat[, i] <- sna::degree(BRprob[[i]])
}
# show boxplot of degree centrality sorted by the degree cent score in
the
# original similarity matrix
boxplot(t(dg.mat[order(rowSums(d_data1BR))], ]), main = "Degree")

```

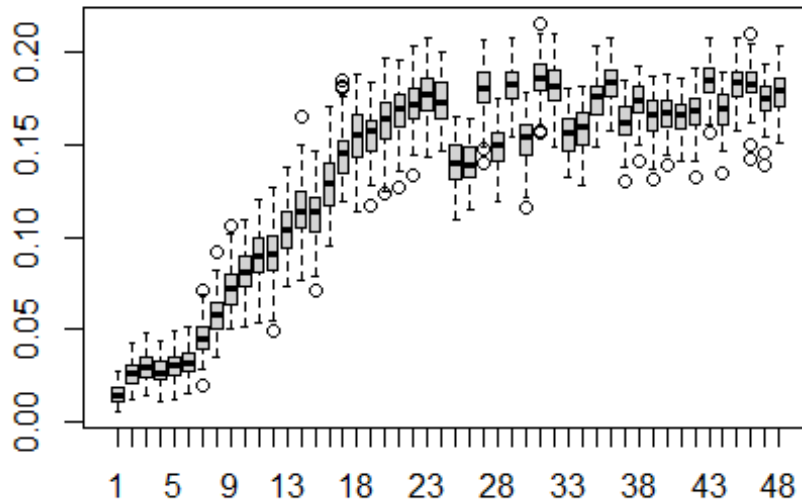


```

ev.mat <- matrix(NA, nrow(d_data1BR), nsim)
for (i in 1:nsim) {
  ev.mat[, i] <- sna::evcent(BRprob[[i]])
}
# show boxplot of eigenvector centrality sorted by the EV cent score in
the
# original similarity matrix
boxplot(t(ev.mat[order(sna::evcent(d_data1BR))], ]), main = "Eigenvector
")

```

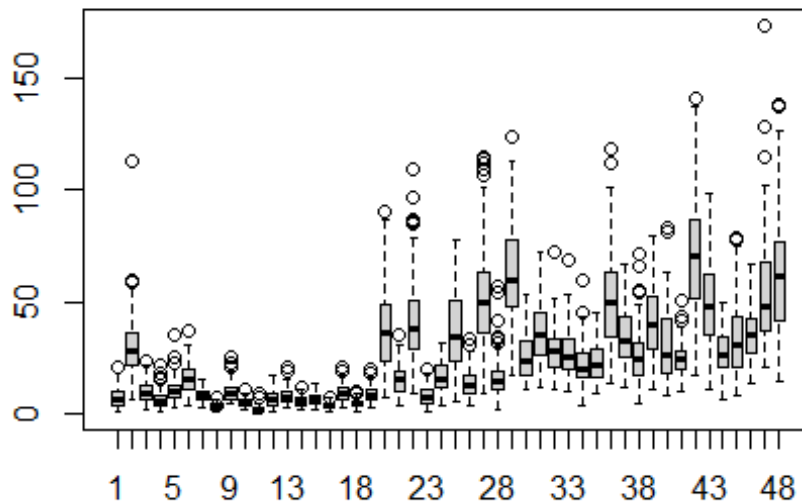
Eigenvector



```
bw.mat <- matrix(NA, nrow(d_data1BR), nsim)
for (i in 1:nsim) {
  bw.mat[, i] <- sna::betweenness(BRprob[[i]])
}
# show boxplot of betweenness centrality sorted by the betweenness cent
# score in the original similarity matrix
boxplot(t(bw.mat[order(betweenness_w(d_data1BR)[, 2]), ]), main = "Betw
eenness")

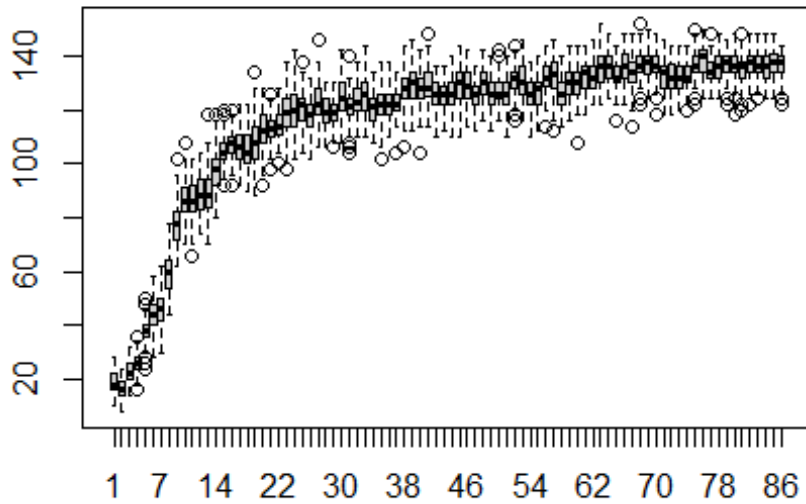
## Warning in as.tnet(net, type = "weighted one-mode tnet"): There were
self-loops
## in the edgelist, these were removed
```

Betweenness



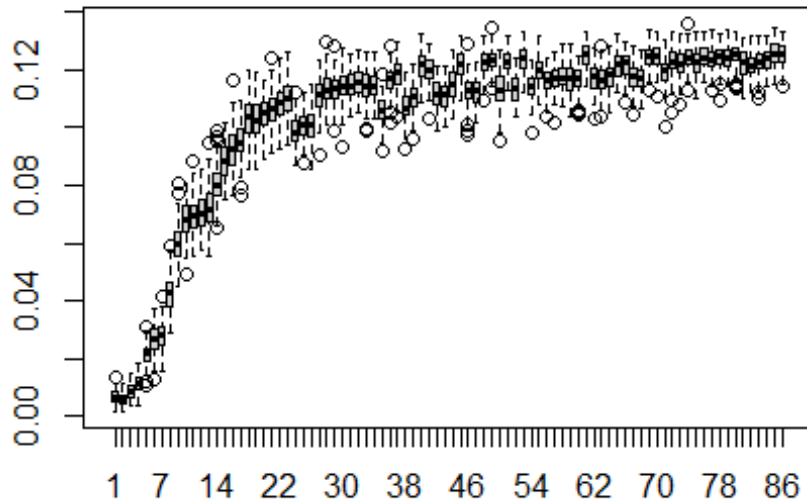
```
# Run the script on the BR similarity matrix  
BRprob2 <- net.prob(d_data2BR)  
# set up matrix and calculate eigenvector centrality for every replicat  
e  
dg.mat <- matrix(NA, nrow(d_data2BR), nsim)  
for (i in 1:nsim) {  
  dg.mat[, i] <- sna::degree(BRprob2[[i]])  
}  
# show boxplot of degree centrality sorted by the degree cent score in  
the  
# original similarity matrix  
boxplot(t(dg.mat[order(rowSums(d_data2BR)), ]), main = "Degree")
```

Degree



```
ev.mat <- matrix(NA, nrow(d_data2BR), nsim)
for (i in 1:nsim) {
  ev.mat[, i] <- sna::evcent(BRprob2[[i]])
}
# show boxplot of eigenvector centrality sorted by the EV cent score in
the
# original similarity matrix
boxplot(t(ev.mat[order(sna::evcent(d_data2BR)), ]), main = "Eigenvector
")
```

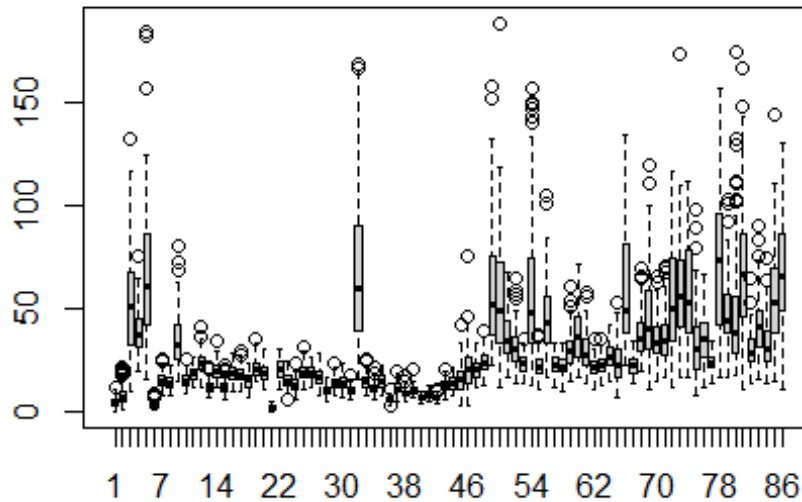
Eigenvector



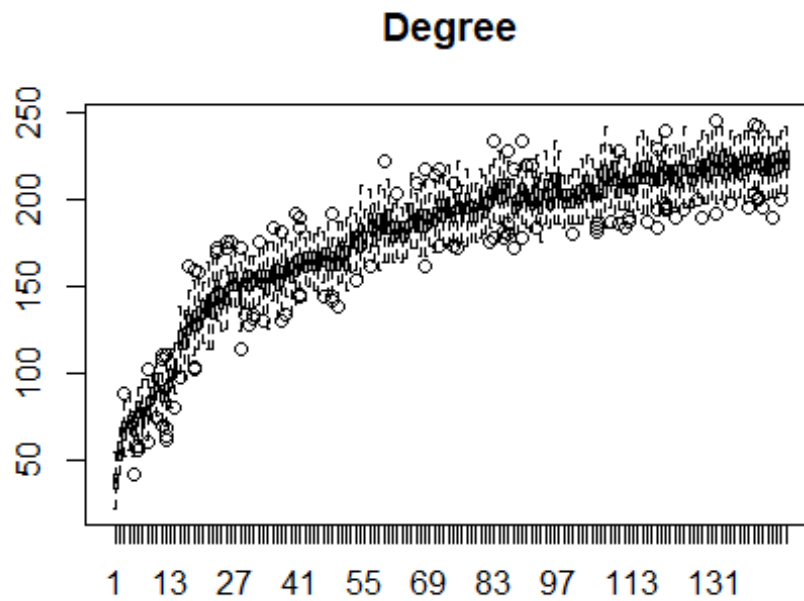
```
bw.mat <- matrix(NA, nrow(d_data2BR), nsim)
for (i in 1:nsim) {
  bw.mat[, i] <- sna::betweenness(BRprob2[[i]])
}
# show boxplot of betweenness centrality sorted by the betweenness cent
# score in the original similarity matrix
boxplot(t(bw.mat[order(betweenness_w(d_data2BR)[, 2]), ]), main = "Betw
eenness")

## Warning in as.tnet(net, type = "weighted one-mode tnet"): There were
self-loops
## in the edgelist, these were removed
```

Betweenness



```
# Run the script on the BR similarity matrix  
BRprob3 <- net.prob(d_data3BR)  
# set up matrix and calculate eigenvector centrality for every replicat  
e  
dg.mat <- matrix(NA, nrow(d_data3BR), nsim)  
for (i in 1:nsim) {  
  dg.mat[, i] <- sna::degree(BRprob3[[i]])  
}  
# show boxplot of degree centrality sorted by the degree cent score in  
the  
# original similarity matrix  
boxplot(t(dg.mat[order(rowSums(d_data3BR)), ]), main = "Degree")
```

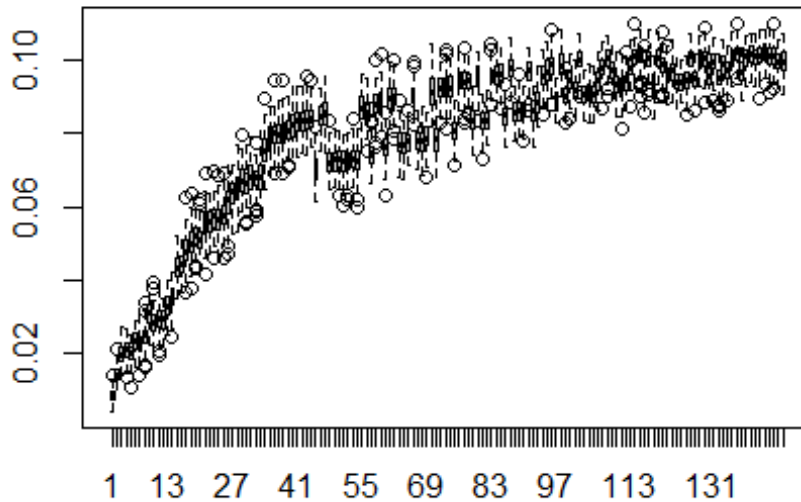



```

ev.mat <- matrix(NA, nrow(d_data3BR), nsim)
for (i in 1:nsim) {
  ev.mat[, i] <- sna::evcent(BRprob3[[i]])
}
# show boxplot of eigenvector centrality sorted by the EV cent score in
the
# original similarity matrix
boxplot(t(ev.mat[order(sna::evcent(d_data3BR)), ]), main = "Eigenvector
")

```

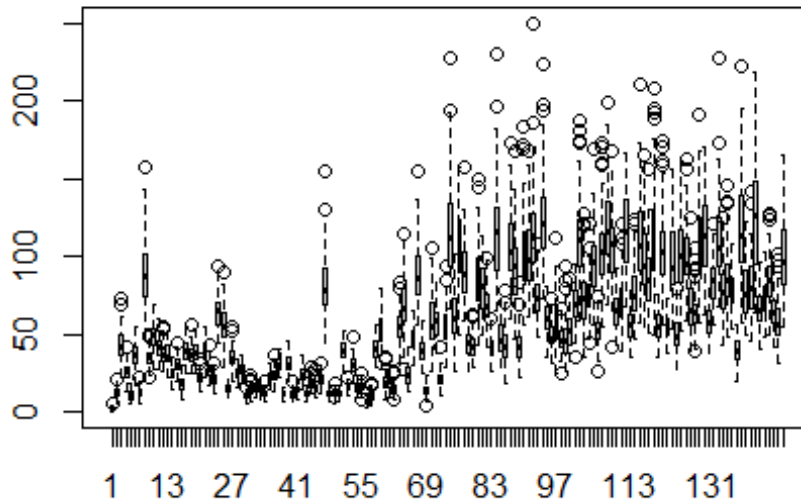
Eigenvector



```
bw.mat <- matrix(NA, nrow(d_data3BR), nsim)
for (i in 1:nsim) {
  bw.mat[, i] <- sna::betweenness(BRprob3[[i]])
}
# show boxplot of betweenness centrality sorted by the betweenness cent
# score in the original similarity matrix
boxplot(t(bw.mat[order(betweenness_w(d_data3BR)[, 2]), ]), main = "Betw
eenness")

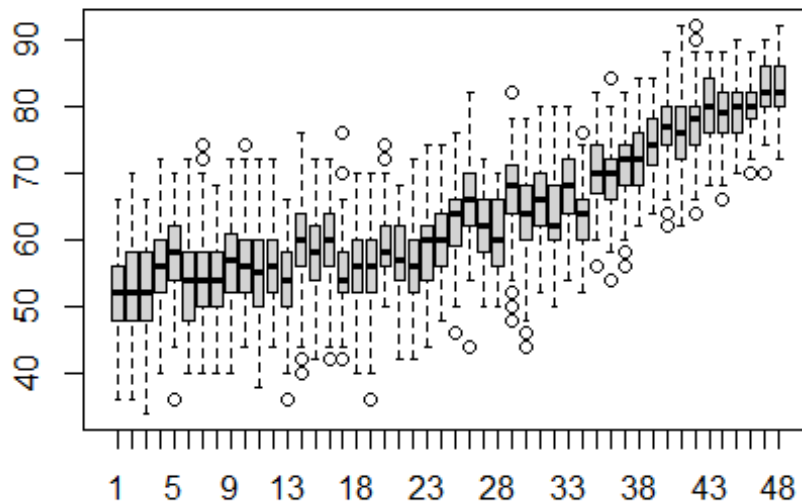
## Warning in as.tnet(net, type = "weighted one-mode tnet"): There were
self-loops
## in the edgelist, these were removed
```

Betweenness



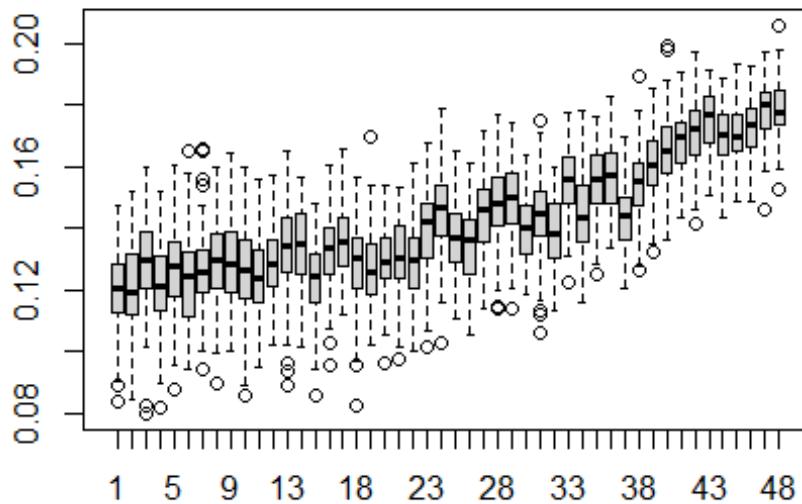
```
# Run the script on the X2 distance matrix
Xprob <- net.prob(d_data1X01)
# set up matrix and calculate eigenvector centrality for every replicat
e
dg.mat <- matrix(NA, nrow(d_data1X01), nsim)
for (i in 1:nsim) {
  dg.mat[, i] <- sna::degree(Xprob[[i]])
}
# show boxplot of degree centrality sorted by the degree cent score in
the
# original distance matrix
boxplot(t(dg.mat[order(rowSums(d_data1X01))]), ), main = "Degree")
```

Degree



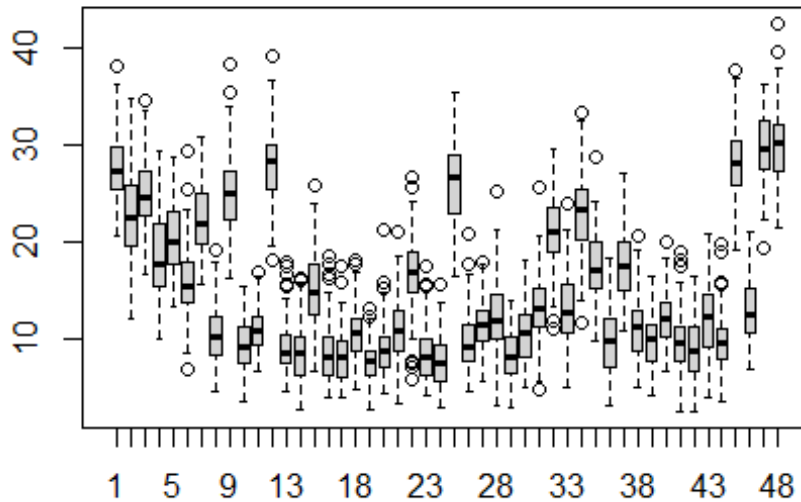
```
ev.mat <- matrix(NA, nrow(d_data1X01), nsim)
for (i in 1:nsim) {
  ev.mat[, i] <- sna::evcent(Xprob[[i]])
}
# show boxplot of eigenvector centrality sorted by the EV cent score in
the
# original distance matrix
boxplot(t(ev.mat[order(sna::evcent(d_data1X01)), ]), main = "Eigenvecto
r")
```

Eigenvector



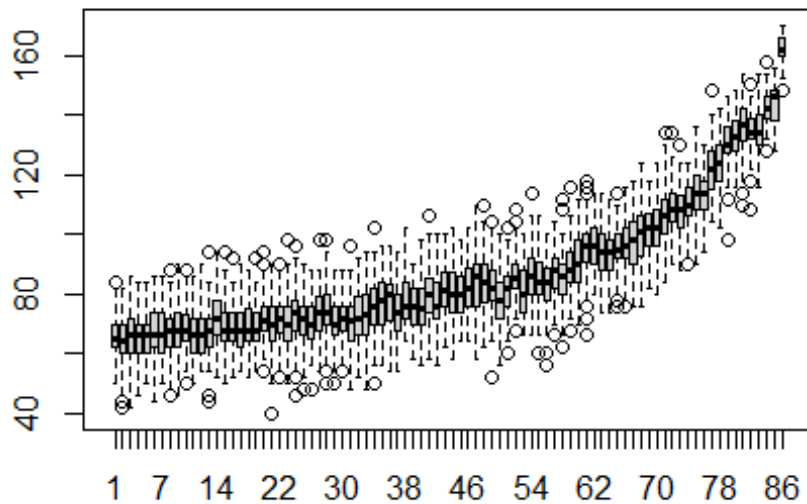
```
bw.mat <- matrix(NA, nrow(d_data1X01), nsim)
for (i in 1:nsim) {
  bw.mat[, i] <- sna::betweenness(Xprob[[i]])
}
# show boxplot of betweenness centrality sorted by the betweenness cent
# score in the original distance matrix
boxplot(t(bw.mat[order(betweenness_w(d_data1X01)[, 2]), ]), main = "Bet
weenness")
```

Betweenness



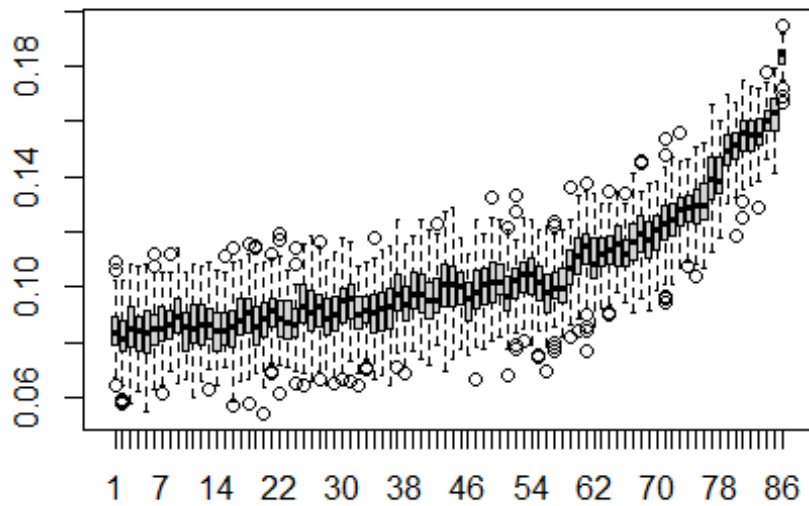
```
# Run the script on the X2 distance matrix
Xprob2 <- net.prob(d_data2X01)
# set up matrix and calculate eigenvector centrality for every replicat
e
dg.mat <- matrix(NA, nrow(d_data2X01), nsim)
for (i in 1:nsim) {
  dg.mat[, i] <- sna::degree(Xprob2[[i]])
}
# show boxplot of degree centrality sorted by the degree cent score in
the original distance matrix
boxplot(t(dg.mat[order(rowSums(d_data2X01))]), ), main = "Degree")
```

Degree



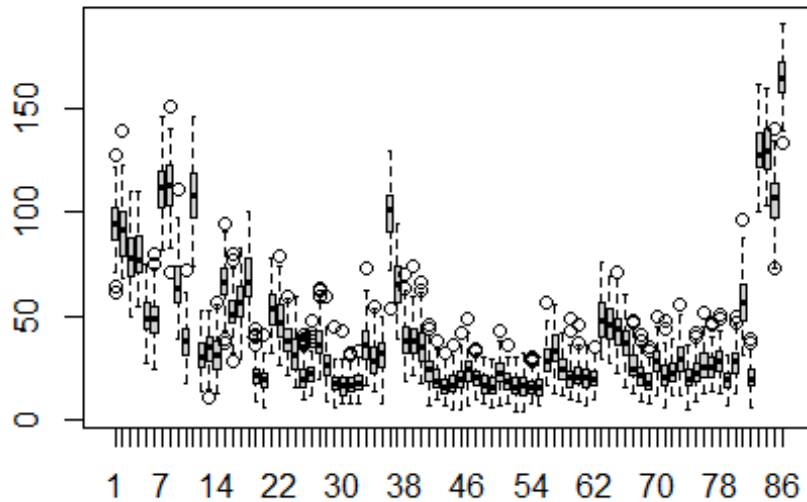
```
ev.mat <- matrix(NA, nrow(d_data2X01), nsim)
for (i in 1:nsim) {
  ev.mat[, i] <- sna::evcent(Xprob2[[i]])
}
# show boxplot of eigenvector centrality sorted by the EV cent score in
the
# original distance matrix
boxplot(t(ev.mat[order(sna::evcent(d_data2X01)), ]), main = "Eigenvecto
r")
```

Eigenvector



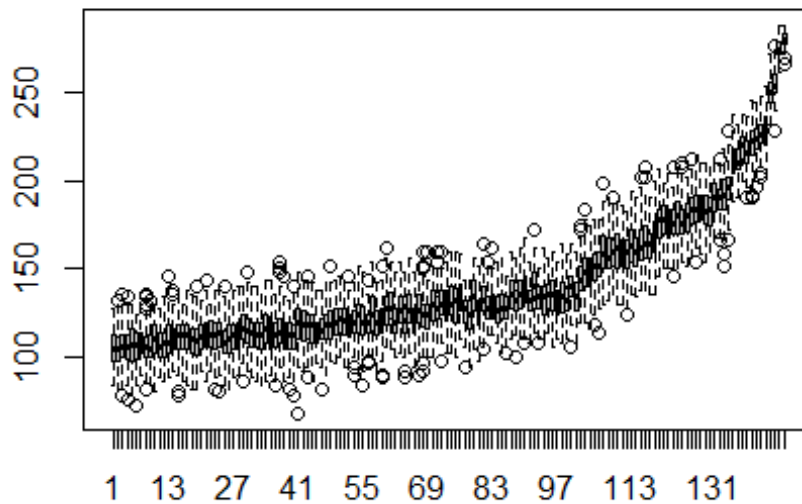
```
bw.mat <- matrix(NA, nrow(d_data2X01), nsim)
for (i in 1:nsim) {
  bw.mat[, i] <- sna::betweenness(Xprob2[[i]])
}
# show boxplot of betweenness centrality sorted by the betweenness cent
# score in the original distance matrix
boxplot(t(bw.mat[order(betweenness_w(d_data2X01)[, 2]), ]), main = "Bet
weenness")
```


Betweenness



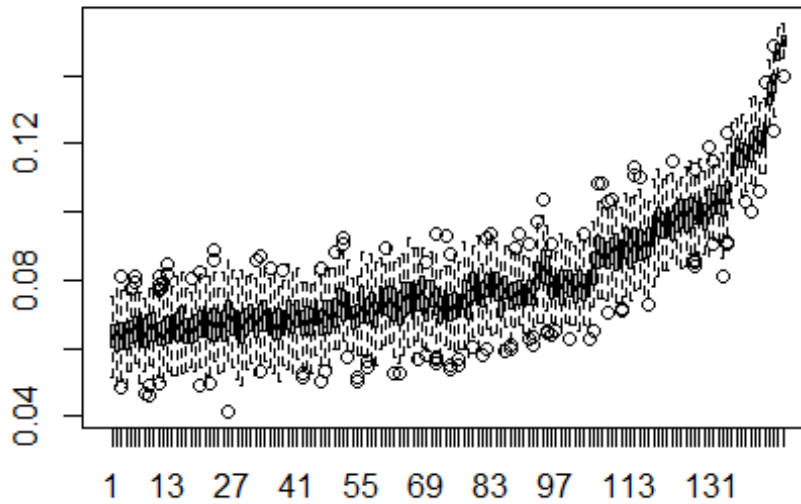
```
# Run the script on the X2 distance matrix
Xprob3 <- net.prob(d_data3X01)
# set up matrix and calculate eigenvector centrality for every replicat
e
dg.mat <- matrix(NA, nrow(d_data3X01), nsim)
for (i in 1:nsim) {
  dg.mat[, i] <- sna::degree(Xprob3[[i]])
}
# show boxplot of degree centrality sorted by the degree cent score in
the
# original distance matrix
boxplot(t(dg.mat[order(rowSums(d_data3X01))]), ), main = "Degree")
```

Degree



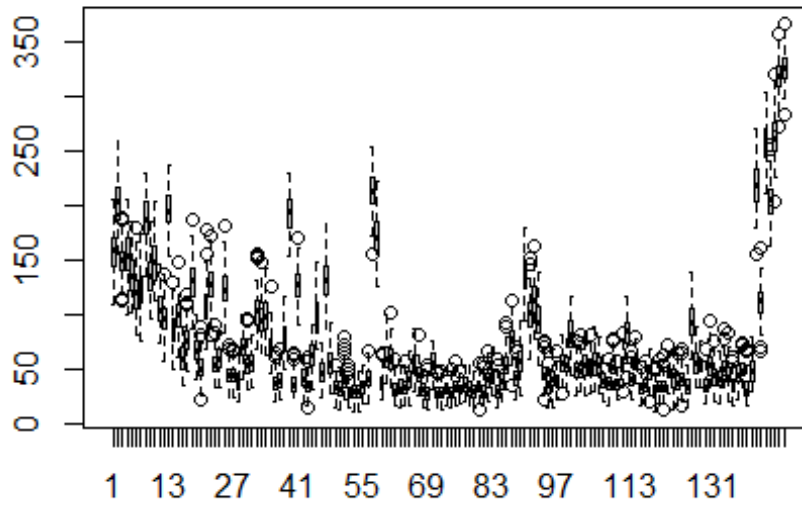
```
ev.mat <- matrix(NA, nrow(d_data3X01), nsim)
for (i in 1:nsim) {
  ev.mat[, i] <- sna::evcent(Xprob3[[i]])
}
# show boxplot of eigenvector centrality sorted by the EV cent score in
the
# original distance matrix
boxplot(t(ev.mat[order(sna::evcent(d_data3X01)), ]), main = "Eigenvecto
r")
```

Eigenvector



```
bw.mat <- matrix(NA, nrow(d_data3X01), nsim)
for (i in 1:nsim) {
  bw.mat[, i] <- sna::betweenness(Xprob3[[i]])
}
# show boxplot of betweenness centrality sorted by the betweenness cent
# score in the original distance matrix
boxplot(t(bw.mat[order(betweenness_w(d_data3X01)[, 2]), ]), main = "Bet
weenness")
```

Betweenness



Appendix F: Supplemental Data for Chapter 8

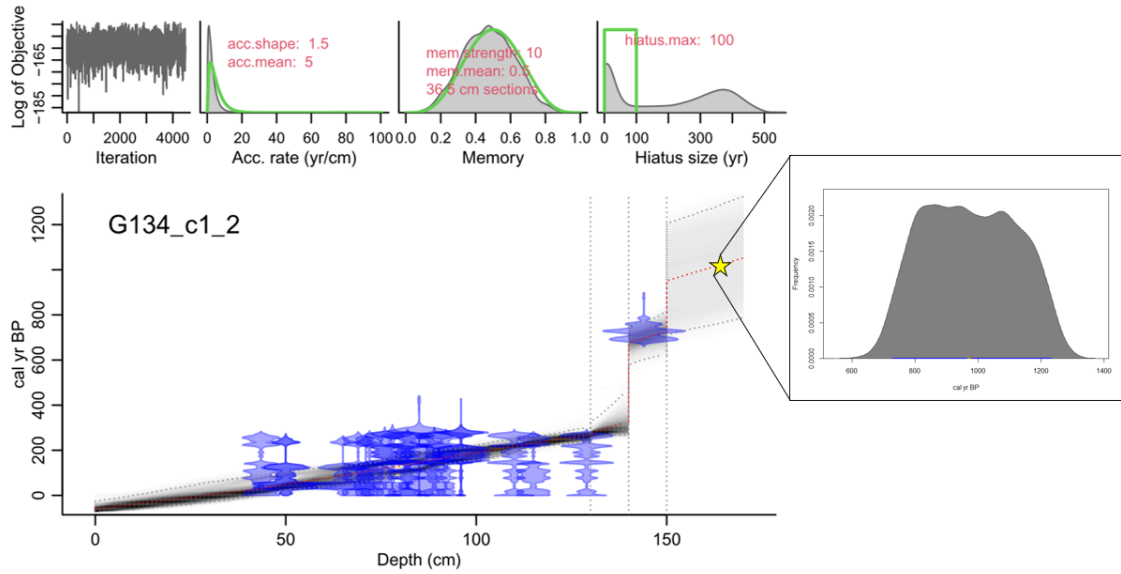
Supplemental Code: Bayesian Accumulation Model for G134 (coded in R v. 4.0.2).

```
##Code to produce an age-depth Bayesian estimate from 14C datapoints
library(rbacon)

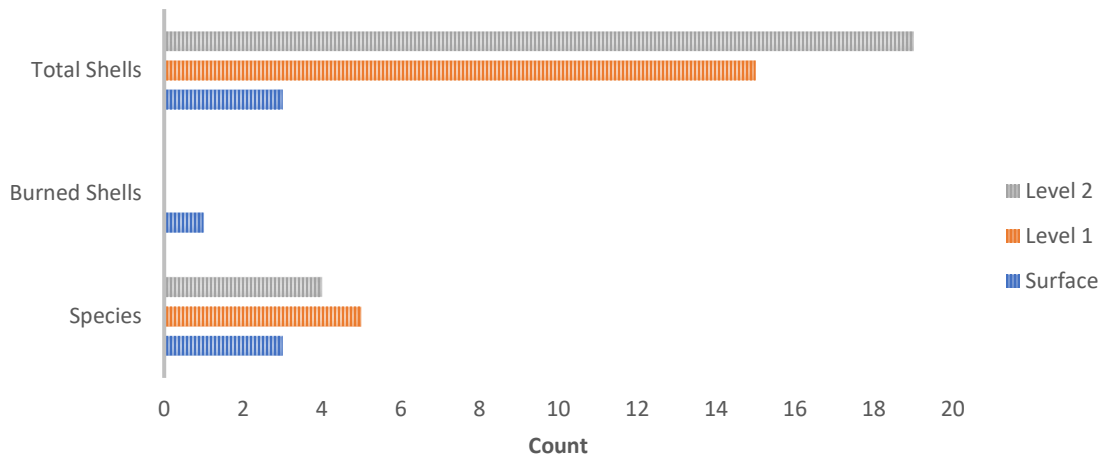
Bacon(
  "G134",
  coredir = "Bacon_runs",
  prob = 0.95,
  d.min = 0,
  d.max = 170, #can change the maximum if we want to estimate deeper layers
  d.by = 1,
  depth.unit = "cm",
  age.unit = "yr",
  unit = depth.unit,
  acc.shape = 1.5,
  acc.mean = 2, #value was tested and changed according to program prior
  estimates
  mem.strength = 10,
  mem.mean = 0.5,
  boundary = NA,
  hiatus.depths = c(130, 140, 150), #inferred hiatuses from excavations
  hiatus.max = 100,
  add = c(),
  after = 1e-04/5, #5 is actually the thick value
  cc = 3, #sets calibration to SHCal20
  ccdir = "",
  postbomb = 0,
  t.a = 3,
  t.b = 4,
  normal = FALSE,
  suggest = TRUE,
  accept.suggestions = FALSE,
  reswarn = c(10, 200),
  remember = TRUE,
  ask = TRUE,
  run = TRUE,
  defaults = "defaultBacon_settings.txt",
  sep = ",",
  dec = ".",
  runname = "", #can update this to give each output specific file name
  slump = c(),
  remove = FALSE,
  BCAD = FALSE,
  ssize = 2000,
  th0 = c(),
  burnin = min(500, 2000), #2000 = ssize
  MinAge = c(),
  MaxAge = c(),
  MinYr = MinAge,
  MaxYr = MaxAge,
  cutoff = 0.01,
```

```
plot.pdf = TRUE,  
dark = 1,  
date.res = 100,  
age.res = 200,  
yr.res = age.res,  
close.connections = TRUE,  
verbose = TRUE  
)
```

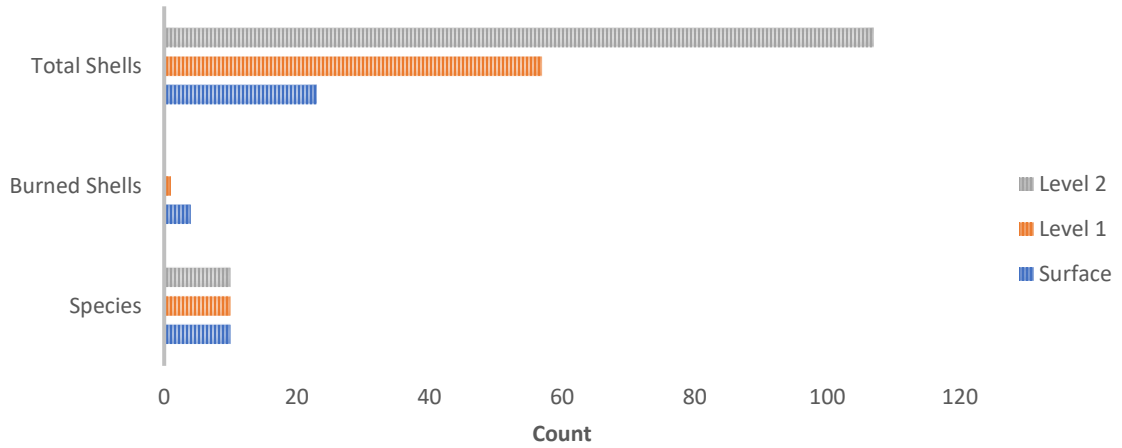
Supplemental Figures and Tables



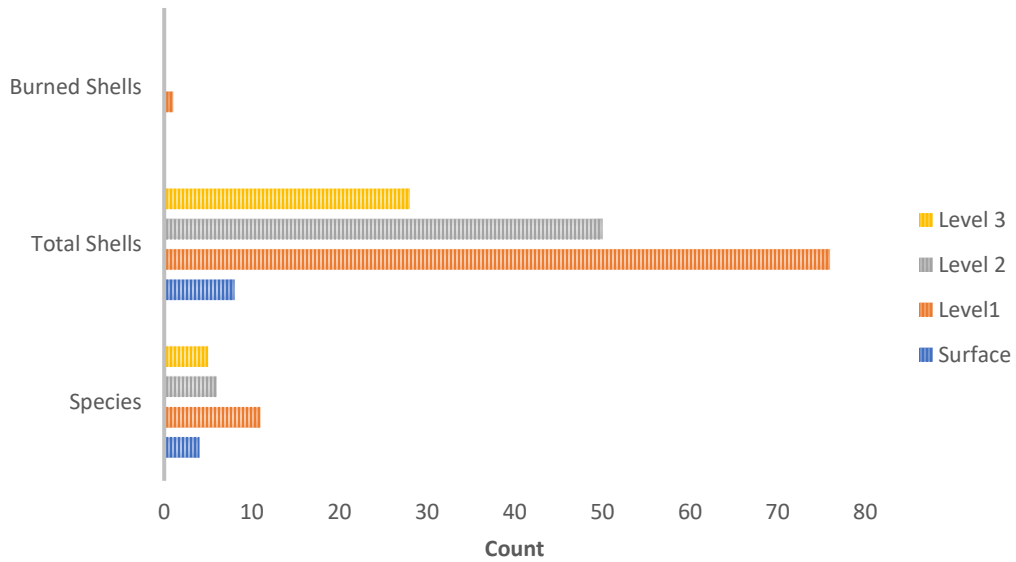
Supplemental Figure F-1: Bayesian age depth estimation model of G134 using only class 1 and class 2 14C dates. See caption of Figure 4 for details on each plot. Age estimations are comparable with the model shown in Figure 4. Star and associated histogram show depth and age-depth estimation for the lithic recovered from the unit [mean (red): 975 cal. BP, median (green): 970 cal. BP, 95% range (blue): 728.-1233 cal. BP].



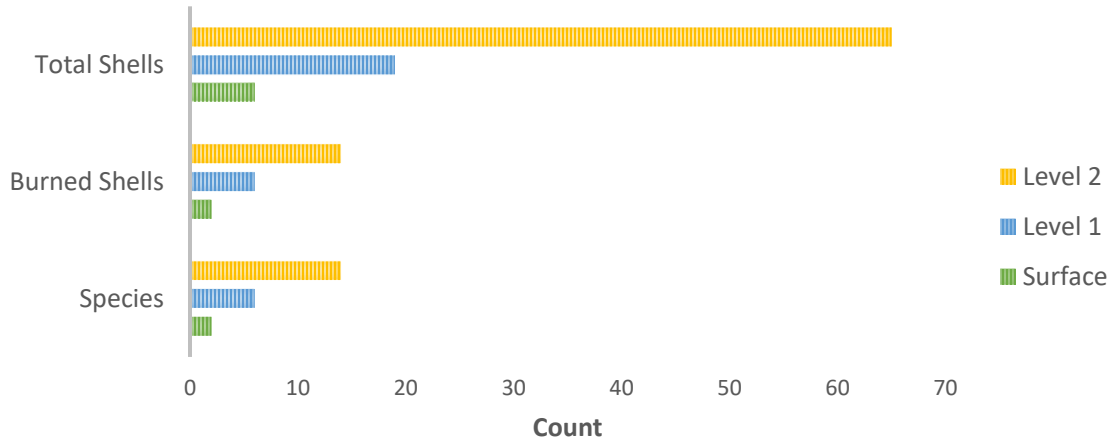
Supplemental Figure F-2: Count of marine shell material recovered from G123 Unit 1.



Supplemental Figure F-3: Count of marine shell material recovered from G123 Unit 2.



Supplemental Figure F-4: Count of marine shell materials recovered from G123 Unit 3.



Supplemental Figure F-5: Count of marine shell material recovered from G-15-2020 by stratigraphic level.

Supplemental Table F-1: Charcoal Samples and their chronometric hygiene ranks and associations.

Sample ID	Depth (cm)	Cultural Context	Material Type Rank	Association Rank	¹⁴ C Rank	Hygiene Class
AMP1	8	Artifacts	2	1	1	2
AMP2	26	Artifacts (faunal, ceramic)	2	1	2	3
AMP3	27	Artifacts (faunal, ceramic)	2	1	2	3
G123-1	14	Artifacts (Marine shell)	2	1	2	3
G123-2	16	Artifacts (Marine shell)	2	1	2	3
G123-3	22	Artifacts (Marine shell)	2	1	2	3
G123-4	16.5	Artifacts (Marine shell)	2	1	1	2
G123-5	20	Artifacts (Marine shell)	2	1	1	2
BELA1	13	Artifacts (faunal, ceramic)	2	1	1	2
BELA2	20	Artifacts (faunal, ceramic)	2	1	1	2
BELA3	18	Artifacts (Marine shell and eggshell)	2	1	1	2
BELA4	21	Artifacts (faunal, ceramic)	2	1	2	3
BELA5	20	Artifacts (faunal, ceramic)	2	1	1	2
G134-1	21	Artifacts (ceramic)	2	1	2	3
G134-2	20	Artifacts (ceramic)	2	1	2	3
G134-3	19	Artifacts (ceramic)	2	1	2	3
G134-4	34	Artifacts (marine shell ceramic)	2	2	2	3
G134-5	38	Artifacts (faunal)	2	1	2	3
G134-6	38	Artifacts (faunal)	2	1	2	3
G134-7	43	Artifacts (faunal)	2	1	2	3
G134-8	40	Artifacts (faunal)	2	1	2	3
G134-10	43.5	Artifacts (faunal)	1	1	1	1
G134-11	47	Artifacts (faunal)	2	1	1	2
G134-13	50	Artifacts (faunal, metal)	1	1	2	2
G134-14	50	Artifacts (faunal, metal)	1	1	2	2
G134-F1-1	57	Feature	2	1	2	3
G134-F2-1	65	Feature	1	1	2	2
G134-15	68	Artifacts (faunal, ceramic)	1	1	2	2
G134-16	66	Artifacts (faunal, ceramic)	2	1	2	3
G134-17	68	Artifacts (faunal, ceramic)	2	1	2	3
G134-18	68	Artifacts (faunal, ceramic)	2	1	2	3
G134-19	68	Artifacts (faunal, ceramic)	2	1	2	3
G134-20	69	Artifacts (faunal, ceramic)	1	1	1	1
G134-23	71	Artifacts (faunal, ceramic)	1	1	2	2
G134-24	71	Artifacts (faunal, ceramic)	2	1	2	3
G134-26	73.5	Artifacts (faunal)	2	1	2	3
G134-27	76	Artifacts (faunal, ceramic)	1	1	2	2

G134-28	72	Artifacts (faunal)	1	1	2	2
G134-30	82	Artifacts (faunal, ceramic)	2	1	2	3
G134-31	82	Artifacts (faunal, ceramic)	1	1	1	1
G134-32	77	Artifacts (faunal)	2	1	2	3
G134-33	79	Artifacts (faunal, ceramic)	2	1	2	3
G134-34	78	Artifacts (faunal, ceramic)	2	1	1	2
G134-35	84	Artifacts (faunal)	2	1	2	3
G134-36	82	Artifacts (faunal, ceramic)	2	1	1	2
G134-37	85	Artifacts (faunal, ceramic)	2	1	1	2
G134-38	81	Artifacts (faunal, ceramic)	2	1	2	3
G134-39	90	Artifacts (faunal, ceramic)	2	1	2	3
G134-40	90	Artifacts (faunal, ceramic)	2	1	2	3
G134-41	92	Artifacts (faunal, ceramic)	2	1	1	2
G134-42	89	Artifacts (faunal, ceramic)	1	1	2	2
G134-43	96	Artifacts (faunal, ceramic, metal)	1	1	1	1
G134-44	87	Artifact (ceramic)	1	1	2	1
G134-45	96	Artifacts (faunal, ceramics, metal)	2	1	1	2
G134-46	109	Artifacts (faunal, ceramic)	2	1		
G134-47	110	Artifacts (faunal, ceramic)	2	1	1	2
G134-48	115	Artifacts (faunal, ceramic)	2	1	1	2
G134-49	129	Artifacts (ceramic)	2	1	1	2
G134-50	144	Artifacts (faunal, ceramic)	2	1	1	2

References

AAA Ethics Forum

2012 Principles of Professional Responsibility. <http://ethics.americananthro.org/ethics-statement-0-preamble/>, accessed September 16, 2020.

AAG

Statement of Professional Ethics | AAG.

http://www.aag.org/cs/about_aag/governance/statement_of_professional_ethics, accessed April 14, 2021.

Agapiou, Athos, Dimitrios Alexakis, Apostolos Sarris, and Diofantos Hadjimitsis

2014 Evaluating the Potentials of Sentinel-2 for Archaeological Perspective. *Remote Sensing* 6(3):2176–2194. DOI:10.3390/rs6032176.

Agapiou, Athos, and Vasiliki Lysandrou

2015 Remote sensing archaeology: Tracking and mapping evolution in European scientific literature from 1999 to 2015. *Journal of Archaeological Science: Reports* 4:192–200. DOI:10.1016/j.jasrep.2015.09.010.

Akaike, Hirotugu

1974 A New Look at the Statistical Model Identification. In *Selected Papers of Hirotugu Akaike*, edited by Emanuel Parzen, Kunio Tanabe, and Genshiro Kitagawa, pp. 215–222. Springer New York, New York, NY.

Alexakis, Dimitrios, Apostolos Sarris, Theodoros Astaras, and Konstantinos Albanakis

2011 Integrated GIS, remote sensing and geomorphologic approaches for the reconstruction of the landscape habitation of Thessaly during the neolithic period. *Journal of Archaeological Science* 38(1):89–100.

Allan, J. A., and T. S. Richards

1983 Use of satellite imagery in archaeological surveys. *Libyan Studies* 14(4):8.

Allee, W. C., and Edith S. Bowen

1932 Studies in animal aggregations: mass protection against colloidal silver among goldfishes. *Journal of Experimental Zoology* 61(2):185–207.

Allibert, Claude

2008 Austronesian Migration and the Establishment of the Malagasy Civilization: Contrasted Readings in Linguistics, Archaeology, Genetics and Cultural Anthropology. *Diogenes* 55(2):7–16. DOI:10.1177/0392192108090734.

Altschul, Jeffrey H.

1988 Models and the Modeling Process. In *Quantifying the Present and Predicting the Past: Theory, Method, and Application of Archaeological Predictive Modeling*, edited by

W. James Judge and Lynne Sebastian, pp. 61–96. US Department of the Interior, Bureau of Land Management, Denver.

Altschul, Jeffrey H., Keith W. Kintigh, Mark Aldenderfer, Elise Alonzi, Ian Armit, Juan Antonio Barceló, Christopher S. Beekman, Penny Bickle, Douglas W. Bird, Scott E. Ingram, Elena Isayev, Andrew W. Kandel, Rachael Kiddey, H el ene Timpoko Kienon-Kabor e, Franco Niccolucci, Corey S. Ragsdale, Beth K. Scaffidi, and Scott G. Ortman
2020 Opinion: To understand how migrations affect human securities, look to the past. *Proceedings of the National Academy of Sciences* 117(34):20342–20345.
DOI:10.1073/pnas.2015146117.

Altschul, Jeffrey H., Keith W. Kintigh, Terry H. Klein, William H. Doelle, Kelley A. Hays-Gilpin, Sarah A. Herr, Timothy A. Kohler, Barbara J. Mills, Lindsay M. Montgomery, and Margaret C. Nelson
2017 Opinion: Fostering synthesis in archaeology to advance science and benefit society. *Proceedings of the National Academy of Sciences* 114(42):10999–11002.

 lvarez Larrain, Alina, Catriel Greco, and Myriam Tarrag o
2021 Participatory mapping and UAV photogrammetry as complementary techniques for landscape archaeology studies: an example from north-western Argentina. *Archaeological Prospection* 28(1):47–61. DOI:10.1002/arp.1794.

 lvarez Larrain, Alina, and Michael K. McCall
2019 Participatory Mapping and Participatory GIS for Historical and Archaeological Landscape Studies: a Critical Review. *Journal of Archaeological Method and Theory* 26(2):643–678. DOI:10.1007/s10816-018-9385-z.

Amelot, X.
2017 Dire la nature   Madagascar. In *Dire l’oc ean Indien*, 1:pp. 32–53.
OSOI/Universit  de La R union-Epica, Saint-Denis de La R union.

An, Li
2012 Modeling human decisions in coupled human and natural systems: Review of agent-based models. *Ecological Modelling* 229:25–36.
DOI:10.1016/j.ecolmodel.2011.07.010.

Anderson, Atholl
2019 Was there mid Holocene habitation in Madagascar? A reconsideration of the OSL dates from Lakaton’i Anja. *antiquity* 93(368):478–487.

Anderson, Atholl, Geoffrey Clark, Simon Haberle, Tom Higham, Malgosia Nowak-Kemp, Amy Prendergast, Chantal Radimilahy, Lucien M. Rakotozafy, Ramilisonina, Jean-Luc Schwenninger, Malika Virah-Sawmy, and Aaron Camens
2018 New evidence of megafaunal bone damage indicates late colonization of Madagascar. Edited by Si n E. Halcrow. *PLOS ONE* 13(10):e0204368.
DOI:10.1371/journal.pone.0204368.

Angulo, Elena, Gloria M. Luque, Stephen D. Gregory, John W. Wenzel, Carmen Bessa-Gomes, Ludek Berec, and Franck Courchamp
2018 Review: Allee effects in social species. *Journal of Animal Ecology* 87(1):47–58. DOI:10.1111/1365-2656.12759.

Andavadoaka Monthly Climate Averages
Andavadoaka Monthly Climate Averages. *WorldWeatherOnline.com*.
<https://www.worldweatheronline.com/andavadoaka-weather/toliara/mg.aspx>, accessed October 23, 2020.

Anquandah, James
1987 The stone circle sites of Komaland, northern Ghana, in West African archaeology. *The African Archaeological Review* 5(1):171–180. DOI:10.1007/BF01117091.

Anschuetz, K. F., R. H. Wilhusen, and C. L. Scheick
2001 An Archaeology of Landscapes: Perspectives and Directions. *Journal of Archaeological Research* 9(2):157–211.

Appels, Willemijn M., Chris B. Graham, Jim E. Freer, and Jeffrey J. McDonnell
2015 Factors affecting the spatial pattern of bedrock groundwater recharge at the hillslope scale. *Hydrological Processes* 29(21):4594–4610.

Arazi, Noemie
2011 Safeguarding archaeological cultural resources in Africa—Policies, methods and issues of (non) compliance. *African Archaeological Review* 28(1):27–38.

Ashley, Ceri Z., Alexander Antonites, and Per Ditlef Fredriksen
2016 Mobility and African archaeology: an introduction. *Azania: Archaeological Research in Africa* 51(4):417–434. DOI:10.1080/0067270X.2016.1233766.

Astuti, Rita
1995 *The People of the Sea: Identity and decent among the Vezo of Madagascar*. Cambridge University Press, Cambridge.

Atalay, S.
2012 *Community-based archaeology: Research with, by, and for indigenous and local communities*. University of California Press.

Baddeley, A. J., and M. N. M. van Lieshout
1995 Area-interaction point processes. *Annals of the Institute of Statistical Mathematics* 47(4):601–619. DOI:10.1007/BF01856536.

Baddeley, A., R. Turner, J. Møller, and M. Hazelton
2005 Residual analysis for spatial point processes (with discussion). *Journal of the*

Royal Statistical Society: Series B (Statistical Methodology) 67(5):617–666.
DOI:10.1111/j.1467-9868.2005.00519.x.

Baddeley, Adrian, Ege Rubak, and Jesper Møller
2011 Score, pseudo-score and residual diagnostics for spatial point process models. *Statistical Science* 26(4):613–646.

Baddeley, Adrian, Ege Rubak, and Rolf Turner
2015 *Spatial point patterns: methodology and applications with R*. CRC Press.

Baggio, Jacopo A., Shauna B. BurnSilver, Alex Arenas, James S. Magdanz, Gary P. Kofinas, and Manlio De Domenico
2016 Multiplex social ecological network analysis reveals how social changes affect community robustness more than resource depletion. *Proceedings of the National Academy of Sciences* 113(48):13708–13713. DOI:10.1073/pnas.1604401113.

Bailey, Geoff
1981 Concepts, time-scales and explanations in economic prehistory. *Economic archaeology* 96:97–117.
2008 Time perspectivism: origins and consequences. In *Time in Archaeology: Time Perspectivism Revisited*, edited by S. Holdaway and L. Wandsnider, pp. 13–30. University of Utah Press, Salt Lake City.

Barret, Jean-Baptiste
1985 Sarodrano: étude d'un site archéologique côtier du sud-ouest malgache. Unpublished Masters, Université de Paris, Paris.

Barton, Kamil
2019 *MuMIn: Multi-Model Inference*.

Basso, Keith H.
1996 Wisdom Sits in Places: Notes on a Western Apache Landscape. In *Senses of Place*, edited by Steven Feld and Keith H. Basso, pp. 53–90. SAR Press, Santa Fe.

Battistini, R., and P. Verin
1972 Man and the Environment in Madagascar. In *Biogeography and Ecology in Madagascar*, edited by R. Battistini and G. Richard-Vindard, 21:pp. 311–337. Springer Netherlands, Dordrecht.

Beaujard, Philippe
2007 East Africa, the Comoros Islands and Madagascar before the sixteenth century: On a neglected part of the world system. *Azania: Archaeological Research in Africa* 42(1):15–35. DOI:10.1080/00672700709480448.
2011 The first migrants to Madagascar and their introduction of plants: linguistic and ethnological evidence. *Azania: Archaeological Research in Africa* 46(2):169–189. DOI:10.1080/0067270X.2011.580142.

- Beck, Anthony, Graham Philip, Maamoun Abdulkarim, and Daniel Donoghue
2007 Evaluation of Corona and Ikonos high resolution satellite imagery for archaeological prospection in western Syria. *Antiquity* 81(311):161–175.
DOI:10.1017/S0003598X00094916.
- Bell, Adrian Viliami, and Bruce Winterhalder
2014 The Population Ecology of Despotism. *Human Nature* 25(1):121–135.
DOI:10.1007/s12110-014-9190-7.
- Bennett, Rebecca, Dave Cowley, and Véronique De Laet
2014 The data explosion: tackling the taboo of automatic feature recognition in airborne survey data. *Antiquity* 88(341):896–905. DOI:10.1017/S0003598X00050766.
- Bennett, Rebecca, Kate Welham, Ross A. Hill, and Andrew L. J. Ford
2012 The Application of Vegetation Indices for the Prospection of Archaeological Features in Grass-dominated Environments. *Archaeological Prospection* 19(3):209–218.
DOI:10.1002/arp.1429.
- Bentham, Jeremy
1791 *Panopticon or the Inspection House*. T. Payne, London.
- Besairie, H.
1964 Carte géologique de Madagascar. Service Géologique de Madagascar, Antananarivo, 1:1,000,000 (color), 3 sheets.
- Bescoby, D.J.
2006 Detecting Roman land boundaries in aerial photographs using Radon transforms. *Journal of Archaeological Science* 33(5):735–743. DOI:10.1016/j.jas.2005.10.012.
- Bettinger, Robert L.
1980 Explanatory/predictive models of hunter–gatherer adaptation. In *Advances in archaeological method and theory*, pp. 189–255. Elsevier.
- Bevan, A., E. Crema, and A. Palmisano
2013 Intensities, interactions and uncertainties: Some new approaches to archaeological distributions. In *Computational Approaches to Archaeological Spaces*, edited by A. Bevan and M. Lake, pp. 27–52. Left Coast Press, Walnut Creek.
- Bevan, A., E. Jobbová, C. Helmke, and J. J. Awe
2013 Directional layouts in central lowland Maya settlement. *Journal of Archaeological Science* 40(5):2373–2383. DOI:10.1016/j.jas.2013.01.011.
- Bevan, Andrew, and James Conolly
2011 Terraced fields and Mediterranean landscape structure: An analytical case study

from Antikythera, Greece. *Ecological Modelling* 222(7):1303–1314.
DOI:10.1016/j.ecolmodel.2010.12.016.

Bevan, Andrew, and Mark Lake

2016 Intensities, interactions, and uncertainties: Some new approaches to archaeological distributions. In *Computational approaches to archaeological spaces*, pp. 27–52. Routledge.

Bevan, Andrew, and Alan Wilson

2013 Models of settlement hierarchy based on partial evidence. *Journal of Archaeological Science* 40(5):2415–2427. DOI:10.1016/j.jas.2012.12.025.

Bewley, Robert, Andrew Wilson, David Kennedy, David Mattingly, Rebecca Banks, Michael Bishop, Jennie Bradbury, Emma Cunliffe, Michael Fradley, and Richard Jennings

2016 Endangered archaeology in the Middle East and North Africa: Introducing the EAMENA project. In *CAA2015. Keep the Revolution Going: Proceedings of the 43rd Annual Conference on Computer Applications and Quantitative Methods in Archaeology*, 1:pp. 919.

Biagetti, Stefano, Stefania Merlo, Elhadi Adam, Augustin Lobo, Francesc C. Conesa, Jasper Knight, Hayette Bekrani, Enrico R. Crema, Jonas Alcaina-Mateos, and Marco Madella

2017 High and Medium Resolution Satellite Imagery to Evaluate Late Holocene Human–Environment Interactions in Arid Lands: A Case Study from the Central Sahara. *Remote Sensing* 9(4):351. DOI:10.3390/rs9040351.

Bini, Monica, Ilaria Isola, Giovanni Zanchetta, Adriano Ribolini, Andrea Ciampalini, Ilaria Baneschi, Daniela Mele, and Anna Lucia D’Agata

2018 Identification of Leveled Archeological Mounds (Höyük) in the Alluvial Plain of the Ceyhan River (Southern Turkey) by Satellite Remote-Sensing Analyses. *Remote Sensing* 10(2):241. DOI:10.3390/rs10020241.

Bird, Douglas W., Rebecca Bliege Bird, Brian F. Coddling, and Nyalangka Taylor

2016 A Landscape Architecture of Fire: Cultural Emergence and Ecological Pyrodiversity in Australia’s Western Desert. *Current Anthropology* 57(S13):S65–S79. DOI:10.1086/685763.

Bivand, Roger, Tim Keitt, and Barry Rowlingson

2019 *rgdal: Bindings for the “Geospatial” Data Abstraction Library*.

Bivand, Roger, and Nicholas Lewin-Koh

2019 *maptools: Tools for Handling Spatial Objects*.

Bivand, Roger, and Colin Rundel

2019 *rgaos: Interface to Geometry Engine - Open Source (‘GEOS’)*.

- Bivand, Roger S., Edzer J. Pebesma, Virgilio Gomez-Rubio, and Edzer Jan Pebesma
2013 *Applied spatial data analysis with R*. 2nd ed. Springer, New York.
- Blaauw, Maarten, and J. Andrés Christen
2011 Flexible paleoclimate age-depth models using an autoregressive gamma process. *Bayesian analysis* 6(3):457–474.
- Blaauw, Maarten, J. Andrés Christen, and Marco A. Aquino Lopez
2021 *rbacon: Age-Depth Modelling using Bayesian Statistics*.
- Blaschke, T.
2010 Object based image analysis for remote sensing. *ISPRS Journal of Photogrammetry and Remote Sensing* 65(1):2–16. DOI:10.1016/j.isprsjprs.2009.06.004.
- Bliege Bird, R., D. W. Bird, B. F. Coddling, C. H. Parker, and J. H. Jones
2008 The “fire stick farming” hypothesis: Australian Aboriginal foraging strategies, biodiversity, and anthropogenic fire mosaics. *Proceedings of the National Academy of Sciences* 105(39):14796–14801. DOI:10.1073/pnas.0804757105.
- Bliege Bird, Rebecca, and Douglas W. Bird
2020 Climate, landscape diversity, and food sovereignty in arid Australia: The firestick farming hypothesis. *American Journal of Human Biology*. DOI:10.1002/ajhb.23527, accessed March 26, 2021.
- Bliege Bird, Rebecca, Chloe McGuire, Douglas W. Bird, Michael H. Price, David Zeanah, and Dale G. Nimmo
2020 Fire mosaics and habitat choice in nomadic foragers. *Proceedings of the National Academy of Sciences*:201921709. DOI:10.1073/pnas.1921709117.
- Blurton Jones, Nicholas
1986 Bushman birth spacing: A test for optimal interbirth intervals. *Ethology and Sociobiology* 7(2):91–105. DOI:10.1016/0162-3095(86)90002-6.
- de Boer, Erik J., Rik Tjallingii, Maria I. Véléz, Kenneth F. Rijdsdijk, Anouk Vlug, Gert-Jan Reichart, Amy L. Prendergast, Perry G.B. de Louw, F.B. Vincent Florens, Cláudia Baider, and Henry Hooghiemstra
2014 Climate variability in the SW Indian Ocean from an 8000-yr long multi-proxy record in the Mauritian lowlands shows a middle to late Holocene shift from negative IOD-state to ENSO-state. *Quaternary Science Reviews* 86:175–189. DOI:10.1016/j.quascirev.2013.12.026.
- Boivin, Nicole, Alison Crowther, Richard Helm, and Dorian Q. Fuller
2013 East Africa and Madagascar in the Indian Ocean world. *Journal of World Prehistory* 26(3):213–281. DOI:10.1007/s10963-013-9067-4.

- Borie, César, César Parcero-Oubiña, Youngsang Kwon, Diego Salazar, Carola Flores, Laura Olguín, and Pedro Andrade
 2019 Beyond Site Detection: The Role of Satellite Remote Sensing in Analysing Archaeological Problems. A Case Study in Lithic Resource Procurement in the Atacama Desert, Northern Chile. *Remote Sensing* 11(7):869. DOI:10.3390/rs11070869.
- Brainerd, George W.
 1951 The Place of Chronological Ordering in Archaeological Analysis. *American Antiquity* 16(4):301–313.
- Brandolini, Filippo, and Francesco Carrer
 2020 *Terra, Silva et Paludes* . Assessing the Role of Alluvial Geomorphology for Late-Holocene Settlement Strategies (Po Plain – N Italy) Through Point Pattern Analysis. *Environmental Archaeology*:1–15. DOI:10.1080/14614103.2020.1740866.
- Braun, David P.
 1983 Pots as Tools. In *Archaeological Hammers and Theories*, edited by J. A. Moore and A. S. Keene, pp. 107–134. Academic Press, New York.
- Breeze, Paul S., Nick A. Drake, Huw S. Groucutt, Ash Parton, Richard P. Jennings, Tom S. White, Laine Clark-Balzan, Ceri Shipton, Eleanor M.L. Scerri, Christopher M. Stimpson, Rémy Crassard, Yamandú Hilbert, Abdullah Alsharekh, Abdulaziz Al-Omari, and Michael D. Petraglia
 2015 Remote sensing and GIS techniques for reconstructing Arabian palaeohydrology and identifying archaeological sites. *Quaternary International* 382:98–119. DOI:10.1016/j.quaint.2015.01.022.
- Breiman, Leo
 2001 Random forests. *Machine learning* 45(1):5–32.
- Brenan, P.
 1972 The Geology of Madagascar. In *Biogeography and Ecology in Madagascar*, edited by R. Battistini and G. Richard-Vindard, 21:pp. 27–86. Springer Netherlands, Dordrecht.
- Breunig, Peter, Katharina Neumann, and Wim Van Neer
 1996 New research on the Holocene settlement and environment of the Chad Basin in Nigeria. *African Archaeological Review* 13(2):111–145. DOI:10.1007/BF01956304.
- Brodie, Neil, Morag M. Kersel, Christina Luke, and Kathryn Walker Tubb (editors)
 2006 *Archaeology, Cultural Heritage, and the Antiquities Trade*. University Press of Florida, Gainesville.
- Brosnan, Tanya, Matthew W. Becker, and Carl P. Lipo
 2018 Coastal groundwater discharge and the ancient inhabitants of Rapa Nui (Easter

Island), Chile. *Hydrogeology Journal*. DOI:10.1007/s10040-018-1870-7, accessed October 6, 2018.

Brughmans, Tom

2010 Connecting the Dots: Towards Archaeological Network Analysis. *Oxford Journal of Archaeology* 29(3):277–303. DOI:<https://doi.org/10.1111/j.1468-0092.2010.00349.x>.

2013 Thinking Through Networks: A Review of Formal Network Methods in Archaeology. *Journal of Archaeological Method and Theory* 20(4):623–662. DOI:10.1007/s10816-012-9133-8.

Brunon-Ernst, A.

2013 Deconstructing panopticism into the plural panopticons. In *Beyond Foucault: New perspectives on Bentham's panopticon*, edited by A. Brunon-Ernst, pp. 17–42. Ashgate Publishing.

Buffa, Danielle

2019 Biby in 3D: First Digitized Collection of Malagasy Fauna presented at the 14th Madagascar Workshop, University of Toronto, October 25-26, 2019, Toronto, Canada.

Buffa, Danielle, George Manahira, Zafy Maharesy Chrisostome, Felicia Fenomanana, Roger Samba, François Lahiniriko, Voahirana Vavisoa, Patricia Soafiavy, Ricky Justome, Harson Leonce, Laurence Hubertine, Briand Venance Pierre, Carnah Tahirisoa, Christophe Colombe, Fleurita Soamampionona Lovanirina, Vanillah Andriankaja, Rivo Robison, and Kristina Douglass

in review Adorning Localities: An Investigation of Shell Beads in Holocene Southwestern Madagascar. *The Journal of Island and Coastal Archaeology*.

Burney, David A.

1997 Tropical islands as paleoecological laboratories: gauging the consequences of human arrival. *Human Ecology* 25(3):437–457.

1999 Rates, Patterns, and Processes of Landscape Transformation and Extinction in Madagascar. In *Extinctions in Near Time*, edited by Ross D. E. MacPhee, pp. 145–164. Springer US, Boston, MA.

Burnham, Kenneth P., and David R. Anderson

2002 *Model selection and multimodel inference: a practical information-theoretic approach*. 2nd ed. Springer, New York.

CAA International

2018 Ethics Policy - CAA International. <https://caa-international.org/about/ethics-policy/>, accessed September 16, 2020.

Calleja, Javier F., Otilia Requejo Pagés, Nelson Díaz-Álvarez, Juanjo Peón, Natalia Gutiérrez, Esperanza Martín-Hernández, Alejandro Cebada Relea, David Rubio Melendi, and Paulino Fernández Álvarez

2018 Detection of buried archaeological remains with the combined use of satellite

multispectral data and UAV data. *International Journal of Applied Earth Observation and Geoinformation* 73:555–573. DOI:10.1016/j.jag.2018.07.023.

Capper, J. E.

1907 Photographs of Stonehenge as seen from a war balloon. *Archaeologia* 60:571.

Caraher, William R., Dimitri Nakassis, and David K. Pettegrew

2006 Siteless Survey and Intensive Data Collection in an Artifact-rich Environment: Case Studies from the Eastern Corinthia, Greece. *Journal of Mediterranean Archaeology* 19(1):7–43. DOI:10.17613/M6RK7G.

Carleton, W. Christopher, and Mark Collard

2019 Recent Major Themes and Research Areas in the Study of Human-Environment Interaction in Prehistory. *Environmental Archaeology*:1–17. DOI:10.1080/14614103.2018.1560932.

Carneiro, R. L.

1970 A Theory of the Origin of the State: Traditional theories of state origins are considered and rejected in favor of a new ecological hypothesis. *Science* 169(3947):733–738. DOI:10.1126/science.169.3947.733.

Carrero-Pazos, Miguel

2019 Density, intensity and clustering patterns in the spatial distribution of Galician megaliths (NW Iberian Peninsula). *Archaeological and Anthropological Sciences* 11(5):2097–2108. DOI:10.1007/s12520-018-0662-2.

Carrero-Pazos, Miguel, Andrew Bevan, and Mark W. Lake

2019 The spatial structure of Galician megalithic landscapes (NW Iberia): A case study from the Monte Penide region. *Journal of Archaeological Science* 108:104968. DOI:10.1016/j.jas.2019.05.004.

Carrero-Pazos, Miguel, Julián Bustelo-Abuín, Víctor Barbeito-Pose, and Carlos Rodríguez-Rellán

2020 Locational preferences and spatial arrangement in the barrow landscape of Serra do Barbanza (North-western Iberia). *Journal of Archaeological Science: Reports* 31:102351. DOI:10.1016/j.jasrep.2020.102351.

Casana, Jesse

2014 Regional-Scale Archaeological Remote Sensing in the Age of Big Data. *Advances in Archaeological Practice* 2(03):222–233. DOI:10.7183/2326-3768.2.3.222.

2020 Global-Scale Archaeological Prospection using CORONA Satellite Imagery: Automated, Crowd-Sourced, and Expert-led Approaches. *Journal of Field Archaeology* 45(sup1):S89–S100. DOI:10.1080/00934690.2020.1713285.

Casana, Jesse, and Elise Jakoby Laugier

2017 Satellite imagery-based monitoring of archaeological site damage in the Syrian

civil war. Edited by Peter F. Biehl. *PLOS ONE* 12(11):e0188589.
DOI:10.1371/journal.pone.0188589.

Cerrillo-Cuenca, Enrique

2017 An approach to the automatic surveying of prehistoric barrows through LiDAR. *Quaternary International* 435:135–145. DOI:10.1016/j.quaint.2015.12.099.

Cerrillo-Cuenca, Enrique, and Primitiva Bueno-Ramírez

2019 Counting with the invisible record? The role of LiDAR in the interpretation of megalithic landscapes in south-western Iberia (Extremadura, Alentejo and Beira Baixa). *Archaeological Prospection*:1–14. DOI:10.1002/arp.1738.

de Certeau, Michel

1984 *The Practice of Everyday Life*. Translated by Steven Rendell. University of California Press, Berkeley.

Charnov, Eric L.

1976 Optimal Foraging, the Marginal Value Theorem. *Theoretical Population Biology* 9(2):129–136.

Chase, A. F., D. Z. Chase, C. T. Fisher, S. J. Leisz, and J. F. Weishampel

2012 Geospatial revolution and remote sensing LiDAR in Mesoamerican archaeology. *Proceedings of the National Academy of Sciences* 109(32):12916–12921.
DOI:10.1073/pnas.1205198109.

Chase, Adrian S. Z., Diane Chase, and Arlen Chase

2020 Ethics, New Colonialism, and Lidar Data: A Decade of Lidar in Maya Archaeology. *Journal of Computer Applications in Archaeology* 3(1):51–62.
DOI:10.5334/jcaa.43.

Chen, Fulong, Rosa Lasaponara, and Nicola Masini

2017 An overview of satellite synthetic aperture radar remote sensing in archaeology: From site detection to monitoring. *Journal of Cultural Heritage* 23:5–11.
DOI:10.1016/j.culher.2015.05.003.

Cinner, Joshua E.

2008 Le rôle des tabous dans la conservation des ressources côtières à Madagascar. *Ressources marines et traditions, bulletin de la CPS* 22:15–23.

Clark, C. D., S. M. Garrod, and M. Parker Pearson

1998 Landscape archaeology and remote sensing in southern Madagascar. *International Journal of Remote Sensing* 19(8):1461–1477. DOI:10.1080/014311698215298.

Clark, G. A.

1994 Migration as an explanatory concept in paleolithic archaeology. *Journal of Archaeological Method and Theory* 1(4):305–343. DOI:10.1007/BF02242740.

- Codding, Brian F., and Douglas W. Bird
2015 Behavioral ecology and the future of archaeological science. *Journal of Archaeological Science* 56:9–20. DOI:10.1016/j.jas.2015.02.027.
- Codding, Brian F., and Terry L. Jones
2013 Environmental productivity predicts migration, demographic, and linguistic patterns in prehistoric California. *Proceedings of the National Academy of Sciences* 110(36):14569–14573. DOI:10.1073/pnas.1302008110.
- Coelho, João d'Oliveira, Robert L. Anemone, and Susana Carvalho
2021 Unsupervised learning of satellite images enhances discovery of late Miocene fossil sites in the Urema Rift, Gorongosa, Mozambique. *PeerJ* 9:e11573. DOI:10.7717/peerj.11573.
- Cohen, Anna, Sarah Klassen, and Damian Evans
2020 Ethics in Archaeological Lidar. *Journal of Computer Applications in Archaeology* 3(1):76–91.
- Colloredo-Mansfeld, Mia, Francisco J. Laso, and Javier Arce-Nazario
2020 Drone-Based Participatory Mapping: Examining Local Agricultural Knowledge in the Galapagos. *Drones* 4(4):62. DOI:10.3390/drones4040062.
- Colwell, Chip
2016 Collaborative Archaeologies and Descendant Communities. *Annual Review of Anthropology* 45(1):113–127. DOI:10.1146/annurev-anthro-102215-095937.
- Conrad, O., B. Bechtel, M. Bock, H. Dietrich, E. Fischer, L. Gerlitz, J. Wehberg, V. Wichmann, and J. Böhner
2015 System for Automated Geoscientific Analyses (SAGA) v. 2.1.4. *Geoscientific Model Development* 8(7):1991–2007. DOI:10.5194/gmd-8-1991-2015.
- Contreras, Daniel A.
2016 Correlation is not enough: Building better arguments in the archaeology of human-environment interactions. In *The Archaeology of Human-environment Interactions*, pp. 17–36. Routledge.
- Cooper, Jago, and Lindsay Duncan
2019 Applied Archaeology in the Americas: Evaluating Archaeological Solutions to the Impacts of Global Environmental Change. In *The Oxford Handbook of Historical Ecology and Applied Archaeology*, edited by Christian Isendahl and Daryl Stump, pp. 440–458. Oxford University Press.
- Cooper, Jago, and Payson Sheets
2012 *Surviving sudden environmental change: answers from archaeology*. University Press of Colorado, Boulder.

- Costenbader, Elizabeth, and Thomas W. Valente
2003 The stability of centrality measures when networks are sampled. *Social networks* 25(4):283–307.
- Crema, Enrico R, and Andrew Bevan
2021 Inference from large sets of radiocarbon dates: software and methods. *Radiocarbon* 63(1):23–39. DOI:10.1017/RDC.2020.95.
- Cripps, G., and A. Harris
2009 Community creation and management of the Velondriake marine protected area. *Blue Ventures Conservation, London. Available at.*
- Cripps, Garth
2009 Understanding migration amongst the traditional fishers of West Madagascar. *Blue Ventures Conservation Report for ReCoMaP.*
- Crossland, Zoë
2001 Time and the ancestors: landscape survey in the Andrantsay region of Madagascar. *Antiquity* 75(290):825–836. DOI:10.1017/S0003598X00089407.
- Crowley, Brooke E., Laurie R. Godfrey, Richard J. Bankoff, George H. Perry, Brendan J. Culleton, Douglas J. Kennett, Michael R. Sutherland, Karen E. Samonds, and David A. Burney
2017 Island-wide aridity did not trigger recent megafaunal extinctions in Madagascar. *Ecography* 40(8):901–912. DOI:10.1111/ecog.02376.
- Crowther, Alison, Leilani Lucas, Richard Helm, Mark Horton, Ceri Shipton, Henry T. Wright, Sarah Walshaw, Matthew Pawlowicz, Chantal Radimilahy, and Katerina Douka
2016 Ancient crops provide first archaeological signature of the westward Austronesian expansion. *Proceedings of the National Academy of Sciences* 113(24):6635–6640.
- Crumley, Carole L.
1979 Three Locational Models: An Epistemological Assessment for Anthropology and Archaeology. *Advances in Archaeological Method and Theory* 2:141–173.
- Custer, Jay F., Timothy Eveleigh, Vytautas Klemas, and Ian Wells
1986 Application of Landsat Data and Synoptic Remote Sensing to Predictive Models for Prehistoric Archaeological Sites: An Example from the Delaware Coastal Plain. *American Antiquity* 51(03):572–588. DOI:10.2307/281753.
- David, Nicholas, Judy Sterner, and Kodzo Gavua
1988 Why Pots are Decorated. *Current Anthropology* 29(3):365–389.
- Davis, Dylan S.
2017 The Applicability of Short-Wave Infrared (SWIR) Imagery for Archaeological

Landscape Classification on Rapa Nui (Easter Island), Chile. *Alpenglow: Binghamton University Undergraduate Journal of Research and Creative Activity* 3(1):7.

2019 Object-based image analysis: a review of developments and future directions of automated feature detection in landscape archaeology. *Archaeological Prospection* 26(2):155–163. DOI:10.1002/arp.1730.

2020a Studying human responses to environmental change: Trends and trajectories of archaeological research. *Environmental Archaeology* 25(4):367–380.

DOI:10.1080/14614103.2019.1639338.

2020b Geographic disparity in machine intelligence approaches for archaeological remote sensing research. *Remote Sensing* 12(1):921. DOI:10.3390/rs12060921.

2020c Defining what we study: The contribution of machine automation in archaeological research. *Digital Applications in Archaeology and Cultural Heritage* 18:e00152. DOI:10.1016/j.daach.2020.e00152.

2021 Theoretical repositioning of automated remote sensing archaeology: Shifting from features to ephemeral landscapes. *Journal of Computer Applications in Archaeology* 4(1):94–109. DOI:10.5334/jcaa.72.

Davis, Dylan S., Vanillah Andriankaja, Tahirisoa Lorine Carnat, Zafy Maharesy Chrisostome, Christophe Colombe, Felicia Fenomanana, Laurence Hubertine, Ricky Justome, François Lahiniriko, Harson Léonce, George Manahira, Briand Venance Pierre, Razafimagnefa Roi, Patricia Soafiavy, Faralahy Victorian, Vavisoa Voahirana, Barthélémy Manjakahery, and Kristina Douglass

2020 Satellite-based remote sensing rapidly reveals extensive record of Holocene coastal settlement on Madagascar. *Journal of Archaeological Science* 115:105097.

DOI:10.1016/j.jas.2020.105097.

Davis, Dylan S., Robert J. DiNapoli, and Kristina Douglass

2020 Integrating point process models, evolutionary ecology, and traditional knowledge improves landscape archaeology: A case from Southwest Madagascar. *Geosciences* 10(8):267. DOI:10.3390/geosciences10080287.

Davis, Dylan S., Robert J. DiNapoli, Matthew C. Sanger, and Carl P. Lipo

2020 The integration of lidar and legacy datasets provides improved explanations for the spatial patterning of shell rings in the American Southeast. *Advances in Archaeological Practice* 8(4):361–375. DOI:10.1017/aap.2020.18.

Davis, Dylan S., and Kristina Douglass

2020 Aerial and Spaceborne Remote Sensing in African Archaeology: A Review of Current Research and Potential Future Avenues. *African Archaeological Review* 37(1):9–24. DOI:10.1007/s10437-020-09373-y.

Davis, Dylan S., Carl P. Lipo, and Matthew C. Sanger

2019 A comparison of automated object extraction methods for mound and shell-ring identification in coastal South Carolina. *Journal of Archaeological Science: Reports* 23:166–177. DOI:10.1016/j.jasrep.2018.10.035.

Davis, Dylan S., Tanambelo Rasolondrainy, George Manahira, Sean W. Hixon, Vanillah Andriankaja, Laurence Hubertine, Ricky Justome, François Lahiniriko, Harson Léonce, Razafimagnefa Roi, Faralahy Victorian, Marius Brenah Jean Clovis, Vavisoa Voahirana, Tahirisoa Lorine Carina, Augustin Jean Yves, Zafy Maharesy Chrisostome, Barthélémy Manjakahery, and Kristina Douglass

In Review Evidence for extensive social networks as risk-mitigation strategies on Southwest Madagascar. *Antiquity*.

Davis, Dylan S., and Matthew C. Sanger

2021 Ethical Challenges in the Practice of Remote Sensing and Geophysical Archaeology. *Archaeological Prospection* 28(3):269–276. DOI:10.1002/arp.1837.

Davis, Dylan S., Matthew C. Sanger, and Carl P. Lipo

2019 Automated mound detection using lidar and object-based image analysis in Beaufort County, South Carolina. *Southeastern Archaeology* 38(1):23–37. DOI:10.1080/0734578X.2018.1482186.

De Laet, V., E. Paulissen, and M. Waelkens

2007 Methods for the extraction of archaeological features from very high-resolution Ikonos-2 remote sensing imagery, Hisar (southwest Turkey). *Journal of Archaeological Science* 34(5):830–841. DOI:10.1016/j.jas.2006.09.013.

De Laet, Véronique, Gertrud van Loon, Athena Van der Perre, Iris Deliever, and Harco Willems

2015 Integrated remote sensing investigations of ancient quarries and road systems in the Greater Dayr al-Barshā Region, Middle Egypt: a study of logistics. *Journal of Archaeological Science* 55:286–300. DOI:10.1016/j.jas.2014.10.009.

Denbow, James R.

1979 *Cenchrus ciliaris*: an ecological indicator of Iron Age middens using aerial photography in eastern Botswana. *South African Journal of Science* 75(9):405–408.

Dennis, L. Meghan

2020 Digital Archaeological Ethics: Successes and Failures in Disciplinary Attention. *Journal of Computer Applications in Archaeology* 3(1):210–218. DOI:10.5334/jcaa.24.

Deschamps, Hubert

1959 *Les migrations intérieures passées et présentes à Madagascar*. Éditions Berger-Levrault, Paris.

Dewar, R. E., C. Radimilahy, H. T. Wright, Z. Jacobs, G. O. Kelly, and F. Berna

2013 Stone tools and foraging in northern Madagascar challenge Holocene extinction models. *Proceedings of the National Academy of Sciences* 110(31):12583–12588. DOI:10.1073/pnas.1306100110.

Dewar, R. E., and A. F. Richard

2007a Evolution in the hypervariable environment of Madagascar. *Proceedings of the National Academy of Sciences* 104(34):13723–13727. DOI:10.1073/pnas.0704346104.

2007b Evolution in the hypervariable environment of Madagascar. *Proceedings of the National Academy of Sciences* 104(34):13723–13727. DOI:10.1073/pnas.0704346104.

Dewar, Robert E.

1984 Extinctions in Madagascar: the loss of the subfossil fauna. In *Quarternary Extinctions*, edited by P. S. Martin and R. G. Klein, pp. 574–593. University of Arizona Press, Tuscon.

1997 Does It Matter that Madagascar is an Island? *Human Ecology* 25(3):481–489.

Dewar, Robert E., and Alison F. Richard

2012 Madagascar: A History of Arrivals, What Happened, and Will Happen Next. *Annual Review of Anthropology* 41(1):495–517. DOI:10.1146/annurev-anthro-092611-145758.

Dewar, Robert E., and Henry T. Wright

1993 The culture history of Madagascar. *Journal of World Prehistory* 7(4):417–466. DOI:10.1007/BF00997802.

DiNapoli, Robert J., Carl P. Lipo, Tanya Brosnan, Terry L. Hunt, Sean Hixon, Alex E. Morrison, and Matthew Becker

2019 Rapa Nui (Easter Island) monument (ahu) locations explained by freshwater sources. Edited by John P. Hart. *PLOS ONE* 14(1):e0210409.

DOI:10.1371/journal.pone.0210409.

DiNapoli, Robert J., and Alex E. Morrison

2017 Human behavioural ecology and Pacific archaeology. *Archaeology in Oceania* 52(1):1–12. DOI:10.1002/arco.5124.

Dodge, Yadolah

2008 Chi-Square Distance. In *The Concise Encyclopedia of Statistics*, pp. 68–70. Springer New York, New York, NY.

Domic, A. I., Sean W. Hixon, M. I. Velez, S. J. Ivory, Kristina Douglass, M. Brenner, and Douglas J. Kennett

In Review Influence of Late Holocene climate change and human land-use on terrestrial and aquatic ecosystems in southwest Madagascar. *Frontiers in Ecology and Evolution*.

Douglass, Kristina

2016 An Archaeological Investigation of Settlement and Resource Exploitation Patterns in the Velondriake Marine Protected Area, Southwest Madagascar, ca. 900 BC to AD 1900. Unpublished PhD Dissertation, Yale University.

2017 The Diversity of Late Holocene Shellfish Exploitation in Velondriake, Southwest Madagascar. *The Journal of Island and Coastal Archaeology* 12(3):333–359. DOI:10.1080/15564894.2016.1216480.

Douglass, Kristina, Annie R. Antonites, Eréndira M. Quintana Morales, Alicia Grealy, Michael Bunce, Chriselle Bruwer, and Charlotte Gough
2018 Multi-analytical approach to zooarchaeological assemblages elucidates Late Holocene coastal lifeways in southwest Madagascar. *Quaternary International* 471:111–131. DOI:10.1016/j.quaint.2017.09.019.

Douglass, Kristina, and Jago Cooper
2020 Archaeology, environmental justice, and climate change on islands of the Caribbean and southwestern Indian Ocean. *Proceedings of the National Academy of Sciences* 117(5):8254–8262. DOI:10.1073/pnas.1914211117.

Douglass, Kristina, Sean Hixon, Henry T. Wright, Laurie R. Godfrey, Brooke E. Crowley, Barthélémy Manjakahery, Tanambelo Rasolondrainy, Zoë Crossland, and Chantal Radimilahy
2019 A critical review of radiocarbon dates clarifies the human settlement of Madagascar. *Quaternary Science Reviews* 221:105878. DOI:10.1016/j.quascirev.2019.105878.

Douglass, Kristina, Eréndira Quintana Morales, George Manahira, Felicia Fenomanana, Roger Samba, Francois Lahiniriko, Zafy Maharesy Chrisostome, Voahirana Vavisoa, Patricia Soafiavy, Ricky Justome, Harson Leonce, Laurence Hubertine, Briand Venance Pierre, Carnah Tahirisoa, Christoph Sakisy Colomb, Fleurita Soamampionona Lovanirina, Vanillah Andriankaja, and Rivo Robison
2019 Toward a just and inclusive environmental archaeology of southwest Madagascar. *Journal of Social Archaeology* 19(3):307–332. DOI:10.1177/1469605319862072.

Douglass, Kristina, Eréndira M. Quintana Morales, Tanambelo Rasolondrainy, George Manahira, Barthélémy Manjakahery, Rosily, Adolphe Ediedy, Florence Mampibay, Heritiana Rabekoto, Patricia Rasoafiavy, Zafy Chrisostome Maharesy, Danielle Buffa, Dylan S. Davis, and Eric Burkhart
In Preparation The Vezo Ecological Knowledge Exchange. *Journal of Ethnobiology*.

Douglass, Kristina, and Tanambelo Rasolondrainy
2021 Social memory and niche construction in a hypervariable environment. *American Journal of Human Biology*. DOI:10.1002/ajhb.23557, accessed January 4, 2021.

Douglass, Kristina, Jonathan Walz, Eréndira Quintana-Morales, Richard Marcus, Garth Myers, and Jacques Pollini
2019 Historical perspectives on contemporary human-environment dynamics in southeast Africa. *Conservation Biology* 33(2):260–274. DOI:10.1111/cobi.13244.

Douglass, Kristina, and Jens Zinke

- 2015 Forging Ahead By Land and By Sea: Archaeology and Paleoclimate Reconstruction in Madagascar. *African Archaeological Review* 32(2):267–299. DOI:10.1007/s10437-015-9188-5.
- Dunn, Christine E.
2007 Participatory GIS — a people’s GIS? *Progress in Human Geography* 31(5):616–637. DOI:10.1177/0309132507081493.
- Dunnavant, Justin P.
2021 Have Confidence in the Sea: Maritime Maroons and Fugitive Geographies. *Antipode* 53(3):884–905. DOI:10.1111/anti.12695.
- Dunnell, Robert C.
1992 The Notion Site. In *Space, Time, and Archaeological Landscapes*, edited by Jacqueline Rossignol and LuAnn Wandsnider, pp. 21–41. Springer US, Boston, MA.
- Dunnell, Robert C., and William S. Dancey
1983 The Siteless Survey: A Regional Scale Data Collection Strategy. *Advances in Archaeological Method and Theory* 6:267–287. DOI:10.1016/B978-0-12-003106-1.50012-2.
- Ehrman-Solberg, Kevin, Bonnie Keeler, Kate Derickson, and Kirsten Delegard
2020 Mapping a path towards equity: reflections on a co-creative community praxis. *GeoJournal*:1–10.
- El-Baz, Farouk
1998 Aeolian deposits and palaeo-rivers of the eastern Sahara. Significance to archaeology and groundwater exploration. *Sahara (Segrate)*(10):55–66.
- Ellis, Erle C.
2021 Land Use and Ecological Change: A 12,000-Year History. *Annual Review of Environment and Resources* 46(1):1–33. DOI:10.1146/annurev-environ-012220-010822.
- Ellis, Erle C., Nicolas Gauthier, Kees Klein Goldewijk, Rebecca Bliege Bird, Nicole Boivin, Sandra Díaz, Dorian Q. Fuller, Jacquelyn L. Gill, Jed O. Kaplan, Naomi Kingston, Harvey Locke, Crystal N. H. McMichael, Darren Ranco, Torben C. Rick, M. Rebecca Shaw, Lucas Stephens, Jens-Christian Svenning, and James E. M. Watson
2021 People have shaped most of terrestrial nature for at least 12,000 years. *Proceedings of the National Academy of Sciences* 118(17):e2023483118. DOI:10.1073/pnas.2023483118.
- Ellison, James, Peter Robertshaw, Diane Gifford-Gonzalez, Roderick J. McIntosh, Ann B. Stahl, Christopher R. DeCorse, Larry H. Robbins, Susan Kent, Adoum Ngaba-Waye, and Mohamed Sahnouni
1996 The future of African archaeology. *The African Archaeological Review*:5–34.

Elsawah, Sondoss, Tatiana Filatova, Anthony J. Jakeman, Albert J. Kettner, Moira L. Zellner, Ioannis N. Athanasiadis, Serena H. Hamilton, Robert L. Axtell, Daniel G. Brown, Jonathan M. Gilligan, Marco A. Janssen, Derek T. Robinson, Julie Rozenberg, Isaac I. T. Ullah, and Steve J. Lade

2020 Eight grand challenges in socio-environmental systems modeling. *Socio-Environmental Systems Modelling* 2:16226. DOI:10.18174/sesmo.2020a16226.

Erdman, Chandra, and John W. Emerson

2008 bcp: An R Package for Performing a Bayesian Analysis of Change Point Problems. *Journal of Statistical Software* 23:1–13. DOI:10.18637/jss.v023.i03.

Erlandson, Jon McVey

2012 As the world warms: rising seas, coastal archaeology, and the erosion of maritime history. *Journal of Coastal Conservation* 16(2):137–142. DOI:10.1007/s11852-010-0104-5.

ESRI

2020 *ArcGIS*. Environmental Systems Research Institute, Inc., Redlands, CA.

Eubanks, V.

2017 *Automating inequality: How high-tech tools profile, police, and punish the poor*. St. Martin's Press.

Evans, D. H., R. J. Fletcher, C. Pottier, J.-B. Chevance, D. Soutif, B. S. Tan, S. Im, D. Ea, T. Tin, S. Kim, C. Cromarty, S. De Greef, K. Hanus, P. Baty, R. Kuszinger, I. Shimoda, and G. Boornazian

2013 Uncovering archaeological landscapes at Angkor using lidar. *Proceedings of the National Academy of Sciences* 110(31):12595–12600. DOI:10.1073/pnas.1306539110.

Eve, Stuart J., and Enrico R. Crema

2014 A house with a view? Multi-model inference, visibility fields, and point process analysis of a Bronze Age settlement on Leskernick Hill (Cornwall, UK). *Journal of Archaeological Science* 43:267–277.

Evers, S. J. T., and Caroline Seagle

2012 Stealing the sacred: Why 'global heritage' discourse is perceived as a frontal attack on local heritage-making in Madagascar. *Madagascar Conservation & Development* 7(2S):97–106.

Evers, T. M.

1975 Recent iron age research in the eastern Transvaal, South Africa. *The South African Archaeological Bulletin*:71–83.

Exelis Visual Information Solutions

2009 *ENVI*. Exelis Visual Information Solutions, Boulder, Colorado.

- Faina, Peterson, Stephen J. Burns, Laurie R Godfrey, Brooke E. Crowley, Nick Scroxton, David McGee, Michael R. Sutherland, and Lovasoa Ranivoharimanana
2021 Comparing the paleoclimates of northwestern and southwestern Madagascar during the late Holocene: implications for the role of climate in megafaunal extinction. *Malagasy Nature* 15:108–127.
- Fisher, Michael, Michael Fradley, Pascal Flohr, Bijan Rouhani, and Francesca Simi
2021 Ethical considerations for remote sensing and open data in relation to the endangered archaeology in the Middle East and North Africa project. *Archaeological Prospection* 28(3). DOI:10.1002/arp.1816, accessed March 25, 2021.
- Fishman, Ram Mukul, Tobias Siegfried, Pradeep Raj, Vijay Modi, and Upmanu Lall
2011 Over-extraction from shallow bedrock versus deep alluvial aquifers: Reliability versus sustainability considerations for India’s groundwater irrigation. *Water Resources Research* 47(6).
- Foucault, Michel
1995 *Discipline and Punish: The Birth of the Prison*. Vintage Books, New York.
- Fournier, Gabriel
1973 Villages fortifiés et histoire du peuplement à Madagascar. *Archéologie médiévale* 3(1):432–435. DOI:10.3406/arcme.1973.1277.
- Fradley, Michael, and Nichole Sheldrick
2017 Satellite imagery and heritage damage in Egypt: a response to Parcak et al.(2016). *Antiquity* 91(357):784–792.
- Francioni, Francesco, and Federico Lenzerini
2006 The obligation to prevent and avoid destruction of cultural heritage: From Bamiyan to Iraq. In *Art and Cultural Heritage: Law, Policy and Practice*, edited by Barbara T. Hoffman, pp. 28–40. Cambridge University Press, Cambridge.
- Freeland, Travis, Brandon Heung, David V. Burley, Geoffrey Clark, and Anders Knudby
2016 Automated feature extraction for prospection and analysis of monumental earthworks from aerial LiDAR in the Kingdom of Tonga. *Journal of Archaeological Science* 69:64–74. DOI:10.1016/j.jas.2016.04.011.
- Freeman, Jacob, and Jacopo A. Baggio
2017 The effect of ownership on ecosystem management among human foragers. *Quaternary International*. DOI:10.1016/j.quaint.2017.12.004, accessed January 13, 2019.
- Fretwell, Stephen Dewitt, and Henry L. Lucas
1969 On territorial behavior and other factors influencing habitat distribution in birds: I. Theoretical development. *Acta Biotheoretica* 19(1):16–36. DOI:10.1007/BF01601953.

- Fritz-Vietta, Nadine V.M., H. Stone Tahirindraza, and Susanne Stoll-Kleemann
 2017 Local people's knowledge with regard to land use activities in southwest Madagascar – Conceptual insights for sustainable land management. *Journal of Environmental Management* 199:126–138. DOI:10.1016/j.jenvman.2017.05.034.
- Fuentes, Agustin
 2016 The Extended Evolutionary Synthesis, Ethnography, and the Human Niche: Toward an Integrated Anthropology. *Current Anthropology* 57(S13):S13–S26. DOI:10.1086/685684.
- Fuller, D. Q., T. Denham, M. Arroyo-Kalin, L. Lucas, C. J. Stevens, L. Qin, R. G. Allaby, and M. D. Purugganan
 2014 Convergent evolution and parallelism in plant domestication revealed by an expanding archaeological record. *Proceedings of the National Academy of Sciences* 111(17):6147–6152. DOI:10.1073/pnas.1308937110.
- Gabrielli, Christopher P., J. J. McDonnell, and W. T. Jarvis
 2012 The role of bedrock groundwater in rainfall–runoff response at hillslope and catchment scales. *Journal of Hydrology* 450:117–133.
- Galič, Maša, Tjerk Timan, and Bert-Jaap Koops
 2017 Bentham, Deleuze and Beyond: An Overview of Surveillance Theories from the Panopticon to Participation. *Philosophy & Technology* 30(1):9–37. DOI:10.1007/s13347-016-0219-1.
- Gallivan, Martin, Danielle Moretti-Langholtz, and Buck Woodard
 2011 Collaborative archaeology and strategic essentialism: Native empowerment in Tidewater Virginia. *Historical Archaeology* 45(1):10–23.
- Gao, Bo-Cai
 1996 NDWI—A normalized difference water index for remote sensing of vegetation liquid water from space. *Remote sensing of environment* 58(3):257–266.
- García-Granero, Juan José, Carla Lancelotti, and Marco Madella
 2015 A tale of multi-proxies: integrating macro- and microbotanical remains to understand subsistence strategies. *Vegetation History and Archaeobotany* 24(1):121–133. DOI:10.1007/s00334-014-0486-7.
- Gard, J., and Raymond Mauny
 1961 Découverte de tumulus dans la région de Diourbel (Sénégal). *Notes Africaines* 89:10–11.
- Garzelli, A., F. Nencini, L. Alparone, B. Aiazzi, and S. Baronti
 2004 Pan-sharpening of multispectral images: a critical review and comparison. In

IGARSS 2004. 2004 IEEE International Geoscience and Remote Sensing Symposium, 1:pp. 84.

Gautier, L., and S. M. Goodman

2003 Introduction to the flora of Madagascar. In *The Natural History of Madagascar*, edited by S. M. Goodman and Jonathan P. Benstead, pp. 221–250. University of Chicago Press, Chicago.

Getis, Arthur, and J. Keith Ord

1992 The Analysis of Spatial Association by Use of Distance Statistics. *Geographical Analysis* 24. Advances in Spatial Science:189–206. DOI:10.1007/978-3-642-01976-0_10.

Godfrey, Laurie R, and Kristina Douglass

in press New insights into the relationship between human ecological pressures and the vertebrate extinctions. In *The New Natural History of Madagascar*, edited by S. M. Goodman. Princeton University Press, Princeton.

Godfrey, Laurie R., Nick Scroxton, Brooke E. Crowley, Stephen J. Burns, Michael R. Sutherland, Ventura R. Pérez, Peterson Faina, David McGee, and Lovasoa Ranivoharimanana

2019 A new interpretation of Madagascar’s megafaunal decline: The “Subsistence Shift Hypothesis.” *Journal of Human Evolution* 130:126–140. DOI:10.1016/j.jhevol.2019.03.002.

Gogarty, Brendan, and Meredith Hagger

2008 The laws of man over vehicles unmanned: The legal response to robotic revolution on sea, land and air. *JL Inf. & Sci.* 19:73.

Gommery, Dominique, Beby Ramanivosoa, Martine Faure, Claude Guérin, Patrice Kerloc’h, Frank Sénégas, and Hervé Randrianantenaina

2011 Les plus anciennes traces d’activités anthropiques de Madagascar sur des ossements d’hippopotames subfossiles d’Anjohibe (Province de Mahajanga). *Comptes Rendus Palevol* 10(4):271–278. DOI:10.1016/j.crpv.2011.01.006.

Gondal, Neha, and Paul D. McLean

2013 What makes a network go round? Exploring the structure of a strong component with exponential random graph models. *Social networks* 35(4):499–513.

Gordon, R. J.

1997 *Picturing bushmen: The Denver African expedition of 1925*. Ohio University Press.

Gorelick, Noel, Matt Hancher, Mike Dixon, Simon Ilyushchenko, David Thau, and Rebecca Moore

2017 Google Earth Engine: Planetary-scale geospatial analysis for everyone. *Remote sensing of Environment* 202:18–27.

Graeber, David, and David Wengrow

2021 *The Dawn of Everything: A New History of Humanity*. First Edition. Farrer, Straus and Giroux, New York.

Grandidier, Alfred, and Guillaume Grandidier

1903 *Collections des ouvrages anciens concernant Madagascar*. Vol. Tome I. Ouvrages ou extraits d'ouvrages portugais, hollandais, anglais, français, allemands, italiens, espagnols et latins relatifs à Madagascar: 1500 à 1613. Comité de Madagascar, Paris.

1904 *Collections des ouvrages anciens concernant Madagascar*. Vol. Tome II. Ouvrages ou extraits d'ouvrages français (jusqu'à 1630), portugais, hollandais, anglais, allemands, italiens, espagnols et latins relatifs à Madagascar (1613 à 1640). Comité de Madagascar, Paris.

1906 *Collections des ouvrages anciens concernant Madagascar*. Vol. Tome IV. Les Aventures de Robert Drury pendant ses quinze années de captivité à Madagascar (1701-1717 et 1719-1720). Comité de Madagascar, Paris.

1907 *Collections des ouvrages anciens concernant Madagascar*. Vol. Tome IV. Ouvrages ou extraits d'ouvrages anglais, hollandais, portugais, espagnols, suédois et russes (1718-1800). Comité de Madagascar, Paris.

Granovetter, Mark S.

1973 The Strength of Weak Ties. *American Journal of Sociology* 78(6):1360–1380.

Green, Adam S., and Cameron A. Petrie

2018 Landscapes of Urbanization and De-Urbanization: A Large-Scale Approach to Investigating the Indus Civilization's Settlement Distributions in Northwest India. *Journal of Field Archaeology*:1–16. DOI:10.1080/00934690.2018.1464332.

Green, Ernestene L.

1973 Location analysis of prehistoric Maya sites in Northern British Honduras. *American Antiquity* 38(3):279–293.

Green, Lesley Fordred, David R. Green, and Eduardo Góes Neves

2003 Indigenous Knowledge and Archaeological Science: The Challenges of Public Archaeology in the Reserva Uaçá. *Journal of Social Archaeology* 3(3):366–398. DOI:10.1177/14696053030033005.

Griffin, William D.

2009 The Matitanana Archaeological Project: Culture History and Social Complexity in the Seven Rivers Region of Southeastern Madagascar. Unpublished PhD Thesis.

Grove, C. A., J. Zinke, F. Peeters, W. Park, T. Scheufen, S. Kasper, B. Randriamanantsoa, M. T. McCulloch, and G.-J. A. Brummer

2012 Madagascar corals reveal Pacific multidecadal modulation of rainfall since 1708. *Climate of the Past Discussions* 8(2):787–817. DOI:10.5194/cpd-8-787-2012.

- Grove, C., Jens Zinke, F. Peeters, Wonsun Park, T. Scheufen, S. Kasper, B. Randriamanantsoa, Malcolm McCulloch, and G. Brummer
2013 Madagascar corals reveal a multidecadal signature of rainfall and river runoff since 1708. *Climate of the Past* 9(2):641–656.
- d’Alpoim Guedes, Jade A., Stefani A. Crabtree, R. Kyle Bocinsky, and Timothy A. Kohler
2016 Twenty-first century approaches to ancient problems: Climate and society. *Proceedings of the National Academy of Sciences* 113(51):14483–14491. DOI:10.1073/pnas.1616188113.
- Gupta, Neha, Sue Blair, and Ramona Nicholas
2020 What We See, What We Don’t See: Data Governance, Archaeological Spatial Databases and the Rights of Indigenous Peoples in an Age of Big Data. *Journal of Field Archaeology* 45(sup1):S39–S50. DOI:10.1080/00934690.2020.1713969.
- Guyot, Alexandre, Laurence Hubert-Moy, and Thierry Lorho
2018 Detecting Neolithic Burial Mounds from LiDAR-Derived Elevation Data Using a Multi-Scale Approach and Machine Learning Techniques. *Remote Sensing* 10(2):225. DOI:10.3390/rs10020225.
- Hacıgüzeller, Piraye
2012 GIS, critique, representation and beyond. *Journal of Social Archaeology* 12(2):245–263. DOI:10.1177/1469605312439139.
- Haggerty, K.
2006 Tear down the walls: On demolishing the panopticon. In *Theorising surveillance: The panopticon and beyond*, edited by D. Lyon, pp. 23–45. Willan Publishing.
- Haight, Frank Avery
1967 Handbook of the Poisson distribution.
- Hamer, Wolfgang B., Daniel Knitter, Sonja B. Grimm, Benjamin Serbe, Berit Valentin Eriksen, Oliver Nakoinz, and Rainer Duttman
2019 Location Modeling of Final Palaeolithic Sites in Northern Germany. *Geosciences* 9(10):430. DOI:10.3390/geosciences9100430.
- Haney, William M.
2015 Protecting tribal skies: Why Indian tribes possess the sovereign authority to regulate tribal airspace. *Am. Indian L. Rev.* 40:1.
- Hanna, Jonathan A., and Christina M. Giovas
2019 An Islandscape IFD: Using the Ideal Free Distribution to Predict Pre-Columbian Settlements from Grenada to St. Vincent, Eastern Caribbean. *Environmental Archaeology*:1–18. DOI:10.1080/14614103.2019.1689895.

Hansford, James P., Patricia C. Wright, Ventura R. Pérez, Kathleen M. Muldoon, Samuel T. Turvey, and Laurie R. Godfrey

2020 Evidence for early human arrival in Madagascar is robust: A response to Mitchell. *The Journal of Island and Coastal Archaeology*:1–7.

DOI:10.1080/15564894.2020.1771482.

Hansford, James, Patricia C. Wright, Armand Rasoamiamanana, Ventura R. Pérez, Laurie R. Godfrey, David Errickson, Tim Thompson, and Samuel T. Turvey

2018 Early Holocene human presence in Madagascar evidenced by exploitation of avian megafauna. *Science Advances* 4(9):eaat6925. DOI:10.1126/sciadv.aat6925.

Harlan, Jack R., and Ann B. Stemler

2011 The races of sorghum in Africa. In *Origins of African Plant Domestication*, edited by Jack R. Harlan, pp. 465–478. Walter de Gruyter.

Harmanşah, Ömür

2015 ISIS, Heritage, and the Spectacles of Destruction in the Global Media. *Near Eastern Archaeology* 78(3):170–177.

Harris, Alasdair

2007 “To live with the Sea” Development of the Velondriake community-managed protected area network, southwest Madagascar. *Madagascar Conservation & Development* 2(1).

Harris, Ar

2011 Out of sight but no longer out of mind: A climate of change for marine conservation in Madagascar. *Madagascar Conservation & Development* 6(1).

DOI:10.4314/mcd.v6i1.68058, accessed October 10, 2019.

Harrower, Michael J., Jared Schuetter, Joy McCorriston, Prem K. Goel, and Matthew J. Senn

2013 Survey, Automated Detection, and Spatial Distribution Analysis of Cairn Tombs in Ancient Southern Arabia. In *Mapping Archaeological Landscapes from Space*, 5:pp. 259–268. Springer New York, New York, NY.

Hartmann, W., J. Silvester, and P. Hayes

1999 *The colonising camera: Photographs in the making of Namibian history*. Juta and Company.

Hausmann, Sonja, Isabelle Larocque-Tobler, Pierre J.H. Richard, Reinhard Pienitz, Guillaume St-Onge, and Falko Fye

2011 Diatom-inferred wind activity at Lac du Sommet, southern Québec, Canada: A multiproxy paleoclimate reconstruction based on diatoms, chironomids and pollen for the past 9500 years. *The Holocene* 21(6):925–938. DOI:10.1177/0959683611400199.

- Hay, Geoffrey J., and Guillermo Castilla
2008 Geographic Object-Based Image Analysis (GEOBIA): A new name for a new discipline. In *Object-Based Image Analysis*, edited by T. Blaschke, S. Lang, and G. Hay, pp. 75–89. Springer, Heidelberg, Berlin, New York.
- Heaton, Timothy J., Peter Köhler, Martin Butzin, Edouard Bard, Ron W. Reimer, William EN Austin, Christopher Bronk Ramsey, Pieter M. Grootes, Konrad A. Hughen, and Bernd Kromer
2020 Marine20—the marine radiocarbon age calibration curve (0–55,000 cal BP). *Radiocarbon* 62(4):779–820.
- Heckenberger, Michael, and Eduardo Góes Neves
2009 Amazonian Archaeology. *Annual Review of Anthropology* 38(1):251–266. DOI:10.1146/annurev-anthro-091908-164310.
- Hengl, Tomislav, Gerard BM Heuvelink, Bas Kempen, Johan GB Leenaars, Markus G. Walsh, Keith D. Shepherd, Andrew Sila, Robert A. MacMillan, Jorge Mendes de Jesus, and Lulseged Tamene
2015 Mapping soil properties of Africa at 250 m resolution: Random forests significantly improve current predictions. *PloS one* 10(6).
- Hennekam, Rick, Jens Zinke, Erik van Sebille, Malou ten Have, Geert-Jan A. Brummer, and Gert-Jan Reichart
2018 Cocos (Keeling) corals reveal 200 years of multidecadal modulation of southeast Indian Ocean hydrology by Indonesian throughflow. *Paleoceanography and Paleoclimatology* 33(1):48–60.
- Heslin, Alison, Natalie Delia Deckard, Robert Oakes, and Arianna Montero-Colbert
2019 Displacement and Resettlement: Understanding the Role of Climate Change in Contemporary Migration. *Loss and Damage from Climate Change*:237–258. DOI:10.1007/978-3-319-72026-5_10.
- Hesse, Ralf
2010 LiDAR-derived Local Relief Models - a new tool for archaeological prospection. *Archaeological Prospection* 17(2):67–72. DOI:10.1002/arp.374.
- Heurtebize, G., and P. Vérin
1974 Premières découvertes sur l'ancienne culture de l'intérieur de l'Androy (Madagascar). Archéologie de la vallée du Lambomaty sur la haute Manambovo. *Journal de la Société des Africanistes* 44(2):113–121. DOI:10.3406/jafr.1974.1752.
- Hijmans, Robert J.
2019 *raster: Geographic Data Analysis and Modeling*.
- Hixon, Sean W., Jason H. Curtis, Mark Brenner, Kristina G. Douglass, Alejandra I.

- Domic, Brendan J. Culleton, Sarah J. Ivory, and Douglas J. Kennett
 2021 Drought coincided with, but does not explain, late holocene megafauna extinctions in SW Madagascar. *Climate* 9(9):138.
- Hixon, Sean W., Kristina Douglass, Lucien M. Rakotozafy, G. Clark, Atholl Anderson, Simon Haberle, and Douglas J. Kennett
 2021 Late Holocene spread of pastoralism coincides with endemic megafaunal extinction in Madagascar. *Proceedings of the Royal Society B* 288(1955):20211204. DOI:10.1098/rspb.2021.1204.
- Hixon, Sean W., Emma A. Elliott Smith, Brooke E. Crowley, George H. Perry, Jeannot Randrianasy, Jean Freddy Ranaivoarisoa, Douglas J. Kennett, and Seth D. Newsome
 2018 Nitrogen isotope ($\delta^{15}\text{N}$) patterns for amino acids in lemur bones are inconsistent with aridity driving megafaunal extinction in south-western Madagascar. *Journal of Quaternary Science* 33(8):958–968. DOI:10.1002/jqs.3073.
- Hobson, Matthew S.
 2019 EAMENA training in the use of satellite remote sensing and digital technologies in heritage management: Libya and Tunisia workshops 2017–2019. *Libyan Studies* 50:63–71.
- Hogg, Alan G, Timothy J Heaton, Quan Hua, Jonathan G Palmer, Chris SM Turney, John Southon, Alex Bayliss, Paul G Blackwell, Gretel Boswijk, Christopher Bronk Ramsey, Charlotte Pearson, Fiona Petchey, Paula Reimer, Ron Reimer, and Lukas Wacker
 2020 SHCal20 SOUTHERN HEMISPHERE CALIBRATION, 0–55,000 YEARS CAL BP. *Radiocarbon*:1–20. DOI:10.1017/RDC.2020.59.
- Hogg, Robert V., Joseph McKean, and Allen T. Craig
 2005 *Introduction to mathematical statistics*. Pearson Education.
- Hopp, Luisa, and Jeffrey J. McDonnell
 2009 Connectivity at the hillslope scale: Identifying interactions between storm size, bedrock permeability, slope angle and soil depth. *Journal of Hydrology* 376(3–4):378–391.
- Howey, Meghan C. L., Michael W. Palace, and Crystal H. McMichael
 2016 Geospatial modeling approach to monument construction using Michigan from A.D. 1000–1600 as a case study. *Proceedings of the National Academy of Sciences* 113(27):7443–7448. DOI:10.1073/pnas.1603450113.
- Hua, Quan, Jocelyn C. Turnbull, Guaciara M. Santos, Andrzej Z. Rakowski, Santiago Ancapichún, Ricardo De Pol-Holz, Samuel Hammer, Scott J. Lehman, Ingeborg Levin, and John B. Miller
 2021 Atmospheric radiocarbon for the period 1950–2019. *Radiocarbon*:1–23.
- Huete, A.R

1988 A soil-adjusted vegetation index (SAVI). *Remote Sensing of Environment* 25(3):295–309. DOI:10.1016/0034-4257(88)90106-X.

Huffman, Thomas N.

1986 Archaeological evidence and conventional explanations of southern Bantu settlement patterns. *Africa* 56(3):280–298.

Huntington, Henry, Terry Callaghan, Shari Fox, and Igor Krupnik

2004 Matching Traditional and Scientific Observations to Detect Environmental Change: A Discussion on Arctic Terrestrial Ecosystems. *Ambio*:18–23.

Ichikawa, Dorj, and Koji Wakamori

2018 The Integrated Use of Landsat, Sentinel-2 and PlanetScope Satellite Data for Crop Monitoring. In *IGARSS 2018-2018 IEEE International Geoscience and Remote Sensing Symposium*, pp. 7707–7710. IEEE.

IDMC

2020 *Mid-Year Figures: Internal Displacement from January to June 2020*. Internal Displacement Monitoring Centre, Geneva.

2021 *Global Report on Internal Displacement 2021: Internal displacement in a changing climate*. Internal Displacement Monitoring Centre, Geneva.

Iida, Taku

2005 The past and present of the coral reef fishing economy in Madagascar: implications for self determination in resource use. *Senri Ethnological Studies* 67:237–258.

Ingold, Tim

1993 The Temporality of the Landscape. *World Archaeology* 25(2):152–174.

Inomata, Takeshi, Daniela Triadan, Flory Pinzón, Melissa Burham, José Luis Ranchos, Kazuo Aoyama, and Tsuyoshi Haraguchi

2018 Archaeological application of airborne LiDAR to examine social changes in the Ceibal region of the Maya lowlands. Edited by John P. Hart. *PLOS ONE* 13(2):e0191619. DOI:10.1371/journal.pone.0191619.

Iovita, Radu, David R. Braun, Matthew J. Douglass, Simon J. Holdaway, Sam C. Lin, Deborah I. Olszewski, and Zeljko Rezek

2021 Operationalizing niche construction theory with stone tools. *Evolutionary Anthropology: Issues, News, and Reviews* n/a(n/a).

DOI:<https://doi.org/10.1002/evan.21881>, accessed January 21, 2021.

IPCC

2018 *Global Warming of 1.5 °C: an IPCC special report on the impacts of global warming of 1.5 °C above pre-industrial levels and related global greenhouse gas emission pathways, in the context of strengthening the global response to the threat of*

- climate change, sustainable development, and efforts to eradicate poverty.*
Intergovernmental Panel on Climate Change, Incheon, Republic of Korea.
2021 *Climate Change 2021: The Physical Science Basis. Contribution of Working Group I to the Sixth Assessment Report of the Intergovernmental Panel on Climate Change.* Edited by V. Masson-Delmotte, P. Zhai, A. Pirani, S. L. Connors, C. Péan, S. Berger, N. Caud, Y. Chen, L. Goldfarb, M. I. Gomis, M. Huang, K. Leitzell, E. Lonnoy, J. B. R. Matthews, T. K. Maycock, T. Waterfield, O. Yelekçi, R. Yu, and B. Zhou. Cambridge University Press.
- 2022 *Climate Change 2022: Impacts, Adaptation and Vulnerability.* Edited by H.-O. Pörtner, D. C. Roberts, M. Tignor, E. S. Poloczanska, K. Mintenbeck, A. Alegria, M. Craig, S. Langsdorf, S. Löschke, V. Möller, A. Okem, and B. Rama. Contribution of Working Group II to the Sixth Assessment Report of the Intergovernmental Panel on Climate Change. Cambridge University Press.
- Jahjah, Munzer, Carlo Ulivieri, Antonio Invernizzi, and Roberto Parapetti
2007 Archaeological remote sensing application pre-post war situation of Babylon archaeological site—Iraq. *Acta Astronautica* 61(1–6):121–130.
DOI:10.1016/j.actaastro.2007.01.034.
- Janssen, Marco A., Örjan Bodin, John M. Anderies, Thomas Elmqvist, Henrik Ernstson, Ryan R. J. McAllister, Per Olsson, and Paul Ryan
2006 Toward a Network Perspective of the Study of Resilience in Social-Ecological Systems. *Ecology and Society* 11(1). accessed November 12, 2021.
- Jazwa, Christopher S., and Stephen A. Collins-Elliott
2021 An ecological model of settlement expansion in northwestern Morocco. *Quaternary International*. DOI:10.1016/j.quaint.2020.12.037, accessed March 28, 2021.
- Jazwa, Christopher S., Douglas J. Kennett, Bruce Winterhalder, and Terry L. Joslin
2017 Territoriality and the rise of despotic social organization on western Santa Rosa Island, California. *Quaternary International*. DOI:10.1016/j.quaint.2017.11.009, accessed October 2, 2018.
- Jenks, George F.
1967 The data model concept in statistical mapping. *International yearbook of cartography* 7:186–190.
- Jensen, John R.
2007 *Remote Sensing of the Environment: An Earth Resource Perspective.* 2nd ed. Pearson Prentice Hall, Upper Saddle River, NJ.
- Jochim, Michael A.
1976 *Hunter-gatherer subsistence and settlement: a predictive model.* 330.901 JOC. CIMMYT.
- Johnson, Katharine M., and William B. Ouimet

2014 Rediscovering the lost archaeological landscape of southern New England using airborne light detection and ranging (LiDAR). *Journal of Archaeological Science* 43:9–20. DOI:10.1016/j.jas.2013.12.004.

Jones, Clive G., Jorge L. Gutiérrez, James E. Byers, Jeffrey A. Crooks, John G. Lambrinos, and Theresa S. Talley
2010 A framework for understanding physical ecosystem engineering by organisms. *Oikos* 119(12):1862–1869.

Jones, Clive G., John H. Lawton, and Moshe Shachak
1994 Organisms as ecosystem engineers. In *Ecosystem management*, pp. 130–147. Springer.

Jones, Peta
1978 An approach to stone settlement typology of the late Iron Age: stone walling on the Klip River 27 10's 29 10'e. *African Studies* 37(1):83–97.

Judge, W. James, and Lynne Sebastian (editors)
1988 *Quantifying the Present and Predicting the Past: Theory, Method, and Application of Archaeological Predictive Modeling. us Department of the Interior*. Bureau of Land Management, Denver.

Jury, M. R.
2003 The Climate of Madagascar. In *The Natural History of Madagascar*, edited by Steven M. Goodman and Jonathan P. Benstead, pp. 75–87. University of Chicago Press, Chicago.

Kar, Nandini, Carmala N. Garzione, Carlos Jaramillo, Timothy Shanahan, Victor Carlotto, Alex Pullen, Federico Moreno, Veronica Anderson, Enrique Moreno, and John Eiler
2016 Rapid regional surface uplift of the northern Altiplano plateau revealed by multiproxy paleoclimate reconstruction. *Earth and Planetary Science Letters* 447:33–47. DOI:10.1016/j.epsl.2016.04.025.

Keeney, Joseph, and Robert Hickey
2015 Using satellite image analysis for locating prehistoric archaeological sites in Alaska's Central Brooks Range. *Journal of Archaeological Science: Reports* 3:80–89. DOI:10.1016/j.jasrep.2015.05.022.

Kelly, Robert L.
2005 An Ethnoarchaeological Study of Mobility, Architectural Investment, and Food Sharing among Madagascar's Mikea. *American Anthropologist* 107(3):403–416. DOI:10.1525/aa.2005.107.3.403.

King, Brian H.
2002 Towards a Participatory GIS: Evaluating Case Studies of Participatory Rural

Appraisal and GIS in the Developing World. *Cartography and Geographic Information Science* 29(1):43–52. DOI:10.1559/152304002782064565.

Kintigh, Keith W., Jeffrey H. Altschul, Mary C. Beaudry, Robert D. Drennan, Ann P. Kinzig, Timothy A. Kohler, W. Fredrick Limp, Herbert D. G. Maschner, William K. Michener, Timothy R. Pauketat, Peter Peregrine, Jeremy A. Sabloff, Tony J. Wilkinson, Henry T. Wright, and Melinda A. Zeder
2014 Grand Challenges for Archaeology. *American Antiquity* 79(01):5–24.
DOI:10.7183/0002-7316.79.1.5.

Kirk, Scott Detrich, Amy E. Thompson, and Christopher D. Lippitt
2016 Predictive Modeling for Site Detection Using Remotely Sensed Phenological Data. *Advances in Archaeological Practice* 4(1):87–101.

Klehm, Carla, Adam Barnes, Forrest Follett, Katie Simon, Christopher Kiahtipes, and Sarah Mothulatshipi
2019 Toward archaeological predictive modeling in the Bosutswe region of Botswana: Utilizing multispectral satellite imagery to conceptualize ancient landscapes. *Journal of Anthropological Archaeology* 54:68–83. DOI:10.1016/j.jaa.2019.02.002.

Knitter, Daniel, and Oliver Nakoinz
2018 Point Pattern Analysis as Tool for Digital Geoarchaeology: A Case Study of Megalithic Graves in Schleswig-Holstein, Germany. In *Digital Geoarchaeology: New Techniques for Interdisciplinary Human-Environmental Research*, edited by Christoph Siart, Markus Forbriger, and Olaf Bubbenzer, pp. 45–64. Natural Science in Archaeology. Springer International Publishing, Cham.

Koechlin, Bernard
1975 *Es Vezo du Sud-ouest de Madagascar: Contribution à l'étude de l'éco-système de semi-nomades marins*. Mouton & Co, Paris.

Kowalewski, Stephen A.
2008 Regional Settlement Pattern Studies. *Journal of Archaeological Research* 16(3):225–285. DOI:10.1007/s10814-008-9020-8.

Krasinski, Kathryn E., Brian T. Wygal, Joanna Wells, Richard L. Martin, and Fran Seager-Boss
2016 Detecting Late Holocene cultural landscape modifications using LiDAR imagery in the Boreal Forest, Susitna Valley, Southcentral Alaska. *Journal of Field Archaeology* 41(3):255–270. DOI:10.1080/00934690.2016.1174764.

Kull, Christian A.
2000 Deforestation, Erosion, and Fire: Degradation Myths in the Environmental History of Madagascar. *Environment and History* 6(4):423–450.

Kull, Christian A., Jacques Tassin, Sophie Moreau, Hervé Rakoto Ramiarantsoa, Chantal

- Blanc-Pamard, and Stéphanie M. Carrière
2012 The introduced flora of Madagascar. *Biological Invasions* 14(4):875–888.
DOI:10.1007/s10530-011-0124-6.
- Kvamme, Kenneth L.
1983 *A manual for predictive site location models: examples from the Grand Junction District, Colorado*. Bureau of Land Management, Grand Junction District, Colorado, USA.
- Kwaku Kyem, Peter A.
2004 Of Intractable Conflicts and Participatory GIS Applications: The Search for Consensus amidst Competing Claims and Institutional Demands. *Annals of the Association of American Geographers* 94(1):37–57. DOI:10.1111/j.1467-8306.2004.09401003.x.
- Lachniet, Matthew S.
2009 Climatic and environmental controls on speleothem oxygen-isotope values. *Quaternary Science Reviews* 28(5–6):412–432.
- Laland, Kevin N., and Michael J. O'Brien
2010 Niche Construction Theory and Archaeology. *Journal of Archaeological Method and Theory* 17(4):303–322. DOI:10.1007/s10816-010-9096-6.
- Lambers, Karsten
2018 Airborne and Spaceborne Remote Sensing and Digital Image Analysis in Archaeology. In *Digital Geoarchaeology*, edited by Christoph Siart, Markus Forbriger, and Olaf Bubbenzer, pp. 109–122. Springer International Publishing, Cham.
- Lambers, Karsten, Wouter Verschoof-van der Vaart, and Quentin Bourgeois
2019 Integrating Remote Sensing, Machine Learning, and Citizen Science in Dutch Archaeological Prospection. *Remote Sensing* 11(7):794. DOI:10.3390/rs11070794.
- Lampl, Paul
1968 *Cities and planning in the ancient Near East*. George Braziller, New York.
- Lane, Paul J.
2015 Archaeology in the age of the Anthropocene: A critical assessment of its scope and societal contributions. *Journal of Field Archaeology* 40(5):485–498.
DOI:10.1179/2042458215Y.0000000022.
- Langley, Josephine M
2006 *Vezo Knowledge: Traditional Ecological Knowledge in Andavadoaka, southwest Madagascar*. Blue Ventures.
- Lansing, J. Stephen

2003 Complex Adaptive Systems. *Annual Review of Anthropology* 32(1):183–204. DOI:10.1146/annurev.anthro.32.061002.093440.

LaRocque, Armand, Brigitte Leblon, and Jerald Ek

2019 Detection of potential large Maya settlements in the northern Petén area (State of Campeche, Mexico) using optical and radar remote sensing. *Journal of Archaeological Science: Reports* 23:80–97. DOI:10.1016/j.jasrep.2018.10.020.

Lasaponara, Rosa, Giovanni Leucci, Nicola Masini, and Raffaele Persico

2014 Investigating archaeological looting using satellite images and GEORADAR: the experience in Lambayeque in North Peru. *Journal of Archaeological Science* 42:216–230. DOI:10.1016/j.jas.2013.10.032.

Lasaponara, Rosa, and Nicola Masini

2007 Detection of archaeological crop marks by using satellite QuickBird multispectral imagery. *Journal of Archaeological Science* 34(2):214–221.

2012 Image Enhancement, Feature Extraction and Geospatial Analysis in an Archaeological Perspective. In *Satellite Remote Sensing*, edited by Rosa Lasaponara and Nicola Masini, 16:pp. 17–63. Springer Netherlands, Dordrecht.

2013 Satellite Synthetic Aperture Radar in Archaeology and Cultural Landscape: An Overview. *Archaeological Prospection* 20(2):71–78. DOI:10.1002/arp.1452.

2018 Space-Based Identification of Archaeological Illegal Excavations and a New Automatic Method for Looting Feature Extraction in Desert Areas. *Surveys in Geophysics* 39(6):1323–1346. DOI:10.1007/s10712-018-9480-4.

Lauricella, Anthony, Joshua Cannon, Scott Branting, and Emily Hammer

2017 Semi-automated detection of looting in Afghanistan using multispectral imagery and principal component analysis. *Antiquity* 91(359):1344–1355. DOI:10.15184/aqy.2017.90.

Le Manach, Frédéric, Charlotte Gough, Alasdair Harris, Frances Humber, Sarah Harper, and Dirk Zeller

2012 Unreported fishing, hungry people and political turmoil: the recipe for a food security crisis in Madagascar? *Marine Policy* 36(1):218–225.

DOI:10.1016/j.marpol.2011.05.007.

Lee, Everett S.

1966 A Theory of Migration. *Demography* 3(1):47. DOI:10.2307/2060063.

Lefale, Penehuro Fatu

2010 Ua ‘afa le Aso Stormy weather today: traditional ecological knowledge of weather and climate. The Samoa experience. *Climatic Change* 100(2):317–335.

DOI:10.1007/s10584-009-9722-z.

Leisz, Stephen J.

2013 An Overview of the Application of Remote Sensing to Archaeology During the

Twentieth Century. In *Mapping Archaeological Landscapes from Space*, 5:pp. 11–19. Springer New York, New York, NY.

Lemahieu, Anne, Lucy Scott, Willem S. Malherbe, Paubert Tsimanaoraty Mahatante, José Victor Randrianarimanana, and Shankar Aswani
2018 Local perceptions of environmental changes in fishing communities of southwest Madagascar. *Ocean & Coastal Management* 163:209–221.
DOI:10.1016/j.ocecoaman.2018.06.012.

Lepofsky, Dana, Chelsey Geralda Armstrong, Spencer Greening, Julia Jackley, Jennifer Carpenter, Brenda Guernsey, Darcy Mathews, and Nancy J. Turner
2017 Historical ecology of cultural keystone places of the Northwest Coast. *American Anthropologist* 119(3):448–463.

van Leusen, Martijn, Jos Deeben, Daan Hallewas, Paul Zoetbrood, Hans Kamermans, and Philip Verhagen
2005 A baseline for predictive modelling in the Netherlands. *Predictive modelling for archaeological heritage management: A research agenda*:25–93.

Leutner, Benjamin, Ned Horning, and Jakob Schwalb-Willmann
2019 *RStoolbox: Tools for Remote Sensing Data Analysis*.

Lewontin, R. C.
1974 The Structure of Evolutionary Genetics. In *The Genetic Basis of Evolutionary Change*, pp. 3–16. Columbia University Press, New York.

Li, Bo, Douglas W. Nychka, and Caspar M. Ammann
2010 The Value of Multiproxy Reconstruction of Past Climate. *Journal of the American Statistical Association* 105(491):883–895. DOI:10.1198/jasa.2010.ap09379.

Li, Hanying, Ashish Sinha, Aurèle Anquetil André, Christoph Spötl, Hubert B. Vonhof, Arnaud Meunier, Gayatri Kathayat, Pengzhen Duan, Ny Riavo G. Voarintsoa, Youfeng Ning, Jayant Biswas, Peng Hu, Xianglei Li, Lijuan Sha, Jingyao Zhao, R. Lawrence Edwards, and Hai Cheng
2020 A multimillennial climatic context for the megafaunal extinctions in Madagascar and Mascarene Islands. *Science Advances* 6(42):eabb2459. DOI:10.1126/sciadv.abb2459.

Lightfoot, Dale R., and James A. Miller
1996 Sijilmassa: The rise and fall of a walled oasis in medieval Morocco. *Annals of the association of American geographers* 86(1):78–101.

Lightfoot, Kent G., Rob Q. Cuthrell, Chuck J. Striplen, and Mark G. Hylkema
2013 Rethinking the Study of Landscape Management Practices Among Hunter-Gatherers in North America. *American Antiquity* 78(02):285–301. DOI:10.7183/0002-7316.78.2.285.

- Lim, Jonathan S., Sean Gleason, Warren Jones, and Willard Church
2021 Nuna Nalluyuituq (The Land Remembers): Remembering landscapes and refining methodologies through community-based remote sensing in the Yukon-Kuskokwim Delta, Southwest Alaska. *Archaeological Prospection* 28(3). DOI:10.1002/arp.1840, accessed July 21, 2021.
- Lindbergh, C. A.
1929 The discovery of the ruined Maya cities. *Science* 70:12–13.
- Lipo, Carl P., Robert J. DiNapoli, Mark E. Madsen, and Terry L. Hunt
2021 Population structure drives cultural diversity in finite populations: A hypothesis for localized community patterns on Rapa Nui (Easter Island, Chile). Edited by Borja Esteve-Altava. *PLOS ONE* 16(5):e0250690. DOI:10.1371/journal.pone.0250690.
- Lipo, Carl P., and Terry L. Hunt
2005 Mapping prehistoric statue roads on Easter Island. *Antiquity* 79(303):158–168.
- Liss, Brady, Matthew Howland, and Thomas E. Levy
2018 Testing Google Earth Engine for Remote Sensing in Archaeology: Case Studies from Faynan, Jordan presented at the 83rd Annual Meeting of the Society for American Archaeology, 2018, Washington D. C.
- Lombard, Jacques
1988 *Le royaume sakalava du Menabe, 17è-20è: essai d'analyse d'un système politique à Madagascar*. Vol. 214. IRD Editions.
- Lombardo, Umberto, and Heiko Prümers
2010 Pre-Columbian human occupation patterns in the eastern plains of the Llanos de Moxos, Bolivian Amazonia. *Journal of Archaeological Science* 37(8):1875–1885. DOI:10.1016/j.jas.2010.02.011.
- Luo, Lei, Xinyuan Wang, Huadong Guo, Rosa Lasaponara, Pulong Shi, Nabil Bachagha, Li Li, Ya Yao, Nicola Masini, and Fulong Chen
2018 Google Earth as a powerful tool for archaeological and cultural heritage applications: a review. *Remote Sensing* 10(10):1558.
- Luo, Lei, Xinyuan Wang, Huadong Guo, Rosa Lasaponara, Xin Zong, Nicola Masini, Guizhou Wang, Pulong Shi, Houcine Khatteli, Fulong Chen, Shahina Tariq, Jie Shao, Nabil Bachagha, Ruixia Yang, and Ya Yao
2019 Airborne and spaceborne remote sensing for archaeological and cultural heritage applications: A review of the century (1907–2017). *Remote Sensing of Environment* 232:111280. DOI:10.1016/j.rse.2019.111280.
- Lyons, N.

- 2013 *Where the wind blows us: Practicing critical community archaeology in the Canadian North*. University of Arizona Press.
- MacArthur, Robert H., and Eric R. Pianka
1966 On Optimal Use of a Patchy Environment. *The American Naturalist* 100(916):603–609. DOI:10.1086/282454.
- MacEachern, Scott
2010 Seeing like an oil company's CHM programme: Exxon and archaeology on the Chad Export Project. *Journal of Social Archaeology* 10(3):347–366.
- Maggs, TM O'C
1976 *Iron Age communities of the southern Highveld*. 2. Council of the Natal Museum, Pietermaritzburg.
- Magnini, Luigi, and Cinzia Bettineschi
2019 Theory and practice for an object-based approach in archaeological remote sensing. *Journal of Archaeological Science* 107:10–22. DOI:10.1016/j.jas.2019.04.005.
- Malley, J. D., J. Kruppa, A. Dasgupta, K. G. Malley, and A. Ziegler
2012 Probability Machines: Consistent Probability Estimation Using Nonparametric Learning Machines. *Methods of Information in Medicine* 51(01):74–81. DOI:10.3414/ME00-01-0052.
- Mark, D. M., and A. G. Turk
2003 Landscape categories in Yindjibarndi: Ontology, environment, and language. In , pp. 28–45. Springer, Berlin, Heidelberg.
- Mason, Revil J.
1968 Transvaal and Natal Iron Age settlement revealed by aerial photography and excavation. *African Studies* 27(4):167–180.
- Mattingly, David J., and M. Sterry
2013 The first towns in the central Sahara. *Antiquity* 87(336):503–518.
- McClure, Sarah B., C. Michael Barton, and Michael A. Jochim
2009 Human behavioral ecology and climate change during the transition to agriculture in Valencia, eastern Spain. *Journal of Anthropological Research* 65(2):253–269.
- McCoy, Mark D.
2020 The Site Problem: A Critical Review of the Site Concept in Archaeology in the Digital Age. *Journal of Field Archaeology* 45(sup1):S18–S26. DOI:10.1080/00934690.2020.1713283.
- McMichael, C. H., M. W. Palace, M. B. Bush, B. Braswell, S. Hagen, E. G. Neves, M. R. Silman, E. K. Tamanaha, and C. Czarnecki

2014 Predicting pre-Columbian anthropogenic soils in Amazonia. *Proceedings of the Royal Society B: Biological Sciences* 281(1777):20132475.
DOI:10.1098/rspb.2013.2475.

Menze, B. H., and J. A. Ur

2012 Mapping patterns of long-term settlement in Northern Mesopotamia at a large scale. *Proceedings of the National Academy of Sciences* 109(14):E778–E787.
DOI:10.1073/pnas.1115472109.

Meredith-Williams, M. G., N. Hausmann, G. N. Bailey, G. C. P. King, A. Alsharekh, S. Al Ghamdi, and R. H. Inglis

2014 Mapping, modelling and predicting prehistoric coastal archaeology in the southern Red Sea using new applications of digital-imaging techniques. *World Archaeology* 46(1):10–24. DOI:10.1080/00438243.2014.890913.

Meyer, M., Ingo Pfeffer, and Carsten Jürgens

2019 Automated Detection of Field Monuments in Digital Terrain Models of Westphalia Using OBIA. *Geosciences* 9(3):109. DOI:10.3390/geosciences9030109.

Mille, Adrien

1970 *Contribution à l'étude des villages fortifiés de l'Imerina ancien*. Travaux et Documents II. Antananarivo: Musée d'Art et d'Archeologie de l'Université de Tananarive.

Millican, Kirsty

2012 The Outside Inside: Combining Aerial Photographs, Cropmarks and Landscape Experience. *Journal of Archaeological Method and Theory* 19(4):548–563.
DOI:10.1007/s10816-012-9140-9.

Mills, B. J., J. J. Clark, M. A. Peeples, W. R. Haas, J. M. Roberts, J. B. Hill, D. L. Huntley, L. Borck, R. L. Breiger, A. Clauset, and M. S. Shackley

2013 Transformation of social networks in the late pre-Hispanic US Southwest. *Proceedings of the National Academy of Sciences* 110(15):5785–5790.
DOI:10.1073/pnas.1219966110.

Mills, Barbara J.

2017 Social Network Analysis in Archaeology. *Annual Review of Anthropology* 46(1):379–397. DOI:10.1146/annurev-anthro-102116-041423.

Ministère de l'Environnement, des Eaux, et des Forêts

2006 *Programme d'action nationale 'adaptation au changement climatique*.

Mire, Sada

2017 The Role of Cultural Heritage in the Basic Needs of East African Pastoralists. *African Study Monographs, Supplement* 5:147–157.

Mitchell, Peter

2019 Settling Madagascar: When Did People First Colonize the World's Largest Island? *The Journal of Island and Coastal Archaeology*:1–20.

DOI:10.1080/15564894.2019.1582567.

2020 Debating Madagascar: A reply to Hansford et al.'s response. *The Journal of Island and Coastal Archaeology*:1–6. DOI:10.1080/15564894.2020.1771483.

Mobley, Charles M., and Morley Eldridge

1992 Culturally modified trees in the Pacific Northwest. *Arctic anthropology*:91–110.

Morton, Fred

2013 Settlements, Landscapes and Identities among the Tswana of the Western Transvaal and Eastern Kalahari before 1820. *South African Archaeological Bulletin* 68(197):15–26.

Moser, Stephanie, Darren Glazier, James E. Phillips, Lamya Nasser el Nemr, Mohammed Saleh Mousa, Rascha Nasr Aiesh, Susan Richardson, Andrew Conner, and Michael Seymour

2002 Transforming archaeology through practice: Strategies for collaborative archaeology and the Community Archaeology Project at Quseir, Egypt. *World Archaeology* 34(2):220–248. DOI:10.1080/0043824022000007071.

Mountrakis, Giorgos, Jungho Im, and Caesar Ogole

2011 Support vector machines in remote sensing: A review. *ISPRS Journal of Photogrammetry and Remote Sensing* 66(3):247–259.

DOI:10.1016/j.isprsjprs.2010.11.001.

Mügler, I., G. Gleixner, F. Günther, R. Mäusbacher, G. Daut, B. Schütt, J. Berking, A. Schwalb, L. Schwark, B. Xu, T. Yao, L. Zhu, and C. Yi

2010 A multi-proxy approach to reconstruct hydrological changes and Holocene climate development of Nam Co, Central Tibet. *Journal of Paleolimnology* 43(4):625–648. DOI:10.1007/s10933-009-9357-0.

Myers, Adrian

2010 Camp Delta, Google Earth and the ethics of remote sensing in archaeology. *World Archaeology* 42(3):455–467. DOI:10.1080/00438243.2010.498640.

Napolitano, Matthew F., Robert J. DiNapoli, Jessica H. Stone, Maureece J. Levin, Nicholas P. Jew, Brian G. Lane, John T. O'Connor, and Scott M. Fitzpatrick

2019 Reevaluating human colonization of the Caribbean using chronometric hygiene and Bayesian modeling. *Science Advances* 5(12):eaar7806. DOI:10.1126/sciadv.aar7806.

Nsanziyera, Ange, Hassan Rhinane, Aicha Oujaa, and Kenneth Mubea

2018 GIS and Remote-Sensing Application in Archaeological Site Mapping in the Awsard Area (Morocco). *Geosciences* 8(6):207. DOI:10.3390/geosciences8060207.

- Nyerges, A. Endre, and Glen Martin Green
 2000 The Ethnography of Landscape: GIS and Remote Sensing in the Study of Forest Change in West African Guinea Savanna. *American Anthropologist* 102(2):271–289. DOI:10.1525/aa.2000.102.2.271.
- O’Connell, James F., and Jim Alien
 2012 Forum The Restaurant At The End Of The Universe: Modelling the colonisation of Sahui. *Australian Archaeology* 74(1):5–31.
- O’Connell, James F., and Kristen Hawkes
 1981 Alyawara Plant Use and Optimal Foraging Theory. In *Hunter-gatherer foraging strategies: Ethnographic and archaeological analyses*, edited by Bruce Winterhalder and Eric Alden Smith, pp. 99–125. University of Chicago Press, Chicago.
- Odling-Smee, F. J., Kevin N. Laland, and Marcus W. Feldman
 2003 *Niche construction: The neglected process in evolution*. Princeton University Press.
- Odling-Smee, John, Douglas H. Erwin, Eric P. Palkovacs, Marcus W. Feldman, and Kevin N. Laland
 2013 Niche construction theory: a practical guide for ecologists. *The Quarterly review of biology* 88(1):3–28.
- Oduntan, Gbenga
 2012 *Sovereignty and jurisdiction in the airspace and outer space: legal criteria for spatial delimitation*. Routledge research in international law. Routledge, New York.
 2019 Geospatial Sciences and Space Law: Legal Aspects of Earth Observation, Remote Sensing and Geoscientific Ground Investigations in Africa. *Geosciences* 9(4):149. DOI:10.3390/geosciences9040149.
- Oliver, Jeff
 2007 Beyond the Water’s Edge: Towards a Social Archaeology of Landscape on the Northwest Coast. *Canadian Journal of Archaeology / Journal Canadien d’Archéologie* 31(1):1–27.
- Opitz, Rachel, and Jason Herrmann
 2018 Recent Trends and Long-standing Problems in Archaeological Remote Sensing. *Journal of Computer Applications in Archaeology* 1(1):19–41. DOI:10.5334/jcaa.11.
- Orengo, H.A., and A. Garcia-Molsosa
 2019 A brave new world for archaeological survey: Automated machine learning-based potsherd detection using high-resolution drone imagery. *Journal of Archaeological Science*:105013. DOI:10.1016/j.jas.2019.105013.
- Orengo, Hector A., Francesc C. Conesa, Arnau Garcia-Molsosa, Agustín Lobo, Adam S.

- Green, Marco Madella, and Cameron A. Petrie
 2020 Automated detection of archaeological mounds using machine-learning classification of multisensor and multitemporal satellite data. *Proceedings of the National Academy of Sciences*:202005583. DOI:10.1073/pnas.2005583117.
- Osicki, Aaron, and D. Sjogren
 2005 A review of remote sensing application in archaeological research. *Geography* 795(28):333.
- Östborn, Per, and Henrik Gerding
 2014 Network analysis of archaeological data: a systematic approach. *Journal of Archaeological Science* 46:75–88. DOI:10.1016/j.jas.2014.03.015.
- O’Sullivan, D., and G. L. Perry
 2013 *O’Sullivan, D., & Perry, G. L. (2013). Spatial simulation: exploring pattern and process. John Wiley & Sons. Wiley-Blackwell, Oxford.*
- Pal, M.
 2005 Random forest classifier for remote sensing classification. *International Journal of Remote Sensing* 26(1):217–222. DOI:10.1080/01431160412331269698.
- Pal, M., and P. M. Mather
 2005 Support vector machines for classification in remote sensing. *International Journal of Remote Sensing* 26(5):1007–1011. DOI:10.1080/01431160512331314083.
- Parcak, Sarah
 2007 Satellite remote sensing methods for monitoring archaeological tells in the Middle East. *Journal of field archaeology* 32(1):65–81.
 2019 *Archaeology from Space: How the Future Shapes Our Past*. Henry Holt and Co., New York.
- Parcak, Sarah, David Gathings, Chase Childs, Greg Mumford, and Eric Cline
 2016 Satellite evidence of archaeological site looting in Egypt: 2002–2013. *Antiquity* 90(349):188–205. DOI:10.15184/aqy.2016.1.
- Parcak, Sarah H.
 2009 *Satellite Remote Sensing for Archaeology*. Routledge, New York.
- Parker Pearson, M.
 2010 *Pastoralists, Warriors and Colonists: The Archaeology of Southern Madagascar* (Archaeopress, Oxford).
- Parker Pearson, Mike, Karen Godden, Retsihisatse Rambilisonina, Jean-Luc Schwenninger, Georges Heurtebize, Chantal Radimilahy, and Helen Smith
 2010 *Pastoralists, Warriors and Colonists: The Archaeology of Southern Madagascar*. BAR International Series 2139. Archaeopress, Oxford.

Parker, Sandra

1985 Predictive modeling of site settlement systems using multivariate logistics. In *For concordance in archaeological analysis: Bridging data structure, quantitative technique, and theory*, pp. 173–207. Waveland Press, Prospect Heights, IL.

Parrington, M.

1983 Remote Sensing. *Annual Review of Anthropology* 12:105–124.

Pearson, Mike Parker

1992 Tombs and monumentality in southern Madagascar: preliminary results of the central Androy survey. *Antiquity* 66(253):941–948. DOI:10.1017/S0003598X00044860.

1997 Close encounters of the worst kind: Malagasy resistance and colonial disasters in Southern Madagascar. *World Archaeology* 28(3):393–417.

DOI:10.1080/00438243.1997.9980355.

Pearson, Mike Parker, and Denis Regnier

2018 Collective and single burial in Madagascar. In *Gathered in death: Archaeological and ethnological perspectives on collective burial and social organisation*, edited by Aurore Schmitt, Sylviane Déderix, and Isabelle Crevecoeur, pp. 41–62. UCL Press.

Pebesma, Edzer J., and Roger S. Bivand

2005 Classes and methods for spatial data in R. *R News* 5(2).

Peeples, Matthew A.

2017 Network science and statistical techniques for dealing with uncertainties in archaeological datasets. <http://www.mattpeeples.net/netstats.html>, accessed December 30, 2020.

Peeples, Matthew A., and John M. Roberts

2013 To binarize or not to binarize: relational data and the construction of archaeological networks. *Journal of Archaeological Science* 40(7):3001–3010.

DOI:10.1016/j.jas.2013.03.014.

Penny, Dan, Cameron Zachreson, Roland Fletcher, David Lau, Joseph T. Lizier, Nicholas Fischer, Damian Evans, Christophe Pottier, and Mikhail Prokopenko

2018 The demise of Angkor: Systemic vulnerability of urban infrastructure to climatic variations. *Science Advances* 4(10):eaau4029. DOI:10.1126/sciadv.aau4029.

Petrie, Cameron A., Ravindra N. Singh, Jennifer Bates, Yama Dixit, Charly A. I. French, David A. Hodell, Penelope J. Jones, Carla Lancelotti, Frank Lynam, Sayantani Neogi, Arun K. Pandey, Danika Parikh, Vikas Pawar, David I. Redhouse, and Dheerendra P. Singh

2017 Adaptation to Variable Environments, Resilience to Climate Change: Investigating Land, Water and Settlement in Indus Northwest India. *Current Anthropology* 58(1):1–30. DOI:10.1086/690112.

Piermattei, A., C. Urbinati, E. Tonelli, Ó. Eggertsson, T. Levanič, R. J. Kaczka, C. Andrew, B. R. Schöne, and U. Büntgen
2017 Potential and limitation of combining terrestrial and marine growth records from Iceland. *Global and Planetary Change* 155:213–224.
DOI:10.1016/j.gloplacha.2017.07.010.

Pierron, Denis, Margit Heiske, Harilanto Razafindrazaka, Ignace Rakoto, Nelly Rabetokotany, Bodo Ravololomanga, Lucien M.-A. Rakotozafy, Mireille Mialy Rakotomalala, Michel Razafiarivony, and Bako Rasoarifetra
2017 Genomic landscape of human diversity across Madagascar. *Proceedings of the National Academy of Sciences* 114(32):E6498–E6506.

Pisor, Anne C., and James Holland Jones
2021 Do people manage climate risk through long-distance relationships? *American Journal of Human Biology* 33(4):e23525. DOI:10.1002/ajhb.23525.

Planet Team
2020 *Planet Application Program Interface: In Space for Life on Earth*. San Francisco, CA.

Plekhov, Daniel, and Evan I. Levine
2020 Defining Suitability in Mixed Agropastoral Societies: A Case Study from Bactria in Northern Afghanistan. *Environmental Archaeology*:1–16.
DOI:10.1080/14614103.2020.1777055.

Plog, Fred, and James N. Hill
1971 Explaining variability in the distribution of sites. *The distribution of prehistoric population aggregates*(1):7.

Pollock, Susan
2016 Archaeology and contemporary warfare. *Annual Review of Anthropology* 45:215–231.

Preiser, Rika, Reinette Biggs, Alta De Vos, and Carl Folke
2018 Social-ecological systems as complex adaptive systems: organizing principles for advancing research methods and approaches. *Ecology and Society* 23(4):art46.
DOI:10.5751/ES-10558-230446.

QGIS Development Team
2018 *QGIS Geographic Information System*. Open Source Geospatial Foundation Project.

Quintus, Seth, and Ethan E. Cochrane
2018 The prevalence and importance of niche construction in agricultural development

in Polynesia. *Journal of Anthropological Archaeology* 51:173–186.
DOI:10.1016/j.jaa.2018.06.007.

Quiros, TE Angela L., Don Croll, Bernie Tershy, Miguel D. Fortes, and Peter Raimondi
2017 Land use is a better predictor of tropical seagrass condition than marine protection. *Biological conservation* 209:454–463.

R Core Team

2020 *R: A language and environment for statistical computing*. R Foundation for Statistical Computing, Vienna, Austria.

2021 *R: A language and environment for statistical computing*. R Foundation for Statistical Computing, Vienna, Austria.

Radimilahy, Chantal

2011 Contribution à l'archéologie du Sud-ouest de Madagascar. In *Civilisations des mondes insulaires : (Madagascar, îles du canal de Mozambique, Mascareignes, Polynésie, Guyanes)*, edited by Chantal Radimilahy and Narivelo Rajaonarimanana, pp. 825–853. KARTHALA, Paris.

Radimilahy, Chantal M., and Zoë Crossland

2015 Situating Madagascar: Indian Ocean dynamics and archaeological histories. *Azania: Archaeological Research in Africa* 50(4):495–518.

DOI:10.1080/0067270X.2015.1102942.

Rakotozafy, Lucien M.-A.

1996 Etude de la constitution du régime alimentaire des habitants du site de Mahilaka du XIème au XIVème siècle à partir des produits de fouilles archéologiques. Unpublished PhD, Université d'Antananarivo, Antananarivo.

Ramirez-Gomez, Sara O.I., Carlos A. Torres-Vitolas, Kate Schreckenber, Miroslav Honzák, Gisella S. Cruz-Garcia, Simon Willcock, Erwin Palacios, Elena Pérez-Miñana, Pita A. Verweij, and Guy M. Poppy

2015 Analysis of ecosystem services provision in the Colombian Amazon using participatory research and mapping techniques. *Ecosystem Services* 13:93–107.

DOI:10.1016/j.ecoser.2014.12.009.

Ranger, T.

2001 COLONIALISM, CONSCIOUSNESS AND THE CAMERA. *Past & Present* 171(1):203–215. DOI:10.1093/past/171.1.203.

Rayne, Louise, Jennie Bradbury, David Mattingly, Graham Philip, Robert Bewley, and Andrew Wilson

2017 From Above and on the Ground: Geospatial Methods for Recording Endangered Archaeology in the Middle East and North Africa. *Geosciences* 7(4):100.

DOI:10.3390/geosciences7040100.

Razanatsoa, E., Malika Virah-Sawmy, S. Woodborne, C. Callanan, and L. Gillson
in press Adaptation of subsistence strategies of the southwestern Malagasy in the
face of climate change. *Malagasy Nature*:1–31.

Razanatsoa, Estelle

2019 Impact of human land-use and rainfall variability in tropical dry forests of
southwest Madagascar during the late Holocene. Unpublished PhD Thesis, University of
Cape Town, Cape Town.

Reddix-Small, Brenda

2014 Satellite remote sensing and database management: Who owns the digitized
information relating to indigenous people and their artifacts. *NC Cent. L. Rev.* 37:1.

Redman, Charles L., and Ann P. Kinzig

2003 Resilience of Past Landscapes: Resilience Theory, Society, and the Longue
Durée. *Conservation Ecology* 7(1). accessed November 24, 2021.

Reid, Sean H.

2016 Satellite Remote Sensing of Archaeological Vegetation Signatures in Coastal
West Africa. *African Archaeological Review* 33(2):163–182. DOI:10.1007/s10437-016-
9222-2.

Rennell, Rebecca

2012 Landscape, Experience and GIS: Exploring the Potential for Methodological
Dialogue. *Journal of Archaeological Method and Theory* 19(4):510–525.
DOI:10.1007/s10816-012-9144-5.

Resnik, David B., and Kevin C. Elliott

2019 Using Drones to Study Human Beings: Ethical and Regulatory Issues. *Science
and Engineering Ethics* 25(3):707–718. DOI:10.1007/s11948-018-0032-6.

Rice, Prudence M.

2015 *Pottery Analysis: A Sourcebook*. 2nd ed. The University of Chicago Press,
Chicago.

Richards, T. S.

1989 Evidence of ancient rainwater concentrating structures in northern Egypt as seen
on Landsat MSS imagery. *International Journal of Remote Sensing* 10(6):1135–1140.

Rick, Torben C., and Daniel H. Sandweiss

2020 Archaeology, climate, and global change in the Age of Humans. *Proceedings of
the National Academy of Sciences* 117(15):8250–8253.

Ripley, Brian D.

1977 Modelling spatial patterns. *Journal of the Royal Statistical Society: Series B (Methodological)* 39(2):172–192.

Roberts, John M., Yi Yin, Emily Dorshorst, Matthew A. Peeples, and Barbara J. Mills
2021 Assessing the performance of the bootstrap in simulated assemblage networks. *Social Networks* 65:98–109. DOI:10.1016/j.socnet.2020.11.005.

Robertshaw, Peter

2012 African archaeology, multidisciplinary reconstructions of Africa's recent past, and archaeology's role in future collaborative research. *African Archaeological Review* 29(2–3):95–108.

Robinson, Erick, H. Jabran Zahid, Brian F. Coddling, Randall Haas, and Robert L. Kelly
2019 Spatiotemporal dynamics of prehistoric human population growth: Radiocarbon 'dates as data' and population ecology models. *Journal of Archaeological Science* 101:63–71. DOI:10.1016/j.jas.2018.11.006.

Robinson, William S.

1951 A method for chronologically ordering archaeological deposits. *American antiquity* 16(4):293–301.

Romero, Daniel M., Brian Uzzi, and Jon Kleinberg

2019 Social networks under stress: Specialized team roles and their communication structure. *ACM Transactions on the Web (TWEB)* 13(1):1–24.

Rosenthal, Alfred

1968 Venture Into Space: Early Years of Goddard Space Flight Center. NASA SP-4301. *NASA Special Publication* 4301.

Rowley-Conwy, Peter, and Robert Layton

2011 Foraging and farming as niche construction: stable and unstable adaptations. *Philosophical Transactions of the Royal Society B: Biological Sciences* 366(1566):849–862. DOI:10.1098/rstb.2010.0307.

Roy, Eleanor Ainge

2017 New Zealand river granted same legal rights as human being. *The Guardian*, March 16, 2017, sec. World news.
<https://www.theguardian.com/world/2017/mar/16/new-zealand-river-granted-same-legal-rights-as-human-being>, accessed November 20, 2020.

Rüther, Heinz

2002 An African Heritage Database: The Virtual Preservation of Africa's Past. *International Archives of Photogrammetry, Remote Sensing and Spatial Information Sciences XXXIV(Part6/W6)*:185–192.

Rutkiewicz, Paweł, Ireneusz Malik, Małgorzata Wistuba, and Aleksandra Osika

2019 High concentration of charcoal hearth remains as legacy of historical ferrous metallurgy in southern Poland. *Quaternary International*:S1040618218308371. DOI:10.1016/j.quaint.2019.04.015.

SAA

2016 Ethics in Professional Archaeology. <https://www.saa.org/career-practice/ethics-in-professional-archaeology>, accessed September 16, 2020.

Sadr, Karim

2016a The Impact of Coder Reliability on Reconstructing Archaeological Settlement Patterns from Satellite Imagery: a Case Study from South Africa: Coder Reliability in Archaeological Settlement Pattern Studies. *Archaeological Prospection* 23(1):45–54. DOI:10.1002/arp.1515.

2016b A Comparison of Accuracy and Precision in Remote Sensing Stone-walled Structures with Google Earth, High Resolution Aerial Photography and LiDAR; a Case Study from the South African Iron Age: Accuracy and Precision in Remote Sensing Stone-Walled Structures. *Archaeological Prospection* 23(2):95–104. DOI:10.1002/arp.1532.

Safi, Michael

Ganges and Yamuna rivers granted same legal rights as human beings | World news | The Guardian. *The Guardian*. Newspaper, <https://www.theguardian.com/world/2017/mar/21/ganges-and-yamuna-rivers-granted-same-legal-rights-as-human-beings>, accessed November 20, 2020.

Sanchez, Gabriel M., Michael A. Grone, Alec J. Apodaca, R. Scott Byram, Valentin Lopez, and Roberta A. Jewett

2021 Sensing the Past: Perspectives on Collaborative Archaeology and Ground Penetrating Radar Techniques from Coastal California. *Remote Sensing* 13(2):285.

Saumagne, Charles

1952 La photographie aérienne au service de l'archéologie en Tunisie. *Comptes rendus des séances de l'Académie des Inscriptions et Belles-Lettres* 96(2):287–301.

Schmid, Thomas, Magaly Koch, Michael DiBlasi, and Miruts Hagos

2008 Spatial and spectral analysis of soil surface properties for an archaeological area in Aksum, Ethiopia, applying high and medium resolution data. *CATENA* 75(1):93–101. DOI:10.1016/j.catena.2008.04.008.

Schuetter, Jared, Prem Goel, Joy McCorriston, Jihye Park, Matthew Senn, and Michael Harrower

2013 Autodetection of ancient Arabian tombs in high-resolution satellite imagery. *International Journal of Remote Sensing* 34(19):6611–6635. DOI:10.1080/01431161.2013.802054.

Schwarz, Gideon

1978 Estimating the Dimension of a Model. *The Annals of Statistics* 6(2):461–464.
DOI:10.1214/aos/1176344136.

Scropton, Nick, Stephen J. Burns, David McGee, Ben Hardt, Laurie R. Godfrey, Lovasoa Ranivoharimanana, and Peterson Faina

2017 Hemispherically in-phase precipitation variability over the last 1700 years in a Madagascar speleothem record. *Quaternary Science Reviews* 164:25–36.
DOI:10.1016/j.quascirev.2017.03.017.

Seddon, J. D.

1968 An aerial survey of settlement and living patterns in the Transvaal Iron Age: preliminary report. *African Studies* 27(4):189–194.

Sevara, Christopher, Michael Pregesbauer, Michael Doneus, Geert Verhoeven, and Immo Trinks

2016 Pixel versus object — A comparison of strategies for the semi-automated mapping of archaeological features using airborne laser scanning data. *Journal of Archaeological Science: Reports* 5:485–498. DOI:10.1016/j.jasrep.2015.12.023.

Skibo, James M., Michael B. Schiffer, and Nancy Kowalski

1989 Ceramic Style Analysis in Archaeology and Ethnoarchaeology: Bridging the Analytical Gap. *Journal of Anthropological Archaeology* 8:388–409.

Smith, Bruce D.

2001 Low-Level Food Production. *Journal of Archaeological Research* 9(1):1–43.

Sonnemann, Till, Douglas Comer, Jesse Patsolic, William Megarry, Eduardo Herrera Malatesta, and Corinne Hofman

2017 Semi-Automatic Detection of Indigenous Settlement Features on Hispaniola through Remote Sensing Data. *Geosciences* 7(4):127. DOI:10.3390/geosciences7040127.

Spencer, Christine, and Andrew Bevan

2018 Settlement location models, archaeological survey data and social change in Bronze Age Crete. *Journal of Anthropological Archaeology* 52:71–86.

DOI:10.1016/j.jaa.2018.09.001.

Spengler, Robert N.

2021 Niche Construction Theory in Archaeology: A Critical Review. *Journal of Archaeological Method and Theory*. DOI:10.1007/s10816-021-09528-4, accessed June 7, 2021.

Spriggs, Matthew

1989 The dating of the Island Southeast Asian Neolithic: an attempt at chronometric hygiene and linguistic correlation. *Antiquity* 63(240):587–613.

DOI:10.1017/S0003598X00076560.

Stahl, Ann Brower

1985 Reinvestigation of Kintampo 6 rock shelter, Ghana: implications for the nature of culture change. *The African Archaeological Review* 3(1):117–150.
DOI:10.1007/BF01117457.

(editor)

2005 *African archaeology: A critical introduction*. Blackwell Pub.

Stephens, Lucas, Dorian Fuller, Nicole Boivin, Torben Rick, Nicolas Gauthier, Andrea Kay, Ben Marwick, Chelsey Geralda Armstrong, C. Michael Barton, Tim Denham, Kristina Douglass, Jonathan Driver, Lisa Janz, Patrick Roberts, J. Daniel Rogers, Heather Thakar, Mark Altaweel, Amber L. Johnson, Maria Marta Sampietro Vattuone, Mark Aldenderfer, Sonia Archila, Gilberto Artioli, Martin T. Bale, Timothy Beach, Ferran Borrell, Todd Braje, Philip I. Buckland, Nayeli Guadalupe Jiménez Cano, José M. Capriles, Agustín Diez Castillo, Çiler Çilingiroğlu, Michelle Negus Cleary, James Conolly, Peter R. Coutros, R. Alan Covey, Mauro Cremaschi, Alison Crowther, Lindsay Der, Savino di Lernia, John F. Doershuk, William E. Doolittle, Kevin J. Edwards, Jon M. Erlandson, Damian Evans, Andrew Fairbairn, Patrick Faulkner, Gary Feinman, Ricardo Fernandes, Scott M. Fitzpatrick, Ralph Fyfe, Elena Garcea, Steve Goldstein, Reed Charles Goodman, Jade Dalpoim Guedes, Jason Herrmann, Peter Hiscock, Peter Hommel, K. Ann Horsburgh, Carrie Hritz, John W. Ives, Aripekka Junno, Jennifer G. Kahn, Brett Kaufman, Catherine Kearns, Tristram R. Kidder, François Lanoë, Dan Lawrence, Gyoung-Ah Lee, Maureece J. Levin, Henrik B. Lindskoug, José Antonio López-Sáez, Scott Macrae, Rob Marchant, John M. Marston, Sarah McClure, Mark D. McCoy, Alicia Ventresca Miller, Michael Morrison, Giedre Motuzaite Matuzeviciute, Johannes Müller, Ayushi Nayak, Sofwan Noerwidi, Tanya M. Peres, Christian E. Peterson, Lucas Proctor, Asa R. Randall, Steve Renette, Gwen Robbins Schug, Krysta Ryzewski, Rakesh Saini, Vivian Scheinsohn, Peter Schmidt, Pauline Sebillaud, Oula Seitonen, Ian A. Simpson, Arkadiusz Sołtysiak, Robert J. Speakman, Robert N. Spengler, Martina L. Steffen, Michael J. Storz, Keir M. Strickland, Jessica Thompson, T. L. Thurston, Sean Ulm, M. Cemre Ustunkaya, Martin H. Welker, Catherine West, Patrick Ryan Williams, David K. Wright, Nathan Wright, Muhammad Zahir, Andrea Zerboni, Ella Beaudoin, Santiago Munevar Garcia, Jeremy Powell, Alexa Thornton, Jed O. Kaplan, Marie-José Gaillard, Kees Klein Goldewijk, and Erle Ellis
2019 Archaeological assessment reveals Earth's early transformation through land use. *Science* 365(6456):897–902. DOI:10.1126/science.aax1192.

Steward, Julian

1955 Smallholders, householders: Farm Families and the Ecology of Intensive, Sustainable Agriculture. In *Anthropological Theory: An Introductory History*, edited by Nora Haenn and Richard Wilk, pp. 1–9. New York University Press, New York.

Steward, Julian H., and Frank M. Setzler

1938 Function and Configuration in Archaeology. *American Antiquity* 4(01):4–10.
DOI:10.2307/275356.

- Stiner, Mary C., and Steven L. Kuhn
 2016 Are we missing the “sweet spot” between optimality theory and niche construction theory in archaeology? *Journal of Anthropological Archaeology* 44:177–184. DOI:10.1016/j.jaa.2016.07.006.
- Storozum, Michael J., Steven T. Goldstein, Daniel A. Contreras, Agness O. Gidna, Audax Z.P. Mabulla, Katherine M. Grillo, and Mary E. Prendergast
 2021 The influence of ancient herders on soil development at Luxmanda, Mbulu Plateau, Tanzania. *CATENA* 204:105376. DOI:10.1016/j.catena.2021.105376.
- Stoyan, Dietrich, and Helga Stoyan
 1994 *Fractals, random shapes, and point fields: methods of geometrical statistics*. Vol. 302. John Wiley & Sons Inc.
- Stuiver, Minze, and Henry A Polach
 1977 Discussion Reporting of 14C Data. *Radiocarbon* 19(03):355–363. DOI:10.1017/S0033822200003672.
- Summers, Kyle
 2005 The evolutionary ecology of despotism. *Evolution and Human Behavior* 26(1):106–135. DOI:10.1016/j.evolhumbehav.2004.09.001.
- Sun, Chuanliang, Yan Bian, Tao Zhou, and Jianjun Pan
 2019 Using of Multi-Source and Multi-Temporal Remote Sensing Data Improves Crop-Type Mapping in the Subtropical Agriculture Region. *Sensors* 19(10):2401. DOI:10.3390/s19102401.
- Sussman, Robert W., Glen M. Green, and Linda K. Sussman
 1994 Satellite imagery, human ecology, anthropology, and deforestation in Madagascar. *Human Ecology* 22(3):333–354. DOI:10.1007/BF02168856.
- Tarolli, Paolo, Wenfang Cao, Giulia Sofia, Damian Evans, and Erle C Ellis
 2019 From features to fingerprints: A general diagnostic framework for anthropogenic geomorphology. *Progress in Physical Geography: Earth and Environment* 43(1):95–128. DOI:10.1177/0309133318825284.
- Thabeng, Olaotse L., Stefania Merlo, and Elhadi Adam
 2020 From the Bottom Up: Assessing the Spectral Ability of Common Multispectral Sensors to Detect Surface Archaeological Deposits Using Field Spectrometry and Advanced Classifiers in the Shashi-Limpopo Confluence Area. *African Archaeological Review*. DOI:10.1007/s10437-020-09372-z, accessed March 11, 2020.
- Thabeng, Olaotse Lokwalo, Stefania Merlo, and Elhadi Adam
 2019 High-resolution remote sensing and advanced classification techniques for the prospection of archaeological sites’ markers: The case of dung deposits in the Shashi-

Limpopo Confluence area (southern Africa). *Journal of Archaeological Science* 102:48–60. DOI:10.1016/j.jas.2018.12.003.

Thomas, Julian

1993 The Politics of Vision and the Archaeologies of Landscape. In *Landscape: Politics and Perspectives*, edited by Barbara Bender, pp. 19–48. Berg, Oxford.

1995 The politics of vision and the archaeologies of landscape. In *Landscape, politics and perspectives*, edited by Barbara Bender, pp. 19–48. Berg.

2008 Archaeology, landscape, and dwelling. In *Handbook of landscape archaeology*, edited by B. David and J. Thomas, pp. 300–306. Left Coast Press, California.

Thompson, Victor D., Philip J. Arnold, Thomas J. Pluckhahn, and Amber M. VanDerwarker

2011 Situating Remote Sensing in Anthropological Archaeology. *Archaeological Prospection* 18(3):195–213. DOI:10.1002/arp.400.

Thompson, Victor D., and John A. Turck

2009 Adaptive Cycles of Coastal Hunter-Gatherers. *American Antiquity* 74(2):255–278.

Tilley, Christopher

1994 *A phenomenology of landscape: places, paths, and monuments*. Berg, Oxford.

Traviglia, A., and D. Cottica

2011 Remote sensing applications and archaeological research in the Northern Lagoon of Venice: the case of the lost settlement of Constanciacus. *Journal of Archaeological Science* 38(9):2040–2050. DOI:10.1016/j.jas.2010.10.024.

Traviglia, Arianna, and Andrea Torsello

2017 Landscape Pattern Detection in Archaeological Remote Sensing. *Geosciences* 7(4):128. DOI:10.3390/geosciences7040128.

Trier, Øivind Due, David C. Cowley, and Anders Ueland Waldeland

2019 Using deep neural networks on airborne laser scanning data: Results from a case study of semi-automatic mapping of archaeological topography on Arran, Scotland.

Archaeological Prospection 26(2):165–175. DOI:10.1002/arp.1731.

Trier, Øivind Due, Siri Øyen Larsen, and Rune Solberg

2009 Automatic detection of circular structures in high-resolution satellite images of agricultural land. *Archaeological Prospection* 16(1):1–15. DOI:10.1002/arp.339.

Trimble

2014 *eCognition Developer*. Trimble Germany GmbH, Munich, Germany.

Tucker, Bram

2004 Giving, Scrounging, Hiding, and Selling: Minimal Food Sharing Among Mikea of

Madagascar. In *Research in Economic Anthropology*, 23:pp. 45–68. Emerald (MCB UP), Bingley.

2020 *Où vivre sans boire revisited: Water and political-economic change among Mikea hunter-gatherers of southwestern Madagascar. Economic Anthropology* 7(1):22–37. DOI:10.1002/sea2.12160.

Tucker, Bram, Mr. Tsimitamby, Frances Humber, Sophie Benbow, and Taku Iida
2010 Foraging for Development: A Comparison of Food Insecurity, Production, and Risk among Farmers, Forest Foragers, and Marine Foragers in Southwestern Madagascar. *Human Organization* 69(4):375–386.

Turck, John A., and Victor D. Thompson
2016 Revisiting the resilience of Late Archaic hunter-gatherers along the Georgia coast. *Journal of Anthropological Archaeology* 43:39–55. DOI:10.1016/j.jaa.2016.05.006.

UNOSAT

2014 *Satellite-based damage assessment to cultural heritage sites in Syria.* UNITAR/UNOSAT.

USAID

2016 *Climate Change Risk Profile: Madagascar.*

Venables, W. N., and B. D. Ripley

2002 *Modern Applied Statistics with S.* 4th ed. Springer, New York.

Verhagen, Philip, and Thomas G. Whitley

2012 Integrating Archaeological Theory and Predictive Modeling: a Live Report from the Scene. *Journal of Archaeological Method and Theory* 19(1):49–100. DOI:10.1007/s10816-011-9102-7.

Verhoeven, Geert

2017 Are We There Yet? A Review and Assessment of Archaeological Passive Airborne Optical Imaging Approaches in the Light of Landscape Archaeology. *Geosciences* 7(3):86. DOI:10.3390/geosciences7030086.

Verhoeven, Geert, and Christopher Sevara

2016 Trying to Break New Ground in Aerial Archaeology. *Remote Sensing* 8(11):918. DOI:10.3390/rs8110918.

Vérin, Pierre

1971 Recherches sur le sud-ouest de Madagascar. *Taloha* 4:3–5.

1986 *The History of Civilisation in North Madagascar.* Routledge.

Vérin, Pierre, Conrad P. Kottak, and Peter Gorlin

1969 The Glottochronology of Malagasy Speech Communities. *Oceanic Linguistics* 8(1):26–83.

Vernon, Kenneth B., Peter M. Yaworsky, Jerry Spangler, Simon Brewer, and Brian F. Coddling

2020a Decomposing Habitat Suitability Across the Forager to Farmer Transition. *Environmental Archaeology* 0(0):1–14. DOI:10.1080/14614103.2020.1746880.

2020b Decomposing Habitat Suitability Across the Forager to Farmer Transition. *Environmental Archaeology*:1–14. DOI:10.1080/14614103.2020.1746880.

Verschoof-van der Vaart, Wouter Baernd, and Karsten Lambers

2019 Learning to Look at LiDAR: The Use of R-CNN in the Automated Detection of Archaeological Objects in LiDAR Data from the Netherlands. *Journal of Computer Applications in Archaeology* 2(1):31–40. DOI:10.5334/jcaa.32.

Virah-Sawmy, Malika, Katherine J. Willis, and Lindsey Gillson

2009 Threshold response of Madagascar's littoral forest to sea-level rise. *Global Ecology and Biogeography* 18(1):98–110. DOI:10.1111/j.1466-8238.2008.00429.x.

2010 Evidence for drought and forest declines during the recent megafaunal extinctions in Madagascar. *Journal of Biogeography* 37(3):506–519. DOI:10.1111/j.1365-2699.2009.02203.x.

Voarintsoa, Ny Riavo G., Lixin Wang, L. Bruce Railsback, George A. Brook, Fuyuan Liang, Hai Cheng, and R. Lawrence Edwards

2017 Multiple proxy analyses of a U/Th-dated stalagmite to reconstruct paleoenvironmental changes in northwestern Madagascar between 370CE and 1300CE. *Palaeogeography, Palaeoclimatology, Palaeoecology* 469:138–155. DOI:10.1016/j.palaeo.2017.01.003.

Wadsworth, William Thomas Dowler

2020 Above, Beneath, and Within: Collaborative and Community-Driven Archaeological Remote Sensing Research in Canada. Unpublished Master's Thesis, University of Alberta, Department of Anthropology, Edmonton.

Wallace, Andrea P. C., Julia P. G. Jones, E. J. Milner-Gulland, Graham E. Wallace, Richard Young, and Emily Nicholson

2016 Drivers of the Distribution of Fisher Effort at Lake Alaotra, Madagascar. *Human Ecology* 44(1):105–117. DOI:10.1007/s10745-016-9805-1.

Warne, Kennedy

2019 This river in New Zealand is a legal person. How will it use its voice? *National Geographic*. <https://www.nationalgeographic.com/culture/2019/04/maori-river-in-new-zealand-is-a-legal-person/>, accessed November 20, 2020.

Warren, Robert E.

1990 Predictive modelling in archaeology: a primer. In *Interpreting space: GIS and archaeology*, edited by K. M. Allen, S. W. Green, and E. B. W. Zubrow, pp. 90–111. Taylor and Francis, London.

- Wasserman, Stanley, and Katherine Faust
 1994 *Social Network Analysis. Structural Analysis in the Social Sciences*. Cambridge University Press, Cambridge.
- Weitzel, Elic M., and Brian F. Coddling
 2020 The Ideal Distribution Model and Archaeological Settlement Patterning. *Environmental Archaeology* 0(0):1–8. DOI:10.1080/14614103.2020.1803015.
- Williams, Martin AJ, and Hugues Faure
 1980 *The Sahara and the Nile: Quaternary environments and prehistoric occupation in northern Africa*. Balkema, Rotterdam.
- Wilmshurst, Janet M., Terry L. Hunt, Carl P. Lipo, and Atholl J. Anderson
 2011 High-precision radiocarbon dating shows recent and rapid initial human colonization of East Polynesia. *Proceedings of the National Academy of Sciences* 108(5):1815–1820.
- Winterhalder, Bruce, Douglas J. Kennett, Mark N. Grote, and Jacob Bartruff
 2010 Ideal free settlement of California's Northern Channel Islands. *Journal of Anthropological Archaeology* 29(4):469–490. DOI:10.1016/j.jaa.2010.07.001.
- Wright, David
 2017 *An Introduction to QGIS: National Museums of Kenya Training Manual (August 2017)*. Seoul National University.
- Wright, H. T., and J. A. Rakotoarisoa
 2003 The Rise of Malagasy Societies: New Developments in the Archaeology of Madagascar. In *The Natural History of Madagascar*, edited by Steven M. Goodman and Jonathan P. Benstead, pp. 112–119. University of Chicago Press, Chicago and London.
- Wright, Henry T. (editor)
 2007 *Early State Formation in Central Madagascar: An archaeological survey of Western Avaradrano*. Vol. 43. Museum of Anthropology, University of Michigan, Ann Arbor.
- Wright, Henry T., Pierre Vérin, Ramilisonina, David Burney, Lida Pigott Burney, and Katsumi Matsumoto
 1996 The Evolution of Settlement Systems in the Bay of Boeny and the Mahavavy River Valley, north-western Madagascar. *Azania: Archaeological Research in Africa* 31(1):37–73. DOI:10.1080/00672709609511456.
- Wynne-Jones, Stephanie, and Jeffrey Fleisher (editors)
 2015 *Theory in Africa, Africa in theory: Locating meaning in archaeology*. Routledge, New York.

- Xiao, Wen, Jon Mills, Gabriele Guidi, Pablo Rodríguez-Gonzálvez, Sara Gonizzi Barsanti, and Diego González-Aguilera
2018 Geoinformatics for the conservation and promotion of cultural heritage in support of the UN Sustainable Development Goals. *ISPRS Journal of Photogrammetry and Remote Sensing* 142:389–406. DOI:10.1016/j.isprsjprs.2018.01.001.
- Yates, Donna
2018 Crowdsourcing Antiquities Crime Fighting: A Review of GlobalXplorer°. *Advances in Archaeological Practice* 6(2):173–178. DOI:10.1017/aap.2018.8.
- Yaworsky, Peter M., and Brian F. Coddling
2018 The Ideal Distribution of Farmers: Explaining the Euro-American Settlement of Utah. *American Antiquity* 83(01):75–90. DOI:10.1017/aaq.2017.46.
- Yount, James W., Tsiazonera, and Bram T. Tucker
2001 Constructing Mikea Identity: Past or Present Links to Forest and Foraging. *Ethnohistory* 48(1–2):257–291. DOI:10.1215/00141801-48-1-2-257.
- Zanni, Sara, and Alessandro De Rosa
2019 Remote Sensing Analyses on Sentinel-2 Images: Looking for Roman Roads in Srem Region (Serbia). *Geosciences* 9(1):25. DOI:10.3390/geosciences9010025.
- Zeder, Melinda A.
2012 The Broad Spectrum Revolution at 40: Resource diversity, intensification, and an alternative to optimal foraging explanations. *Journal of Anthropological Archaeology* 31(3):241–264. DOI:10.1016/j.jaa.2012.03.003.
2016 Domestication as a model system for niche construction theory. *Evolutionary Ecology* 30(2):325–348. DOI:10.1007/s10682-015-9801-8.
- Zerbini, Andrea, and Michael Fradley
2018 Higher Resolution Satellite Imagery of Israel and Palestine: Reassessing the Kyl-Bingaman Amendment. *Space Policy* 44–45:14–28. DOI:10.1016/j.spacepol.2018.03.002.
- Zinke, J., W.-Chr. Dullo, G.A. Heiss, and A. Eisenhauer
2004 ENSO and Indian Ocean subtropical dipole variability is recorded in a coral record off southwest Madagascar for the period 1659 to 1995. *Earth and Planetary Science Letters* 228(1–2):177–194. DOI:10.1016/j.epsl.2004.09.028.

Vita

Dylan Scott Davis

EDUCATION

PhD in Anthropology (<i>in progress</i>), The Pennsylvania State University Dissertation Chair: Kristina G. Douglass	2018 – 2022
M.A. in Anthropology, Binghamton University Advisor: Carl P. Lipo	2017 – 2018
B.S. Anthropology & B.A. Geography, Binghamton University (<i>summa cum laude</i>)	2014 – 2017

SELECT PUBLICATIONS

- Davis, D. S.** (2020). Studying human responses to environmental change: Trends and trajectories of archaeological research. *Environmental Archaeology*, 25(4), 367–380.
- Davis, D. S.**, Andriankaja, V., Carnat, T. L., Chrisostome, Z. M., Colombe, C., Fenomanana, F., Hubertine, L., Justome, R., Lahiniriko, F., Léonce, H., Manahira, G., Pierre, B. V., Roi, R., Soafiavy, P., Victorian, F., Voahirana, V., Manjakahery, B., & Douglass, K. (2020). Satellite-based remote sensing rapidly reveals extensive record of Holocene coastal settlement on Madagascar. *Journal of Archaeological Science*, 115, 105097.
- Davis, D. S.**, DiNapoli, R. J., & Douglass, K. (2020). Integrating point process models, evolutionary ecology, and traditional knowledge improves landscape archaeology: A case from Southwest Madagascar. *Geosciences*, 10(8), 267.
- Davis, D. S.** (2019). Object-based image analysis: A review of developments and future directions of automated feature detection in landscape archaeology. *Archaeological Prospection*, 26(2), 155–163.
- Davis, D. S.**, Sanger, M. C., & Lipo, C. P. (2019). Automated mound detection using lidar and object-based image analysis in Beaufort County, South Carolina. *Southeastern Archaeology*, 38(1), 23–37.

SELECT GRANTS

- National Science Foundation (NSF) – Doctoral Dissertation Research Improvement Grant (**co-PI**, PI K. Douglass): Award No. BCS-2039927 (\$31,556, 2021-2023)
- NSF Spatial Archaeometry Research Collaborations – Data and Analytics Grant (**PI**) (\$12,381, 2021-2022)
- National Geographic Society – Enduring Impacts RFP Grant (**co-PI**, PI K. Douglass): Award No. NGS-77912R-21 (\$79,995, 2021-2022)
- NASA Pennsylvania Space Grant Consortium – Mini-Grant (**PI**) (\$4,995, 2020-2021)
- Sigma Xi – Grant in Aid of Research (**PI**) (\$800, 2020-2021)
- Microsoft – AI for Earth Azure Compute Credit Grant (**co-PI**, PI K. Douglass) (\$15,000, 2020-2021)
- Explorers Club – Mamont Scholar Grant (**PI**) (\$2,000, 2020-2021)
- American Philosophical Society – Lewis and Clark Fund for Exploration and Research (**PI**) (\$5,000, 2020-2021)